2025

Geological Survey Paper 15:

Structural Geology of the Northern Tyennan Subdomain, Tasmania — An Overview and Structural Synthesis

Author: D.R. Gray, M.J. Vicary, G.C. Cumming
J.L. Everard and C. Jackman

Date: 25/06/2025

Email: info@mrt.tas.gov.au

Website: www.mrt.tas.gov.au

REPORT No.: GSP15

Isoclinally folded Precambrian quartzite of Hansons Peak (1185 m) with the quartzite ridgeline (photo left) flanking the eastern side of the glacially carved Dove Lake (photo middle right). The craggy dolerite of the northern face of Cradle Mountain (photo right background) is dominated by Little Horn (1355 m) and Weindorfers Tower (1470 m), with Smithies Peak (1527 m) partially hidden behind Weindorfers Tower. The dolerite sill sits above a thin (~ 130 m thickness), flat lying, bedded Permian sedimentary sequence that is unconformable on the quartzite. The Permian unconformity is traversed on the Face Track at ~1240 m.

Note the oblique intersection of a plunging, isoclinal synformal fold in Hansons Peak (peak left) and a plunging antiform (peak right).

Tasmanian Government

Mineral Resources Tasmania

mrt

CONTENTS

ABSTRACT *3*

1.0 INTRODUCTION **4**

2.0 BACKGROUND TO THE NORTHERN TYENNAN SUBDOMAIN **5**

2.1 Geographic Elements **5**

2.2 Previous Mapping **8**

2.3 Litho-tectonic units **9**

2.4 Previous Structural Interpretations **10**

2.5 Nature of the Layering and Foliations **13**

2.6 Key Structural Relationships **14**

2.7 Structural and Metamorphic Petrology **14**

2.8 Metamorphism and Geochronology **14**

2.8.1 Metamorphic P, T Determinations *14*

2.8.2 Geochronology *15*

2.9 Current Work **15**

3.0 NORTHERN TYENNAN SUBDOMAIN GEOLOGY SUMMARY/OVERVIEW **16**

3.1 Major Structural Elements **16**

3.2 Map Pattern and Regional Relationships **18**

3.3 Major Fold Axial Surface Trace Pattern **20**

3.4 Early Isoclinal Fold Pattern **21**

3.5 Lineation Lm Pattern **21**

3.6 Early Fold Axis (FA) and Lineation (Lm) Relationships **23**

3.7 Transport Direction (TD) Pattern **24**

3.8 Younger Overprinting Cleavages and Folds **26**

3.9 Fault Pattern **26**

4.0 REGIONAL STRUCTURAL PROFILES **27**

4.1 Western Profile A-A': Mt Kate-Cradle Mountain-Overland Track Profile **27**

4.2 Middle Profile B-B': Lone Gum Plain Profile **29**

4.3 Eastern Profile C-C': Mersey Valley Profile **29**

5.0 MAJOR STRUCTURES OF THE NORTHERN TYENNAN SUBDOMAIN **31**

5.1 Mt Kate Recumbent Isoclinal Macro-fold (Area 1, Figure 16) **31**

5.1.1 Mt Kate Recumbent Isoclinal Macro-fold Hinge (Area 1a) *31*

5.1.2 Mt Kate Macro-fold "Tail" (Area 1b, Figure 16) *37*

5.1.3 Quartzite-Pelite Upper Limb to Hinge Transition Zone (Area 1c) *37*

5.2 Granite Tor Macro-fold Zone (Area 2, Figure 16) **41**

5.3 Northern Tyennan Chevron Fold Zone (Area 3, Figure 16) **42**

5.3.1 Quartzite-Pelite Structural Transition Zone (Area 3a, Figure 16) *42*

5.3.2 Liena-Borradaile F3 Chevron Fold Zone (Area 3b, Figure 16) *54*

5.3.3 Rowallan Fold Interference Zone (Area 3c, Figure 16) *63*

5.4 Overland Track Zone (Area 4, Figure 16) **75**
5.4.1 North of Lake Windemere *75*
5.4.2 Pine Forest Moor *80*
5.4.3 Old Pelion Hut Track *81*
6.0 IMPLICATIONS OF THE NORTHERN TYEN-NAN SUBDOMAIN STRUCTURE **85**
6.1 The Role of non-coaxial shear in Northern Tyennan Fabric Development **85**
6.2 The Role of non-coaxial shear in Northern Tyennan Fold Development **85**
6.3 Shear Sense Explanation and Implications **87**
6.4 The Mt Kate Macro-fold Geometry **90**
6.5 The Curvature of the Northern Tyennan Subdomain **93**
7.0 CONCLUSIONS **96**
8.0 ACKNOWLEDGEMENTS **96**
9.0 REFERENCES **97**

APPENDICES

APPENDIX 1 - Enlarged maps of foliations, lineations and fold axes for the Northern Tyennan Subdomain **95**
APPENDIX 2 - Structural Measurements **103**

Abstract

The Northern Tyennan subdomain occupies the northernmost part of the Tyennan Domain. It is in part fault-bounded with arcuate form showing distinct curvature and a swing to east-west strike in the northern part. The western boundary of the subdomain is defined by the Tyennan Margin Fault, an inverted Late Cambrian extensional fault that also marks the margin of the Dundas-Fossey Graben. The fault along the northern boundary is covered by Cambro-Ordovician siliciclastic overlap sequences, Tertiary basalt and younger Cenozoic fluvioglacial deposits. The eastern boundary is less distinct defined by erosional remnants of Permian sedimentary rocks intruded by Jurassic dolerite that form the western margin of the Central Plateau.

Structurally the Northern Tyennan subdomain has three main structural elements including 1) the Mt Kate recumbent macro-fold, 2) the Granite Tor fold interference zone and 3) the Liena-Borradaile F3 chevron fold zone. The northern part is dominated by the Mt Kate macro-fold hinge and hinge to lower limb transition where high-grade pelites (garnet schists) form the core of the macro-fold but are also partly preserved on the lower limb at Lake Rowallan. These high-grade rocks represent medium-grade metamorphism to lower amphibolite facies and are the Mersey River Metamorphic Complex (Meffre et al, 2001; Chmielowski & Berry, 2012). Estimated P, T conditions of 550°C ± 50°C and 7.2 ± 1.5 kbars indicate that the high-grade rocks of the MRMC were subducted to depths of at least 20 km prior to exhumation (Mattner, 2015). The MRMC metamorphism has been dated at 502±10 Ma (Berry et al., 2007).

The Mt Kate isoclinal recumbent macro-fold represents a transition from 3 regional macro-folds in the Central Tyennan subdomain into a single major macro-fold in the Northern Tyennan subdomain. This transition also accompanies the marked swing from north-south trend to east-west trend. The outer shell of the Mt Kate macro-fold has "sled-runner" geometry with a short upper, overturned limb and a long, trailing lower limb. This geometry has similarities to the Spry (1962) interpretation of a north-closing Borradaile fold. The inner shell or hinge has quartzite layers in-folded with garnet schist as an asymmetric fold couple, that has curved hinge lines symmetrical about the pronounced east-west lineation Lm trend. Refolding by upright east-west trending folds has produced a mushroom-shaped fold interference pattern due to the inner sheath-fold hinge curvature.

This marked change in structural geometry occurs across Granite Tor. South of Granite Tor the west- and east-closing macro-fold system of the Central Tyennan subdomain appears to dominate. North of Granite Tor the structural geometry is the simple north-closing recumbent isoclinal macro-fold (F2 generation) where the lower limb is refolded by upright tight to open chevron folds (F3 generation). At the junction, or "centre" of apparent curvature just north of Granite Tor, Type 3 fold interference occurs due to refolding by open, northwest-trending folds with a weakly developed, sub-vertical axial surface cleavage (S4/Scc).

The east-west trending Liena-Borradaile F3 chevron fold zone occupies the central and eastern part of the subdomain. The "core" of the chevron fold domain has variably plunging, close to tight, upright chevron folds with both rounded antiformal hinges and cuspate synformal hinges. They have ovoid and partially closed ovoid outcrop patterns typical of sub-vertical, individual conical-shaped sheath folds. The folds show marked plunge variations within a steeply north-dipping axial surface foliation. Multiple zones of these fold hinges define individual hinge domains that are enveloped by strong to intense zones of transposition foliation. These features combined are suggestive of F3 folding as part of a shear-related continuum, considered part of Tyennan sheet ascent-emplacement deformation with subsequent rotation to the current sub-vertical orientation.

The lineation Lm and transport direction TD pattern indicate that the pronounced curvature of the Northern Tyennan subdomain is not due to a simple passive clockwise rotation about an apparent rotation axis. The pattern suggests movement up, and flexing around, a potential curved segment of the Cambrian subduction channel.

Tasmanian Government

Mineral Resources Tasmania

Department of State Growth
www.mrt.tas.gov.au

Structural Geology of the Northern Tyennan Subdomain, Tasmania — An Overview and Structural Synthesis

David R. Gray[1], Michael J. Vicary[2], Grace C. Cumming[2], John L. Everard[2] and Carl Jackman[2]
[1] *Consultant Structural Geologist to Mineral Resources Tasmania*
[2] *Geological Survey Branch - Mineral Resources Tasmania*

ARTICLE INFO

Published: 25 June 2025
Publisher: Mineral Resources Tasmania
Report No.: GSP15

KEYWORDS

Structural Geology
Fold-nappe
Chevron folds
Northern Tyennan region
Medium-P metamorphism

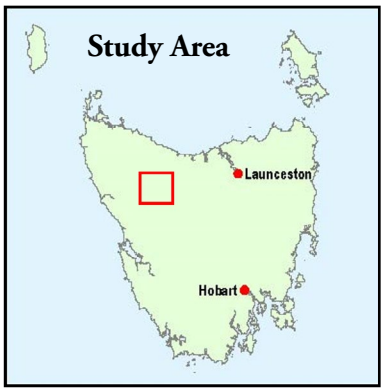

1.0 INTRODUCTION

The Northern Tyennan subdomain occupies the northern part of the Tyennan Domain (Figure 1). It is structurally continuous with the Central Tyennan subdomain to the south. It has a litho-tectonic sequence of Proterozoic high-grade garnet schists overlying Proterozoic low-grade quartzite±phyllite (Spry, 1958; Gee et al., 1970). In map projection the Northern Tyennan subdomain has a ~100 km length and ~70 km width (Figure 2).

The western and northern parts of the Northern Tyennan subdomain are flanked by the Mt Read Volcanic succession within the Dundas-Fossey graben system. The western and northern boundary are defined by the Tyennan Margin fault separating the Proterozoic rocks from the Cambrian Mt Read Volcanics of the Dundas-Fossey graben. Part of the northern boundary is covered by Late Cambro-Ordovician fluvial overlap sequences, and the eastern and southern boundaries by the Permian sedimentary overlap sequence and the Jurassic dolerite sills of the Central Plateau. The Late Cambrian-Ordovician sandstone and conglomerates of the fluvial overlap sequences mark the prominent, north-flanking ranges of the Black Bluff Range, Mt Claude, Mt Van Dyke and Mt Roland (Figure 3).

The Proterozoic age units are part of continental margin deposits that were subducted to depths of ~20 to 60 km beneath an advancing ophiolite sheet during a Cambrian arc-continent collision along the eastern margin of Gondwana (Berry and Crawford, 1988; Berry, 2014, Figure 4.10).

This Tasmanian Geological Survey Paper is part of a series of papers revisiting the structural geology of the Tyennan Domain of Tasmania (Figure 1). The aim of this study has been to re-examine the structure of the Tyennan Proterozoic rocks in the context of Cambrian continental margin subduction-obduction. Deformation of this former Cambrian continental margin beneath the advancing ophiolite sheet has involved crustal-scale stacking of sheets of different metamorphic grade, isoclinal folding and internal sheet deformation, with sheets welded along their contacts by shear zones and/or brittle faulting. Subsequent erosional removal of the ophiolite sheet has provided an exposed 50-100 km window into these underlying rocks (Gray et al., 2024).

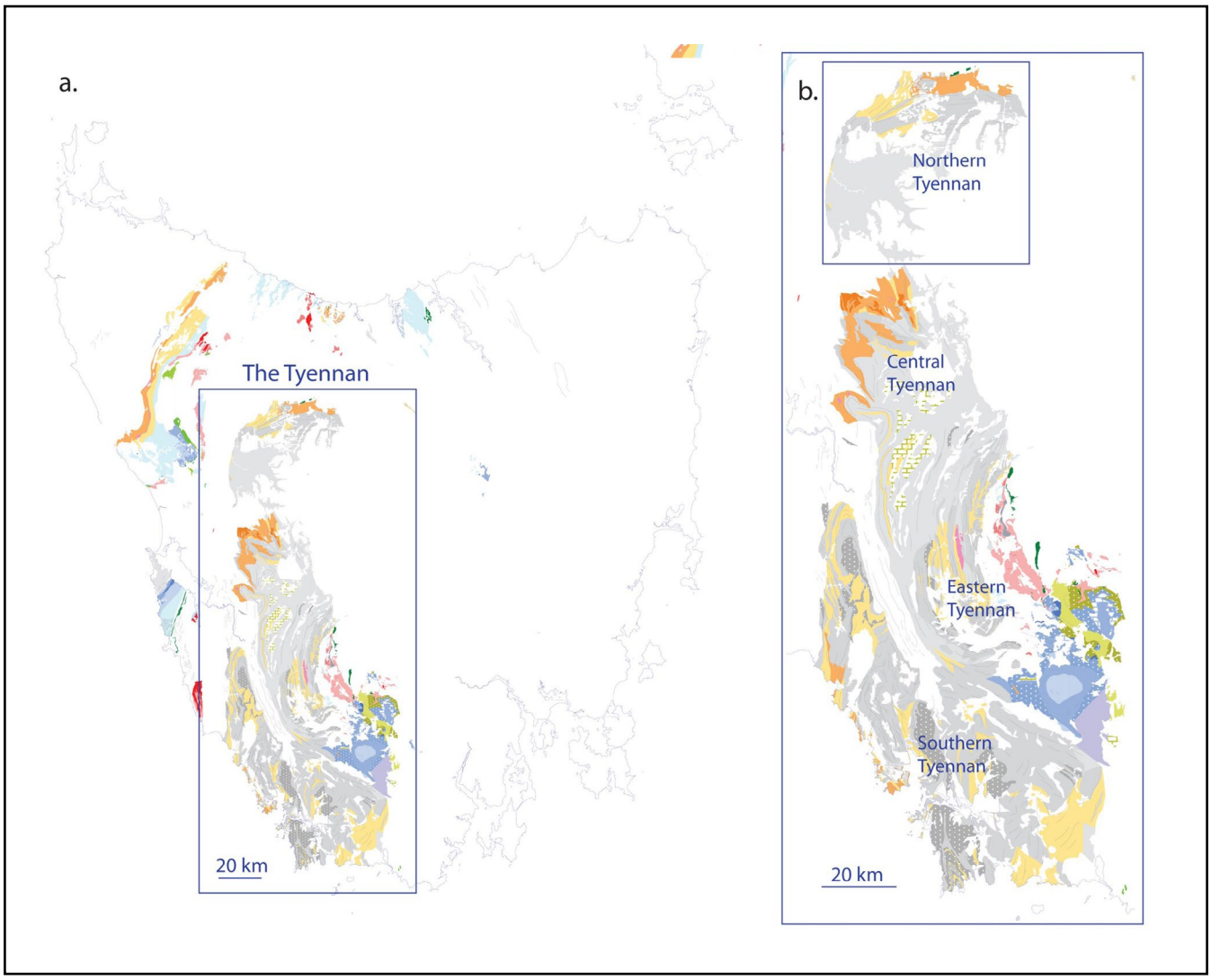

Figure 1. The Tyennan Domain Proterozoic region of Tasmania shown in a). Map base is Mineral Resources Tasmania 1:25,000 and 1:250,000 digital geological atlas. b) Enlarged map with the location of the Northern Tyennan subdomain. The divisions within the Tyennan are after Berry (2014). The approximate Northern Tyennan map sheet polygon boundaries are 5345400 mN (northern boundary), 5165000 mN (southern boundary), 467000 mE (eastern boundary) and 386000 mE (western boundary).

This paper represents a synthesis of the regional structure of the Northern Tyennan subdomain with companion Geological Survey Paper 7 defining the structures and structural relationships in the adjoining Central Tyennan subdomain (Gray and Vicary, 2021).

Appendix 1 provides enlargements of the Northern Tyennan subdomain structural maps.

A1.1: Foliation Sm Map

A1.2; Lineation Lm Map

A1.3: Isocline Fold axis FA Map

Appendix 2 provides a listing of new structural measurement data collected as part of this synthesis.

2.0 BACKGROUND TO THE NORTHERN TYENNAN SUBDOMAIN

2.1 Geographic Elements

The Northern Tyennan subdomain occupies a distinct plateau at ~1220 m dissected by the major, north-flowing Forth and Mersey Rivers in the north and the Murchison and Fury Rivers in the west (Figures 2a and 2b). It is situated on the western edge of the high Central Plateau (Figure 2b). The plateau is a compound landform incorporating a pre-Permian surface, a Tertiary surface of mature river erosion, a post-Tertiary basalt surface and a maturely dissected and young Central Plateau (Spry, 1958). Pleistocene glaciation has further modified these landforms carving U-shaped valleys leaving roches moutonnées and glacio-fluvial deposits of till and varves (Spry, 1958).

Geologically the plateau is punctuated by Proterozoic quartzite and pelite, unconformably overlain by a flat-lying Permian sedimentary sequence intruded by a Jurassic dolerite sill(s) that caps the higher peaks (Figure 3). These dolerite-capped peaks include Cradle Mountain (1545 m), Barn Bluff (1559 m), Mt Oakleigh (1286 m), Mount Pelion West (1560 m), Mount Pelion East (1560 m), Mt Achilles (1363 m), Mount Ossa (1617 m), Cathedral Mountain (1387 m), Mt Hyperion (1480 m), The Acropolis (1481 m) and Mt Gould (1485 m).

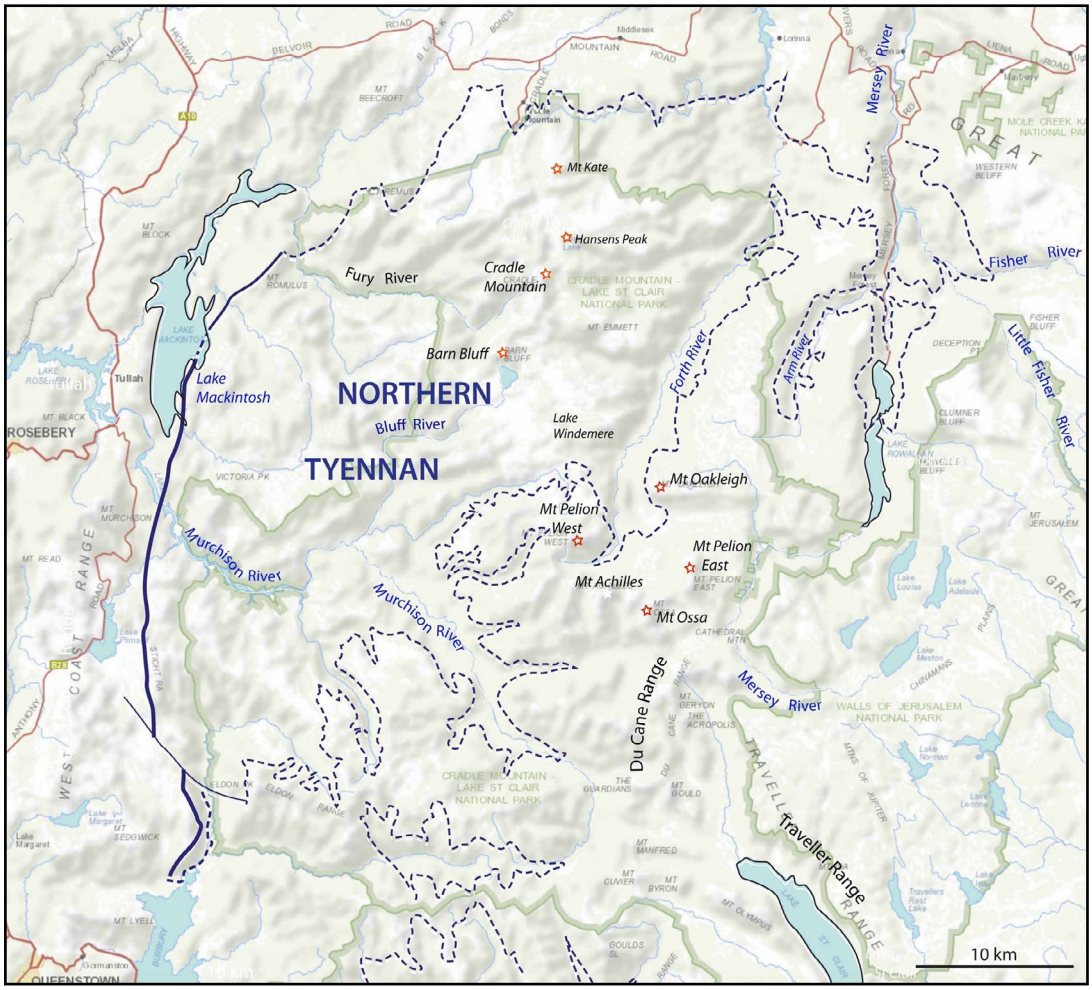

Figure 2a.

ListMap™ topographic map with the dark blue dashed line marking the boundary and outcrops of the Proterozoic rocks of the Northern Tyennan subdomain. Geographic elements including peaks and major rivers are highlighted.

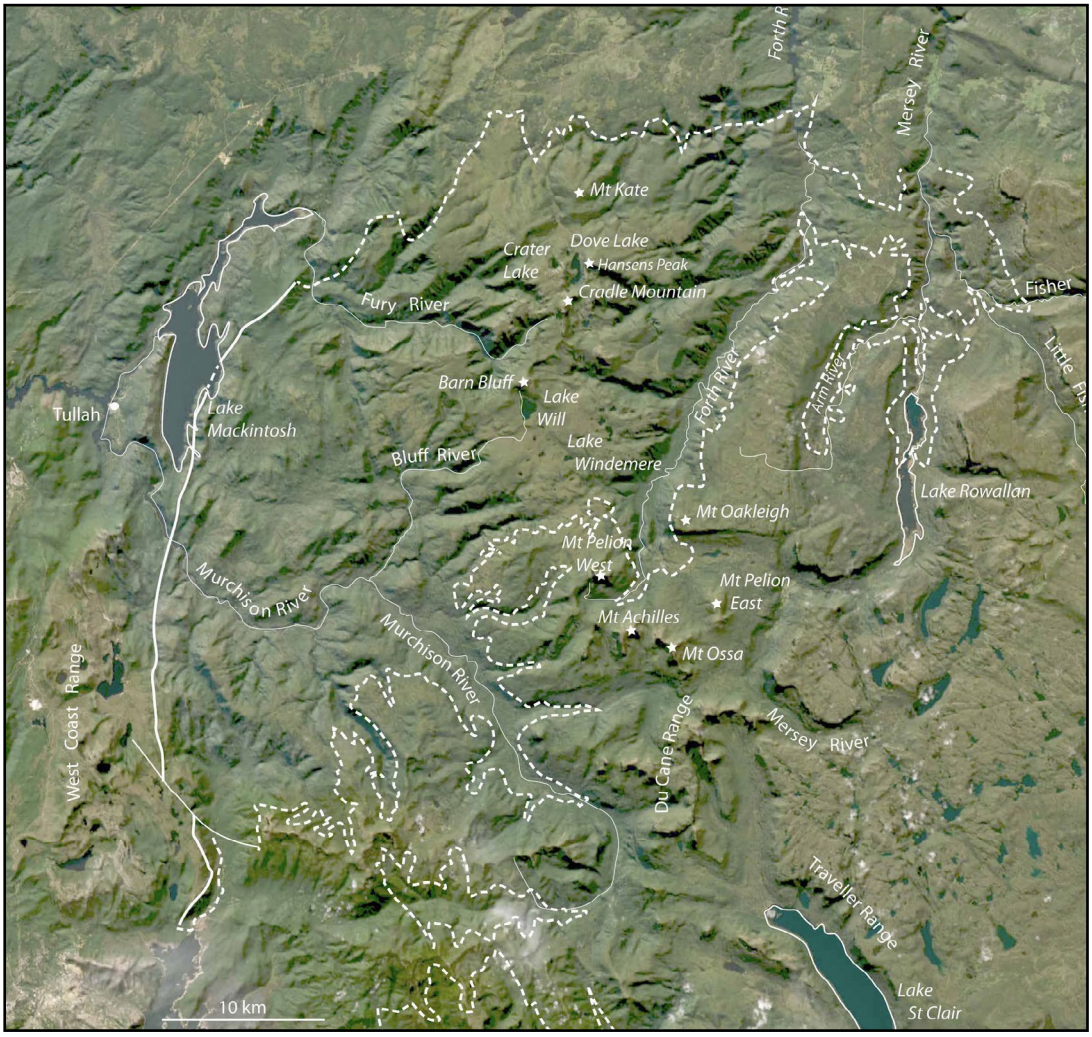

Figure 2b.

ListMap™ Google satellite image of the Northern Tyennan subdomain showing the distinct plateau of the Central Plateau (image right), dissected and glaciated remnant plateau of the central part occupied by the subdomain. The white dashed line marks the outcrop extent and boundaries of the Proterozoic rocks of the subdomain.

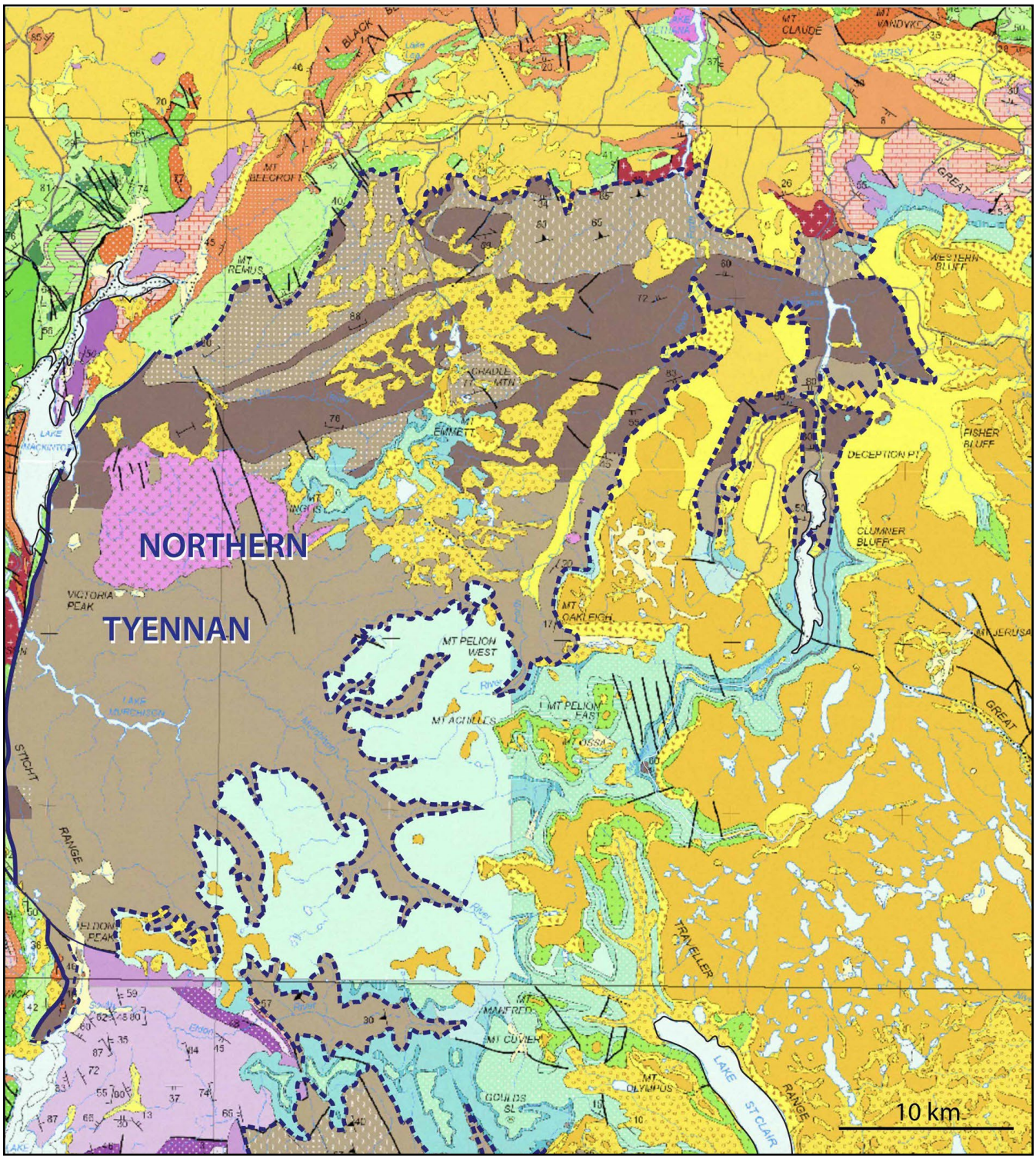

Figure 3. Geological map of the Northern Tyennan subdomain and surrounds. The dark blue dashed line marks the outcrop extent and boundaries of the Proterozoic rocks of the subdomain shown in brown.

Yellow: Quaternary sediments.
Pale orange: Tertiary basalt.
Orange: Jurassic dolerite.
Blue/bright green: Permian glacial sedimentary rocks (map lower centre).
Pink: Devonian granite.
Mauve/purple: Silurian sedimentary rocks.
Pale red-pink pale-pink: Cambro-Ordovician fluvial sedimentary overlap succession.
Light to dark bright green: Cambrian volcanic rocks.
Brown: Proterozoic rocks.
Dark red: Cambrian granite.
Brown: Proterozoic rocks.
Dark brown: Proterozoic pelitic rocks.
Light brown with stipple: Proterozoic high-grade pelitic rocks.

Quartzite peaks include Mt Kate (1156 m), Crater Peak (1270 m), Mount Campbell (1248 m) and Hansons Peak (1185 m), Mount Romulus (966 m) and Quartzite Tor (921 m) with Granite Tor (1034 m) within the Granite Tor granite (Figure 3).

2.2 Previous Mapping

An index map for mapping and structural data sources for the Northern Tyennan subdomain is shown in Figure 4. Allan Spry undertook mapping of the Forth and Mersey valleys for the Tasmanian Hydro-Electric Commission from December 1955 to early March 1956 culminating in Spry (1958, 1962).

Tasmanian Geological Survey mapping by 1) Ian Jennings in the mid to late 1950's resulted in the Explanatory Report One-Mile Geological Map Series Middlesex (Jennings and Burns, 1958; Jennings, 1963), and 2) Denis Gee, Brian Marshall and Kerry Burns in the Cradle Mountain area as part of the 1:63,000 Mackintosh map-sheet (Barton et al., 1966) and Geological Survey Report No. 8 (Gee et al., 1970). A photo-geological map interpretation was undertaken by Hunting Geology and Geophysics Australia Pty Ltd for Alcoa of Australia Limited in 1980 (Hopgood, 1980: Appendix B, Tasmanian Company Report 80-1490).

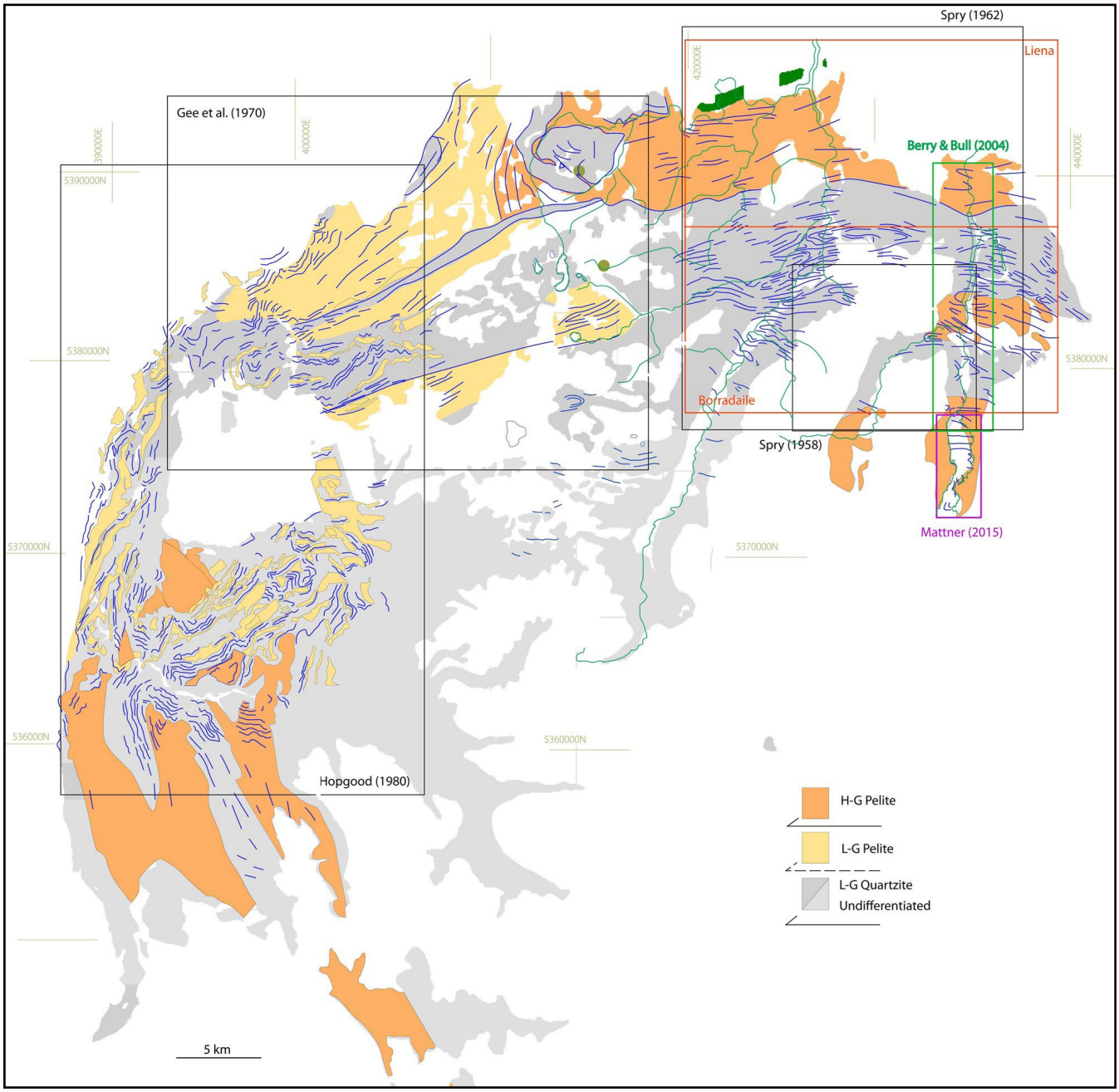

Figure 4. Index map for structural data sources for the Northern Tyennan subdomain. Mapping was initiated in the mid 1950's by Alan Spry (Spry, 1958, 1962) for the Hydro Electricity Commission followed by Geological Survey mapping in the late 1960's (Gee et al., 1970). This was followed by University of Tasmania student mapping in the late 1990's and early 2000's (Berry and Bull, 2004), and a University of Tasmania Honours Thesis by Mattner (2015). Recent Geological Survey mapping on the Liena and Borradaile has been undertaken in 2020-2023 by Cumming et al. (in prep, 2025). The lithologic base map is modified from the Mineral Resources Tasmania 1:250,000 and 1:25,000 digital atlas.

The early work was followed by University of Tasmania undergraduate student structural mapping along the Mersey Valley in the late 1990s and early 2000s included in a Geological Society of Australia Fieldtrip Guide (Berry and Bull, 2004). A University of Tasmania Honours Thesis on the Lake Rowallan area when the Lake level was very low was undertaken in 2015 (Mattner, 2015).

2.3 Litho-tectonic units

The Proterozoic rocks of the Northern Tyennan subdomain (Figure 5) consist of a structurally intercalated, ~7 km thick stack of low-grade (L-G) meta-sedimentary rocks including quartzite (unit 3, Figure 5) and phyllite (unit 2, Figure 5), and high-grade garnet schist (unit 1, Figure 5) and an amphibolite bearing schist of igneous origin (Jennings, 1963; Spry, 1958, 1962; Gee et al., 1970). The high-grade (H-G) metamorphic rocks are part of the Mersey River Metamorphic Complex (Meffre et al., 2000). They are a medium- high-grade metamorphic sequence consisting of interbedded quartz-mica schists and quartzites containing quartz-muscovite-biotite-albite-garnet assemblages (Mattner, 2015). The "stratigraphic" or litho-tectonic package across the Northern Tyennan subdomain was originally divided into Dove and Arm Schist, dominant pelitic schist sequences, Fisher Quartzite, a quartzite dominated sequence, and Howell Group of interlayered quartzite, quartz-mica and garnet-mica schist (Jennings, 1963; Spry, 1958, 1962).

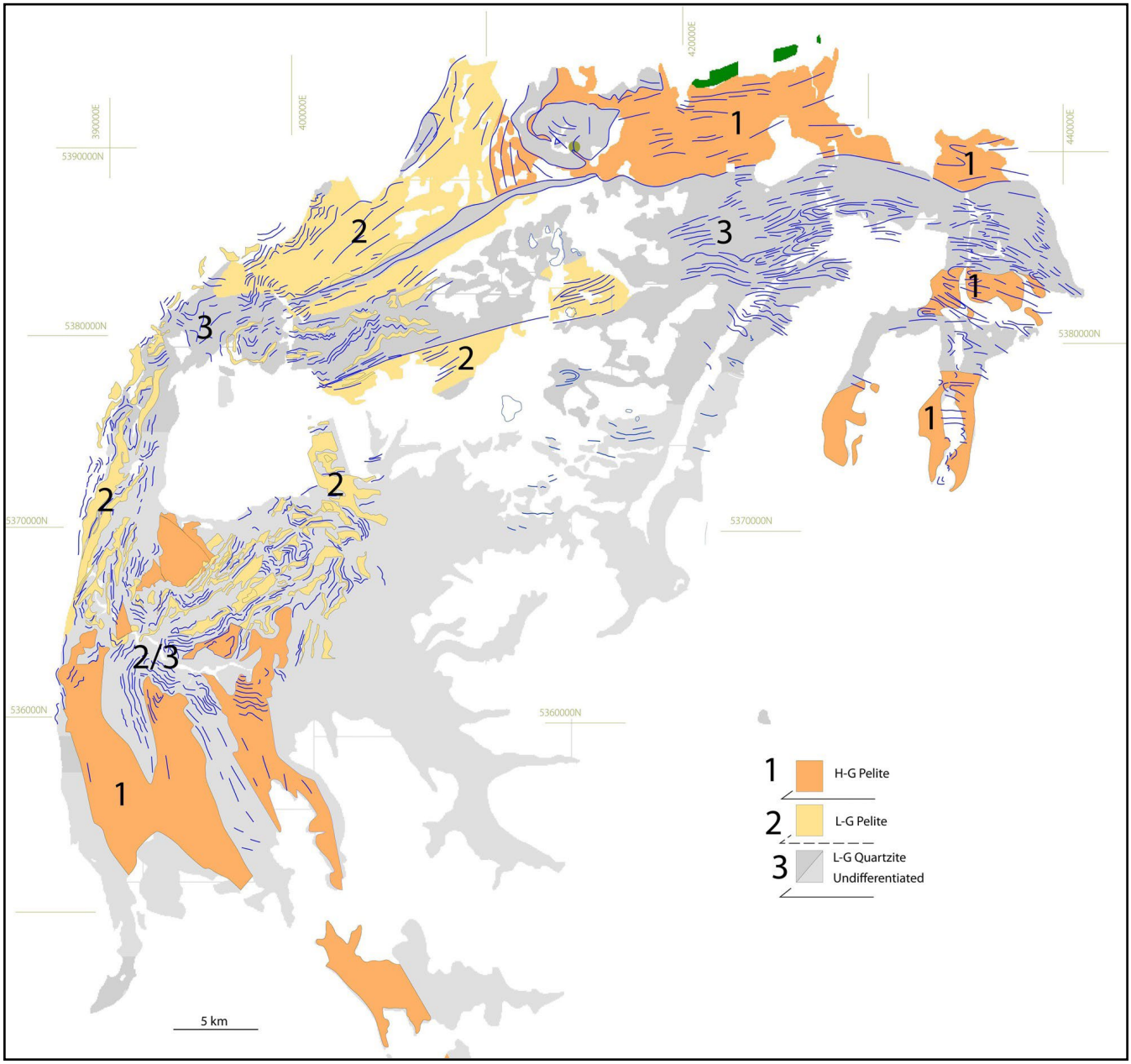

Figure 5. Northern Tyennan subdomain litho-tectonic unit map showing the stacking order based on structural mapping and interpretation. 1: Uppermost unit. 2: Middle unit. 3: Bottom unit. 2/3: interdigitating pelite and quartzite in approximately equal proportions (area south of Granite Tor). Each lithotectonic unit is bounded at the base by a high strain zone.

Form lines in So/Sm are shown by the blue line traces.

H-G: high-grade.

L-G: low-grade.

The lithologic base map is modified from the Mineral Resources Tasmania 1:250,000 and 1:25,000 digital atlas.

Mapping by Gee et al. (1970) showed that well-foliated phyllite dominates the northwestern part of the Northern Tyennan subdomain, particularly in the area of Anio Creek, Devils Ravine and Crisis Creek (Figure 6). In thin section the phyllite consists of a fine segregated layering with thin (~1 mm) lenticles of quartz surrounded by muscovite and chlorite (Gee et al., 1970). The chloritic phyllite is transitional into medium-grained quartz-muscovite schist and then into a coarser-grained garnet schist near Waldheim (Figure 6). The schists are mostly medium-grained quartz-muscovite rocks with albite and less commonly biotite. Garnet schist occurs in the core of the Mt Kate Antiform (Gee et al., 1970) and in parts of the Lake Rowallan area (Mattner, 2015). The garnet schist in the northern part of the Northern Tyennan subdomain was originally defined as the Dove Schist consisting of quartz-mica and garnet-mica schists with little quartzite (Jennings, 1963).

In the Cradle Mountain area:

1. The low-grade meta-sedimentary rocks occur as scattered slices of indurated banded siltstone within the western semi-pelitic belt between Lake Rodway and Granite Tor (Gee et al., 1970). The semi-pelitic belt is made up of structurally intercalated, thin bands of phyllite, schist and schistose quartzite.
2. Quartzite occurs either as a well-bedded, slabby to platy quartzite or as schistose quartzite. The slabby quartzite occurs in the two major quartzite belts in the southern half of the Cradle Mountain area (Figure 6). The schistose quartzite is predominant in the semi-pelitic belt designated the Waldheim High Strain Zone (Figure 6).
3. Foliation-sub-parallel slabs of amphibole schist also occur in the southwest corner of Crater Lake (Gee et al., 1970).

2.4 Previous Structural Interpretations

The earliest structural interpretations were by Jennings and Burns (1958) and Spry (1958, 1962) based on the mapping of geological units (Figures 7, 8 and 9). A series of east-west trending open anticlines and synclines were identified (Figures 7 and 9), although Spry (1962) interpreted a hypothetical Borradaile fold nappe (Figure 8) as an east-west trending, north-closing, recumbent isoclinal macro-fold. This was based on repetition of the schist units and similarities with his Frenchmans Cap interpretation of a Franklin fold-nappe (Spry, 1963).

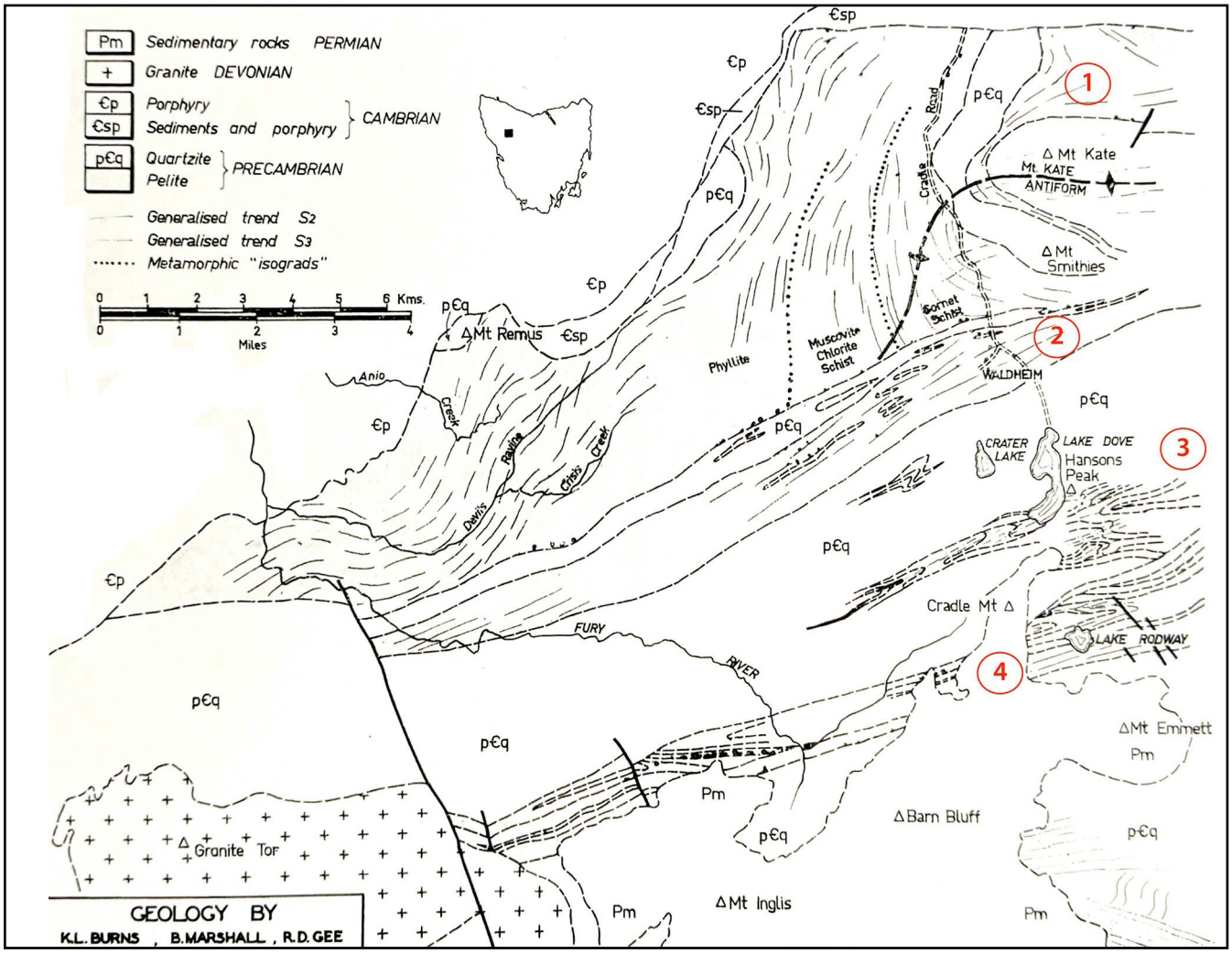

Figure 6. Structural map of the Granite Tor-Cradle Mountain area (Figure1, Gee et al., 1970) showing form lines in the dominant foliation (S2) and crenulation cleavage (S3). Labelled elements include: Circled 1: Mt Kate Antiform; Circled 2: Waldheim High Strain Zone; Circled 3: Cradle Mountain (Crater Lake-Hansons Peak-Twisted Lakes) Folded Zone; Circled 4: Lake Rodway High Strain Zone.

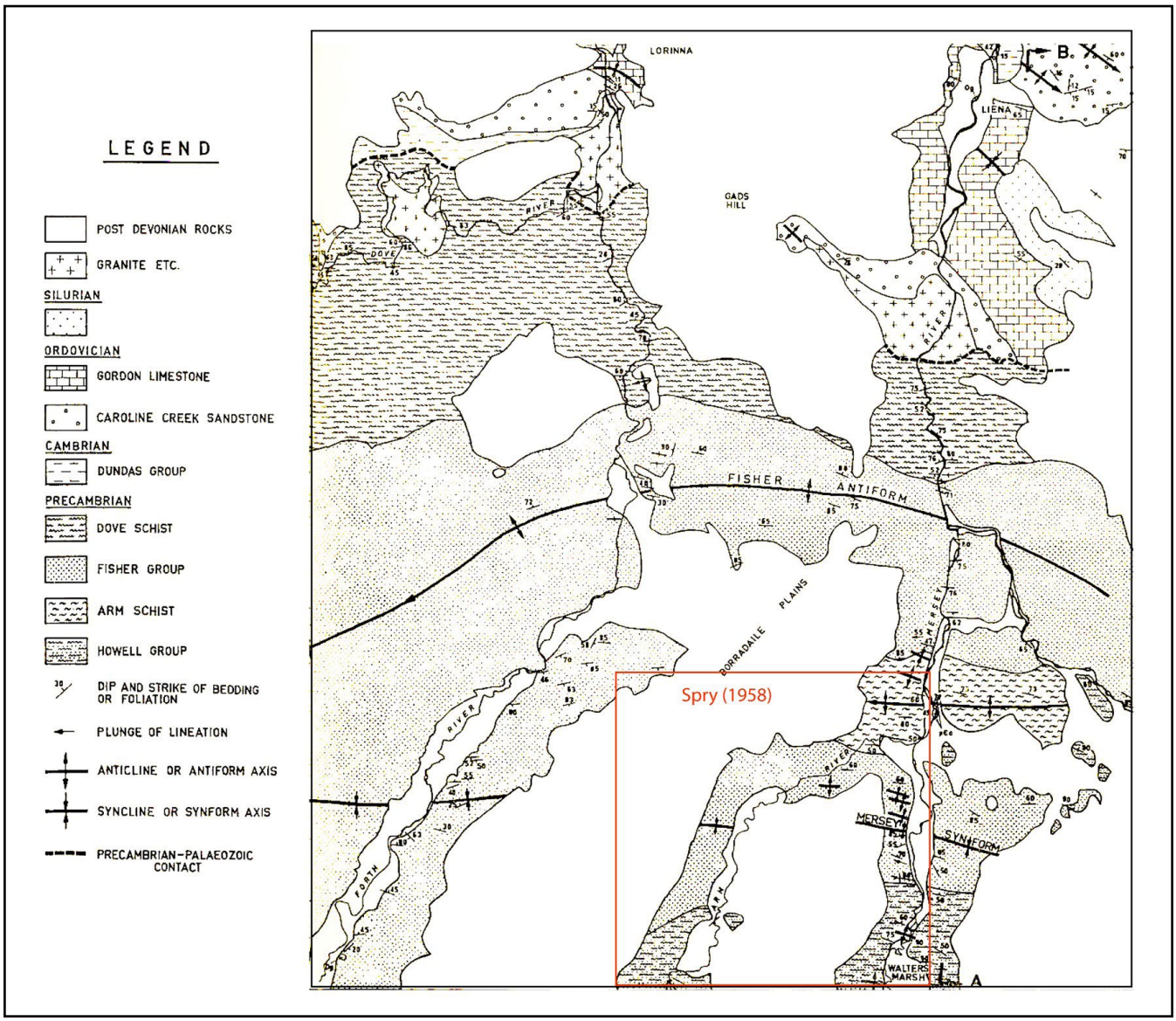

Figure 7. Geological map of the Forth River and Mersey River valleys (fig.1, Spry, 1962). The geology was based on Spry (1958) and Jennings and Burns (1958). Cross-section A-B along the Mersey River shown in Figure 8.

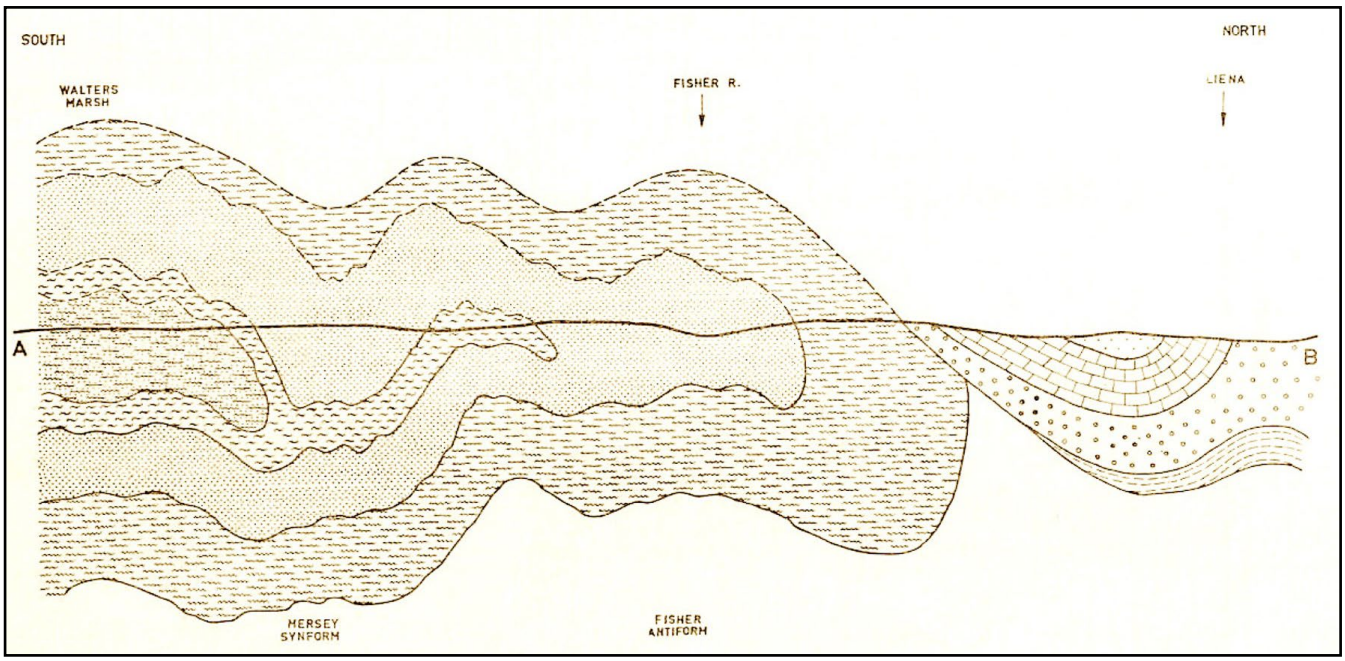

Figure 8. Interpretative cross-section A-B along the Mersey River from Spry (1962, Figure 4). For section location see Figure 7. Geographic place names are shown through the section. The profile shows the hypothetical Borradaile fold nappe. The interpretation was based on repetition of the schist and quartzite layers along the Mersey River profile. The fold-nappe is refolded by the series of younger open anticlines and synclines shown in Figures 7 and 9.

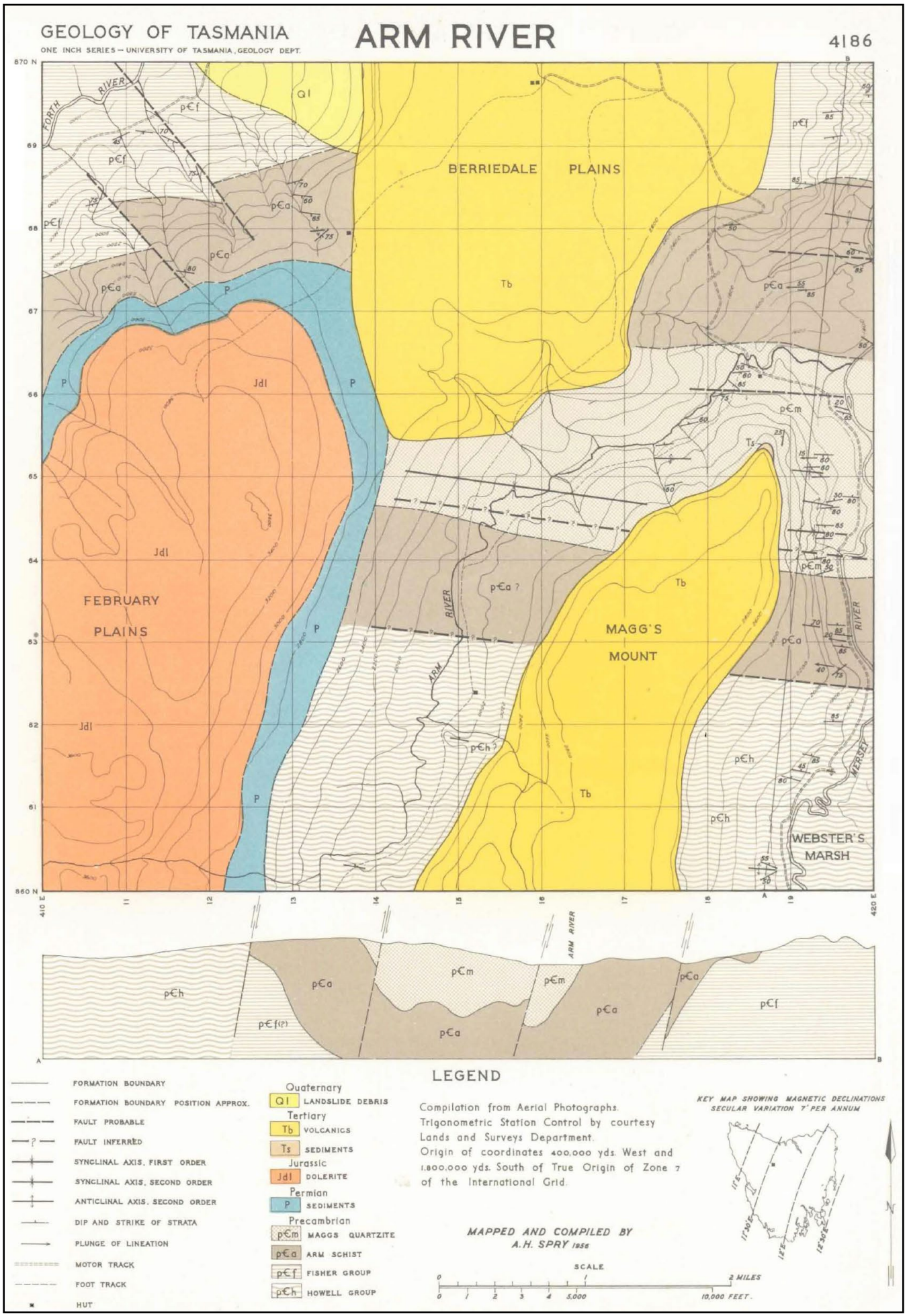

Figure 9. Geological map of the Arm River area with cross-section A-B north-south trending along the Mersey River (Spry, 1958).

Mapping of part of the Mackintosh sheet in the Cradle Mountain area (Gee et al. (1970) included a more detailed structural analysis and form line mapping of foliation (Figure 6). Using this mapping four major structural elements can be identified including the Mt Kate Antiform (circled 1, Figure 6), the Waldheim High Strain Zone (Circled 2, Figure 6), the Cradle Mountain (Crater Lake-Hansons Peak-Twisted Lakes) Folded Zone (Circled 3, Figure 6) and the Lake Rodway Banded/High Strain Zone (Circled 4, Figure 6).

2.5 Nature of the Layering and Foliations

Gee et al. (1970) identified three foliations including a bedding foliation designated as S1, an intense crenulation cleavage/schistosity (S2), and a spaced crenulation cleavage (S3) (Figure 10). The schistosity S2 in most cases is an intense foliation defined by white mica-rich zones or lamellae with ~0.5 mm thickness and spaced at ~1.5 - 2 mm (Figure 11).

To conform to previous Tyennan Geological Survey Publications the following nomenclature has been adopted. There are six types of layering and foliation:

1. *Bedding So:* relatively undeformed bedding
2. *Bedding-parallel foliation So/Sm:* compositional banding sub-parallel to a strong to intense foliation that is folded by recumbent isoclinal folding.
3. *Intense foliation (Sm):* the dominant foliation that is axial surface to the major recumbent isoclinal macro-folds. Associated with this layering is a marked rodding fabric within the Sm layering. This is the regional foliation that envelopes macro- to meso- fold "pods". The pods occur at all scales.
4. *Crenulation cleavages (Scc)* associated with development of transposition layering in the basal high strain zones and to younger folding events.
5. *Shear Band foliation (Sb) or S-C' fabrics* as a form of extensional crenulation cleavage that reflects shear-induced, foliation-oblique late-stage flattening. These zones are essentially secondary shear zones that record the overall shear sense and/or emplacement direction.
6. *Spaced cleavage (Scl)* a younger Devonian cleavage that overprints all three foliations listed above.

There are four types of lineations:

1. *A mineral lineation (Lm)* generally defined by mica and/or elongated quartz grains in the quartzite.
2. *An elongation or stretching lineation (Lelong)* most commonly shown by elongated quartz grains.
3. *A rodding lineation (Lrod)* that changes from an initial intersection lineation at high angle to the regional stretching direction, to a "herringbone" pattern where flattened mesoscopic fold hingelines become curvilinear and pulled apart, to eventually develop a strong, sub-parallel alignment with the regional stretching direction (Lstretch).
4. *A crenulation lineation (Lcren)* as tiny puckers or wrinkles within the foliation.

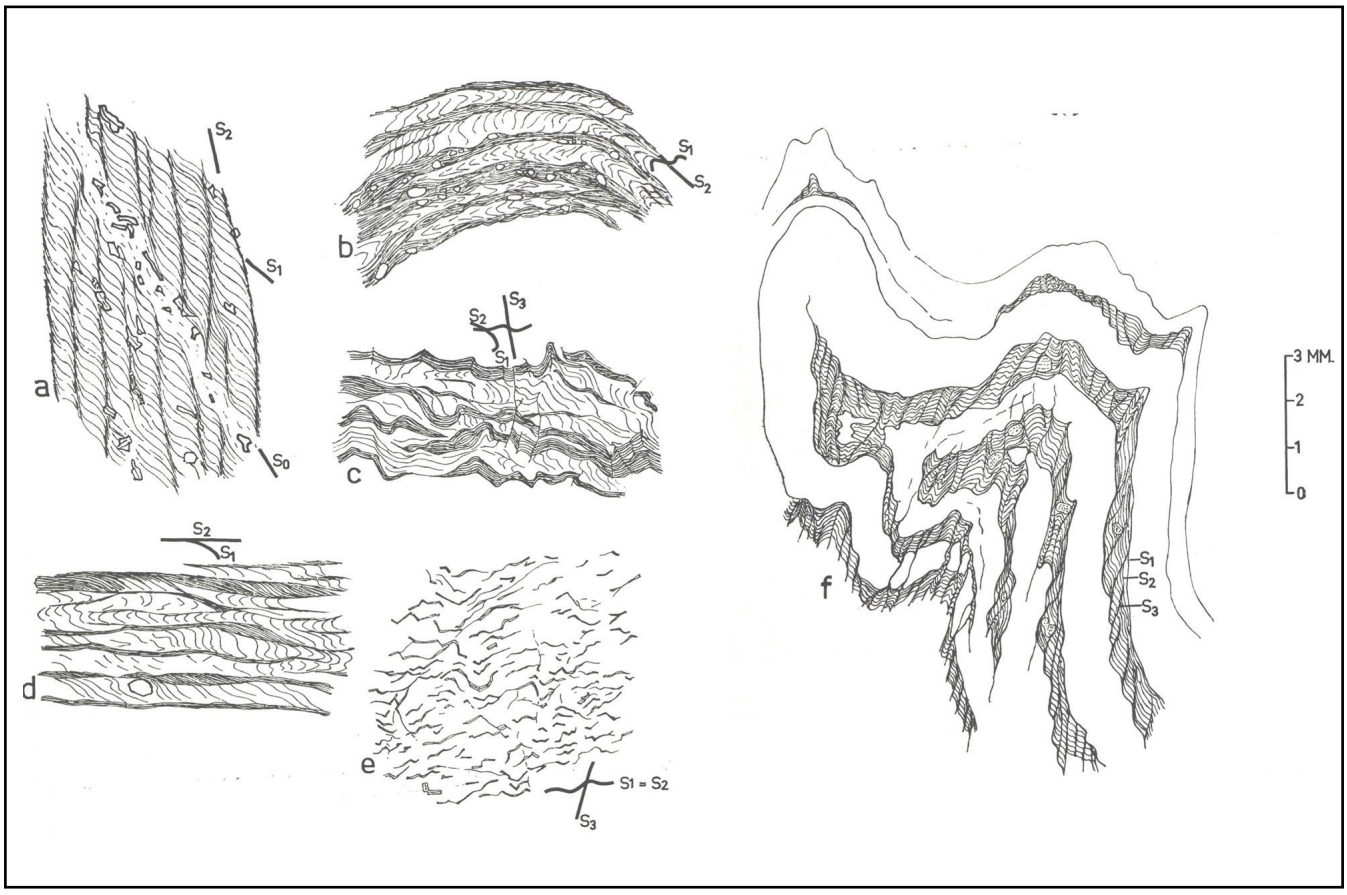

Figure 10. Fabric and microstructural relationships from the Cradle Mountain area (Figure 2, Gee et al., 1970).

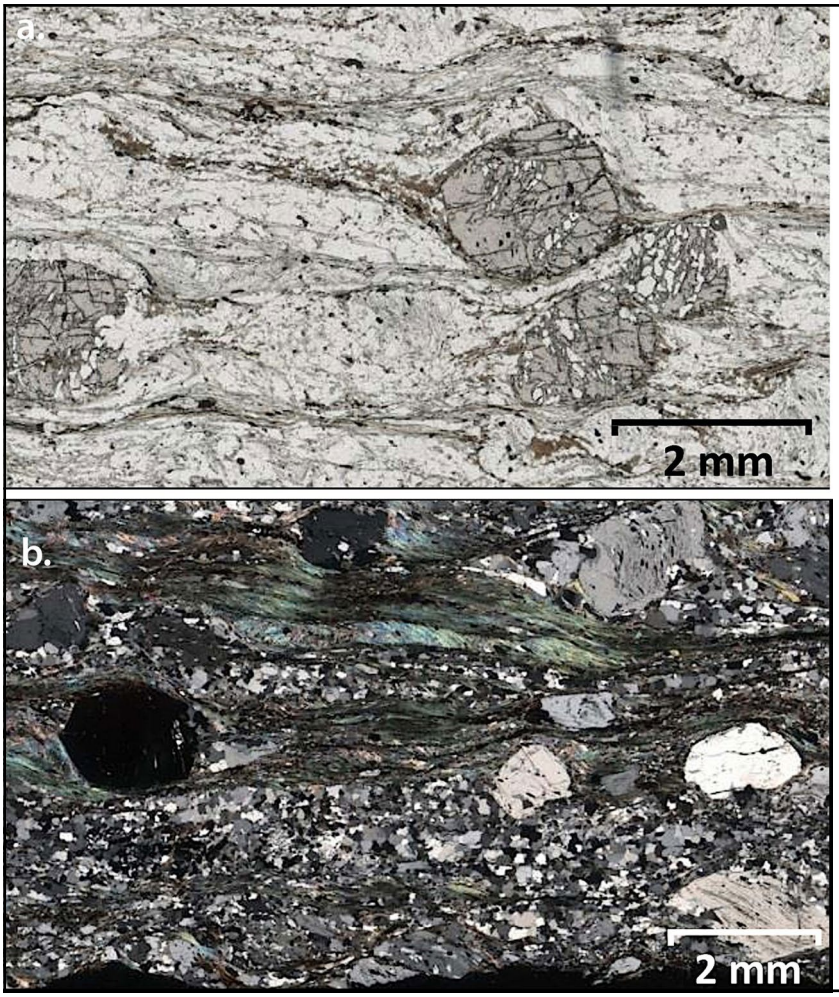

Figure 11. Photomicrographs of the dominant foliation Sm (Photo credits: Sally Mattner).

a) Quartz mica schist with mica rich foliation zones enclosing skeletal garnet and albite (light grey). The garnets are wrapped by fine grained biotite. PPL (fig. 22a, Mattner, 2015).

b) Spaced mica rich selvedges defining the dominant foliation Sm and enclosing inclusion-free garnet and albite porphryoblasts. Many of the albites (light grey) show sigmoidal inclusion trails Si. Crossed polars. (fig. 2.1d, Mattner, 2015).

2.6 Key Structural Relationships

Based on Gee et al. (1970) the following are key relationships for the Northern Tyennan subdomain:

- The S1 bedding foliation is found in both phyllite and schist and parallels a colour and compositional banding up to 10 mm in thickness in quartzite.
- The dominant foliation is an S2 crenulation cleavage/ schistosity (Figure 11). This is transitional into a transposition foliation typified by alternating quartz-micas and mica-rich layering (Figure 10 b, c and d).
- The S3 crenulation cleavage is localised within belts of mesoscopic refolding and transposition foliation development (Figure 10f).
- Fold axes are extremely variable within the axial surface foliation.

2.7 Structural and Metamorphic Petrology

Spry (1962), Gee et al. (1970) and more recently Mattner (2015) have described the structural petrology of the Northern Tyennan schists and quartzites. Fabric relationships (Figure 12) suggest the metamorphism is pre- to syn-D2 (Spry, 1962; Gee et al., 1970; Mattner, 2015).

In the Cradle Mountain area there is a zonal arrangement of metamorphic grade (Gee et al., 1970) including low-grade phyllite, quartz-mica schist up to almandine schist flanking the eastern margin of the Mt Kate macro-fold (Figure 6). Metamorphic discontinuities are associated with major high strain zones, where: 1) Garnet only occurs to the north of the Waldheim High Strain Zone, and 2) The folded belt between Lakes Dove and Rodway and the plateau north of Mt Inglis (Figure 6) has biotite-muscovite-chlorite schists in immediate juxtaposition to chlorite schists and low-grade meta-sedimentary rocks with no metamorphic recrystallisation (Gee et al., 1970)

2.8 Metamorphism and Geochronology

Metamorphism is to lower amphibolite facies (Berry and Bull, 2004; Mattner, 2015) but originally considered to be upper greenschist facies (Gee et al., 1970). Studies of the metamorphism have been undertaken by Gee et al. (1970), Chmielowski (2009), Mattner (2015) and Cumming et al. (in prep, 2025). Metamorphic facies varies from lower greenschist to lower amphibolite in the Liena-Borradaile F3 Chevron Fold Domain (Cumming et al., in prep, 2025).

2.8.1 Metamorphic P, T Determinations

Mattner (2015) established the metamorphic conditions for the Mersey River Metamorphic Complex (MRMC) using:

1. garnet-biotite geothermometry to establish a temperature estimate of 550 ±50 °C.
2. garnet-biotite-plagioclase-quartz (GBPQ) barometry and the GB temperature estimate to get a pressure estimate of 7.2 ± 1.6 kbars.
3. the Si-in-white mica barometer to obtain a peak pressure of 7.5-9 kbars.

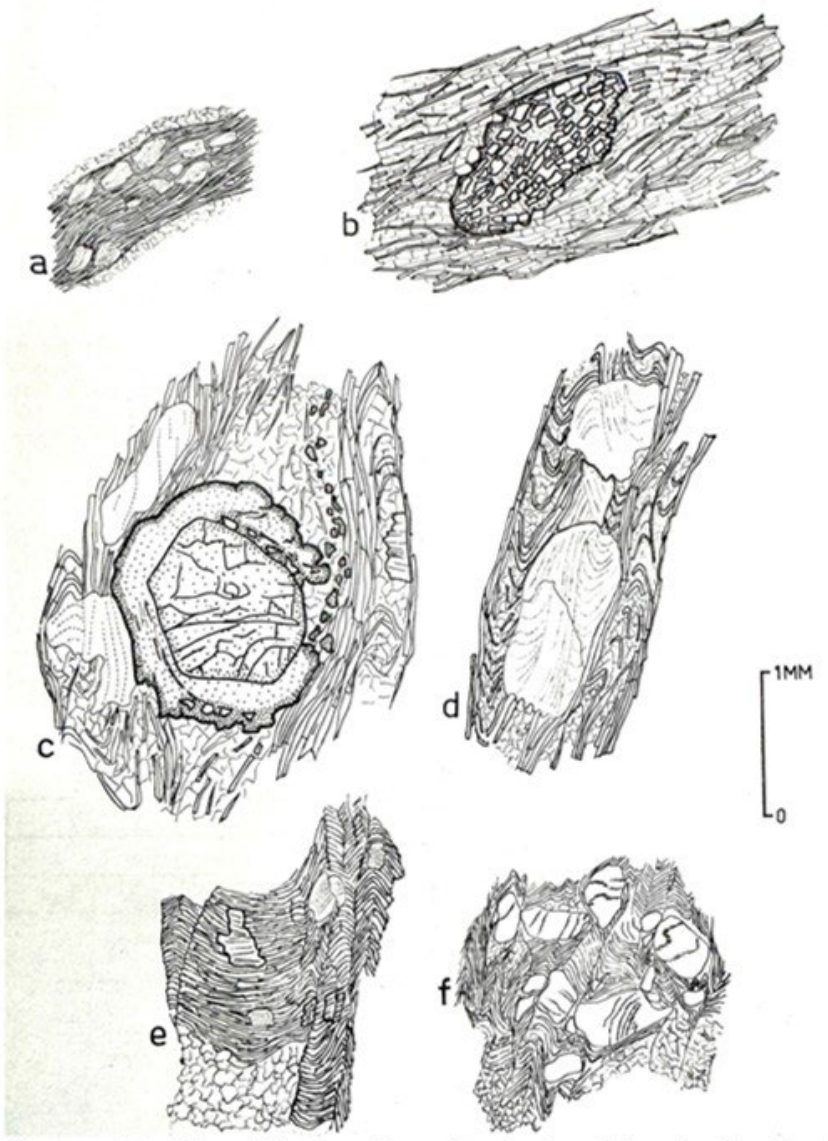

Figure 12. Microfabric mineral relationships in the Cradle Mountain region of the Northern Tyennan subdomain (fig. 3 from Gee et al., 1970).

a) Mica preferred orientation (S2) sub-parallel to compositional layering So/Sm with albite porphyroblasts showing sigmoidal Si (internal inclusion trail) continuous with S2.

b) Mica-quartzite S2 fabric with an idioblastic garnet porphyroblast showing sieve texture synkinematic with S2.

c) Idioblastic garnet showing a xenoblastic rim around an older fractured garnet core enveloped by a strong S2 mica foliation suggesting garnet growth pre- to early S2.

d) Albite porphyroblasts with helicitic inclusion trails reflecting overgrowth of an S2 crenulation fabric late to post-S2.

e) Post S2 chlorite and albite porphyroblasts across the S2 foliation re-crenulated by S3 discrete crenulation cleavages.

f) S3 crenulation cleavages and crenulations in albite-muscovite schist.

Mattner (2015) further argued that 1) an increase in Si and Fe/2+Mg in white micas indicated that MRMC rocks were exposed to increasing pressure conditions during growth of S2, 2) garnet compositionally shows an increase in Mg and a decrease in Mn from core to rim indicating that garnet grew during increasing temperature conditions and 3) the estimated P, T conditions of 550°C ± 50°C and 7.2 ± 1.5 kbars indicate that the high-grade rocks of the MRMC were subducted to depths of at least 20 km prior to exhumation.

2.8.2 Geochronology

The Mersey River Metamorphic Complex has monazite ages of 498±7 Ma (sample 7401) and 502±10 Ma (sample 154328) (Berry et al., 2007; Chmielowski, 2009, p.88). The sample locations are shown in Figure 13. Berry (pers. com., 2024) observed that the monazite in sample 7401 had been texturally altered with probable hydrothermal resetting by the thick overlying Jurassic dolerite sill.

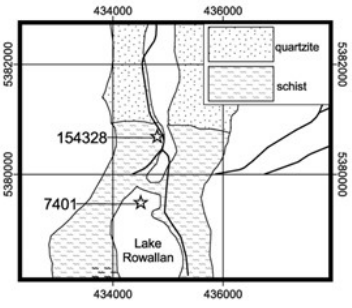

Figure 13. Map of the north end of Lake Rowallan showing the locations of the samples used in monazite dating (fig.5 from Chmielowski, 2009). Sample 7401 is a quartz-muscovite-albite-garnet schist used as a laboratory standard because of consistent monazite grain population. It gave a monazite age of 497±3 Ma and [498±4 Ma] (sample 74001) based on in-house standard and 171 analyses (Chmielowski, 2009, p.127). Sample 154328 is a pelitic schist consisting of fine grained quartz, lesser muscovite, rare biotite, some late stage chlorite and two populations of monazite (Chmielowski, 2009, p.127).

2.9 Current Work

Structural mapping was undertaken 1) in the Cradle Mountain area along the Dove Canyon track (July, 2017), the Lakes Lilla-Crater Lake area (July, 2017), the Hansons Peak - Twisted Lakes - Lake Hanson area (October, 2020), 2) along the Mersey Forest road between Lake Rowallan and Lake Parangana (May, 2017), 3) along the Overland Track (March, 2019) and 4) in the Arm River and Mersey River areas north of Lake Rowallan (January, 2022). This work was followed by revision of the Northern Tyennan structural map accompanied by construction of a major north-south structural profile through the subdomain and a revised regional structural interpretation.

The structural work has been accompanied by a revision of the Mackintosh sheet utilising Lidar, satellite imagery and a Company Exploration Report E.L.2/78 (Speijers, 1980), and new geological mapping of the Liena and Borradaile 1:25,000 map areas undertaken by Cumming, Everard and Jackman (2021-2024).

3.0 NORTHERN TYENNAN SUBDOMAIN GEOLOGY SUMMARY/OVERVIEW

3.1 Major Structural Elements

The Northern Tyennan subdomain consists of three main structural domains that incorporate the major structural elements (Figures 14 and 15). These include the:

1. Mt Kate recumbent macro-fold domain (red dashed envelope, Figure 14).
2. Granite Tor macro-fold interference domain (blue dashed envelope, Figure 14).
3. F3 chevron fold domain (green dashed envelope, Figure 14).

A summary or synopsis of each of these three domains and their internal divisions is given in Figure 15.

These interpretations of the different Northern Tyennan structural domains/elements are based on the following work (Figure 16):

Area 1a: Structural mapping by Gee et al. (1970) and structural mapping by DRG along the Dove Canyon track and boardwalk to Dove Lake (2017, 2020).

Area 1b: Structural mapping by GC, CJ and JLE for the completion of the 1:25,000 Liena and Borradaile sheets in the period 2021-2024.

Area 1c: Structural mapping by Gee et al. (1970).

Area 2: interpretation and Granite Tor map modification using the Alcoa Exploration Lease Report EL by MV.

Area 3a: Structural mapping by Gee et al. (1970) and structural mapping by DRG.

Area 3b: Structural mapping by GC, CJ and JLE for the completion of the 1:25,000 Liena and Borradaile sheets in the period 2021-2024.

Area 3c: Structural mapping by Mattner (2015), DRG (2017) and GC (2022-2024) .

Area 4: Structural traverse along the Overland Track by DRG (2019).

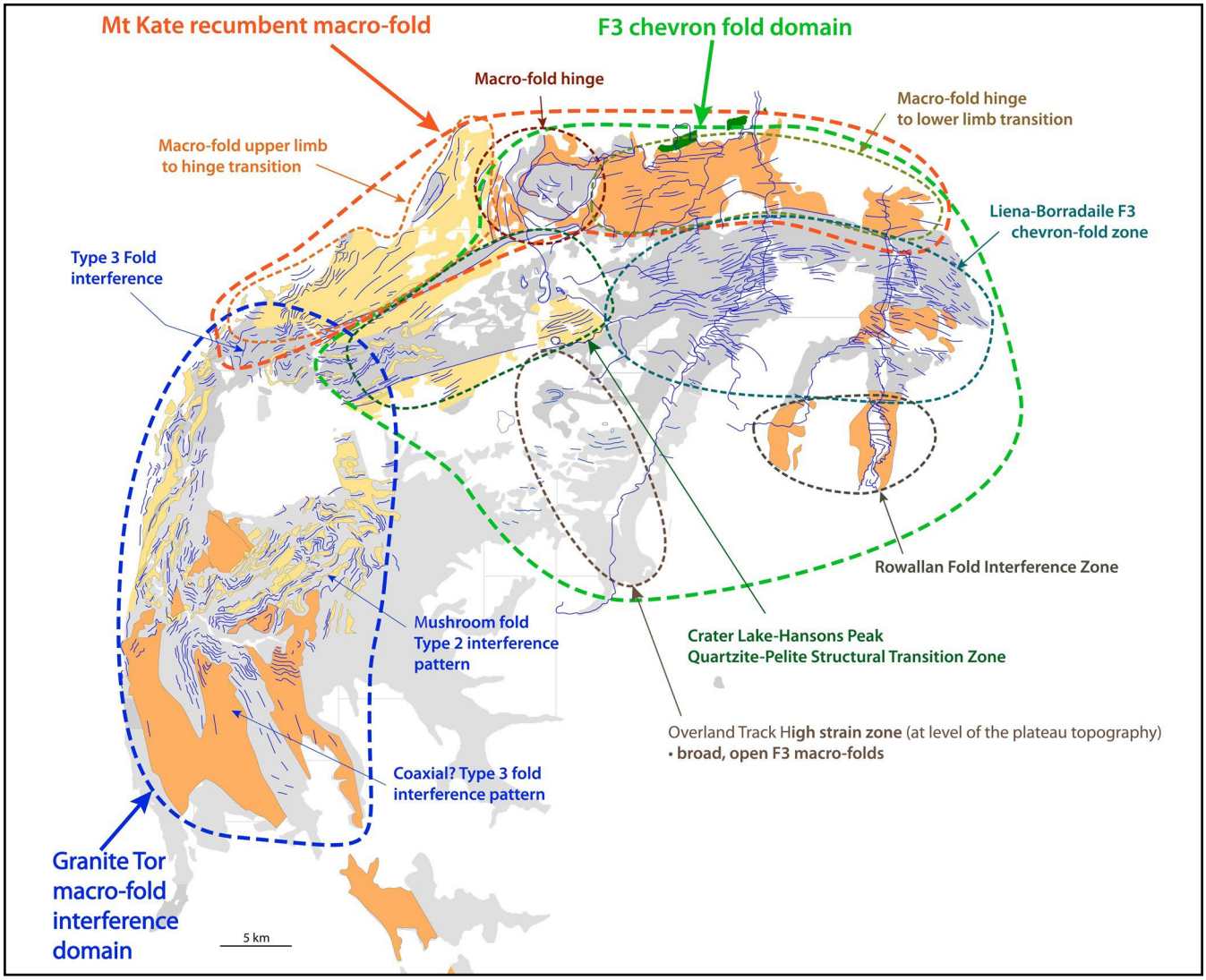

Figure 14. Northern Tyennan subdomain structural domain map. The region consists of three distinct structural domains including the Mt Kate recumbent macro-fold domain, the Granite Tor macro-fold interference domain and the F3 Chevron Fold domain. The lithologic base map is modified from the Mineral Resources Tasmania 1:250,000 and 1:25,000 digital atlas.

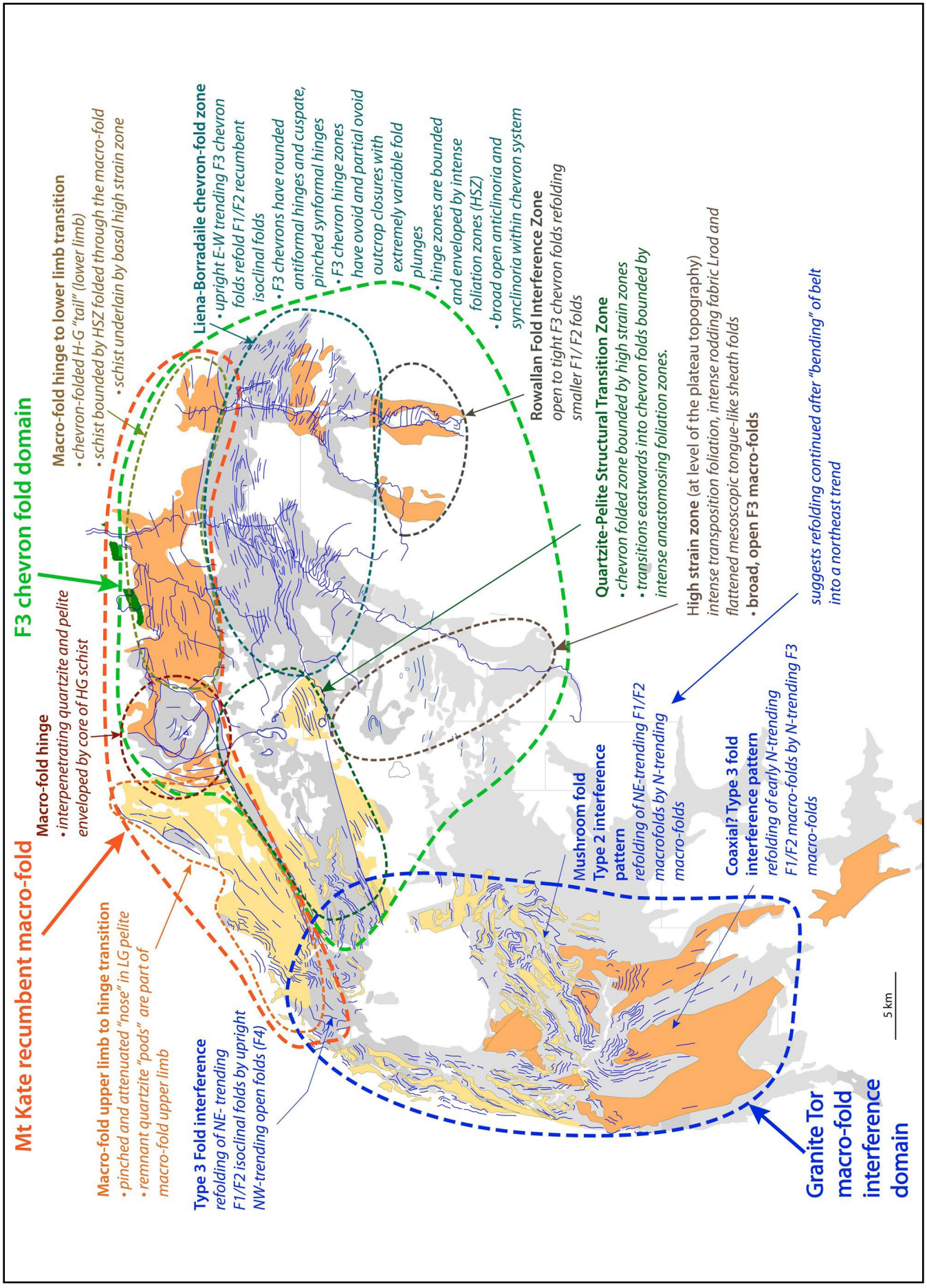

Figure 15. Detailed summary and structural element map of the Northern Tyennan subdomain. Summary descriptions of the components that make up each domain are given. The lithologic base map is modified from the Mineral Resources Tasmania 1:250,000 and 1:25,000 digital atlas.

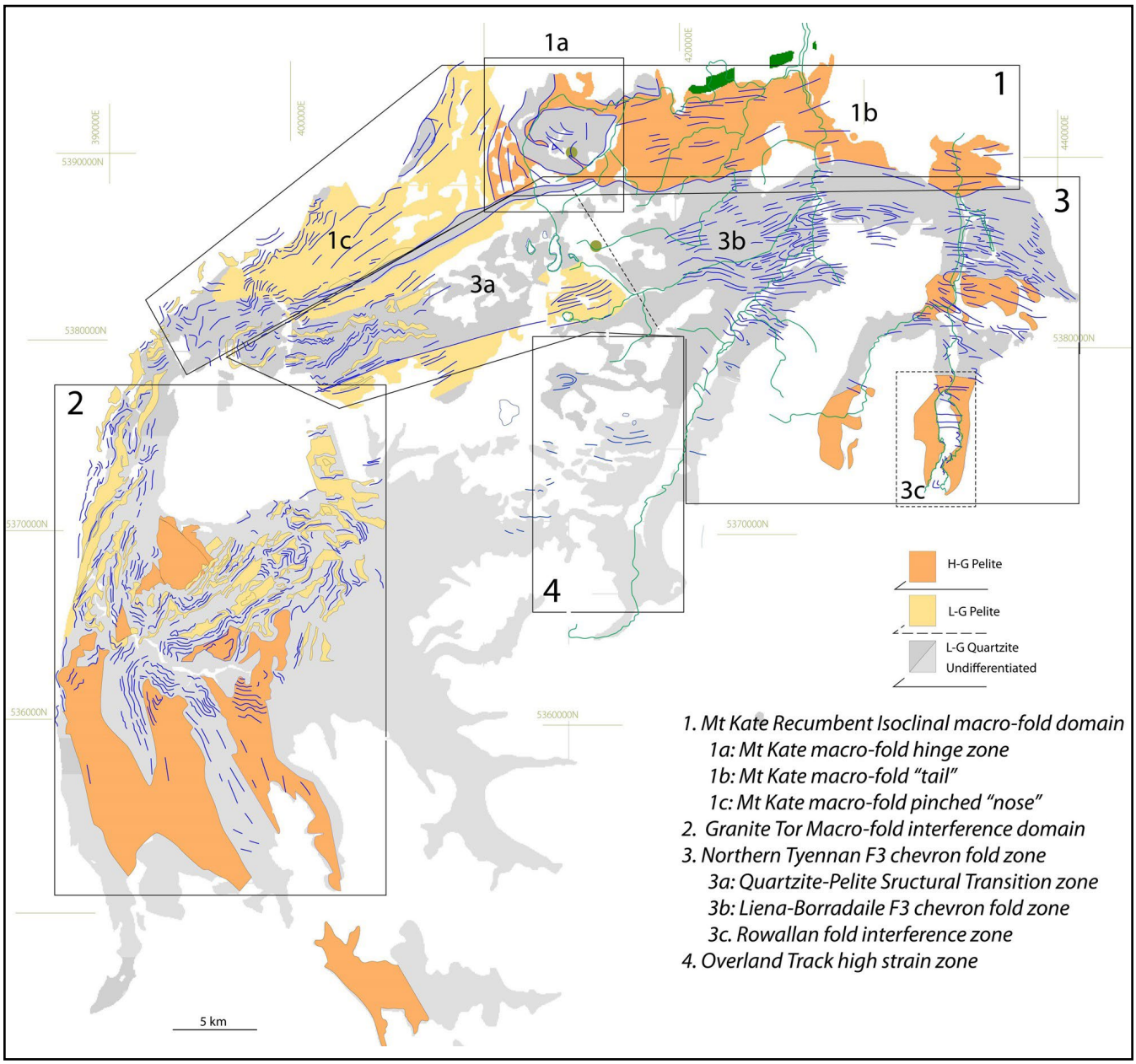

Figure 16. The Northern Tyennan subdomain litho-tectonic map showing polygons of outlined areas that are treated separately in the text. Form lines in So/Sm and Sm are shown by the blue line traces. Map base is from the Mineral Resources Tasmania 1:250,00 digital atlas.

The structures and the structural relationships within the Northern Tyennan subdomain are shown in a schematic 3D geometric model (Figure 17). The sketch summary 3D model is based on the analysis and synthesis of all the structural data and observations presented in Sections 3.0, 4.0 and 5.0 of this publication. The outermost element includes the Mt Kate macro-fold with the southern continuation into a refolded macro-fold system (Figures 17 and 18). South of Granite Tor the macro-fold system is continuous with the Franklin macro-fold (west-closing, synformal F2 hinge, Figure 18) refolded by the Redan Hill (antiformal F3 hinge 2, Figure 18) and Collingwood Plain (synformal F3 hinge 3, Figure 18) of the Central Tyennan subdomain (Gray and Vicary, 2021).

The inner part of the Northern Tyennan subdomain incorporates the Liena-Borradaile F3 chevron fold system that refolds the lower limb of the macro-fold (Figure 17). The chevron folds loose amplitude or die out to the west. The central part has two distinct high strain zones, the Waldheim High Strain Zone (WHSZ) and the Lake Rodway High Strain Zone (LRHSZ). These merge with an anastomosing network of high strain zones through the tight to almost isoclinal chevron folds of the eastern part of the Liena-Borradaile F3 chevron fold zone (Figure 14).

3.2 Map Pattern and Regional Relationships

The northern and western boundary of the Tyennan allochthon shows a marked curvature with a swing from north-trending to north-northeast trending (Cradle Mountain area) to east-trending (Mersey River area) (Figures 14 and 19). It consists of sub-parallel belts of structurally intercalated pelite and quartzite flanked to the north and west by onlapping to faulted Cambrian-Devonian volcanic-sedimentary successions of the Dundas-Fossey Mountain graben system ("troughs") and to the east by the flat-lying Permian succession (Figure 3).

Figure 17. Schematic 3D geometric model of the structures within the Northern Tyennan subdomain. The outermost element includes the Mt Kate macro-fold (red dot-dashed F2 axial surface trace) with the southern continuation into a refolded macro-fold system south of Granite Tor (see Figure 18).

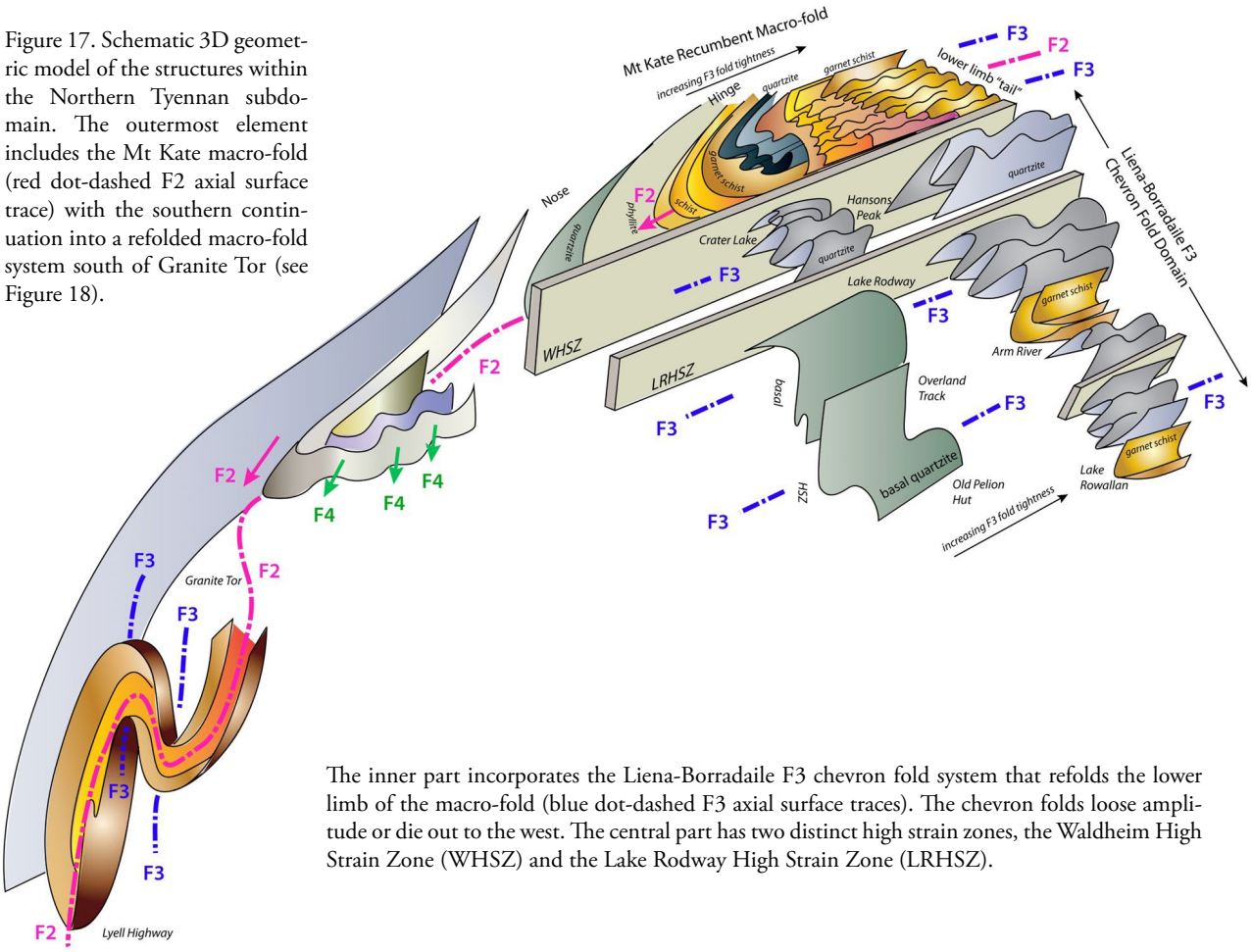

The inner part incorporates the Liena-Borradaile F3 chevron fold system that refolds the lower limb of the macro-fold (blue dot-dashed F3 axial surface traces). The chevron folds loose amplitude or die out to the west. The central part has two distinct high strain zones, the Waldheim High Strain Zone (WHSZ) and the Lake Rodway High Strain Zone (LRHSZ).

Figure 18. The variation and style changes of the outer recumbent macro-fold system that extends from Cradle Mountain as the Mt Kate macro-fold southwards into a coaxially refolded series of macro-folds that include the Franklin macro-fold, the Redan Hill macro-fold and the Collingwood Plain macro-fold to the south in the Central Tyennan subdomain. These are all part of the leading edge macro-fold system (Gray et al., 2024).

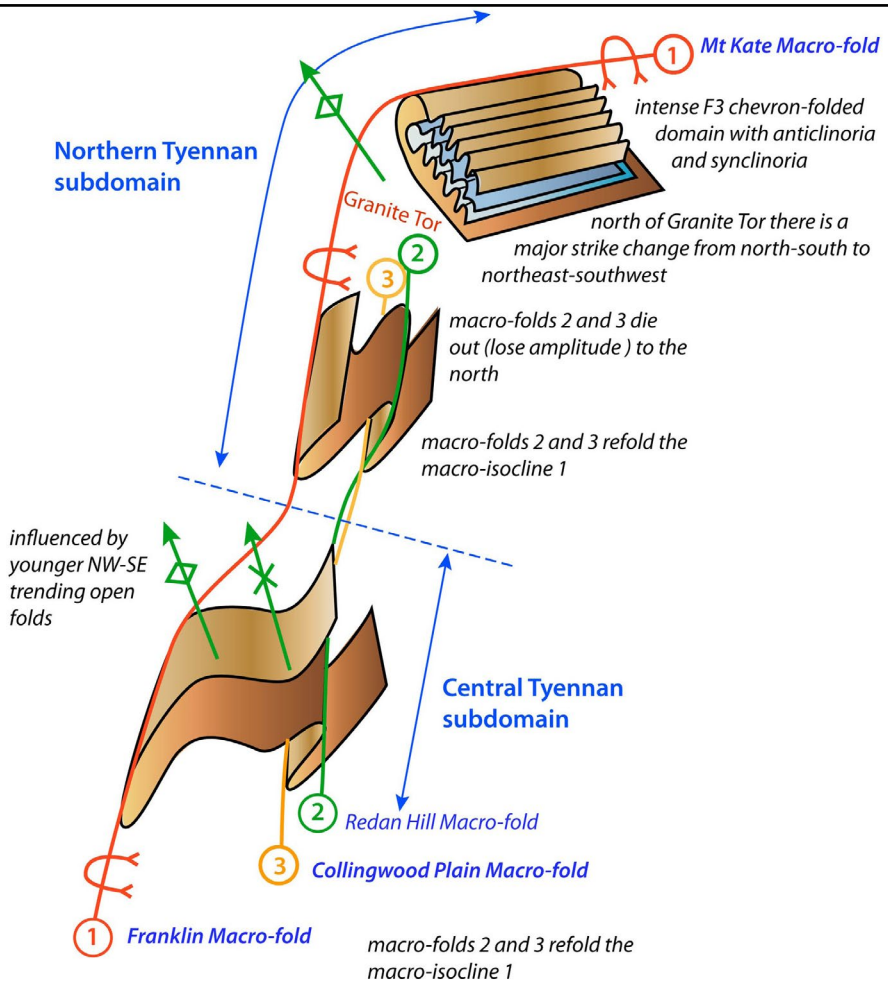

The strike belts of intercalated quartzite and pelite and the high-grade schist follow the exposed margin of the Northern Tyennan subdomain. Other noticeable features (Figure 19) include 1) truncation of the hinge of the Mt Kate recumbent, isoclinal macro-fold by a sub-vertical band of intense transposition layering incorporating pods of quartzite and pelite (dashed red circle 1, Figure 19), 2) a repetition of the high grade schists along the Mersey River valley in eastern part of the subdomain (dashed red circle 2, Figure 19), and 3) a complex fold interference pattern involving intercalated quartzite, low grade pelite and high grade schist south of Granite Tor along the southwest part of the subdomain(dashed red circle 3, Figure 19).

3.3 Major Fold Axial Surface Trace Pattern

The major fold axial surface traces have curved form matching the bend in the Northern Tyennan subdomain (Figure 20). In the northern part the major Mt Kate macro-fold axial surface (red line trace, Figure 20) represents the continuation of the Franklin macro-fold (Figures 18 and 20). This is sub-parallel with the dominant F3 east-west trending axial surface traces (blue line traces, Figure 20) that define the Liena-Borradaile F3 chevron fold domain (see Section 5.3.2).

South of Granite Tor the overall pattern of F1/F2 axial surface traces remains sub-parallel with and refolded by F3 folds but now with an approximate north-south trend. Some second and/or third order F1/F2 folds appear to have axial surface traces in an east-west orientation and are refolded by the north-trending F3 folds to give mushroom-shaped fold interference patterns (Figure 20).

F4 folds (green line traces, Figure 20) are localised within the "bend" just north of Granite Tor.

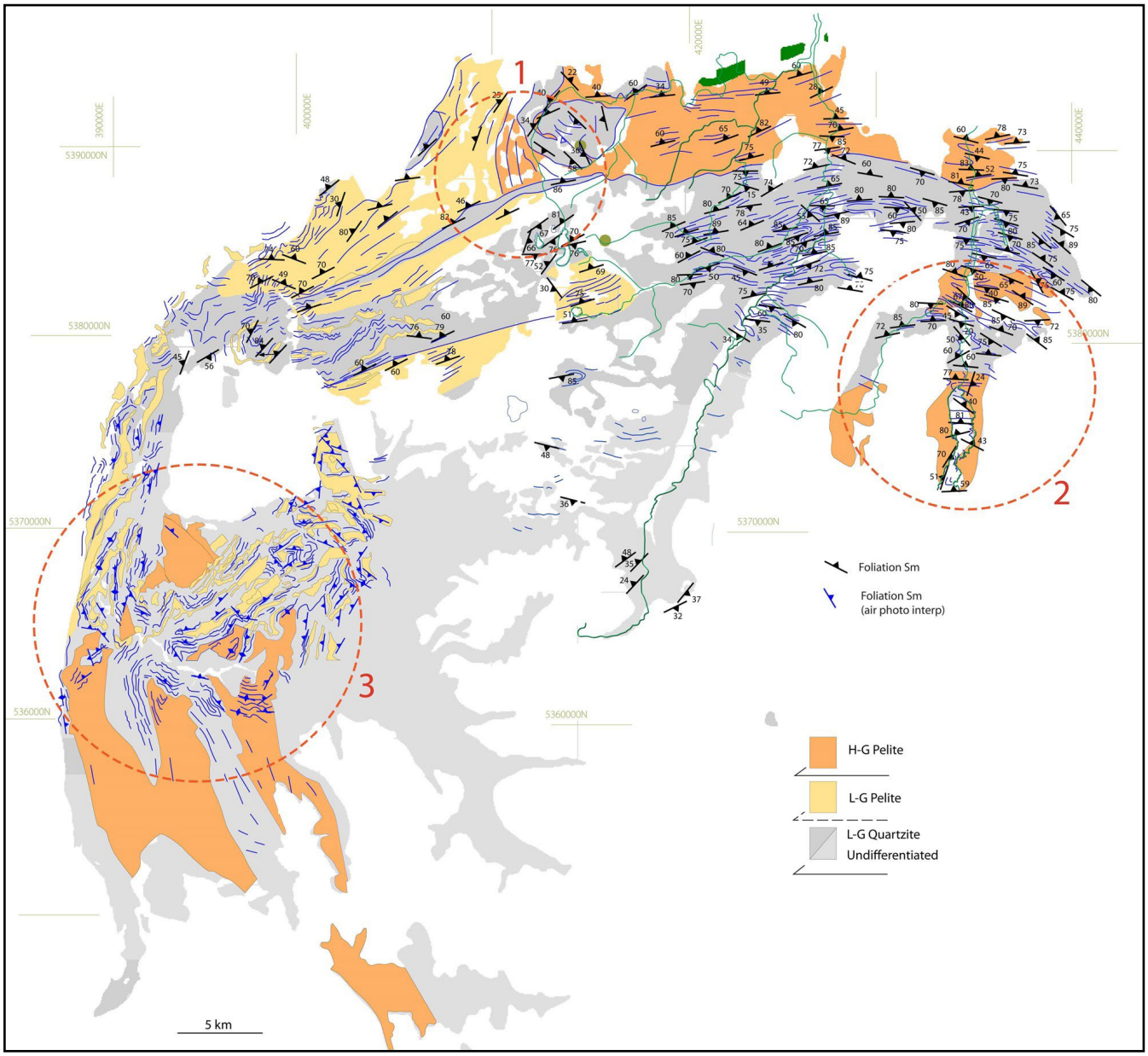

Figure 19. Northern Tyennan Subdomain structural summary map showing foliation Sm attitudes. Black strike/dip symbols are measured foliation attitudes, whereas the blue strike/dip symbols are based on aerial photograph interpretation. Map Base is from the Mineral Resources Tasmania 1:250,00 digital atlas. The dashed red circles labeled 1, 2 and 3 are features referred to in the text.

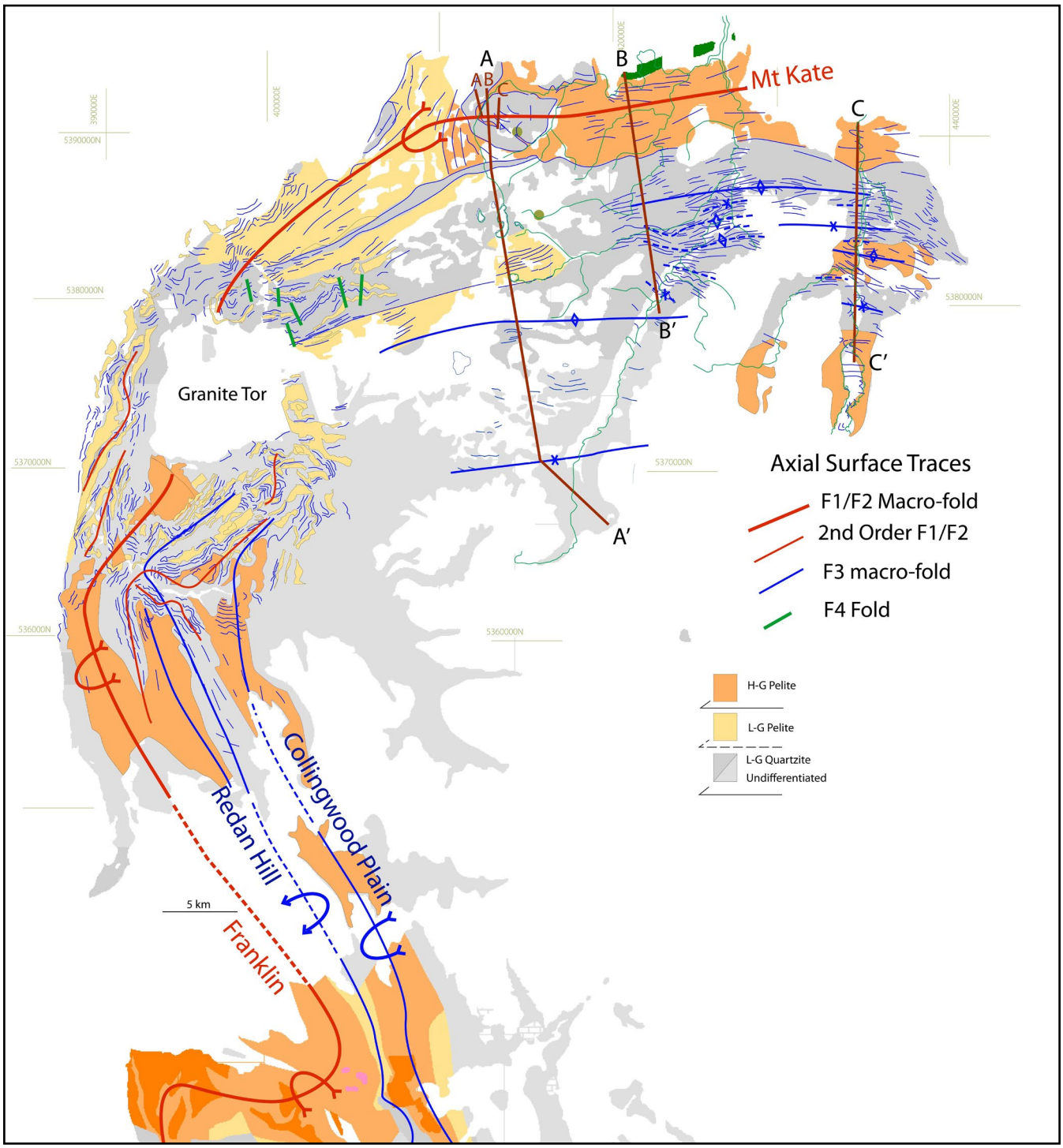

Figure 20. Northern Tyennan subdomain axial surface trace map for F1/F2 macro-folds (heavy red line traces), second order F1/F2 macro-folds (thin red line traces), F3 macro-folds (blue line traces) and F4 folds (green line traces). Positions of regional structural profiles are shown by the dark red lines labeled A-A', B-B' and C-C'. The line segments A, B and C about the north end of A-A' are the profiles across the Mt Kate macro-fold nose (see Figures 37 and 38).

3.4 Early Isoclinal Fold Pattern

The early isocline fold axes are generally east- or west-plunging, but also show northwest and rare southeast plunges as well as northeast and southwest plunges (Figure 21). This fold axis variability reflects refolding by the upright east-west trending chevron fold system (designated F3) as well as by the marked curved hinge lines of the F1/F2 recumbent folds and the chevron folds.

3.5 Lineation Lm Pattern

The mineral/stretching lineation Lm is overall west- plunging (Figure 22). In places though Lm has northwest and rare southeast plunges, as well as northeast and southwest plunges (Figure 22). This lineation plunge/plunge direction variability reflects 1) folding of Lm about small and intermediate-scale F1/F2 isoclines, 2) refolding by the upright east-west trending F3 chevron fold system, and 3) the marked curved nature of both the first and second order F1/F2 folds as well as the F3 chevron fold hinge lines.

A mesoscopic-scale example on the Overland Track at Old Pelion Hut shows the lineation Lm on the upper limb of an isocline in quartzite is at right angles to Lm on the isocline lower isocline limb (see Figure 23).

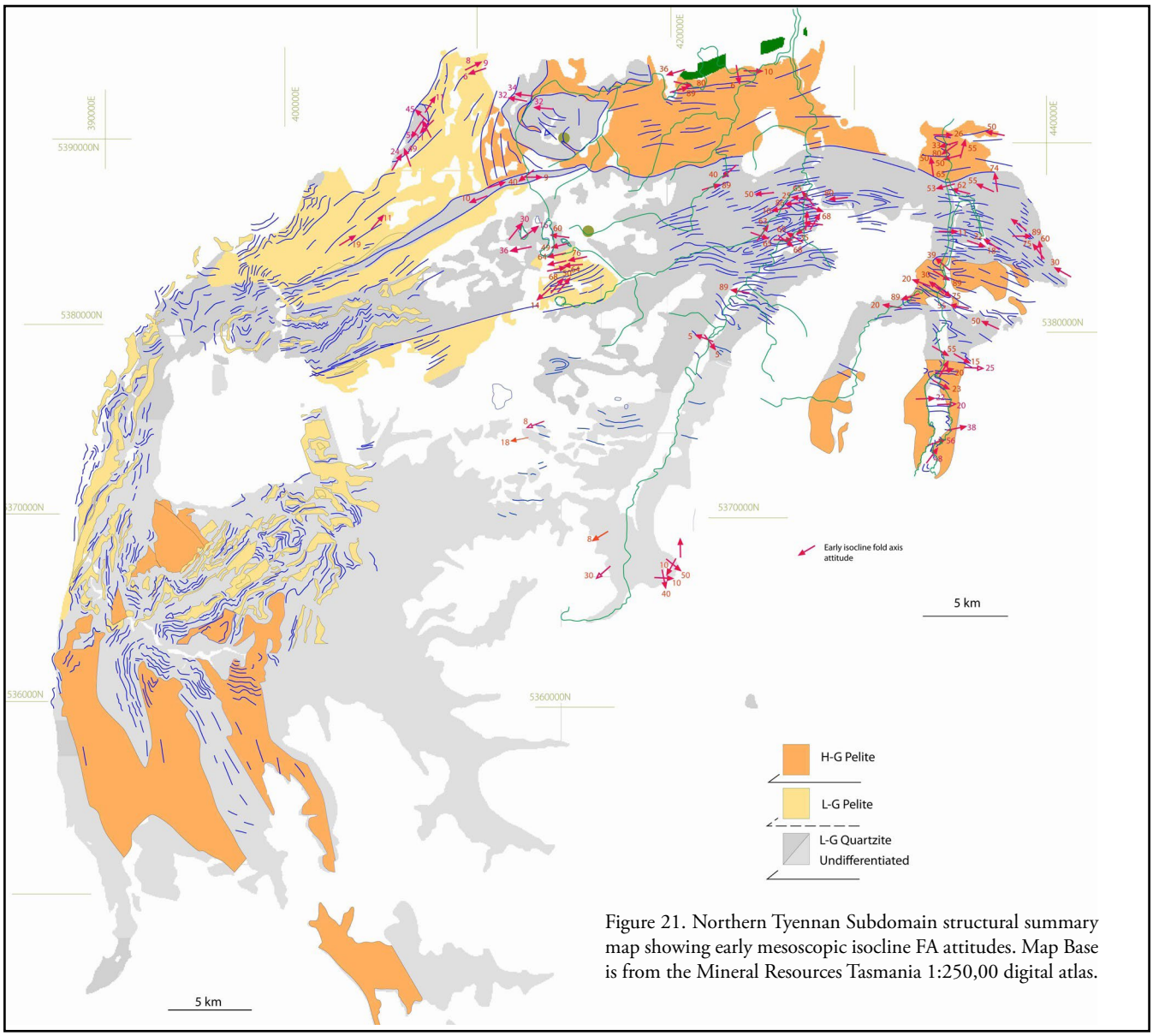

Figure 21. Northern Tyennan Subdomain structural summary map showing early mesoscopic isocline FA attitudes. Map Base is from the Mineral Resources Tasmania 1:250,00 digital atlas.

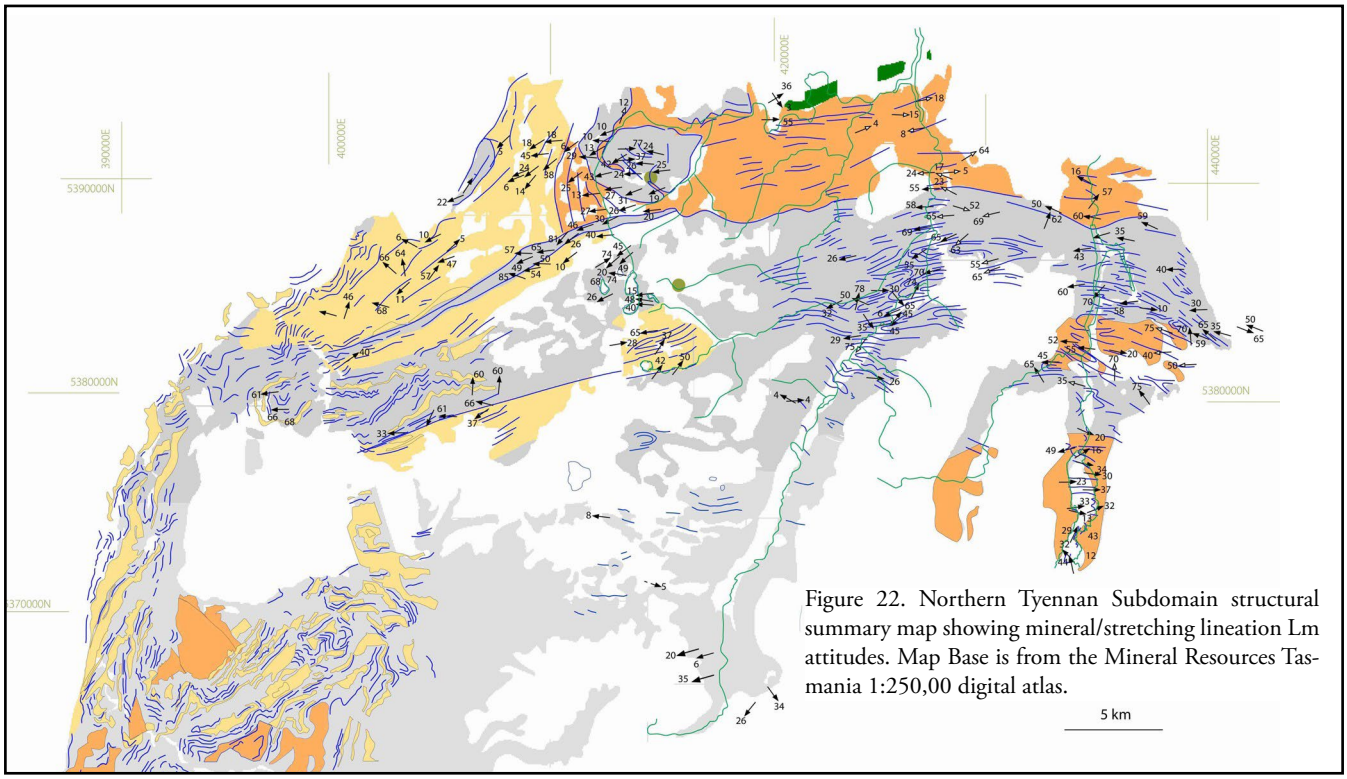

Figure 22. Northern Tyennan Subdomain structural summary map showing mineral/stretching lineation Lm attitudes. Map Base is from the Mineral Resources Tasmania 1:250,00 digital atlas.

3.6 Early Fold Axis (FA) and Lineation (Lm) Relationships

Despite the refolding by the younger upright chevron folds there are two rotation domains of early fold axis (FA) towards the mineral lineation Lm. (Figure 23a). The pattern potentially reflects different limbs of the early Mt Kate recumbent macro-fold. The interpretation requires a marked hinge line curvature of the Mt Kate macro-fold typical of a sheath-like geometry (Figure 23b). The northwest map part shows a clockwise rotation, reflecting the northern limb of a west-closing recumbent fold (Figure 23b). The northeast map part shows counter-clockwise rotation suggestive of the southern hinge-limb of a west-closing macro-fold (Figure 23b).

The geometry of the Mt Kate fold is west-closing (i.e. sheath nose 1, Figure 24) with a curved hinge line and refolded by the F3 chevron folds to give a mushroom fold interference pattern. The rotation domains however, do not match the hinge line position and the perceived medial line orientation. The other issue is that the northern part of the fold is covered by overlap sequences so that the actual geometry may be different to the apparent map geometry.

The interface between the domains may be at a low angle to the present erosion surface, such that it is west dipping and below the erosion surface approximately west of Hansons Creek and above the erosion surface east of Hansons Creek (see coincidence of domain boundary dashed lines, Figure 23a).

The map pattern of the FA^Lm rotation directions requires that the opposing limbs of the upper and lower sheath folds are superimposed in map view (Figure 24). The geometric arrangement requires 1) removal of part of the upper fold limb by erosion (see topographic erosional interface and dashed part of upper limb missing), 2) superposition of the remaining part of the upper fold limb with the underlying right side limb.

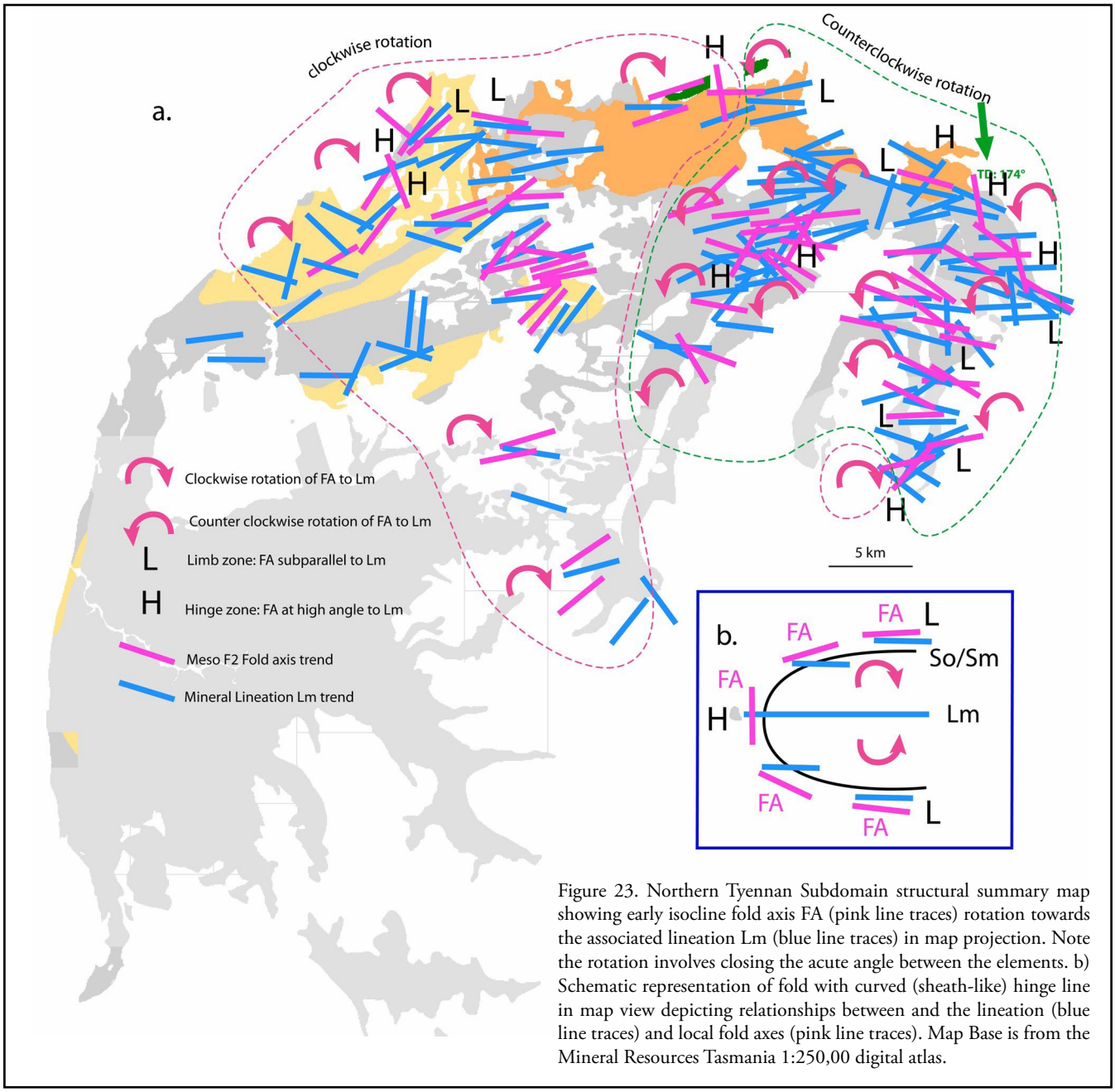

Figure 23. Northern Tyennan Subdomain structural summary map showing early isocline fold axis FA (pink line traces) rotation towards the associated lineation Lm (blue line traces) in map projection. Note the rotation involves closing the acute angle between the elements. b) Schematic representation of fold with curved (sheath-like) hinge line in map view depicting relationships between and the lineation (blue line traces) and local fold axes (pink line traces). Map Base is from the Mineral Resources Tasmania 1:250,00 digital atlas.

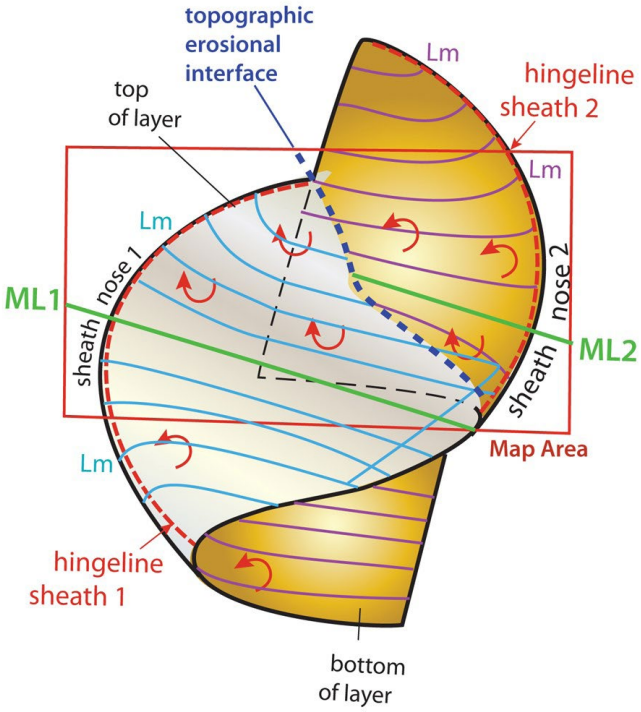

Figure 24. 3D schematic model of the FA^Lm rotation directions through an offset, en echelon asymmetric sheath fold pair. The red rectangle represents the Northern Tyennan subdomain map area. The rectangle captures the FA^Lm rotation directions shown in Figure 23 above. The geometric arrangement requires 1) removal of part of the upper fold limb by erosion (see topographic erosional interface and dashed part of upper limb missing), 2) superposition of the remaining part of the upper fold limb with the underlying right side limb.

This means that the opposing limbs of the upper and lower sheath folds are superimposed in map view.

3.7 Transport Direction (TD) Pattern

The transport direction (Figure 25) can be determined using movement planes derived either from 1) the lineation Lm and the dominant foliation plane Sm (designated MP1), and 2) the shear band intersection with the foliation Sm (designated MP2). For the lineation case (MP1) the shear sense must be derived from other markers such as fabric asymmetry and if this is not available then the approach only provides the orientation of the movement plane and not the sense.

The Lm movement planes (MP1) are considered to represent the shear direction in the "early" stage of the deformation sequence, whereas the shear band movement planes (MP2) most likely indicate the shear direction in the "later" stages of the sequence during strain hardening of the foliation Sm (see Figure 25).

Visually the MP1 movement plane pattern is dominantly west-northwest trending (Figures 26 and 27) but there is a herringbone pattern of interfering east-west, northwest-southeast and north-south trends (Figure 26). As Lm is considered to develop pre- the early F1/F2 macro-folds the MP1 orientation has to be affected by both F2 and F3 folding (see Figure 20), with trend changes across the larger scale macro-fold hinges and limbs, particularly in the core of the Liena-Borradaile zone (Figure 26).

Restored MP2 (shear band derived) movement planes are also west-northwest trending and show east-over-west shear sense (Figure 28). These are interpreted to reflect the strain hardening stage, late within Sm/Lm development, or are part of the subsequent emplacement of the Tyennan sheet. Late stage shear bands and brittle faults in the eastern part of the subdomain have north-south trends with north-over-south shear sense (red arrows, Figure 26).

These support the north-over-south shear sense of Berry and Bull (2004), determined from asymmetric quartz fabrics in a thin quartzite mylonite zone at Rowallan Dam and a consistent southward vergence of F2 folds. There are however, complexities in the shear sense markers at Lake Rowallan (see Section 5.3.3).

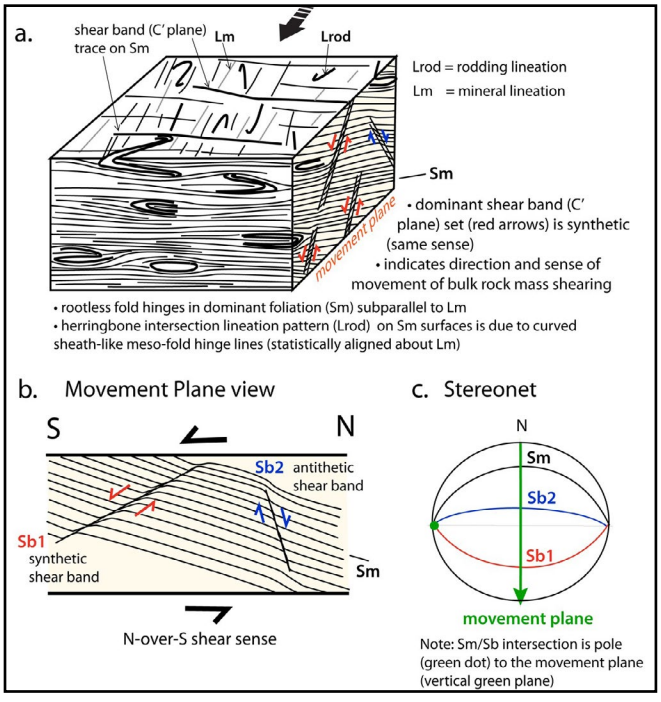

Figure 25. Categorisation of the movement plane in general shear-related deformation. a) Block diagram showing fabric elements formed in a simple shear related deformation with the movement plane as the plane containing the pole to the foliation and the lineation Lm in the foliation (side of the block showing shear bands). b) View of the Movement plane (side of the block) showing shear bands with synthetic (same sense: red arrows) and antithetic (opposite sense: blue arrows). The overall sense of shear is shown by the heavy black arrows. c) Stereonet showing the great circle traces of the synthetic shear band (Sb1: red trace, the antithetic shear band (Sb2: blue trace), the foliation Sm (black trace) and the movement plane (green trace).

Figure 26: Northern Tyennan Subdomain structural summary map showing transport directions based on movement plane determinations from foliation Sm and lineation Lm measurements (MP1 green data) and shear band data with Sm restored to the horizontal (MP2 blue arrows). Pink arrows are fault and shear band data considered post the development of MP2 movement planes. Map Base is from the Mineral Resources Tasmania 1:250,00 digital atlas.

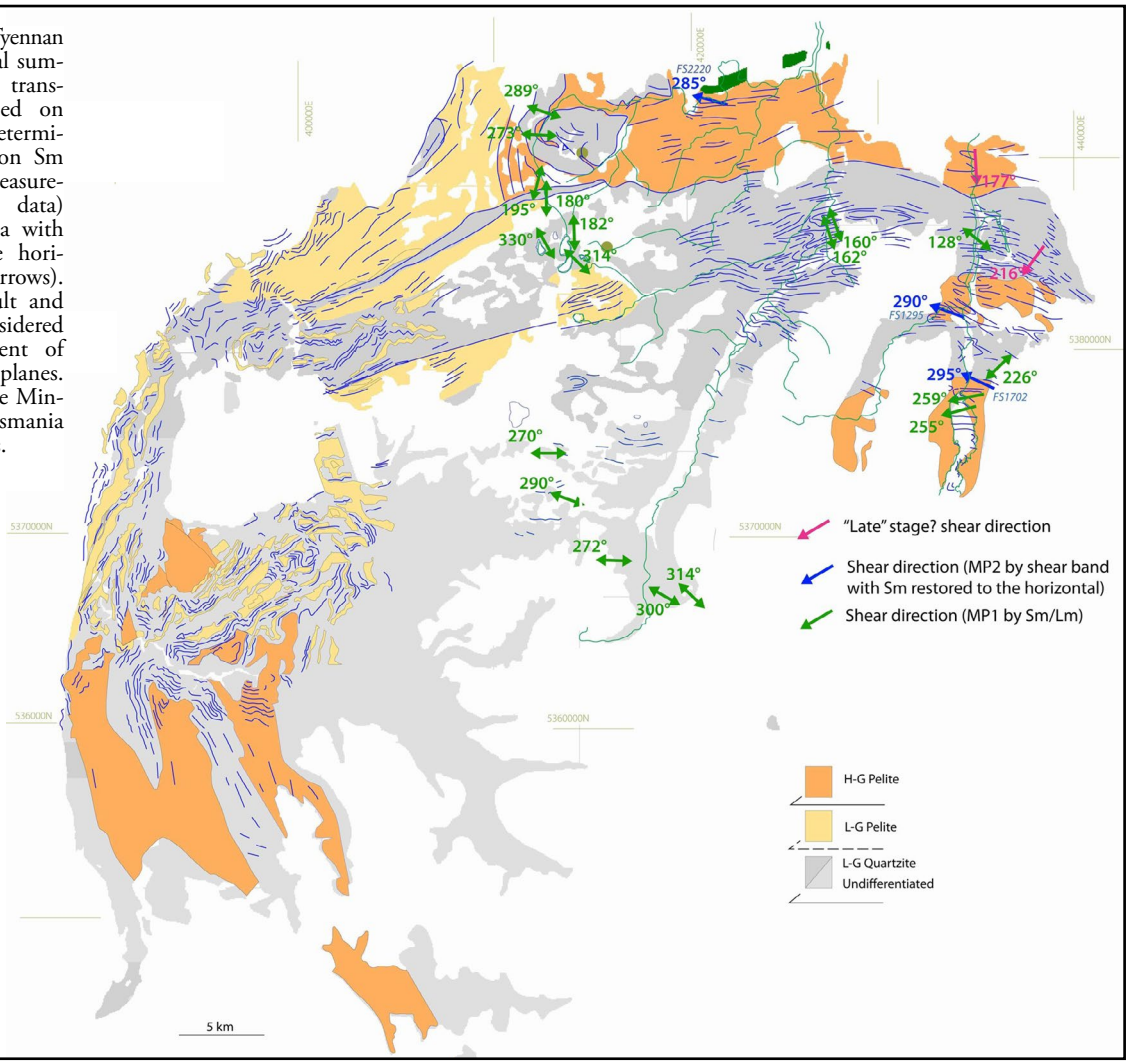

Figure 27. Northern Tyennan Subdomain transport direction summary map with directions from Movement Planes MP1 and MP2 highlighted by the green and blue lines respectively. Heavy lines represent the "generalised" shear direction trends allowing for reorientation of trends through a central folded belt through Dove Lake-Lake Parangana. The generalised MP1 trend is ~280°. The generalised MP2 trend is ~295°. Map Base is from the Mineral Resources Tasmania 1:250,00 digital atlas.

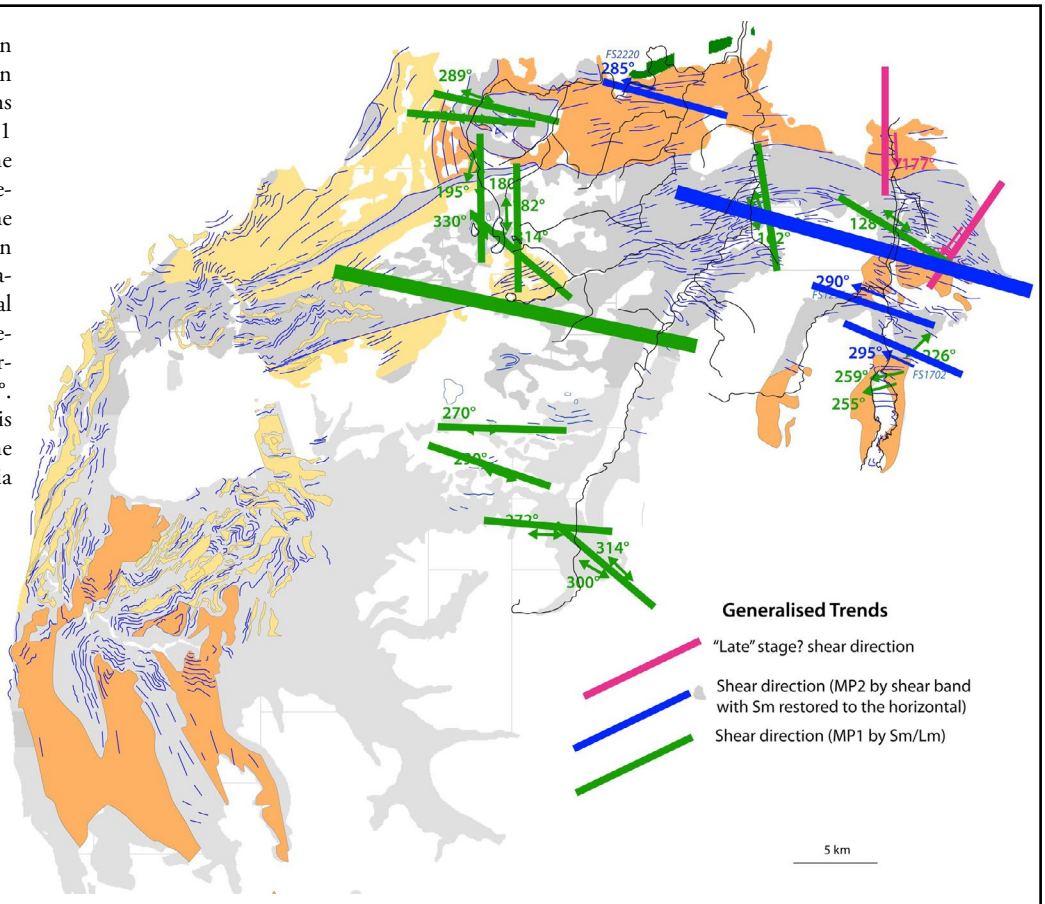

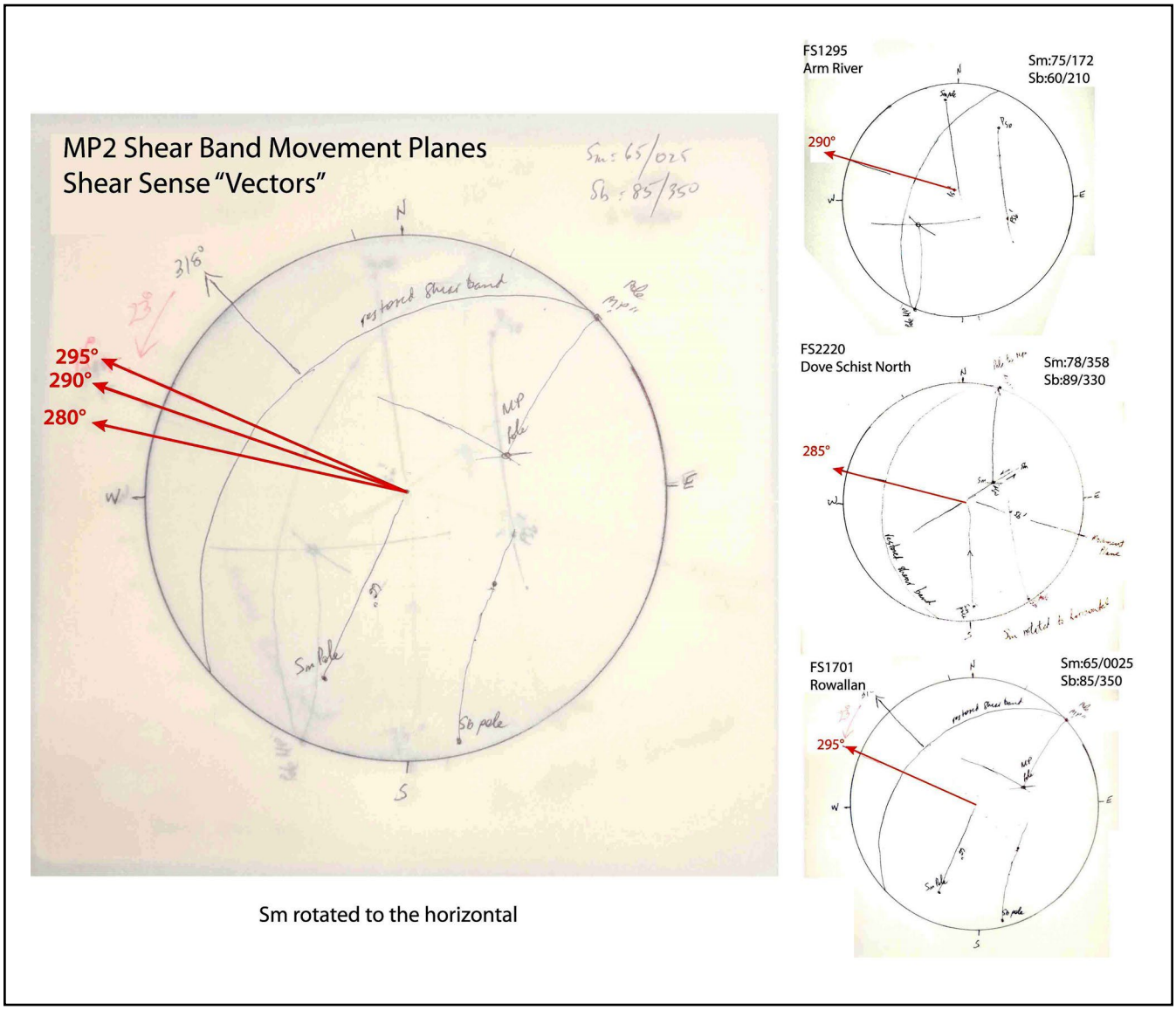

Figure 28. Restored MP2 Shear Band Data for three locations in the Northern Tyennan subdomain. All the shear bands equate to Sb1 in Figure 25 (i.e. synthetic sense shear bands). Each shear band pole and Sm-Sb intersection have been rotated together with the Sm pole to restore Sm to a horizontal attitude. This gives the resultant shear direction within a horizontal plane. a) Total data stereonet plot showing the grouping of the trends with a generalised ~290° shear direction from the stereonets in (b). b) Individual stereonet restorations for FS1295 (Arm River), FS2220 (Dove Schist north) and FS1701 (Rowallan) combined to give the stereonet in (a).

3.8 Younger Overprinting Cleavages and Folds

Two sets of later folds and their associated axial surface crenulation cleavages have been designated as F3 (Scc3) and F4 (Scc4) (Figure 29). The F3 folds are the dominant, east-west trending, upright chevron folds in the Liena-Borradaile domain (Map area 3b, Figure 16). They refold the lower limb of the Mt Kate recumbent macro-fold and the contained early F1/F2 isoclines. They have tight to close geometry but in the Overland Track map area (Map area 4, Figure 16) have open form.

The F4 folds and the axial surface crenulation cleavage are northwest-southeast trending and have open form (Figures 17, 20 and 29). They are linked to the apparent bend of this part of the Northern Tyennan subdomain from the north-south trend to the east-west trend.

3.9 Fault Pattern

Brittle faulting within the Northern Tyennan subdomain is dominated by a series of north-northwest trending, sub-vertical dextral-sense faults (Figure 30). There is also a subsidiary set of E-W trending faults. The data presented is limited to the western part with a fault update being prepared for the eastern part as part of the Liena-Borradaile mapping (Cumming et al., in prep, 2025).

These faults have facilitated the clockwise rotation of the Northern Tyennan subdomain (Gray and Vicary, in prep, 2025). The set of east-west sub-vertical faults are linked to opening of the Dundas-Fossey graben system (Gray and Vicary, in prep, 2025).

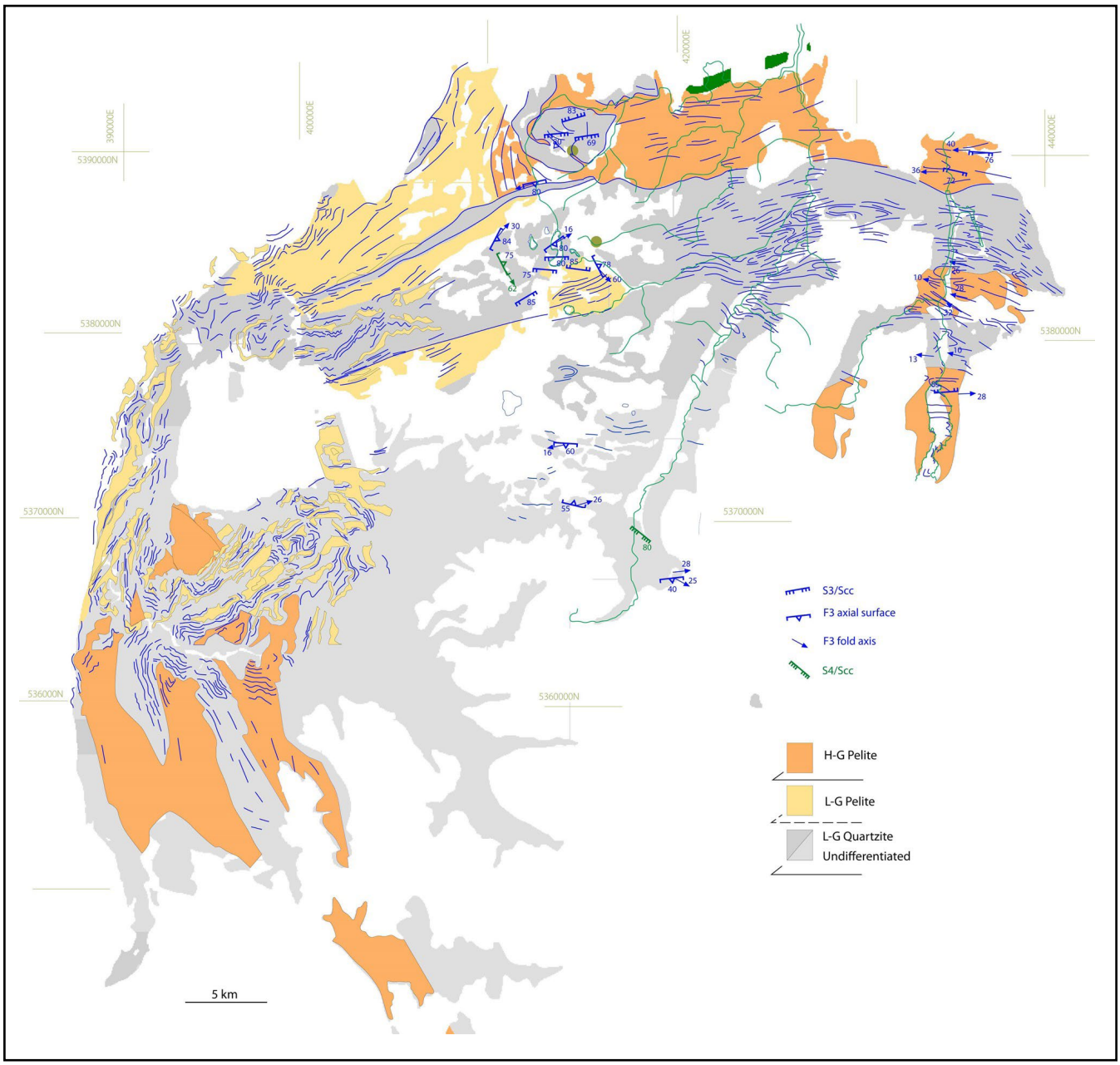

Figure 29. Northern Tyennan Subdomain structural summary map showing foliation S3 and S4 foliation attitudes and fold axis trends. Map Base is from the Mineral Resources Tasmania 1:250,00 digital atlas.

4.0 REGIONAL STRUCTURAL PROFILES

Three north-south profiles across the Northern Tyennan subdomain are presented and discussed. These include a western profile A-A', a middle profile B-B' and an eastern profile C-C' (see Figure 20 for locations). The profiles reflect a changing and transitional structural character towards the eastern part.

4.1 Western Profile A-A': Mt Kate-Cradle Mountain-Overland Track Profile

The western structural profile A-A' (Figure 31) shows three distinct structural elements and/or domains including:

1. The west-closing Mt Kate recumbent macro-fold within high-grade (H-G) schist (Ltpg). The macro-fold has a curved hinge line and sheath-like geometry that in this north-south profile shows an asymmetric north- and south- closing fold pair section and ovoid sectional traces in quartzite through the core of the sheath fold (Area 1a and enlargement, Figure 31). The macro-fold is clearly truncated by the Waldheim High Strain Zone (WHSZ) on the south.

2. A sub-vertical high strain zone interface (Waldheim HSZ) marked by intense transposition foliation and rootless fold hinges transitional into the Crater Lake-Hansons Peak chevron fold zone (Area 3b). The chevron fold zone consists of upright, tight to close F3 folds that refold early F1/F2 isoclinal folds.

3. A southern quartzite domain with broad, open F3 folds within a strongly to intensely foliated quartzite and platy quartzite at the level of the Overland Track (Area 4, Figure 31).

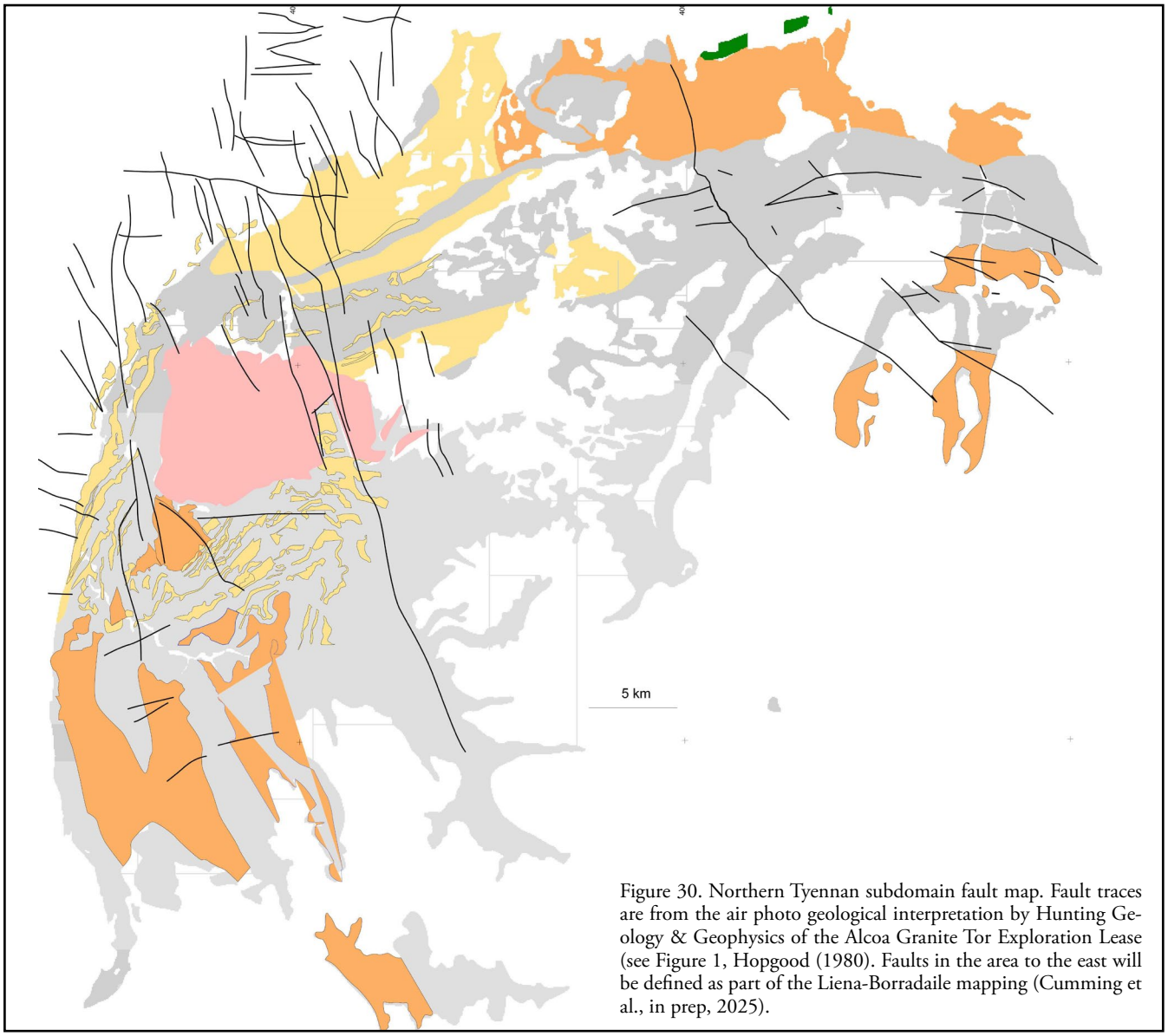

Figure 30. Northern Tyennan subdomain fault map. Fault traces are from the air photo geological interpretation by Hunting Geology & Geophysics of the Alcoa Granite Tor Exploration Lease (see Figure 1, Hopgood (1980). Faults in the area to the east will be defined as part of the Liena-Borradaile mapping (Cumming et al., in prep, 2025).

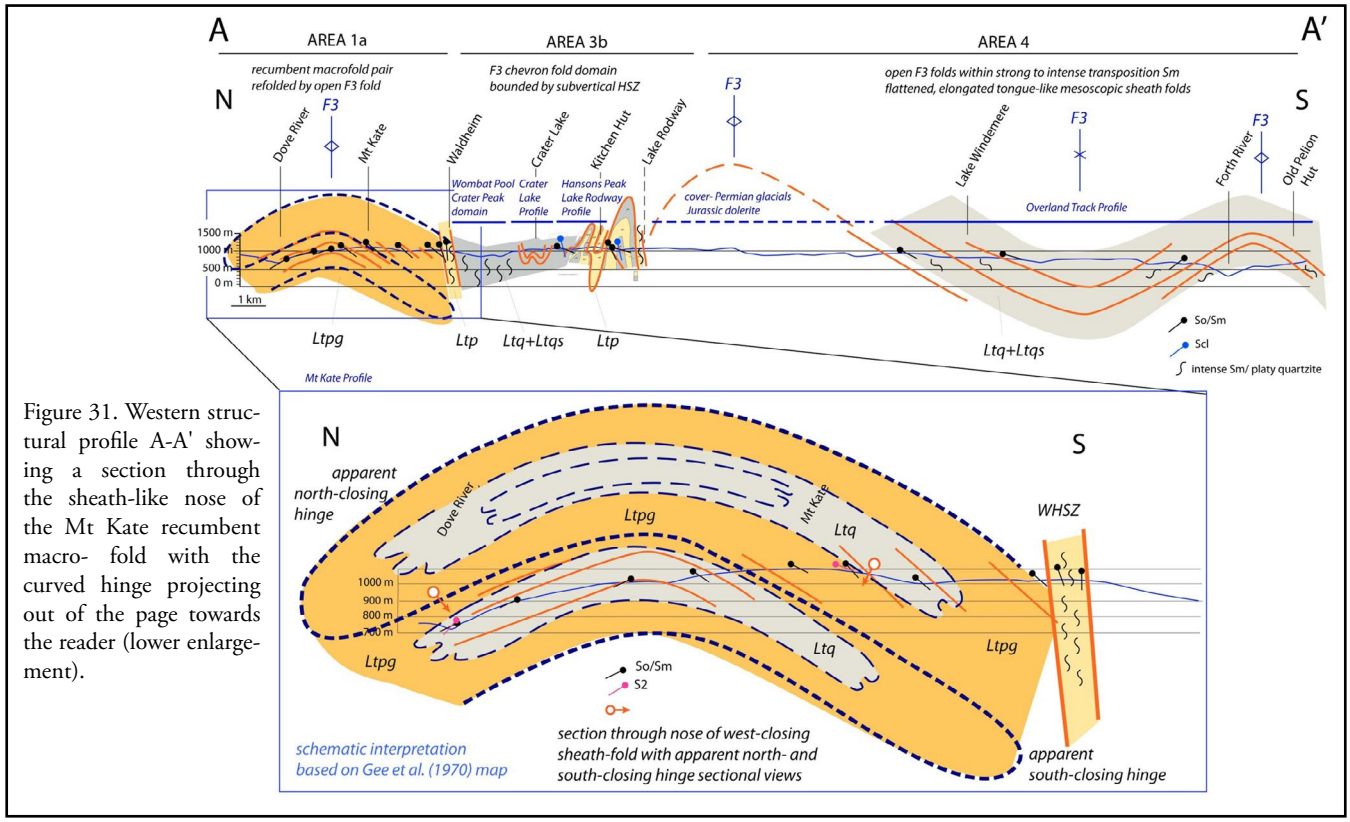

Figure 31. Western structural profile A-A' showing a section through the sheath-like nose of the Mt Kate recumbent macro- fold with the curved hinge projecting out of the page towards the reader (lower enlargement).

4.2 Middle Profile B-B': Lone Gum Plain Profile

The middle Profile B-B' (Figure 32) is located within the F3 chevron folded Liena-Borradaile zone (see Figure 20 for location). It is dominated by upright chevron folds but within a broad open anticlinorium and synclinorium (Figure 32). The F3 Fold hinges vary from tight angular chevron form, where the synformal closures commonly have cuspate to pinched-out form and the antiformal hinges have more rounded form. Many of the fold hinges are separated and bounded by higher strain foliation zones (see Section 5.3.2). A tight to almost isoclinal form of some of the folds suggests they are most likely F2 folds.

The main structural elements include the broad Fisher Anticlinorium and the Mersey Synclinorium as well as an inferred north-closing, recumbent isoclinal fold as continuation of the Mt Kate macro-fold (see red dashed line close-out centred on the Dove River, left side of profile, Figure 32).

4.3 Eastern Profile C-C': Mersey Valley Profile

The easternmost profile C-C' along the Mersey Valley (Figure 33) occurs along the easternmost part of the Northern Tyennan subdomain (Figure 20 for location). This profile is also dominated by upright F3 chevron folds, that refold early F1/F2 isoclinal folds at all scales. Tight to almost isoclinal hinges within the profile are considered second order (km scale) F1/F2 hinges that are coaxially refolded and tightened by the F3 folding (see the interpretation and hinge designation in Figure 33b).

Three different interpretations of profile C-C' are presented based on different construction approaches (Figure 33). Figure 33a is based on the recent Liena-Borradaile sheet mapping and utilises the mapped outcrop traces and structural data collected to produce a profile dominated by chevron folding cut by steep faults but without distinct anticlinoria and synclinoria.

Figures 33b and 33c utilise outcrop sketches and structural data collected along the Mersey Forest road. Figures 33b and 34 show chevron folding but attempts to differentiate between early F1/F2 tight to isoclinal hinges and more open F3 folds that dominate the profile. The variations in structural style at the outcrop scale are shown as insets in Figure 34. Figure 33c is a profile constructed utilising i. structural mapping and profiling data collected by UTAS Third Year mapping students, ii. the litho-stratigraphy of Spry (1958) and iii. the Devonian thrust-detachment model of Woodward et al. (1990).

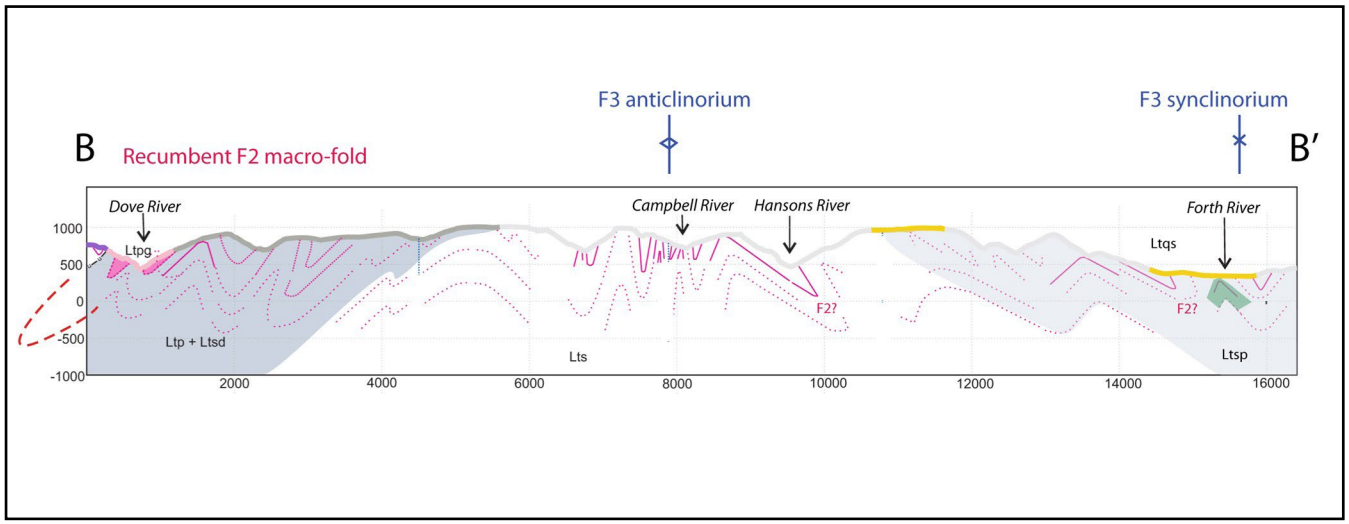

Figure 32. Lone Gum Plain profile (Cumming, in prep, 2025) based on Liena-Borradaile mapping (see section A-A", Figure 78). The main structural elements include an F3 anticlinorium and synclinorium, and an inferred close out to the north of the Mt Kate macro-fold.

Units include:

Ltpg (pink): garnet schist.

Ltp: (dark grey): schist and phyllite (dominantly pelite)

Ltsd: (green): quartz-mica schist

Ltps: phyllite and quartzite

Lts (white): quartzite (dominantly quartzite)

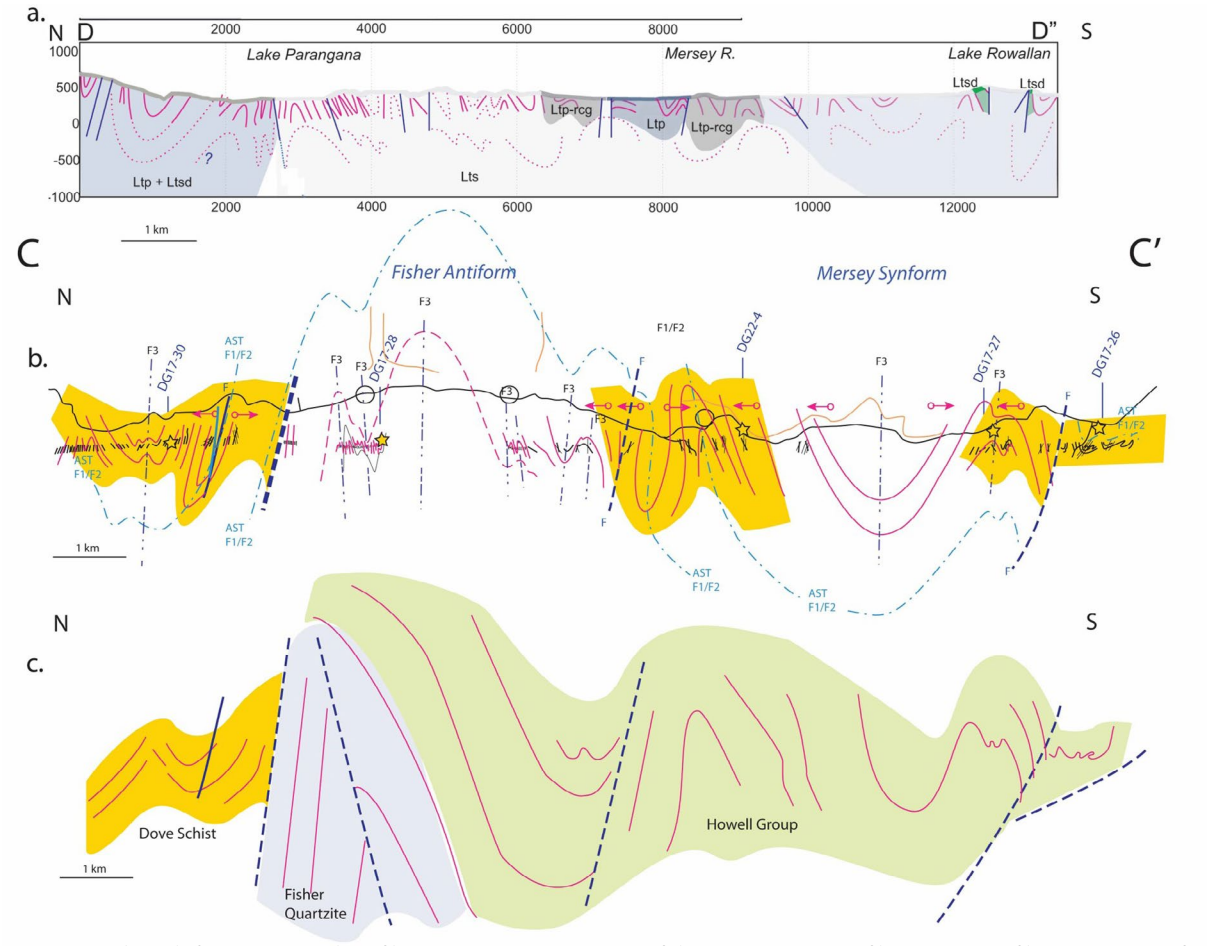

Figure 33. Three different structural profile constructions as versions of the Mersey River Profile C-C'. a) Profile section D-D" from Liena-Borradaile mapping (Cumming et al., in prep, 2025). See legend in Figure 32 above for lithologic units. b) Profile by DRG using structural data collected by DRG and UTas Third year mapping data (provided by Ron Berry). c) Profile by Ron Berry (see Berry & Bull, 2004). The Mersey Forest road provides the structural basis for these three interpretative profiles.

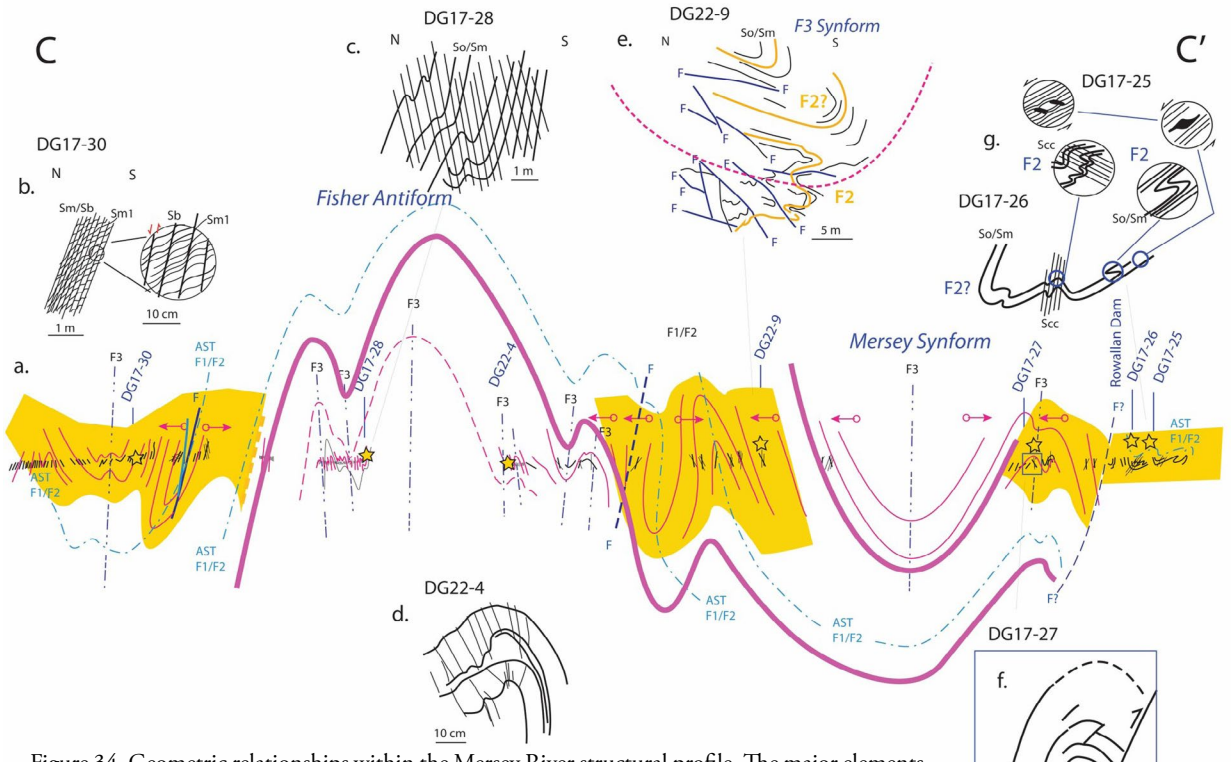

Figure 34. Geometric relationships within the Mersey River structural profile. The major elements include the Fisher Antiform in quartzite and the Mersey Synform in a litho-tectonic package of garnet schist (orange unit)-and quartzite-phyllite (white unit). Cleavage vergence was used to construct the position of the major F3 hinges (shown by the red arrow with circle symbol). The insets show the structural character and style at different positions across the major folds.

5.0 MAJOR STRUCTURES OF THE NORTHERN TYENNAN SUBDOMAIN

5.1 Mt Kate Recumbent Isoclinal Macro-fold (Area 1, Figure 16)

5.1.1 Mt Kate Recumbent Isoclinal Macro-fold Hinge (Area 1a)

The Mt Kate recumbent isoclinal macro-fold occupies the northernmost part of the Northern Tyennan subdomain (Figures 14 and 20). It has a complex, west closing fold hinge zone defined by interpenetrating high-grade garnet schist and quartzite and symmetrical to asymmetrical, alternating south- and north-closing, second-order fold hinges (Figures 35, 36 and 37). These second order folds show curved sheath-like form through the main closure (Figure 37). This hinge line curvature can be seen in the form line map based on the Gee et al. (1970) mapping (Figure 35) and in section C (Figure 38) that shows ovoid fold profiles typical of sheath folds. The second order fold hinges have been interpreted by convergence of the compositional layering So/Sm (Figure 36a). The map pattern reflects interpenetrating quartzite and pelite enveloped by a core of high-grade garnet schist (dark orange unit of Figure 37). Views of these second-order folds within the

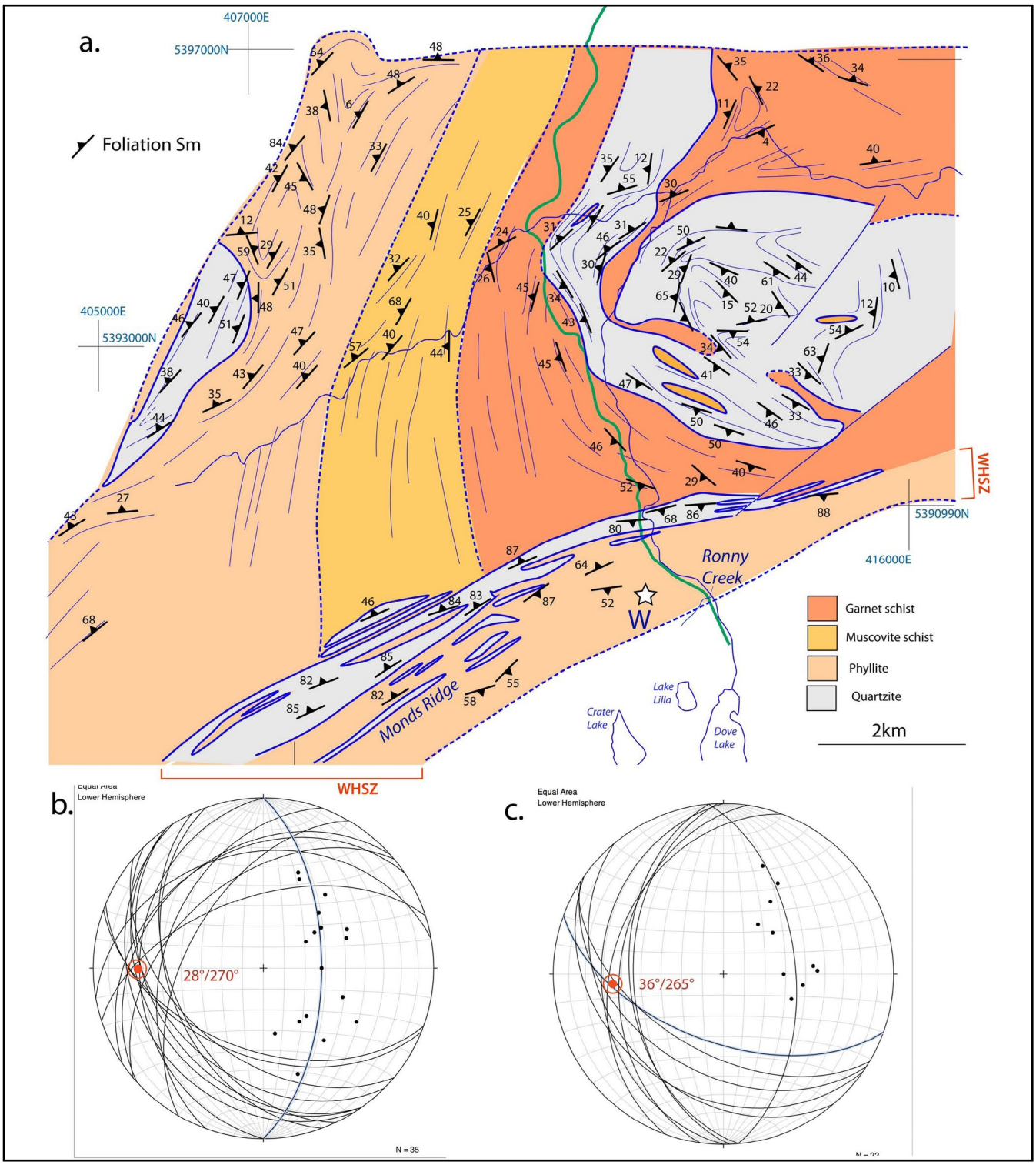

Figure 35. a) Lithological map showing foliation Sm attitudes and form lines on base map from the MRT 1:25,000 digital geological atlas series. b) Stereonet with Sm great circle traces giving a β axis of 28°/270° for the Mt Kate macro-fold (F1/F2 fold axis). c) Stereonet of foliation S2 great circle traces giving a β axis of 36°/265° (F3 fold axis). W: Waldheim. WHSZ: Waldheim High Strain Zone.

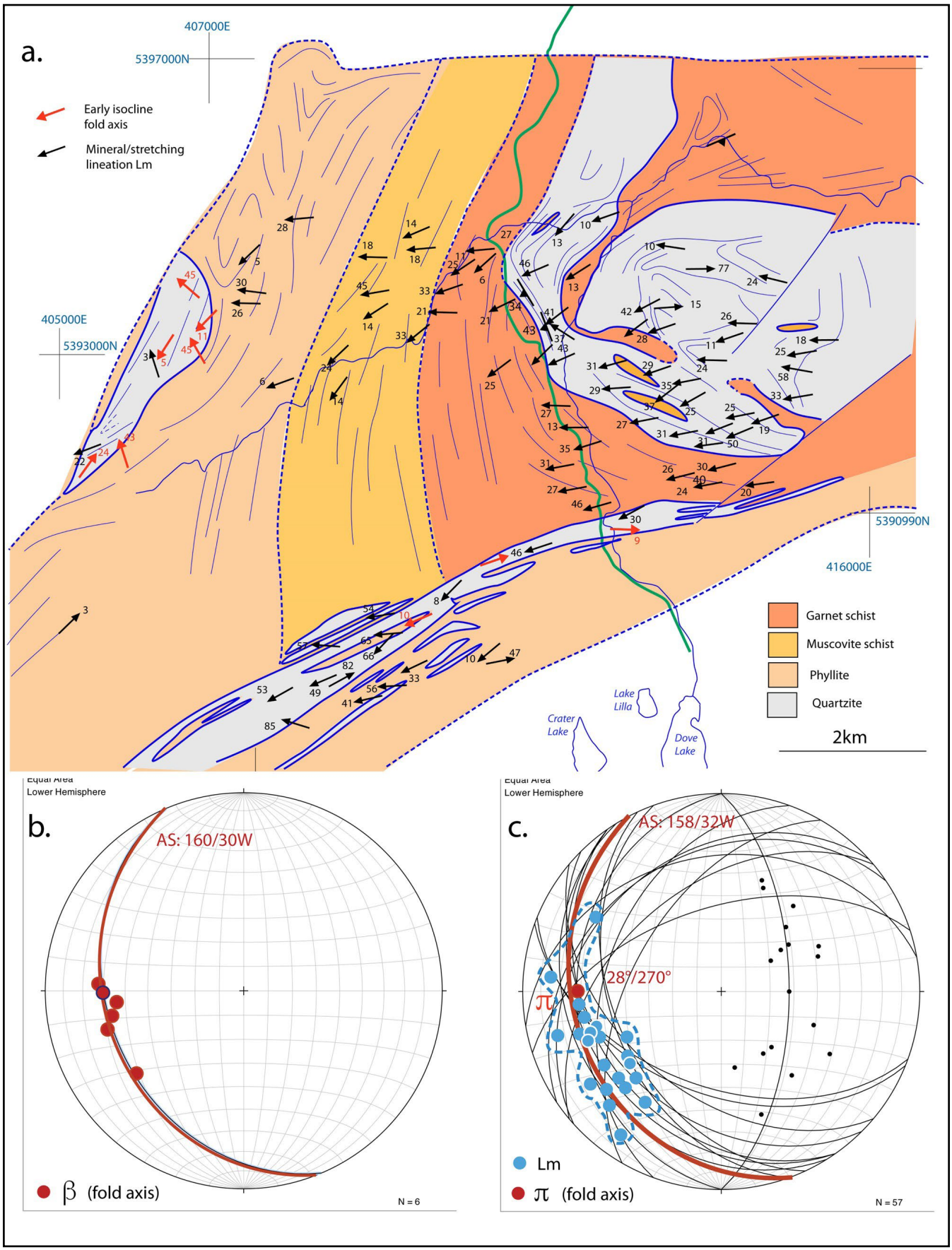

Figure 36. a) Lithological map with form lines showing mineral/stretching lineation Lm and early isocline fold axis attitudes on base map from the MRT 1:25,000 digital geological atlas series. b) Stereonet showing best-fit great circle of the calculated β axes (red dots) from inferred hinges of the second order folds based on mapped Sm convergence. This is the equivalent Mt Kate macro-fold axial surface. c) Stereonet of mineral lineation Lm (blue dots plotted with Sm great circle traces showing an asymmetric girdle spread about the β point along the macro-fold axial surface (158°/32°W).

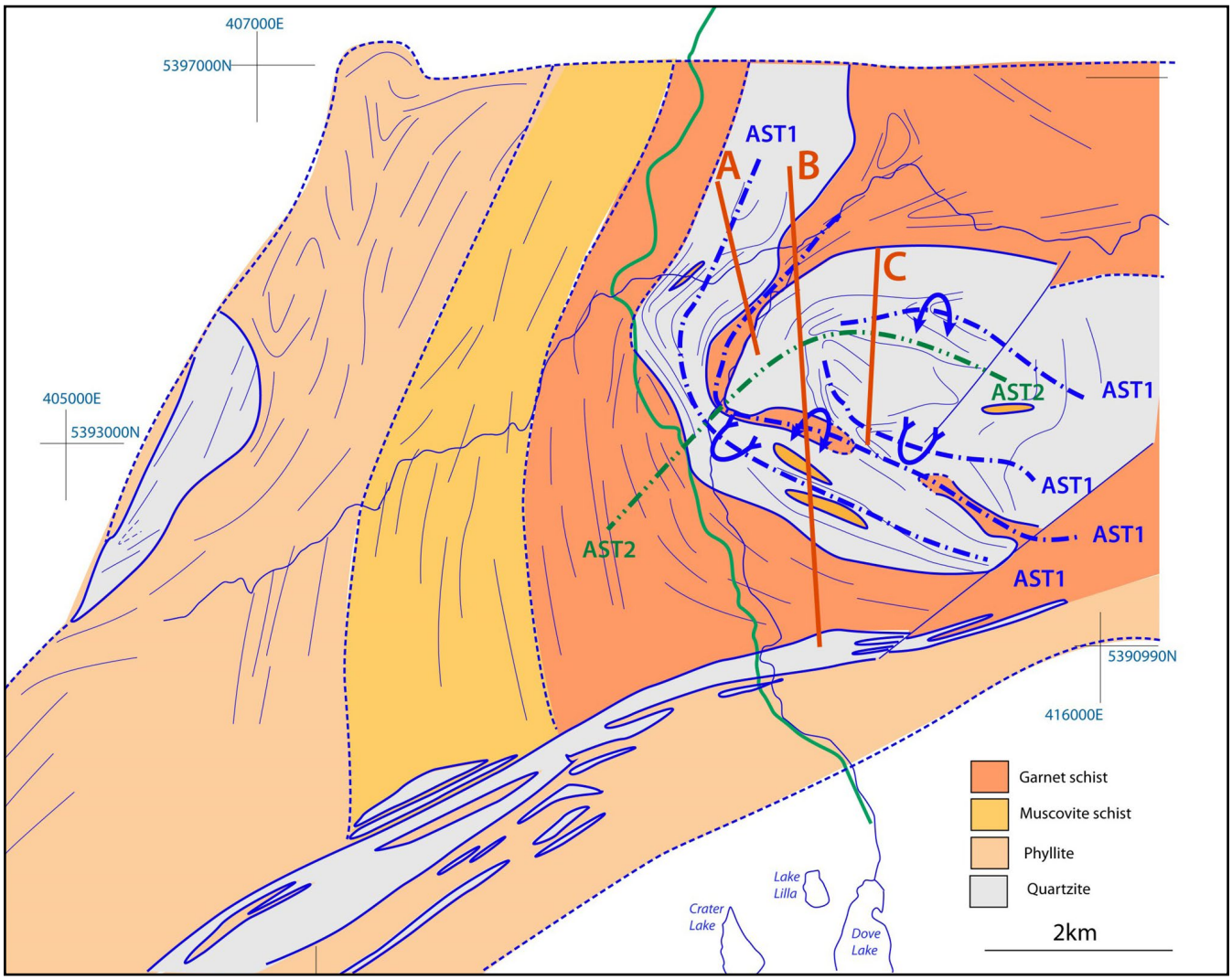

Figure 37. Lithological map with form lines showing macro-fold axial surface traces on base map from the MRT 1:25,000 digital geological atlas series. The blue dash-dot traces (AST1) are the second-order, isoclinal fold hinge-line traces within the major south-closing Mt Kate macro-fold hinge. The green dash-dot (AST2) represents the hinge line trace of the younger anticline that refolds the Mt Kate macro-fold. The locations of structural profiles A, B and C in Figure 38 are shown by the red lines.

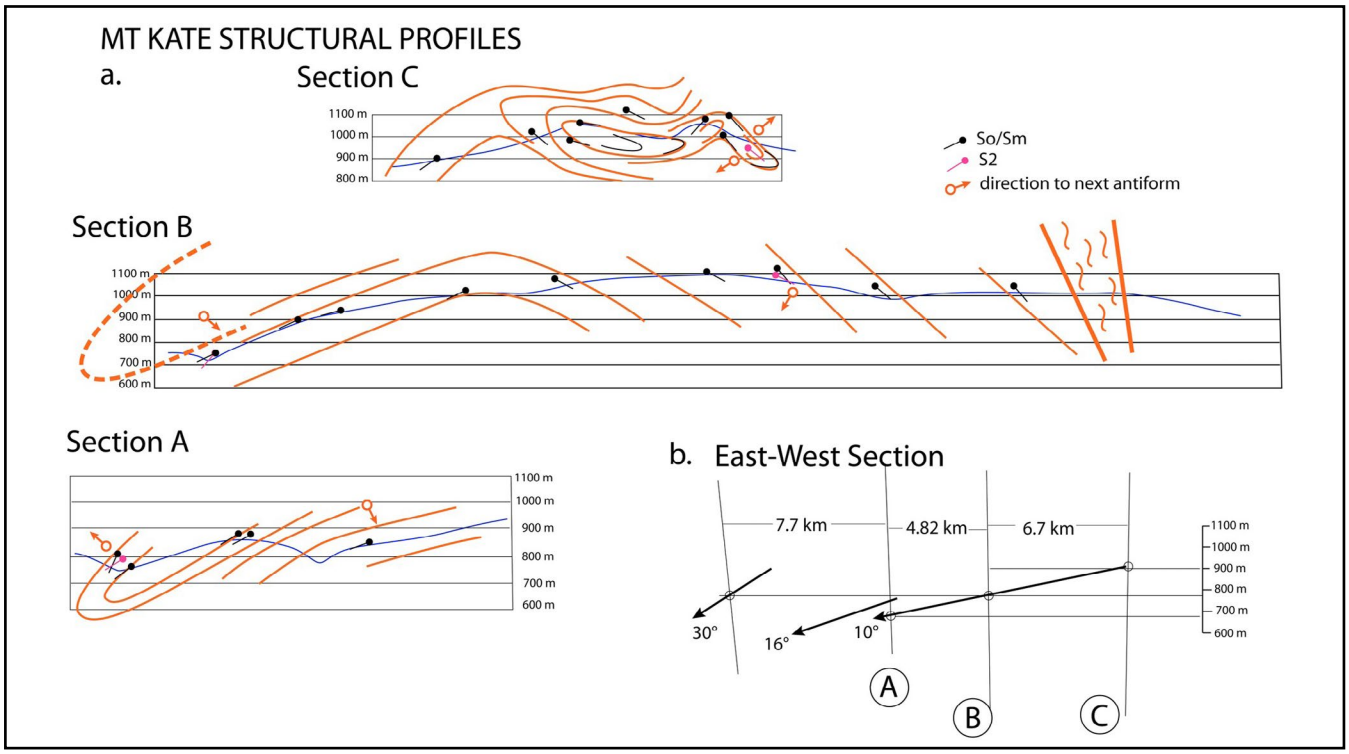

Figure 38. Structural Profiles across the Mt Kate Macro-fold. For locations see Figure 37. a) North-south sections A, B and C. b) East-west profile showing the spacing positions of the sections A, B and C in (a) and the macro-fold plunge in each of the sections (black arrows).

quartzite internal to the high-grade schist can be seen in the Dove Canyon (Figure 41) and Quailes Hill (Figure 42) with the nose shown in the Mt Kate ridgeline (Figure 43). The layering in the hinge of the macro-fold is truncated by a major high strain zone characterised by a steeply dipping, intense foliation Sm (Figure 35).

The Mt Kate macro-fold geometry has a modal 28°/270° (Figure 35b) with an axial surface 160°/30°W (Figure 36b). The serial sections (Figure 38a) however, show that the macro-fold plunge steepens southwards (see the east-west section, Figure 38b). The axial surface fit was determined by using β point stereonet determinations from selected straight-line segments of the mapped curved macro-fold hinge line (Figure 36b) and matched by a great circle best fit to the lineation Lm distribution (Figure 36c).

Originally interpreted as an F3 fold and designated the Mt Kate Antiform by Gee et al. (1970) the earlier recumbent isoclinal macro-fold is broadly arched by the younger, open anticline with a weak, east-west trending axial surface S3 crenulation cleavage.

The map geometry is influenced by a sheath-like form of the F1/F2 macro-fold with curved hinge line (compare Figure 39) and refolding by the open F3 folding, causing an apparent mushroom interference pattern (compare Figures 36, 37 and 40). The interpreted 3D form of the Mt Kate macro-fold is shown schematically in Figure 44. Key geometric elements include the in-folded quartzite layer(s) within the garnet schist, the overall curved hinge line and consistent Lm trend. The diagram represents a restoration from the tilted map view depicted in Figure 37 where the Waldheim High Strain Zone (WHSZ) has been rotated to the horizontal along with the overlying, structurally higher macro-fold hinge. The WHSZ is a higher strain interface within the litho-tectonic stack (Figure 5) and is most likely folded as part of the leading edge fold-nappe.

Figure 39 (Left). Curved mesoscopic fold hinge line in thin quartzite layer with the lateral limb segments rotated towards the mineral lineation Lm shown by the elongation of quartz grains sub-parallel to the red pen. The fold is from the Dove Canyon track just east of the intersection of Stony Creek with Pencil Pine Creek. The hinge line-lineation relationships match those in the Mt Kate macro-fold (Figure 36).

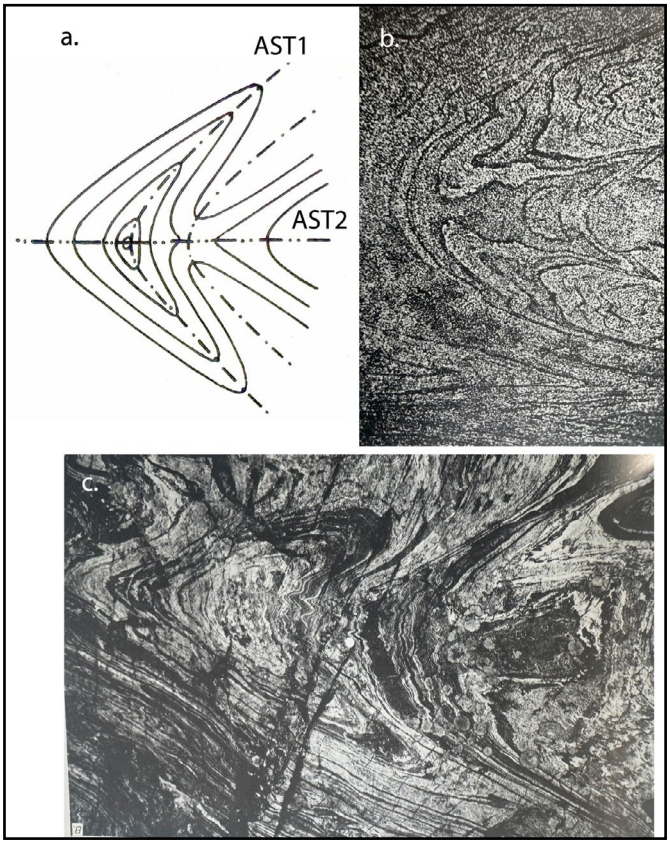

Figure 40 (Right). Mushroom type 2 fold interference in the map pattern relationships of the quartzite layer(s) within the Mt Kate macro-fold hinge shown in Figure 37 (modified from figs. 22.18 and 22.19 in Ramsay & Huber, 1987). The apparent hinge line curvature is largely due to the refolding but hinge line-lineation relationships (Figure 36) suggest a hinge line curvature component may also be related to sheath-fold character. a) Form line pattern with axial surface traces of F1 (AST1) refolded by F2 (AST2). b) Matching outcrop from Loch Hourn, NW Scotland (Photo Credit: John Ramsay). c) Outcrop pattern from the Lepontine nappe of the Swiss Alps (Photo Credit: John Ramsay).

Figure 41. View of cliffs along the east side of the Dove River gorge taken from the Dove Canyon track.

a) and b) are non-annotated and annotated photographs respectively. Form lines in So/Sm (white line traces) show a series of tight to isoclinal fold hinges that are part of a second order south-closing recumbent fold.

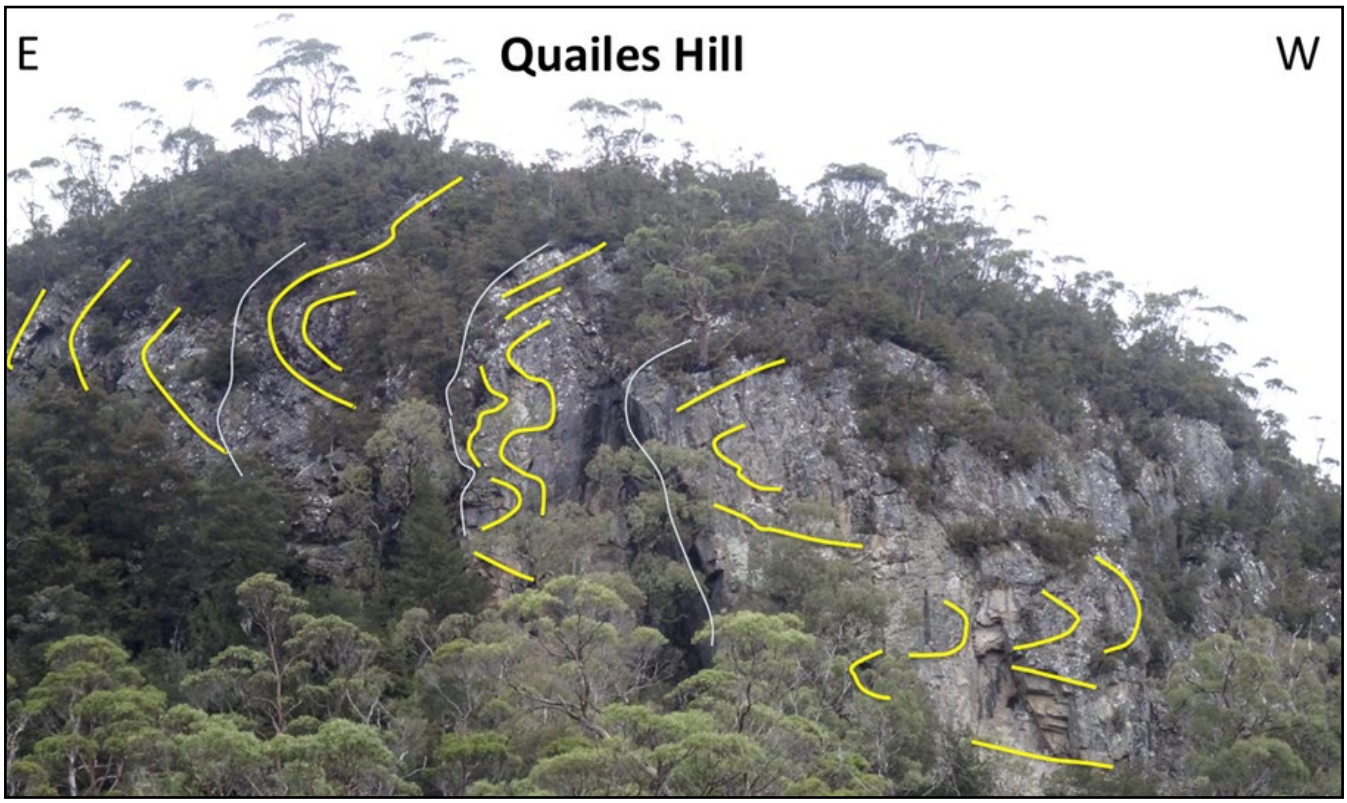

Figure 42. View of Quailes Hill showing an east-closing recumbent isoclinal fold hinge. The view is taken from the Dove Lake-Cradle Mountain boardwalk looking to the south.

Figure 43. View of the Mt Kate ridgeline looking to the northeast from the Dove Canyon track. The ridgeline is held-up by strongly foliated and internally folded quartzite with apparent homoclinal dip in Sm. a) and b) are non-annotated and annotated photographs respectively. The So/Sm enveloping surface is at high angles to the dominant foliation Sm indicating location within the Mt Kate macro-fold hinge

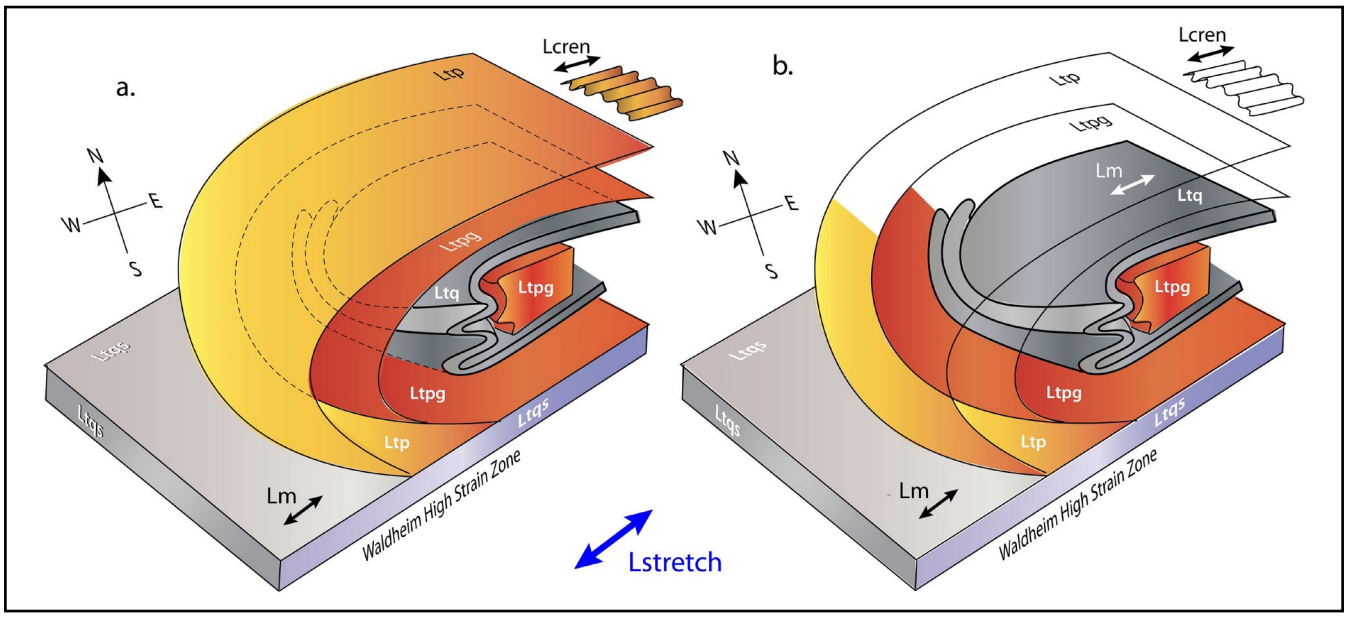

Figure 44. 3D model sketch of the Mt Kate macro-fold geometry with the macro-fold lower limb truncated by the Waldheim High Strain Zone. The macro-fold and underlying high strain zone have been rotated such that the Waldheim HSZ is now sub-horizontal. a) Lithological units shown as shells with low-grade phyllite (yellow-orange: Ltp) enveloping a core of garnet schist (bright orange: Ltpg) and quartzite bands (grey: Ltq). b) The 3D model sketch with the outer layers/shells removed to show the internal geometry of the folded quartzite that outlines the macro-fold hinge zone and the curved sheath-like nature of the second-order fold hinges. Note the sub-parallelism of the early mineral lineation direction (Lm) and the younger crenulation lineation Lcren.

5.1.2 Mt Kate Macro-fold "Tail" (Area 1b, Figure 16)

The "tail" of the Mt Kate macro-fold consists of an east-west trending, elongated belt of high-grade schist that is internally upright chevron folded (Figures 45 and 46). The "tail" represents the hinge to lower limb transition of the Mt Kate macro-fold. It extends from the in-folded quartzite layers at Mt Kate (Figure 38 and left side Figure 45) to the Mersey River (right side, Figure 45). It is strongly foliated, contains mesoscopic isoclinal folds (Figures 47 and 48) and is dominated by upright chevron folds with ~ 1.5-2 km wavelengths.

Fold axis determinations of inferred macro-fold hinge closures within the schist (see stereonets, Figure 45) show varying fold axis trends (red arrows, Figure 45a). These calculated fold plunges appear somewhat randomly oriented but lie on a steeply north-dipping, east-west trending "best-fit" great circle (Figure 45b). This fold axis pattern and relationships are suggestive of curved sheath-like fold hinges typical of folding in simple and general shear where the inferred shear plane is now sub-vertical or steeply north-dipping. The same fold axis pattern is present in the quartzite-pelite sequence of the Liena-Borradaile area to the south (see Section 5.4 below).

At the outcrop scale the structural character of the high-grade schist is typified by zones of transposition layering alternating with zones of mesoscopic chevron folds. The northern and southern boundaries of the high-grade schist belt (see orange lines in Figures 45 and 46) are intensely foliated zones (Figure 49).

5.1.3 Quartzite-Pelite Upper Limb to Hinge Transition Zone (Area 1c)

Area 1c incorporates the westernmost part of the Mt Kate macro-fold. It represents the northwest-dipping, attenuated upper, overturned? limb of the Mt Kate macro-fold. The hinge and hinge to lower limb transition of the macro-fold is truncated by the Waldheim High Strain Zone (section 5.3.1). The Waldheim HSZ is a zone of sub-vertical transposition layering that defines the southern boundary of Area 1c (HSZ, Figure 50). The form lines in Sm suggest there are three distinct structural domains within Area 1c. In the northern part the foliation has a curved pattern reflecting the partial hinge of the macro-fold but overall with a dominant northwest dip and a west- to southwest-plunging mineral stretching lineation Lm (North stereonet inset, Figure 50). In the middle region the form lines reflect open folding with gentle northeast or southwest plunges such that the individual limb segments are either north dipping or northwest dipping (Mid Stereonet inset, Figure 50). The lineations Lm with Sm lie along a great circle (red great circle, Mid stereonet, Figure 50). In the southern part of Area 1c there is a strike change in the form lines from northeast to east-west trending where open folds have a steeply northeast plunge (60°/023°, South stereonet inset, Figure 50). This is a region of fold interference around Granite Tor related to the major strike change and geometric curvature within the Northern Tyennan subdomain (see Section 5.2). The lineations (Lm) within Sm lie along a great circle 246°/62°N (South stereonet, Figure 50). The spread in Lm attitudes most likely reflects local mesoscopic isoclinal folding of the mineral lineation with Lm at divergent angles on opposite limbs (Lake Rodway Zone, Figure 72).

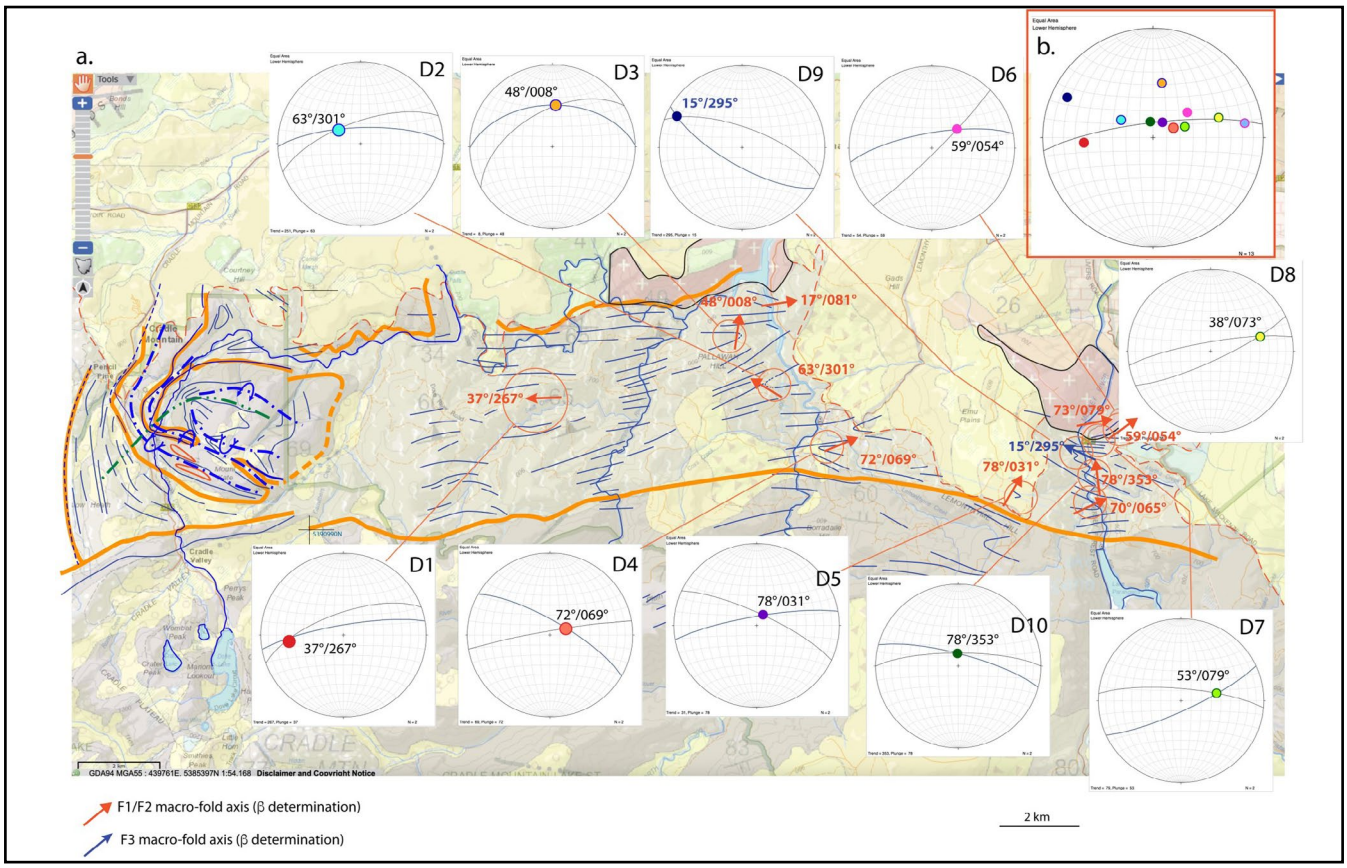

Figure 45. Structural map of the Mt Kate macro-fold nose and eastern elongated "tail ". a) MRT 1:250,000 digital atlas map base showing form lines in Sm (blue line traces), calculated fold axes (red arrows) and β fold axis determinations plunge variations across the macro-fold tail. The inset stereonets show fold plunge at the various circled locations based on Sm attitude data shown in Figure 46. b) Total fold axis stereonet plot with best-fit great circle. The coloured dots (individual fold axis determinations) can be matched with the stereonets listed D1 through D10.

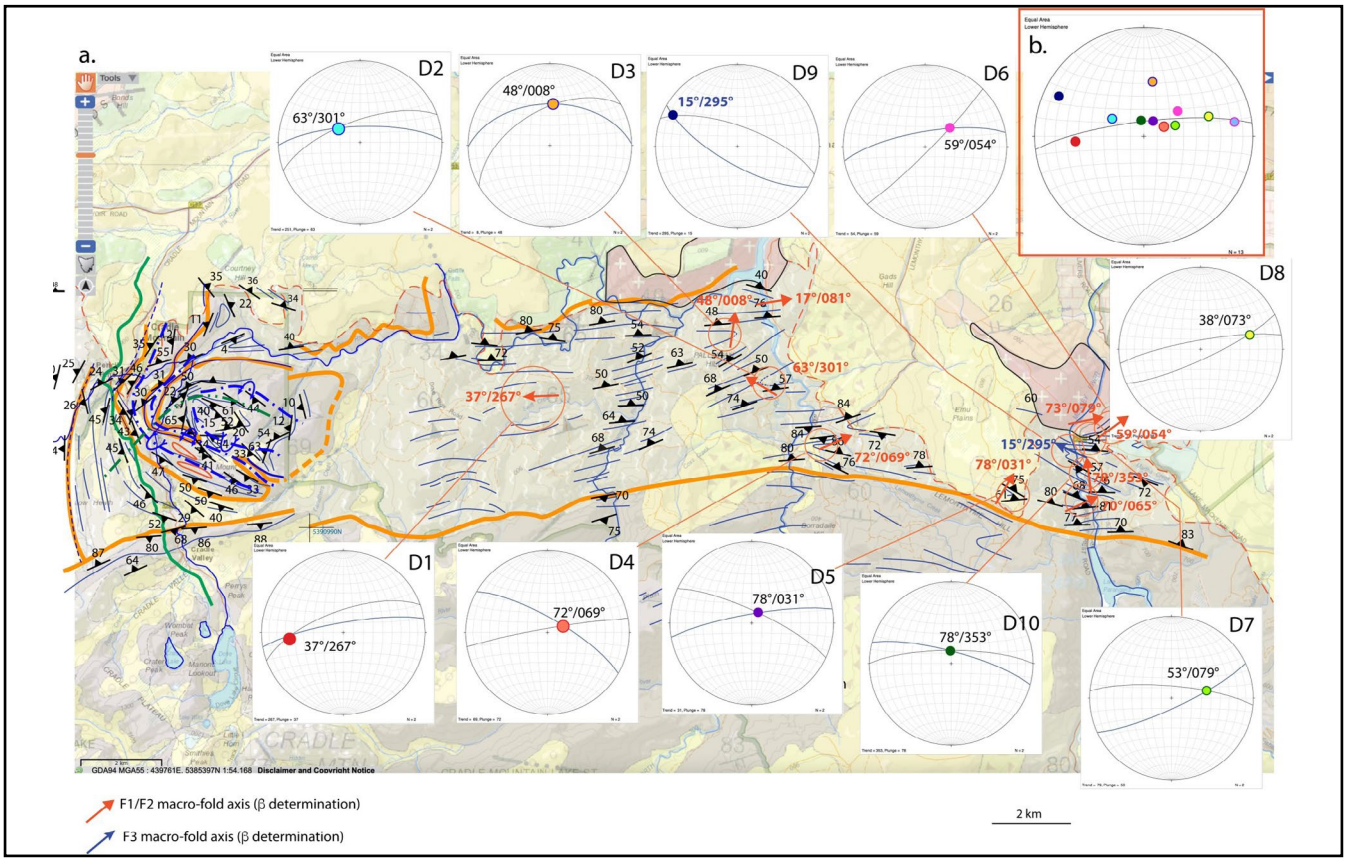

Figure 46. Structural map of the Mt Kate macro-fold nose and eastern elongated "tail ". a) MRT 1:250,000 digital atlas map base showing Sm attitudes (black strike/dip symbols), form lines in Sm (blue line traces), calculated fold axes (red arrows) and β fold axis determinations plunge variations across the macro-fold tail. b) Total fold axis stereonet plot with best-fit great circle. The coloured dots (individual fold axis determinations) can be matched with the stereonets listed D1 through D10.

Figure 47 (Left). Structural character of the high-grade schist in outcrops along Campbells Creek (Photo credits: Carl Jackman). a) Elongated and attenuated steeply dipping chevrons within porphryoblastic, thinly banded mica and quartz-mica schist. (424020E, 5394266N) b) Disrupted and isoclinally folded quartz veins, now pod-like relicts within porphryoblastic schist. (424020E, 5394266N).

Figure 48 (Below). Tight to isoclinal folds in mica schist with thin psammitic bands Lower Martha Creek (435448E, 5392213N) (Photo credit: John Everard).

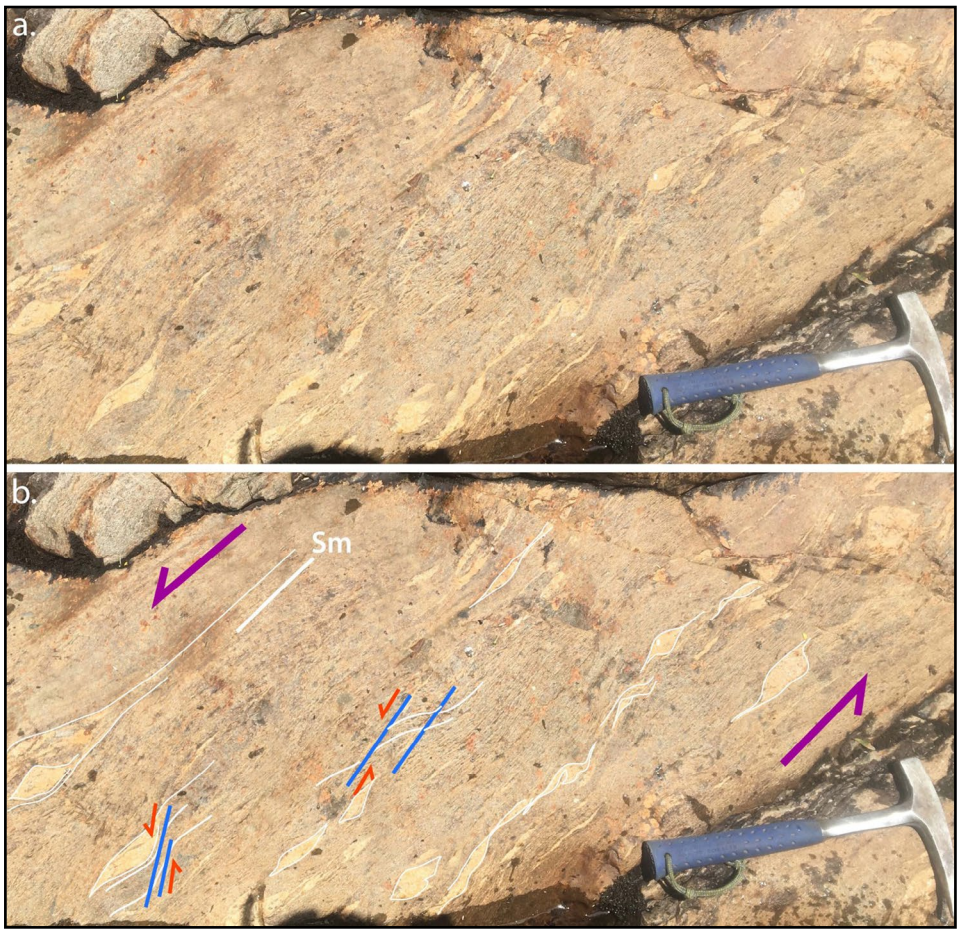

Figure 49 (Left). Intensely foliated schist on the northern boundary of the Dove Schist. The photo is looking to the northeast with the foliation sub-vertical and with east-west strike. a) Non-annotated photo of the transposition layering Sm. b) Annotated photo showing the Sm enclosing relicts of isoclinally folded and disrupted quartz-feldspar veins with strung-out "tails". The bottom left shows sets of shear bands indicating sinistral or east-over-west shear sense. Outcrop along Dove River. (Photo credit: Grace Cumming).

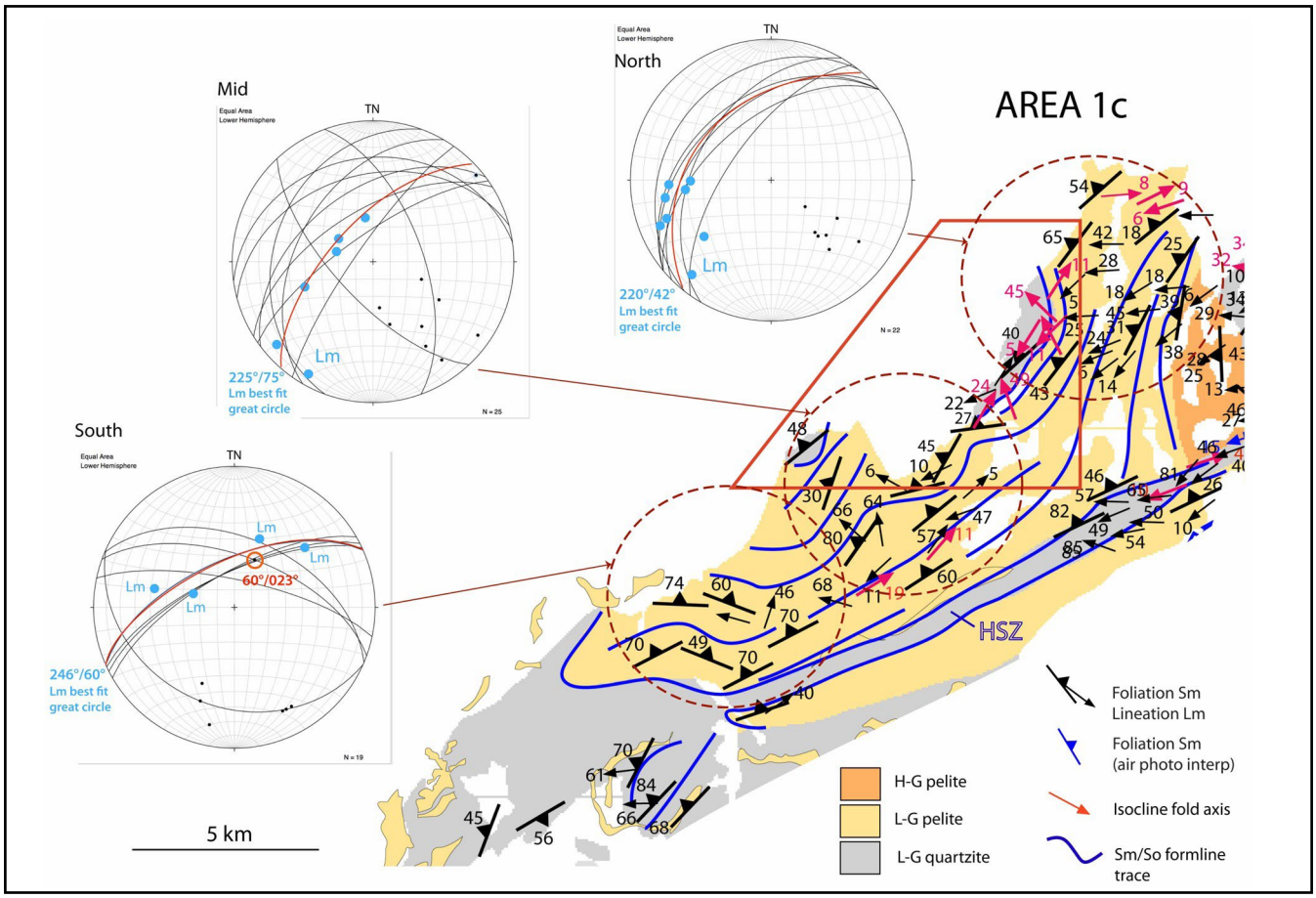

Figure 50. Map area 1c simplified structure map showing litho-tectonic units, foliation form lines (blue line traces) and foliation and lineation data. Bright orange: high-grade pelite (garnet schist). Dull orange: low-grade pelite (phyllite). Grey: quartzite. HSZ: Waldheim High Strain Zone. The base map is from the MRT 1:250,000 digital atlas. All structural data are from the Mackintosh 1:63,360 map sheet (Barton et al., 1966). The red outlined area is the location of Figure 51. The stereonets show great circle traces for Sm and lineation data (blue dots) for the north part, middle part and southern part of the attenuated and truncated nose. The red great circles are best fits to the Lm data.

Quartzite remnants sit at the highest structural position situated along the contact with the Cambrian Mt Read volcanic succession (Figures 50 and 51). The largest quartzite is an elongated and tapered "tadpole-like" pod sub-parallel with the dominant foliation Sm. The foliation envelopes the pod, but appears to locally crosscut the quartzite-pelite contact (Figure 51). Younging is lacking, but geometrically the quartzite lies on the overturned macro-fold limb with a stacking sequence of high-grade schist (fold core) overlying low-grade pelite (phyllite) overlying quartzite (Figures 20 and 44). Fold axes within the quartzite pod lie along a best-fit great circle (233°/44°NW) that approximates the northwest dipping foliation Sm. More likely there appears to be two sets of folds within the pod, one set either northeast or southwest plunging (red FA dots on Stereonet, Figure 51) and the other northwest plunging (blue FA dots on stereonet, Figure 51). The northwest set (blue dots) is related to the F4 folding and the strike curvature of the Northern Tyennan subdomain, whereas the red dots are probably F1/F2 hinges.

5.2 Granite Tor Macro-fold Zone (Area 2, Figure 16)

Area 2 is the southwestern part and north-trending strike belt of the Northern Tyennan subdomain (Figure 16). It consists of interdigitating high-grade pelite, low-grade quartzite and intercalated quartzite-pelite where the pelite bodies have elongated and tapered pod-like form (Figure 52). South of Granite Tor the area is dominated by an apparent mushroom-shaped fold interference pattern (Type 2 fold interference, Ramsay, 1967; Ramsay and Huber, 1987) where the early isoclinal folds are refolded by a north-south fold set into an east-west orientation (Figure 52). This is a continuation of the macro-fold sets from the Central Tyennan subdomain to the south (see Gray and Vicary, 2021).

The structural interpretation of Area 2 is based on an air photo-geological interpretation of an Alcoa Exploration Lease by Hunting Geology and Geophysics (Hopgood, 1980). No geological mapping has been undertaken in this area. Foliation So/Sm attitudes and form lines are derived from the air photos and maps in the original study (Figure 1; Hopgood, 1980).

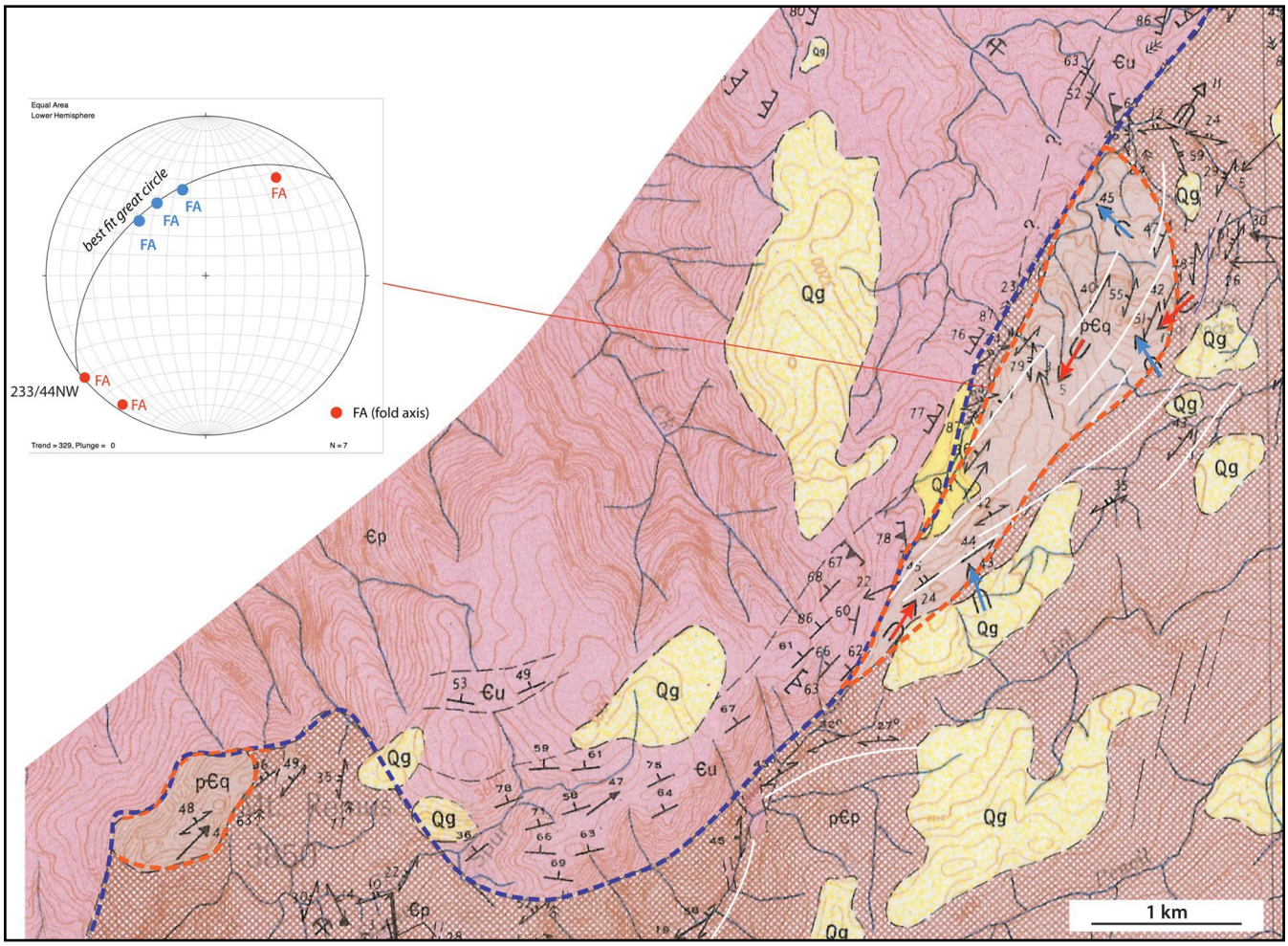

Figure 51. Quartzite remnants as lozenges on the upper limb of the Mt Kate macro-fold preserved along the contact with the Cambrian Mt Read volcanic succession. Base map is part of the Mackintosh 1:63,360 map sheet (Barton et al., 1966). The location of the map polygon is shown in Figure 50. The blue dashed line is the contact with the Cambrian Mt Read Volcanic succession (pink Eu). pEq: quartzite. pEp: pelite (phyllite). Form lines in Sm are shown by the white line traces. The red dashed line traces outline the quartzite remnants. The red and blue arrows are measured fold axes. The inset stereonet (upper left) shows the fold axis distribution and apparent fit to a great circle 233°/44°NW of folds within the northern quartzite lozenge.

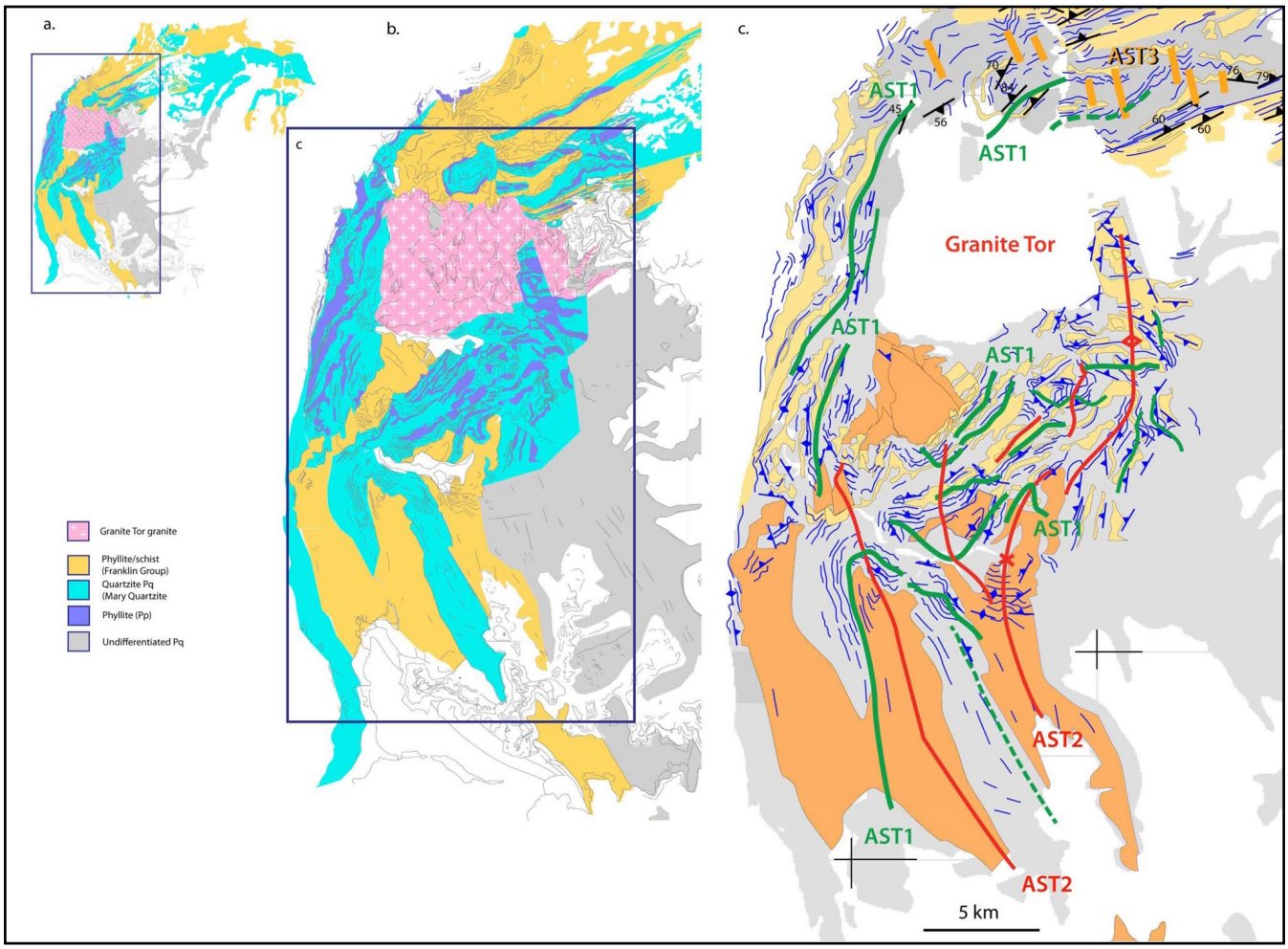

Figure 52. Structural form line map of the Granite Tor Macro-fold zone (Area 2, Figure 16) showing fold interference patterns between three sets of macro-folds. Blue line traces: form lines in So/Sm and the blue strike dip symbols are based on air photo interpretation from Hopgood (1980). Black strike/dip symbols are from the Mackintosh 1:63,360 Map sheet. Axial surface traces (AST) for early F1/F2 macro-folds are shown by the green line traces. Second phase F3 fold axial surface traces (AST2) are shown by the red line traces. Third phase F4 fold axial surface (AST 3) traces are shown by the orange line traces. F4 folds are more local and restricted to the strike change to the northeast just north of Granite Tor (Figures 17 and 20).

5.3 Northern Tyennan Chevron Fold Zone (Area 3, Figure 16)

Area 3 occupies the central and largest part of the Northern Tyennan subdomain (Figure 16). The region is dominated by upright F3 chevron folds and has been designated the Northern Tyennan Chevron Fold Zone. The zone however, shows a marked change in character from the western part (Area 3a, Figure 16) to the middle and eastern part (Area 3b, Figure 16). In the west a broader ~ 1 km wide zone of open to close chevron folds (the Crater Lake-Hansons Peak -Twisted Lake Folded Zone) is bounded by two sub-vertical high strain zones. In the middle and eastern part lozenge shaped chevron fold domains (< 1km in width) contain a series of tight to almost isoclinal chevron folds with extremely variable fold plunges. The lozenge domains are bounded by or are transitional into the high strain steeply dipping, intensely foliated transposition zones. The character is also different in the Lake Rowallan area (Area 3c, Figure 16).

5.3.1 Quartzite-Pelite Structural Transition Zone (Area 3a, Figure 16)

Area 3a represents the western part of Chevron Fold Zone and is made up of a "core" of close to tight, upright chevron folds through the Crater Lake-Lake Hanson area, bounded by sub-vertical zones of transposition foliation and elongated outcrop pods of intercalated quartzite and pelite. These have been designated as the Waldheim High Strain Zone along the northern boundary and the Lake Rodway High Strain zone along the southern boundary. These zones merge with the anastomosing shear zone network that characterises the eastern part (see Section 5.3.2).

Waldheim High Strain Zone

The Waldheim High Strain Zone (Element 2, Figure 16) is an east-northeast trending linear belt some ~2 km in width extending from Ronny Creek on the east through Waldheim to Mond Ridge on the west (Figure 35). It is a belt of structurally intercalated thin quartzite bands and schist containing an intense sub-vertical transposition foliation. At Ronny Creek this foliation is steeply south dipping containing a moderately to steeply west-plunging rodding lineation Lm/Lrod (Figure 53) and rootless isoclinal folds in thin quartzite bands and isolated quartz veins (Figure 54). Fold axes plunge gently west, but in some areas of higher strain these folds have extremely variable plunge within the transposition foliation.

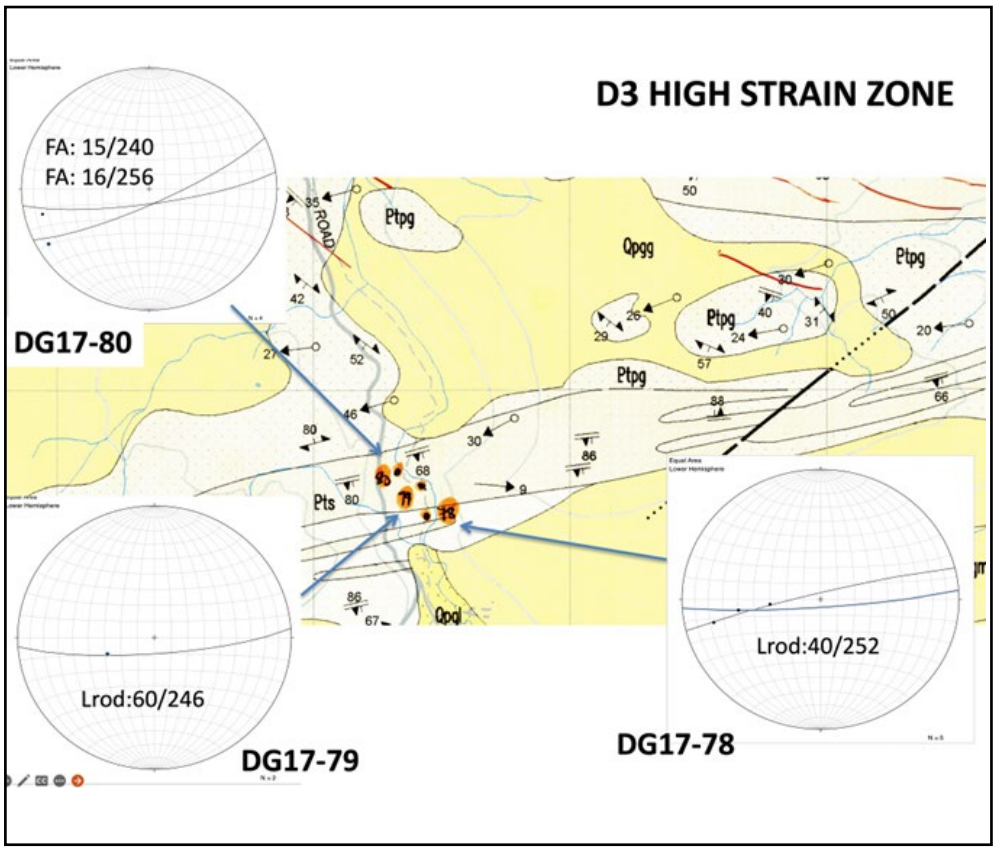

Figure 53 (Left). Map of the Waldheim High Strain Zone in the region where the zone is cut by Ronny Creek. Base map is the MRT 1:25,000 digital atlas. Inset stereonets show the generally steeply south dipping transposition foliation and the moderately to steeply west plunging contained rodding lineation

Figure 54 (Below). Intense north - dipping transposition foliation with lenticular strung out quartz veins in Sm. Outcrop along Dove Lake Boardwalk just north of Roddy Creek carpark.

Narrow local zones of high strain, characterised by intense transposition foliation, rootless isoclinal folds, are part of a transitional zone into the chevron folds at Crater Lake and Hansons Peak (Figures 55, 56, 57, 58, 59 and 60). This marginal zone through Wombat and Crater Peaks shows variable strain with zones of less intense foliation alternating with zones of intense foliation (Figures 55, 56 and 57). The areas of intense foliation show moderately to steeply plunging mineral/stretching lineations and a spread of isocline fold axis plunges within the enclosing foliation (Figure 57a, b). The isoclines have flattened and attenuated form (Figures 57 and 58) and are enveloped by the transposition foliation (Figure 59 and 60) to give an anastomosing network at the outcrop scale (Figure 57). This is repeated at scales > 100's metres across the transitional zone.

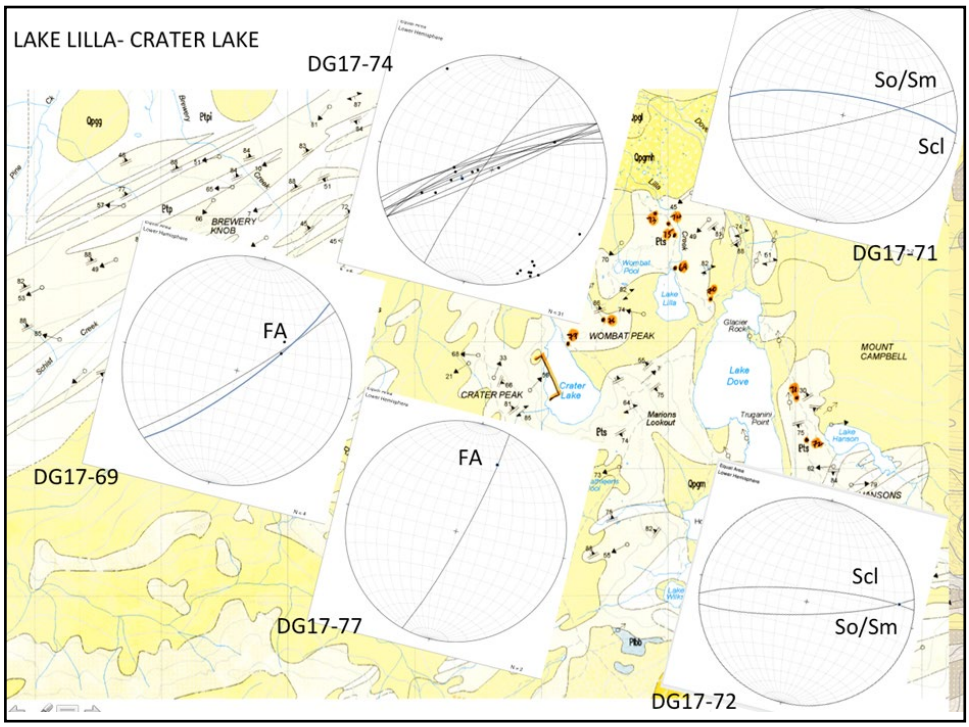

Figure 55 (Left). Map of the transitional zone from the Waldheim High Strain zone through to the Crater Lake Folded Zone. Base map is modified from the Mineral Resources Tasmania 1:25,000 scale digital atlas.

Figure 56 (Below). Structural map and data of the Lake Lilla track, from the Overland Track board walk to Lake Lilla. a) Structural map with pavement outcrop sketches (plan view) and structural attitude data for the outcrop stations DG17-73, DG17-74, DG17-75 and DG17-69. b), c), d) and e are stereonets of the structural data from these outcrop stations.

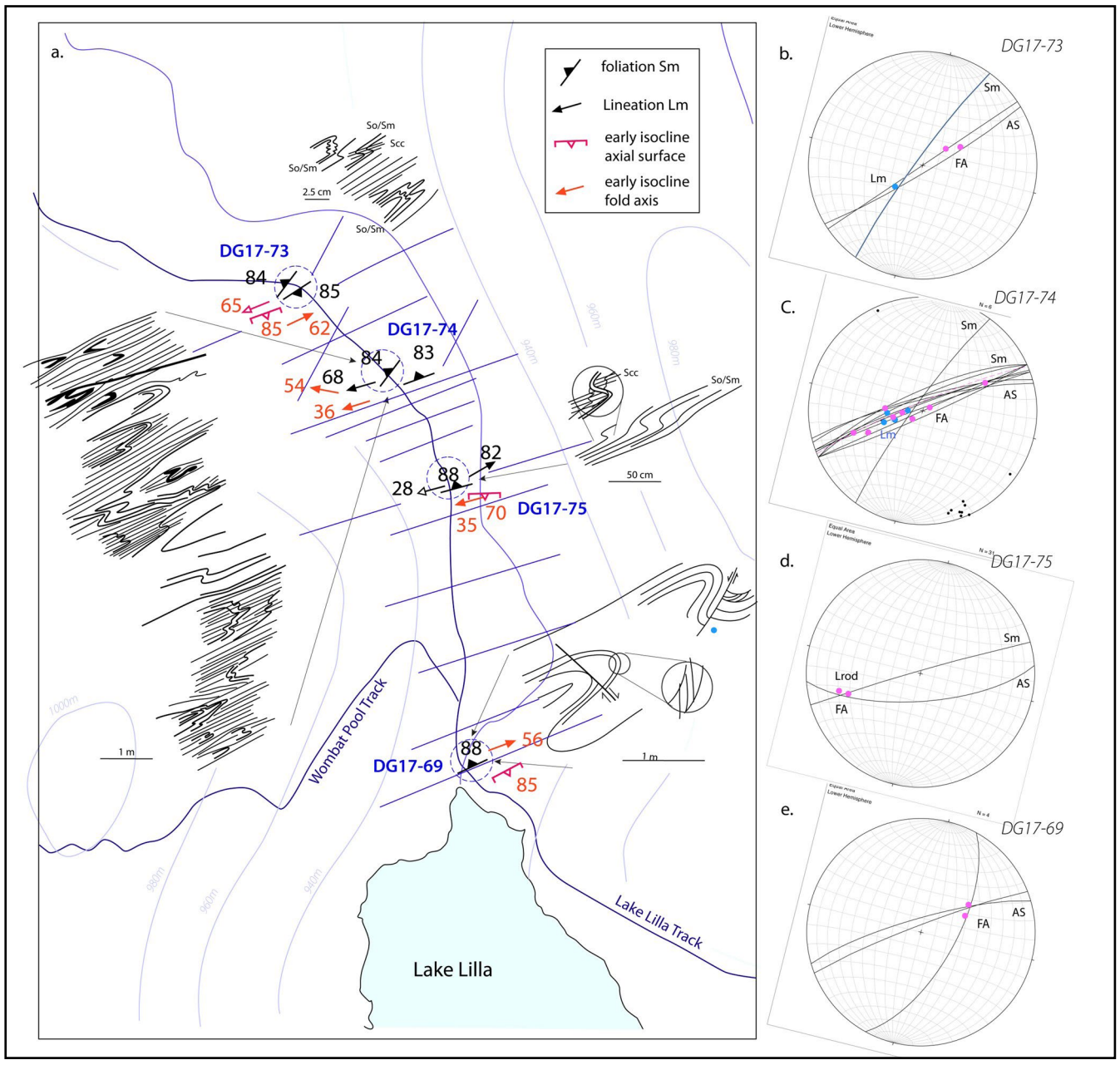

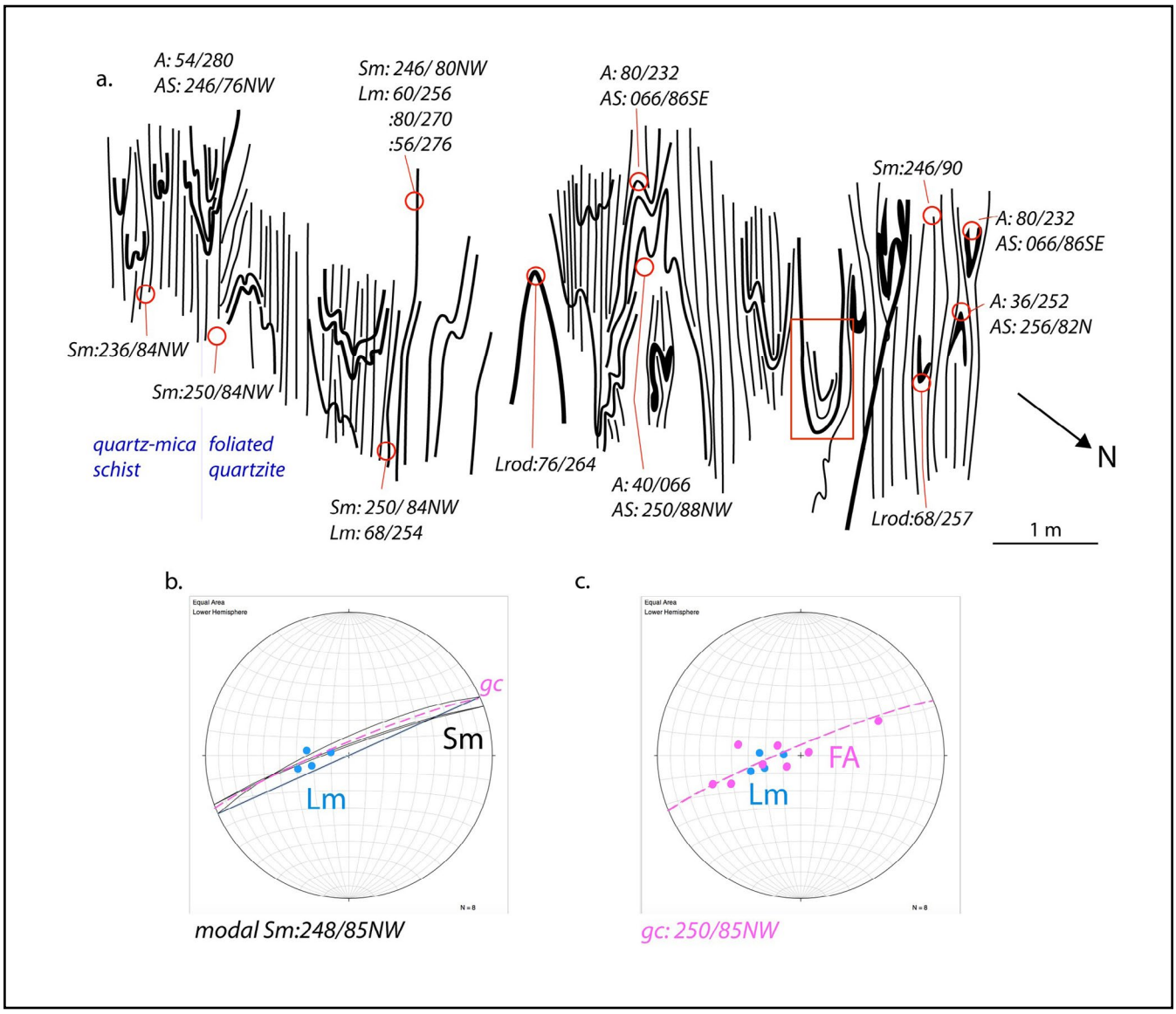

Figure 57. High strain zone along the Lake Lilla track (DG17-74). a) Track pavement map of an intensely foliated high strain zone showing stretched and dismembered isoclinal folds in thin quartzite layers within foliated quartzite (main part of map) and quartz-mica schist (map left). The fold nose highlighted by the red rectangle is shown in Figure 58. The complex, composite nature of the dominant foliation Sm in the quartz-mica schist is shown in Figure 59. b) Stereonet of Sm great circle traces (gc) and lineation Lm data (blue dots) from the map area. c) Stereonet of fold axis (FA) data (pink dots) with lineation (Lm) data (blue dots) superimposed. All structural data are with respect to magnetic north.

The Crater Lake - Hansons Peak - Twisted Lake Folded Zone

The Crater Lake - Hansons Peak - Twisted Lake Folded Zone (eastern part of Area 3a, Figure 16) consists of upright chevron folds that coaxially refold the early F1/F2 isoclinal folds within a quartzite-pelite sequence (Figures 61 and 62). The Folded Zone is bound by the Waldheim High Strain Zone on the north and by the Lake Rodway High Strain Zone on the south (Figures 31 and 61). The zone is transitional eastwards with the Liena-Borradaile Chevron fold domain (Map Area 3b, Figure 16).

Some of the folds have tight to isoclinal form, such as the dominant folds in profile A-A' (Figure 62) and the fold between Marions Lookout and Wombat Peak that extends through the south wall of Crater Lake cirque (Figures 61 and 63). These are considered F1/F2 folds that have been refolded by the more open F3 folds.

The Hansons Peak profile (photo profile PP1, Figure 64) and map (Figures 63 and 65) show the interpreted F1/F2 chevron folds plunging into Dove Lake at 35° to 50° with a β axis of 49°/257° (stereonet upper left, Figure 65). The mineral stretching lineation Lm and the rodding lineation Lrod are sub-parallel and cluster about the β axis (stereonet lower left, Figure 65). Small F3 folds are also coaxial with the β axis (F1/F2). Intrafolial, mesoscopic asymmetric isoclinal folds occur within schistose quartzite along the steeply dipping limbs of these folds (Figure 66). Between Truganini Point and Hansons Lake the Hansons Peak track below Mt Campbell (Figure 63) exposes schistose quartzite (Pts) with an intense, sub-vertical transposition foliation Sm and strung out quartz veins and rootless isoclinal fold pairs in quartz veins (Figure 67). This dominant transposition foliation is overprinted by a steeply north-dipping discrete cleavage (Scl) that is associated with the F3 folding.

Figure 58. Isoclinal fold hinge within the Lake Lilla track high strain zone (see Figure 57 for location). The fold is steeply plunging and has flattened form with long sub-parallel limbs that are enveloped by an intense transposition layering with disrupted and stretched quartz veins.

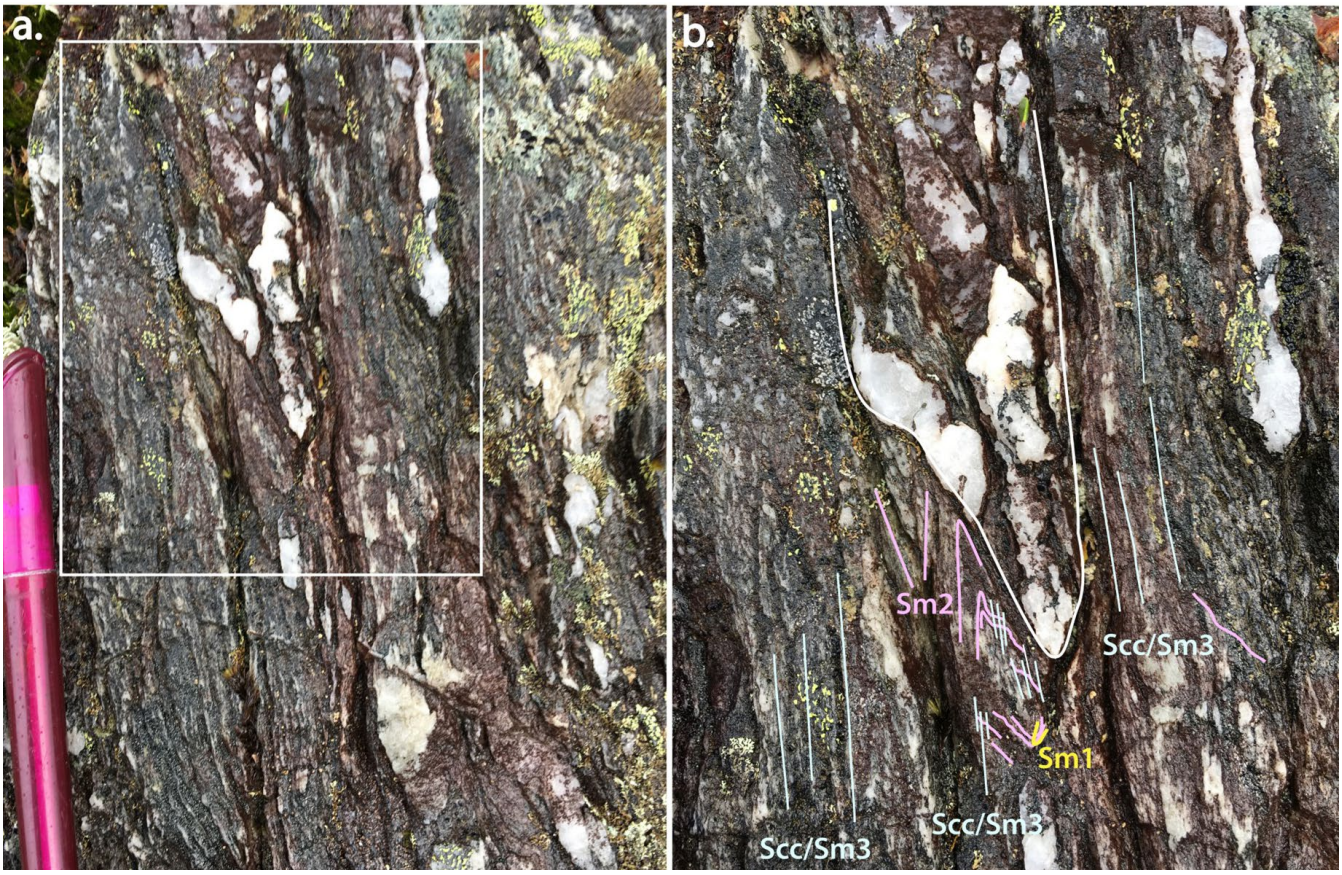

Figure 59. Intense sub-vertical, transposition layering in mica-quartz schist at the south end of the Lake Lilla high strain zone (see left side of Figure 56a). a) Disrupted, isoclinally folded quartz veins within the composite but dominant foliation Sm. b) Enlargement of part of (a) showing the composite, complex nature of overprinting foliations that make up the dominant foliation (Scc/Sm3: blue line traces). An early fabric Sm1 (yellow line traces) is folded by Sm2 (pink line traces) locally preserved within the hinge shadow zone of the folded quartz vein. All elements are enveloped by the dominant foliation Sm3 (blue line traces).

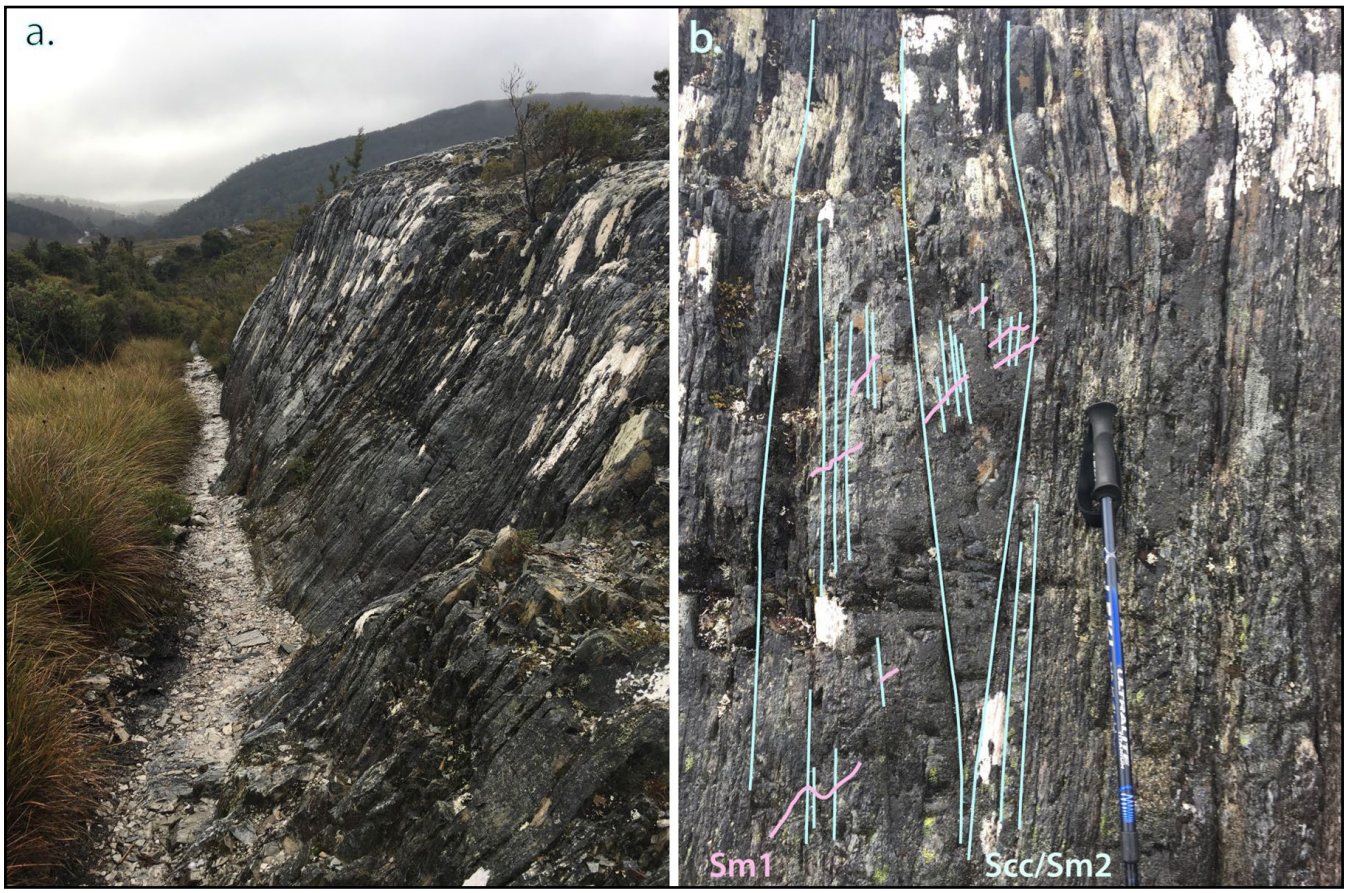

Figure 60. Intensely foliated quartzite along the Lake Lilla Track. a) Steeply dipping composite foliation in the glacially ice-sculptured quartzite wall along the track (location DG17-75, Figure 56). b) Foliated quartzite 15 m south along the track with strong to intense crenulation cleavage Scc/Sm2 (blue line traces) folding an earlier foliation Sm1 (pink line traces).

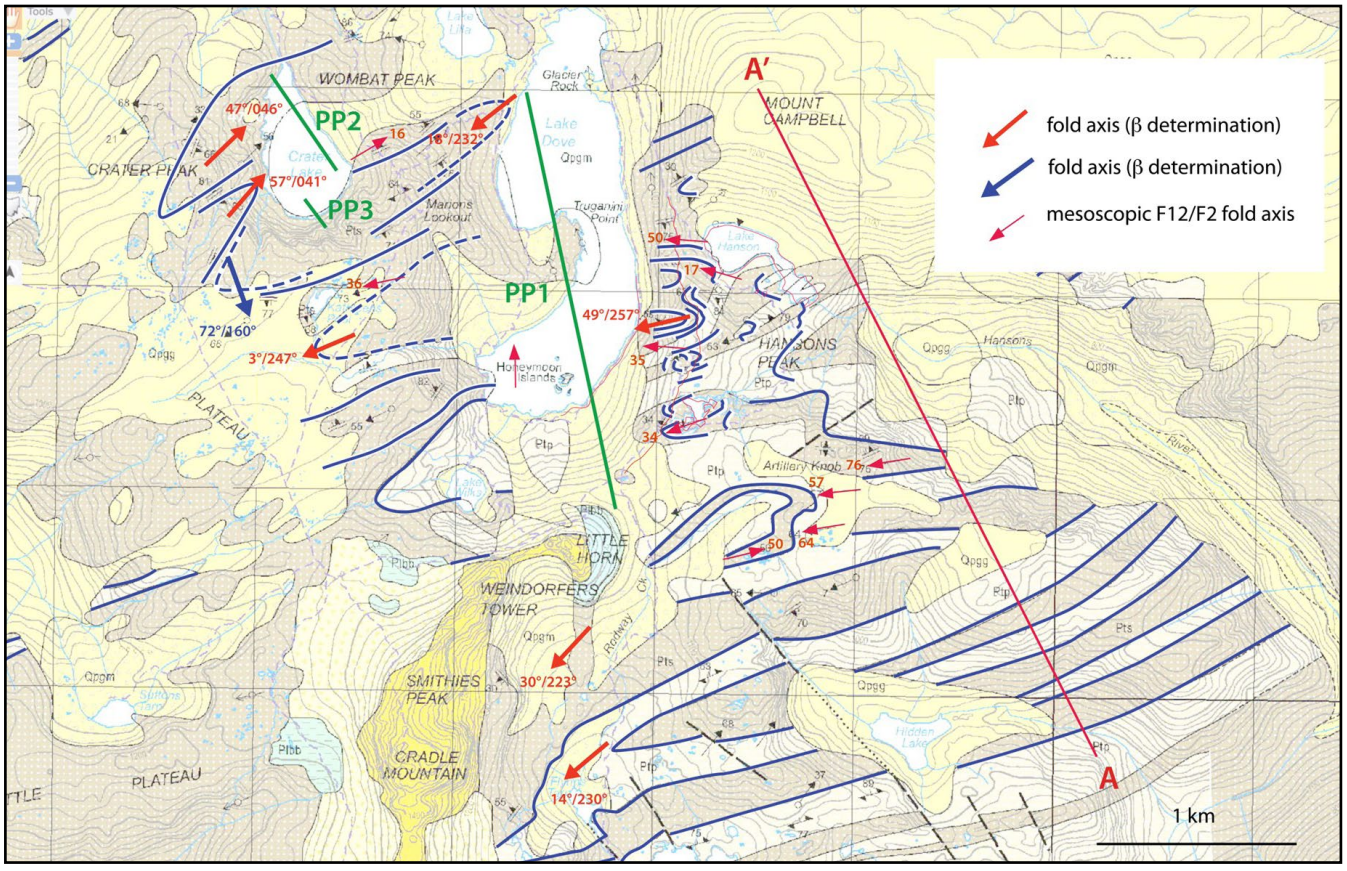

Figure 61. Fold axis and formline map of the Crater Lake-Hansons Peak-Twisted Lake Folded Zone. Base map is the MRT 1;25,000 digital atlas series. The red form line trace is the location of structural profile A-A' (Figure 62) an up plunge map projection profile. The positions of photo profiles PP1 (Figure 64), PP2 (Figure 69) and PP3 (Figure 70) are shown by the green line traces.

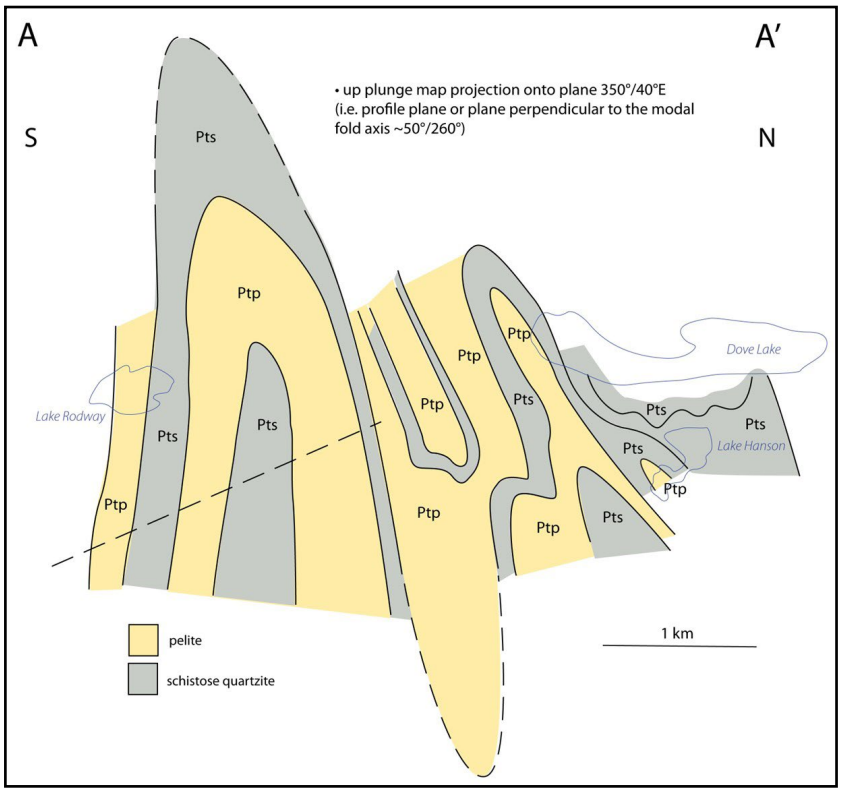

Figure 62 (Left). Tight to isoclinal, upright chevron fold geometry within the Crater Lake-Hansons Peak-Lake Rodway fold zone. The profile A-A' is an up-plunge map projection onto a 350°/40°E profile plane from the MRT digital atlas 1:25,000 map. The position of Dove Lake and Lakes Rodway and Hanson are shown in the tilted map projection. For profile location see Figure 61a (section A-A').

Figure 63 (Below). Structure and form line map of the Cradle Mountain-Dove Lake region with fold structures outlined on the east and west walls of Dove Lake glacial valley. The base map is from the MRT 1:25,000 digital atlas map series. The positions of photo profiles PP1 (Figure 64) and PP4 (Figure 71) are shown by the pink and blue line traces respectively.

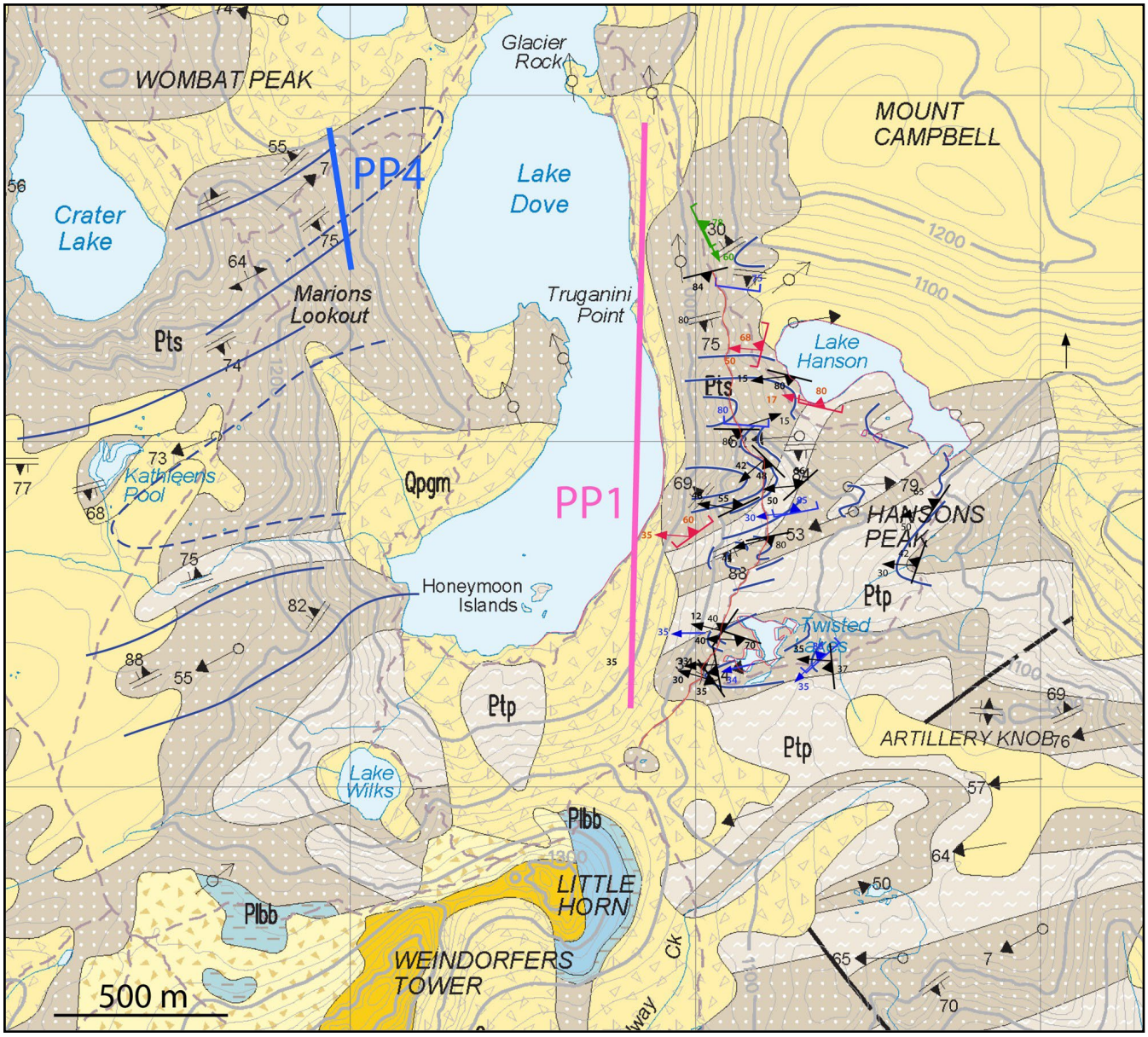

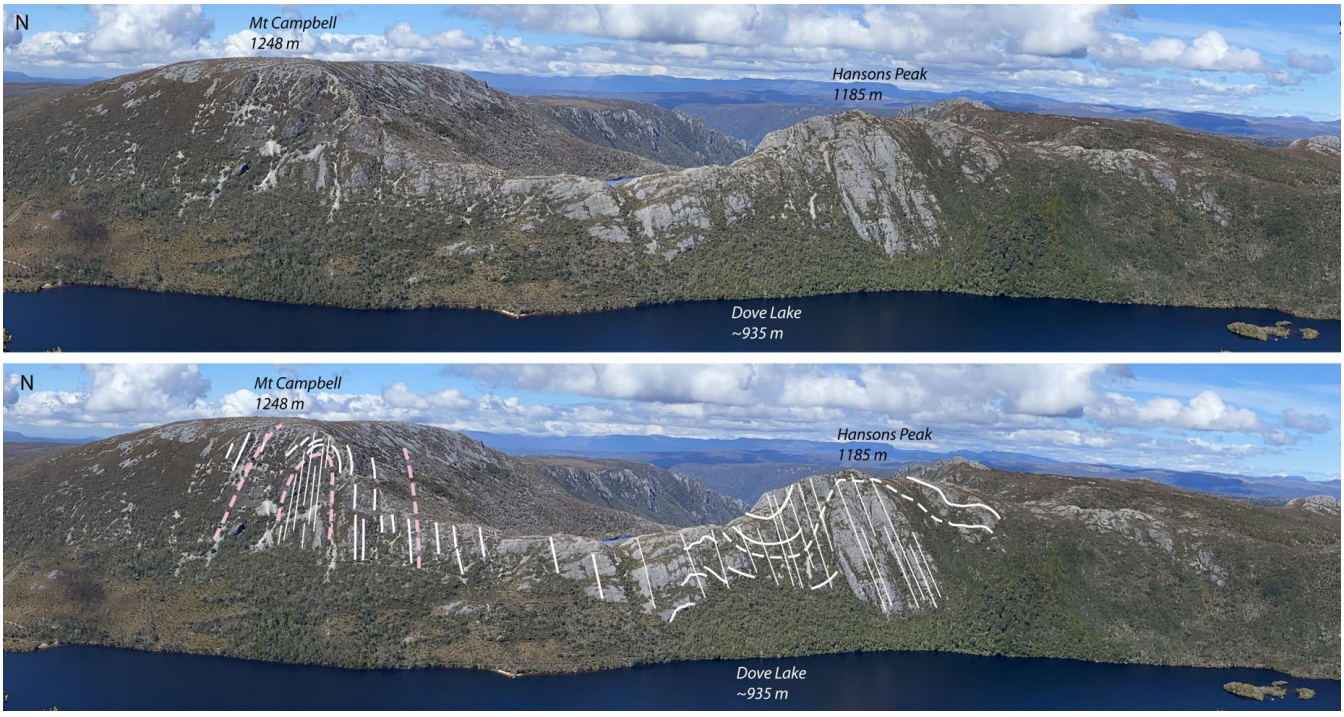

Figure 64. View of the east wall of the Dove Lake glacial cirque wall taken from Marions Lookout (looking east) with Mt Campbell on the left and Hansons Peak on the right (Photo profile PP1). The outlined folds are plunging west at 30°-50° into Dove Lake providing an oblique intersection of the folded So/Sm layering on the east wall of Dove Lake. The position of PP1 is shown on Figures 61 and 63.

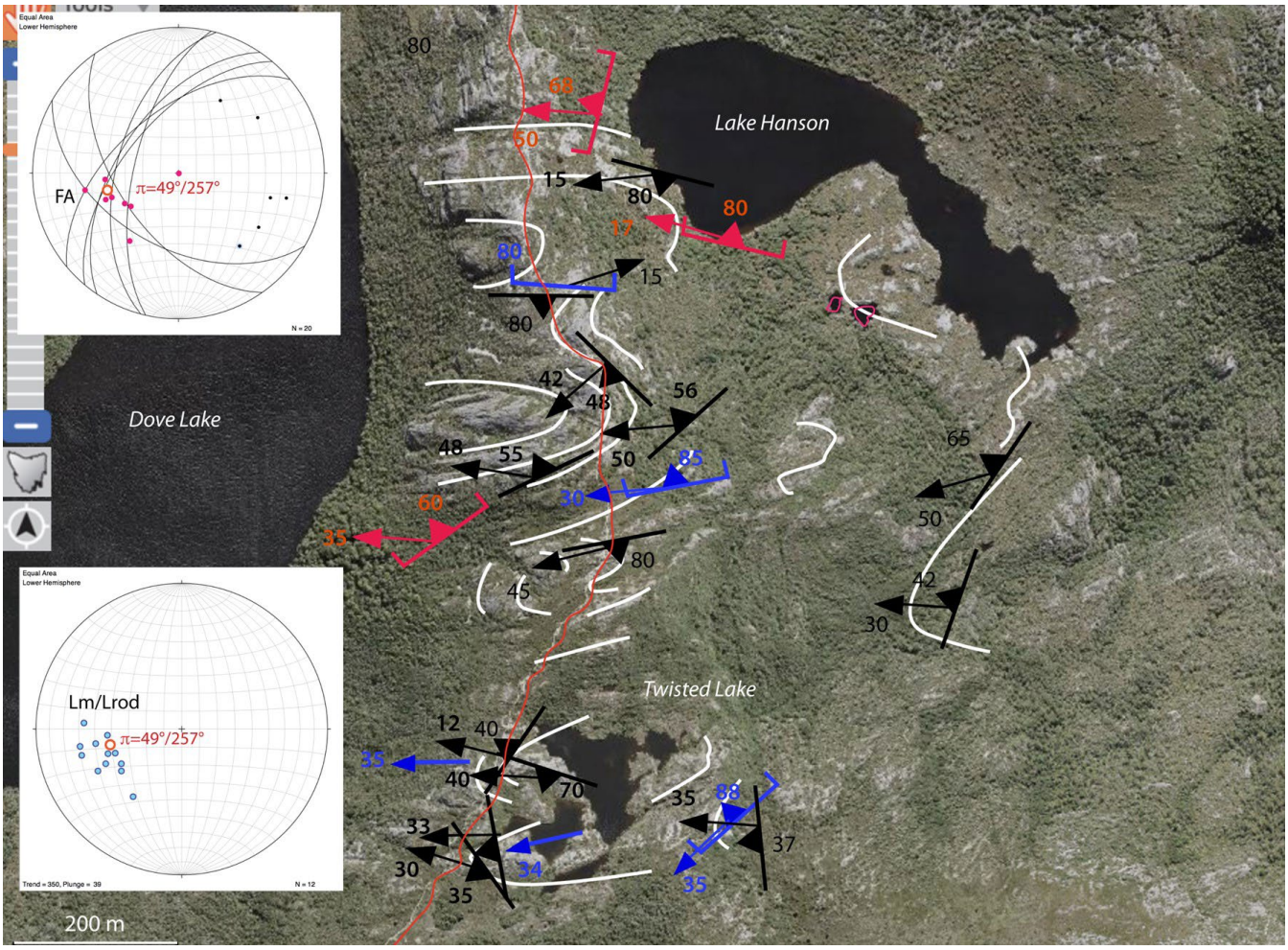

Figure 65. Structural map of the Lake Hanson-Hansons Peak-Twisted Lake area showing form lines in So/Sm (white line traces). Foliation dip and strike are shown by the black symbols with the mineral elongation lineation Lm shown by the black arrows. Isoclinal fold attitudes are shown by the red arrows (fold axis plunge) and red strike and dip symbols (axial surface attitude). Younger close to tight, upright F3 fold attitudes are shown by the blue strike and dip symbols (axial surface attitude) and the blue arrows (fold axis plunge). The inset strereonets show structural data measured across Hanson Peak.
Upper left: Fold axis (red dots) and So/Sm great circle traces with a β intersection of 49°/257°.
Lower left: Mineral lineation Lm and rodding lineation Lrod (blue dots).

Figure 66. Upright, intrafolial asymmetric folds within schistose quartzite along Hansons Peak ridgeline. Fold pairs are bounded by sub-vertical, intensely foliated, schistose quartzite.

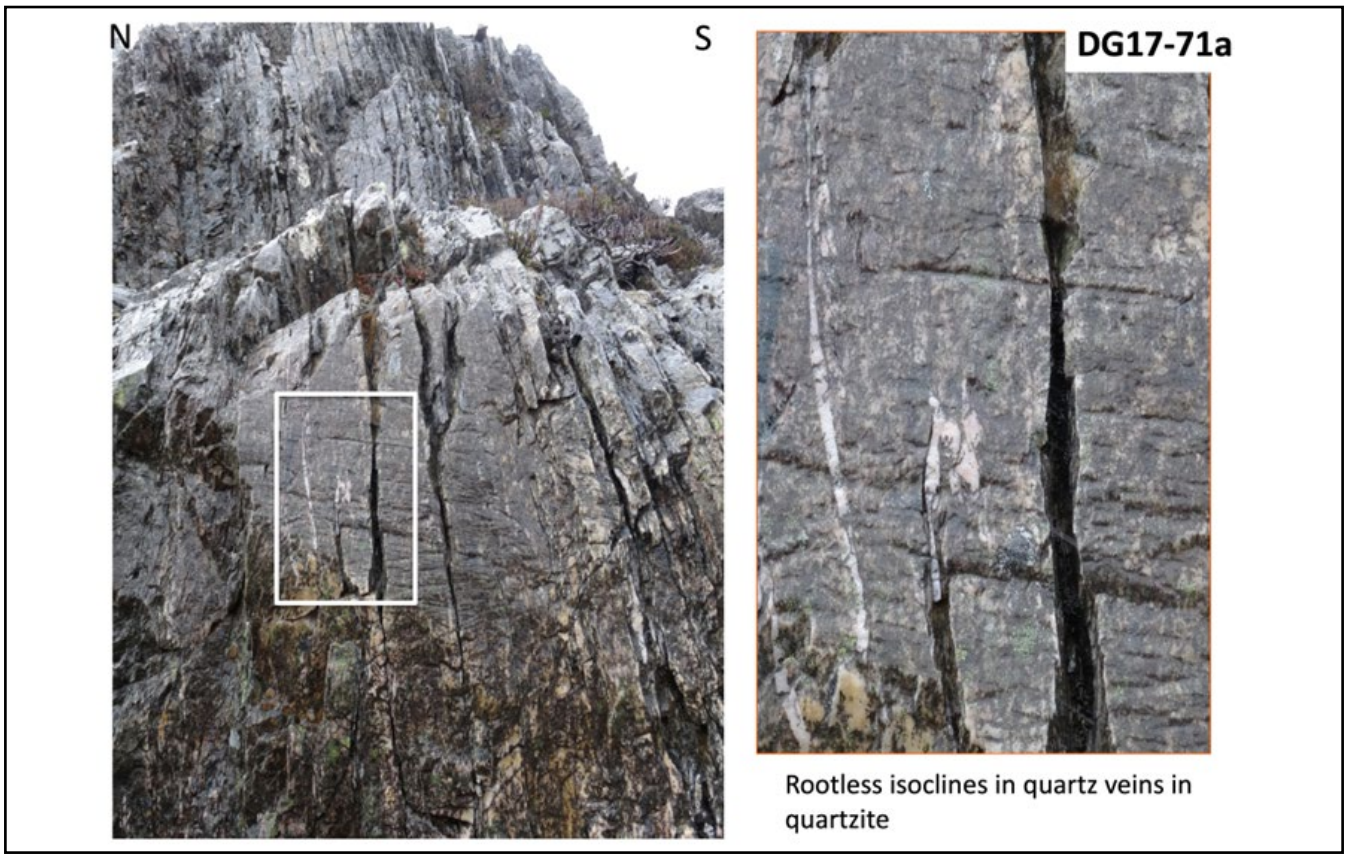

Figure 67. Schistose quartzite (Pts) with an intense, sub-vertical transposition foliation Sm overprinted by a steeply north-dipping discrete cleavage (Scl). The transposition foliation contains strung out quartz veins and rootless isoclinal fold pairs in quartz veins. b) is an enlargement of the white rectangle area in (a).

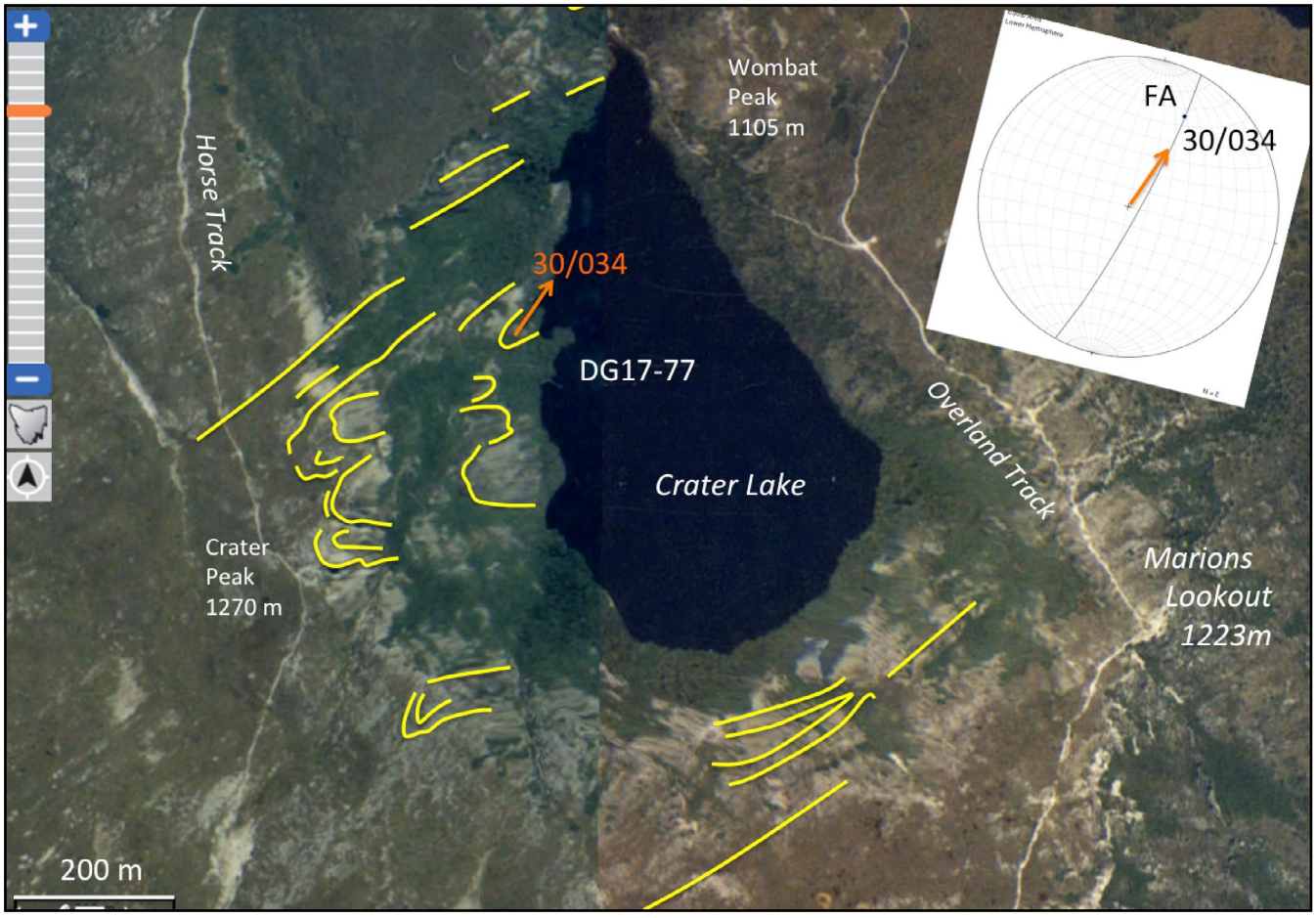

Figure 68. Satellite image of Crater Lake and surrounds showing the Overland Track (white track east of Crater Lake) and Marions Lookout (whitish area at bend in the Overland Track on image bottom right). Form lines in So/Sm are shown by the yellow line traces. The plunge of the antiformal fold hinge line shown in Figure 70 is shown by the red arrow. The recumbent isoclinal fold shown in Figure 69 occurs in the southern wall of Crater Lake glacial cirque. The stereonet (upper right) shows the estimated axial surface attitude and fold plunge) of the antiformal fold.

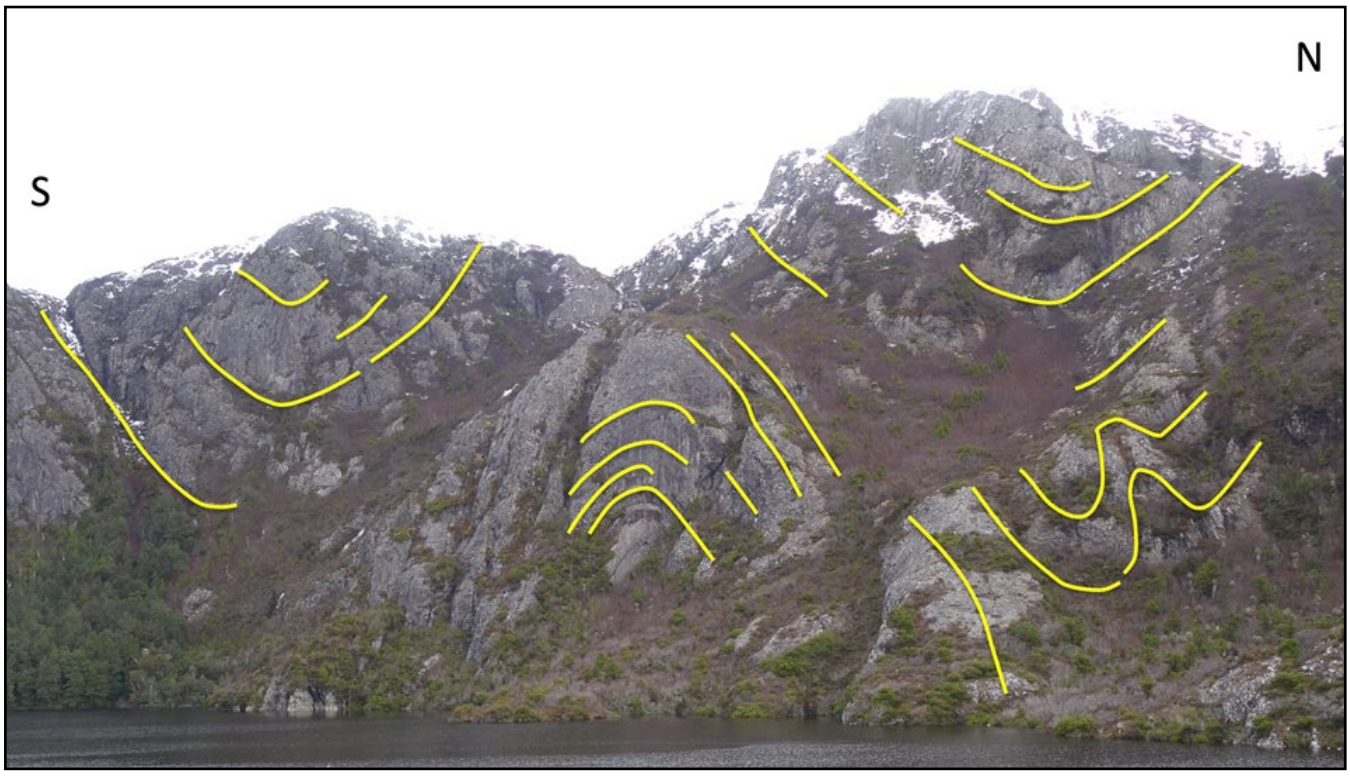

Figure 69. Tight to open, upright folds within the west wall of the Crater Lake cirque. Photo profile PP2 (for location see Figure 61). The central antiformal fold (photo middle) is plunging into Crater Lake at ~30°.

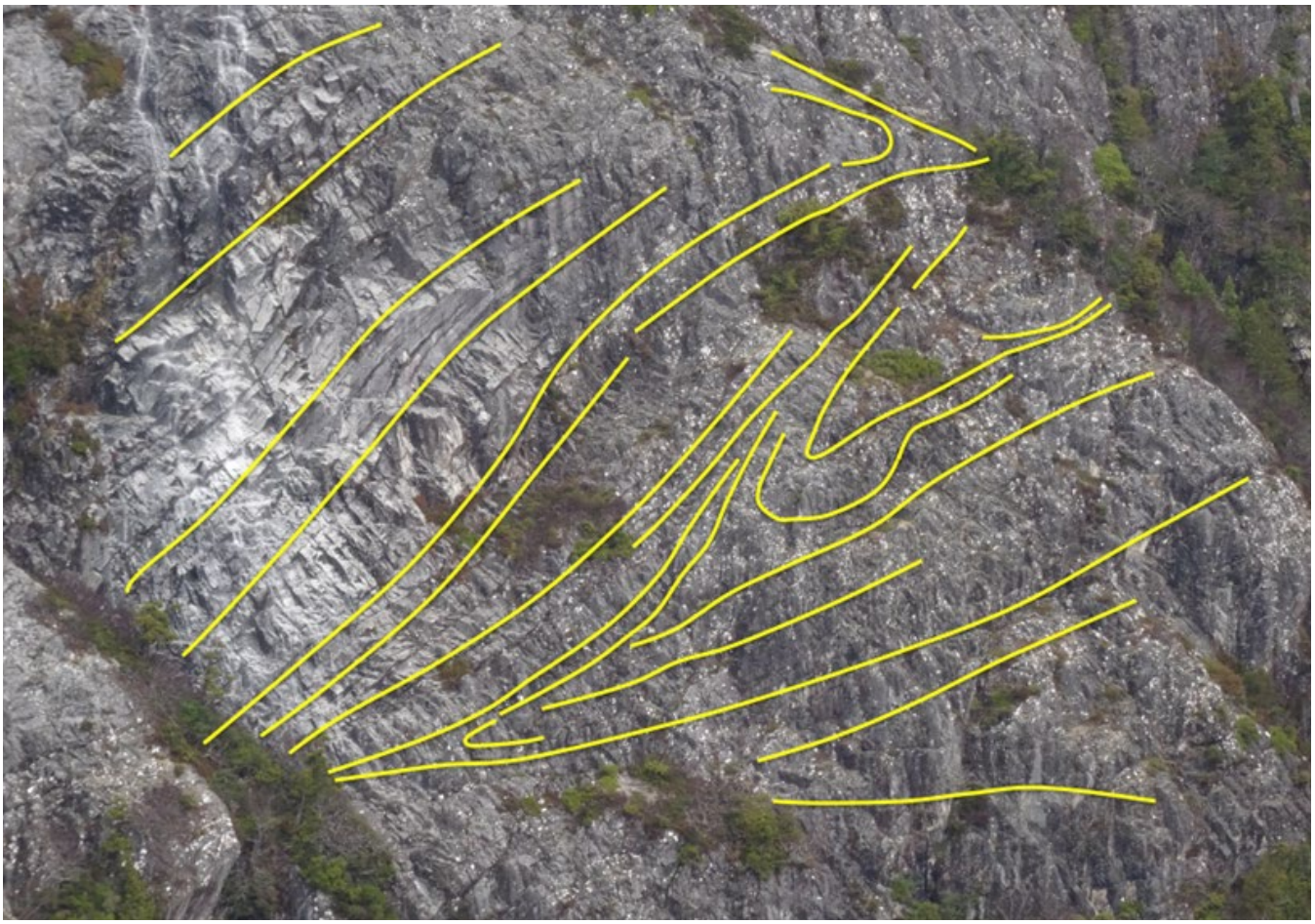

Figure 70. An oblique section of isoclinal folds exposed within the south wall of the Crater Lake cirque. Photo profile PP3 (for location see Figure 61). These early folds are refolded by the upright folds visible in the west wall of Crater Lake cirque (Figures 68 and 69).

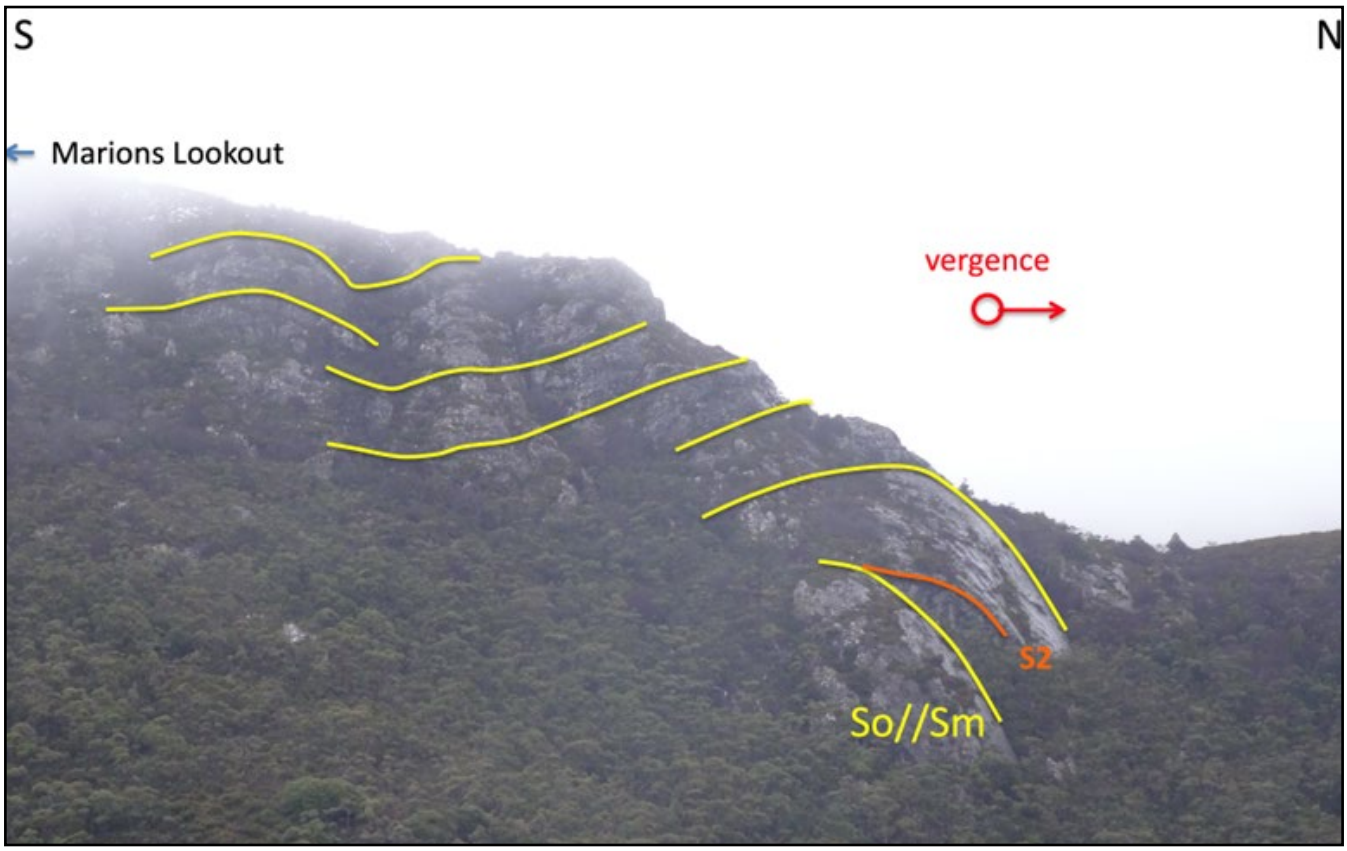

Figure 71. Broad open, upright warps within the west wall of the Dove Lake cirque valley. The ridgeline separates the Crater Lake cirque and the Dove Lake valley. These folds are a continuation of folds exposed in the west wall of Crater Lake cirque. The S2 foliation angular relationship with So/Sm indicates a clockwise rotation of S2 requiring a north-closing recumbent fold hinge to the north (see dashed fold hinge in Figure 63).

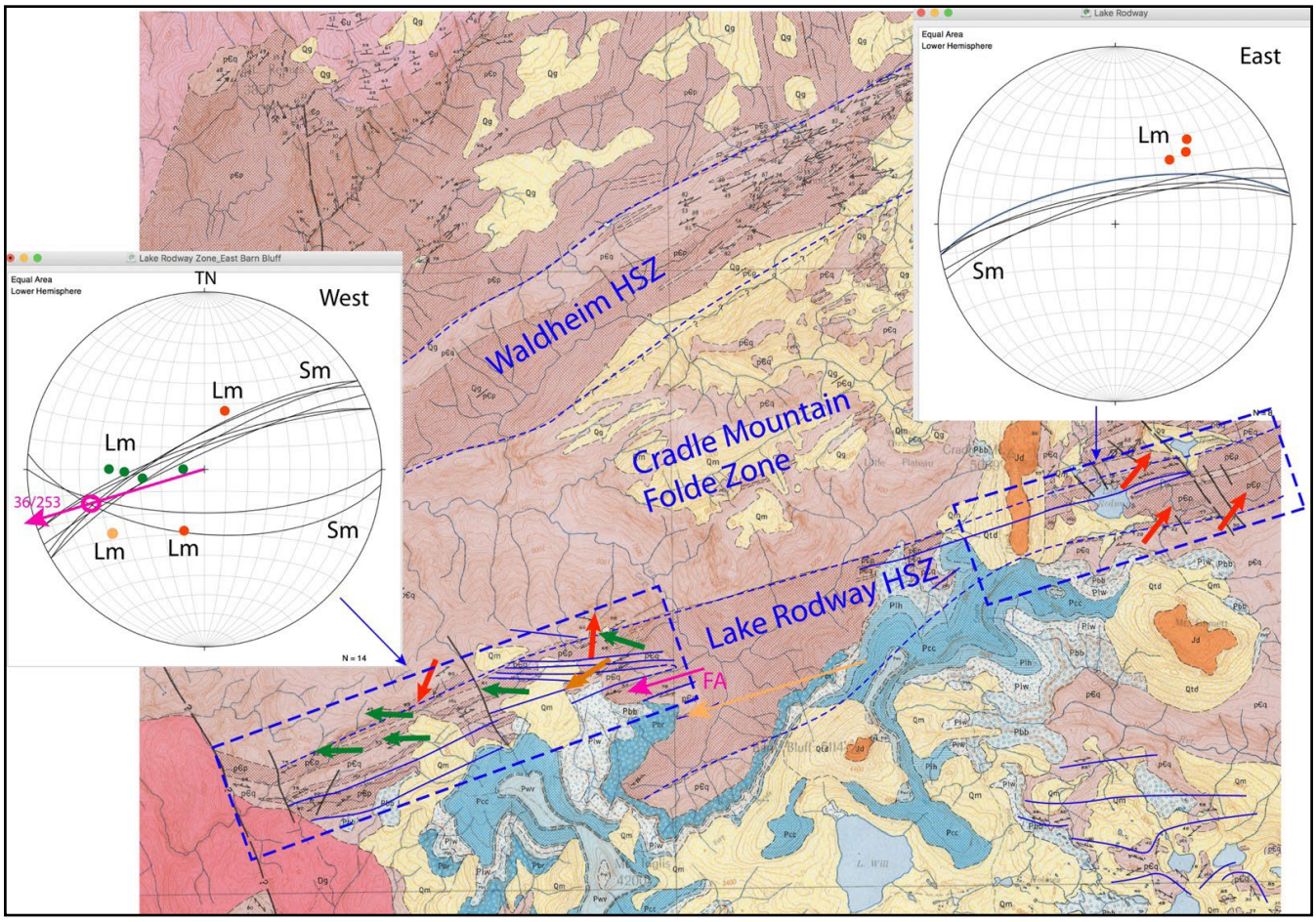

Figure 72. The Lake Rodway High Strain zone defined on the Mackintosh 1:63,500 geological map sheet as base map. The dashed rectangles delineate the eastern and western parts of the zone. The inset stereonets show foliation Sm great circle traces and lineation Lm attitudes as green dots (west plunging) and red dots (northeast and southwest plunging). Tight to isoclinal folding in Sm is implied by the form lines (blue line traces) in the western part and a Beta axis of 36°/253°.

Open F3 folds are exposed in the west wall of Crater Lake (Figures 68 and 69). An oblique intersection of isoclinal F1/F2 folds can be seen in the south wall of Crater Lake (Figure 70).

Lake Rodway Zone

The Lake Rodway Zone (Element 4, Figure 16) is a pelite-dominated, steeply north dipping foliated zone with thin structurally intercalated quartzite bands (Figures 72 and 73). The zone shows both west plunging and north-east plunging stretching lineation directions that reflect isoclinal folding of the early-formed lineation (Figure 72).

5.3.2 Liena-Borradaile F3 Chevron Fold Zone (Area 3b, Figure 16)

The Liena-Borradaile F3 Chevron Fold Zone consists of steeply to moderately plunging F3 chevron folds with long straight limbs and narrow hinge zones (Figures 74, 75, 76 and 77). The significance of the F3 folding was previously recognised by Spry (1962) and Berry and Bull (2004). The overall form of the F3 folds is dependent on lithology. In thin-bedded quartzites the folds have tight chevron form (Figure 74 and 75), whereas in thicker bedded quartzites they have open antiformal hinges and narrow, pinched, cuspate synformal hinges (Figure 76).

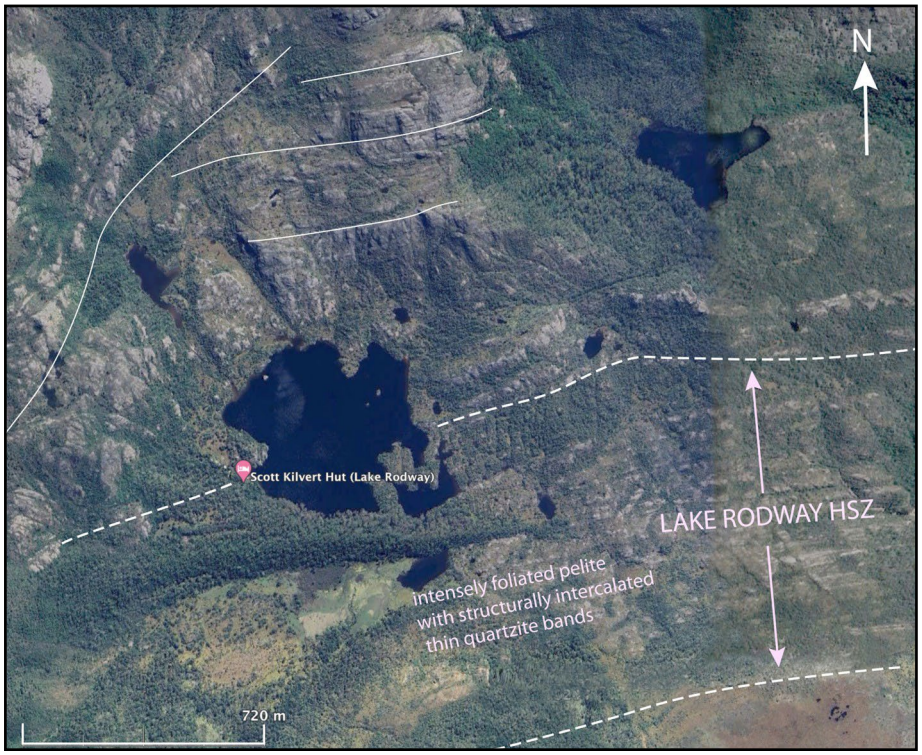

Figure 73 (Left). Google satellite image of the eastern part of the Lake Rodway High Strain Zone. The banded nature is reflected by structurally intercalated, thin, sub-parallel quartzite bands within the pelitic zone. The upper or northern part of the image shows the thicker banded quartzites of the Crater Lake-Hansons Peak Lake Rodway Folded Zone.

Figure 74 (Bottom left). Steeply plunging, mesoscopic isoclinal folds in thin-bedded quartzite. Location is south of Colorado Creek, east of the Mersey Valley road (437906E, 5390156N) (Photo credit: John Everard).

Figure 75 (Bottom right). Tight approaching isoclinal chevron fold form exposed in the west face of Little Plough Hill. Fold plunges are moderate to steep into and out of the face of the hillside (Photo credits: Grace Cumming).

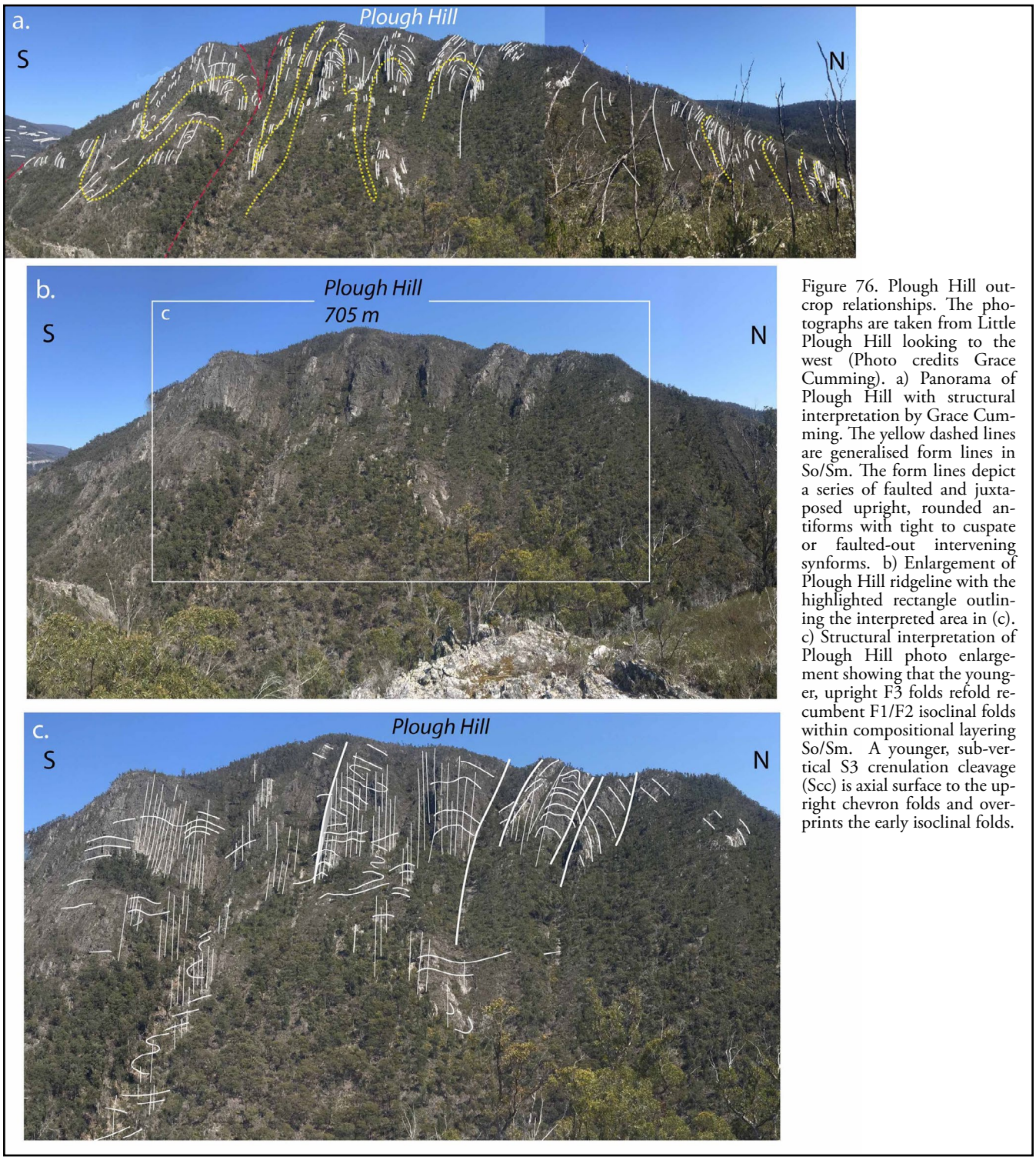

Figure 76. Plough Hill outcrop relationships. The photographs are taken from Little Plough Hill looking to the west (Photo credits Grace Cumming). a) Panorama of Plough Hill with structural interpretation by Grace Cumming. The yellow dashed lines are generalised form lines in So/Sm. The form lines depict a series of faulted and juxtaposed upright, rounded antiforms with tight to cuspate or faulted-out intervening synforms. b) Enlargement of Plough Hill ridgeline with the highlighted rectangle outlining the interpreted area in (c). c) Structural interpretation of Plough Hill photo enlargement showing that the younger, upright F3 folds refold recumbent F1/F2 isoclinal folds within compositional layering So/Sm. A younger, sub-vertical S3 crenulation cleavage (Scc) is axial surface to the upright chevron folds and overprints the early isoclinal folds.

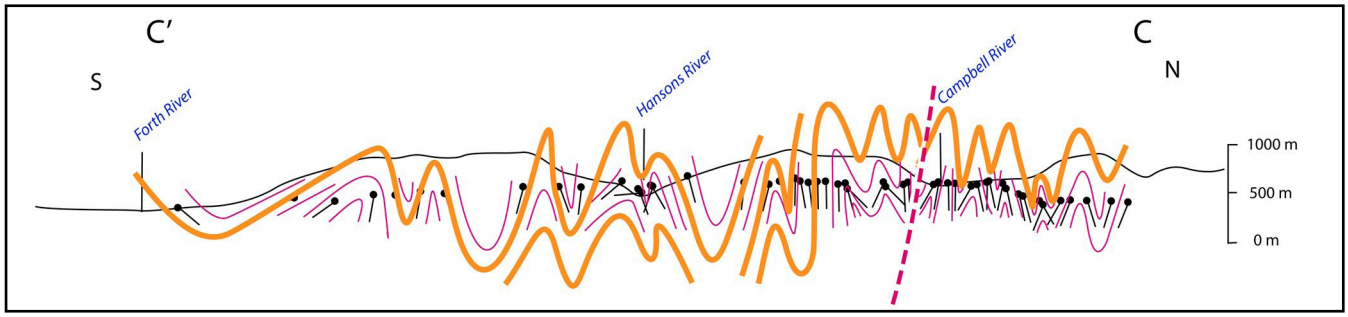

Figure 77. Typical chevron fold profile across the Liena-Borradaile F3 Chevron Fold Zone. The section was constructed using dip/apparent dip marker traces (black pins) and the outcrop traces defined during field mapping. Locally constructed form lines are shown by the pink lines traces. The heavy orange line traces show the overall regional fold geometry. The pink dashed line is a high angle reverse fault.

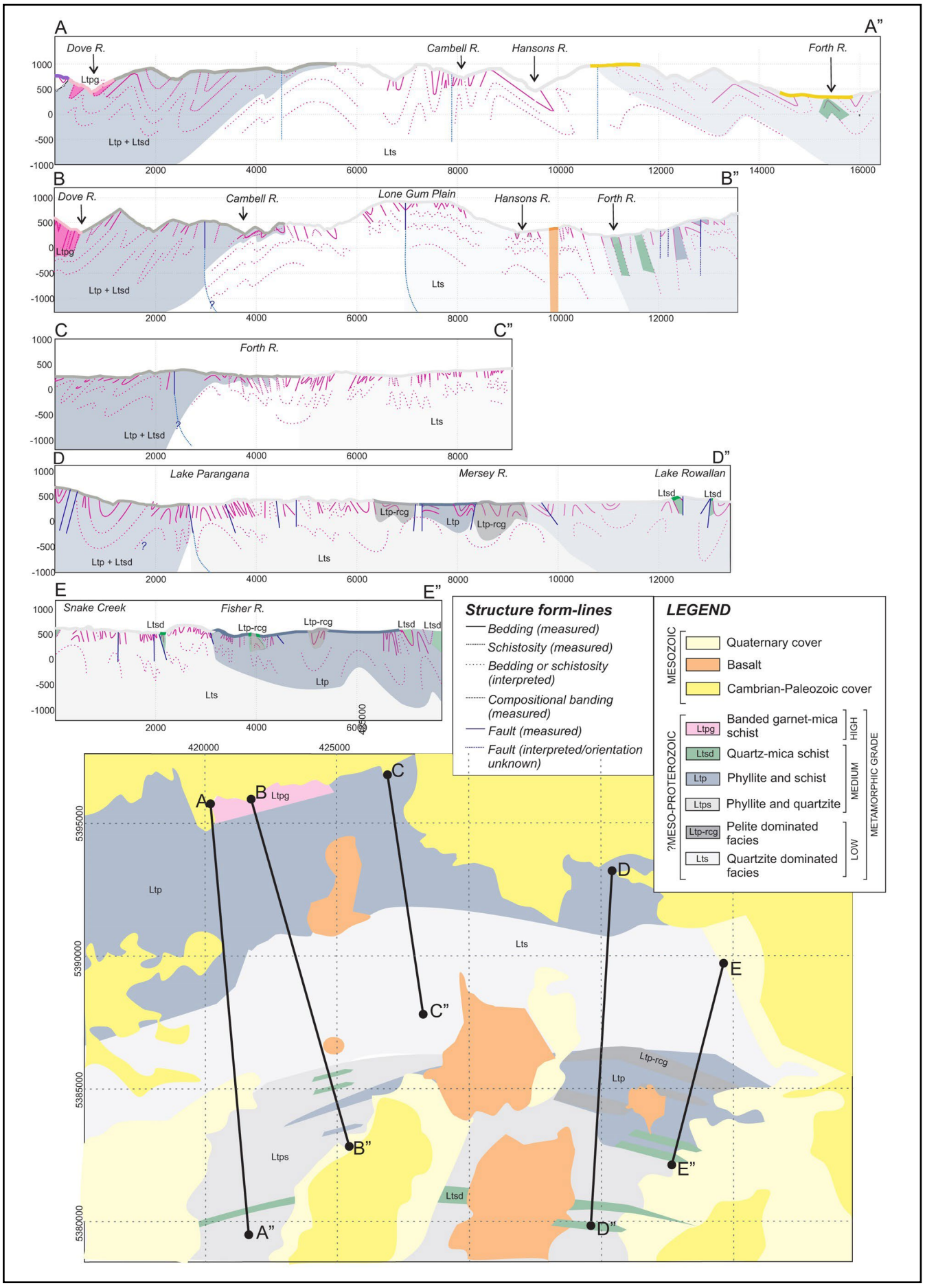

Figure 78. Structural profiles of the Liena-Borradaile F3 Chevron Fold Zone showing the complex chevron fold form of the folds and a series of broad anticlinoria and synclinoria. (Cumming et al., 2025).

The Liena-Borradaile F3 Chevron Fold Zone geometry is one of shear zone bounded lozenges containing steeply to moderately plunging chevron folds with curvilinear fold hinge lines (Figures 78, 79, 80, 81 and 82). The measured and derived individual macro-fold fold hinges/axes show complex and extremely variable fold geometry (Figures 79, 80 and 81). The overall geometry consists of a series of interpenetrating upwards-closing antiformal fold lobes in quartzite and downwards-closing synformal fold lobes in pelite (Figures 80 and 82), both folded within a broad anticlinoria and synclinoria pair (Figure 78). The measured and derived individual macro-fold fold hinges/axes lie within a sub-vertical, east-west trending, steeply north-dipping plane (see stereonets, Figure 80) with the fold axis dispersion reflecting marked hinge line curvature with folding in general shear about a sub-vertical stretch.

The Liena-Borradaile F3 Chevron Fold Zone is dominated by younger, upright F3 chevron folds but there is clear evidence of early recumbent tight to isoclinal folds being refolded by the upright chevron folds. The eastern face of Plough Hill shows early isoclines being refolded by the upright F3 folds (Figure 76c). Along the Arm River a younger synform refolds an intermediate scale (10-20 m width) recumbent fold hinge with complex, mesoscopic, symmetrical M folds cut by a series of brittle faults (Figures 83 and 84).

A small metre-scale example of an antiformal F3 fold hinge in quartzite (Figure 85) shows a slightly fanned spaced cleavage (Figure 85a, b) and a folded lineation Lm (Figure 85c). Analysis of mud cracks on the folded bedding surface (Figure 86a, b) give a ~3:1 XZ strain that may largely reflect development of Sm and the contained Lm.

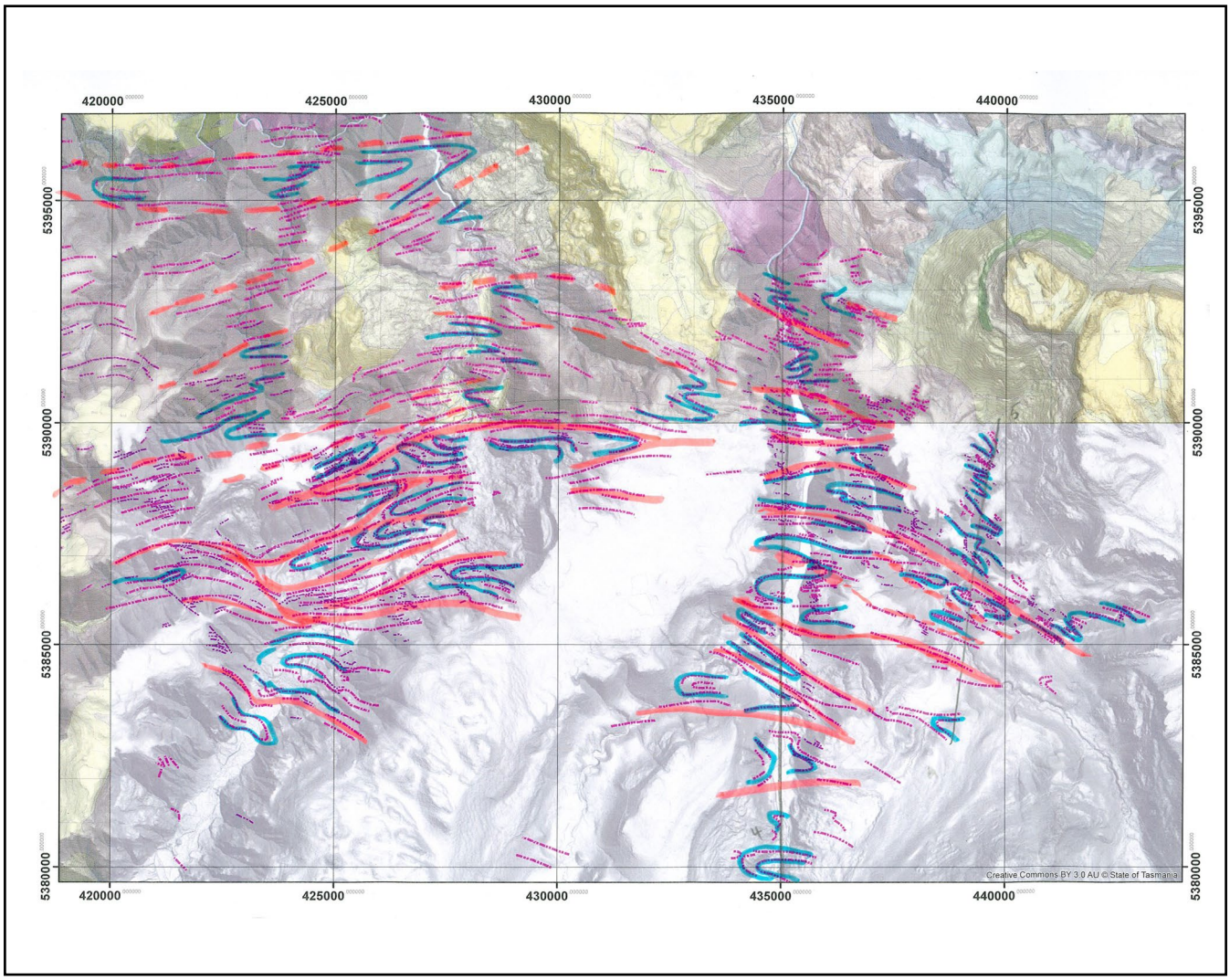

Figure 79. Liena-Borradaile F3 Chevron Fold Zone structure interpretation form line map (Cumming et al., 2025). Blue line traces: form lines in So/Sm. Pink line traces: high strain zones with intense Sm.

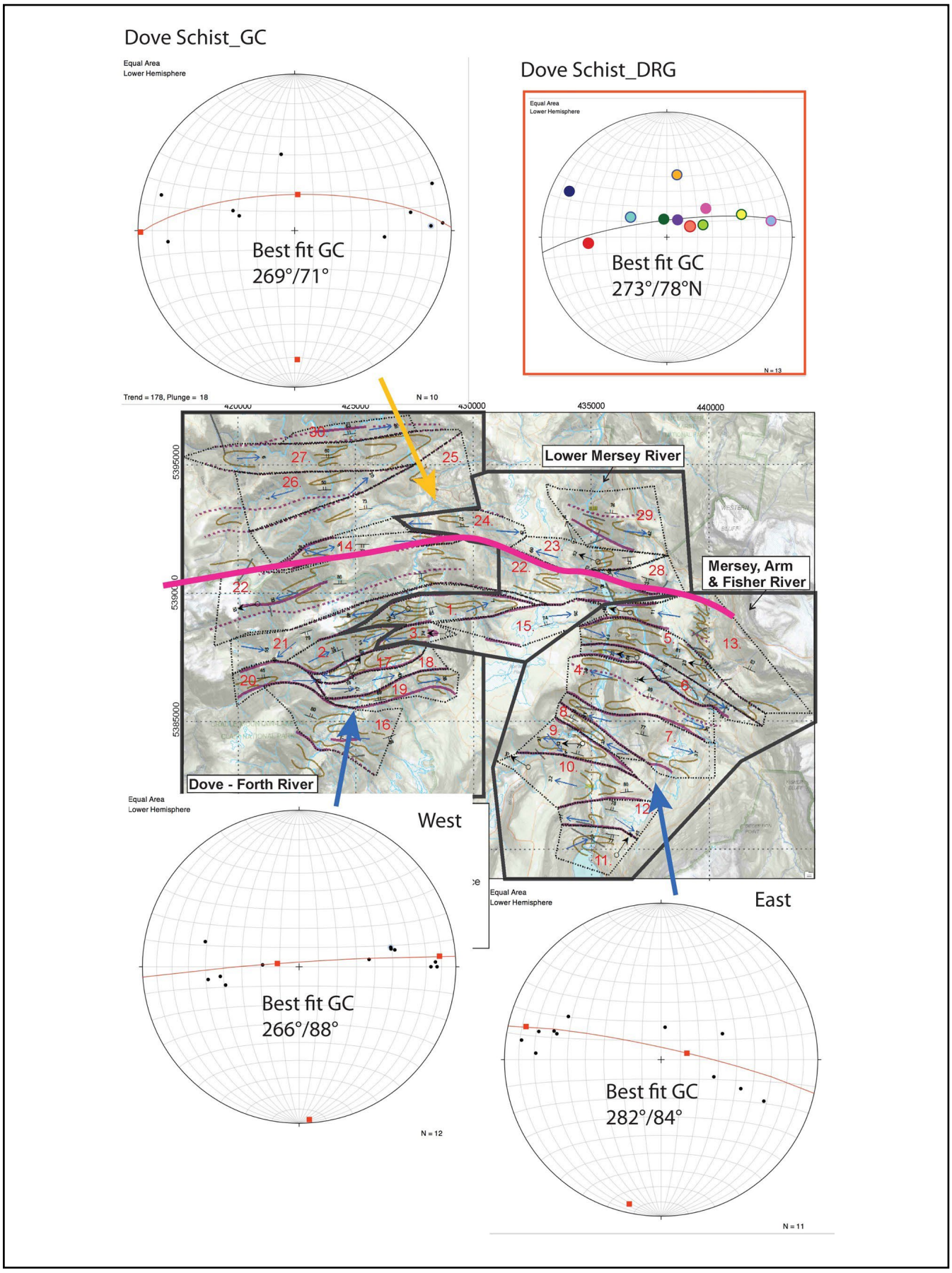

Figure 80. Liena-Borradaile fold hinge domains outlined by anastomosing high strain zone array. The heavy pink line is the southern contact of the Dove Schist. The domains outlined by the purple lines are commonly lozenge-shaped, with outcrop trace patterns of hinges are shown by the khaki line traces. Structural domains within the Liena-Borradaile F3 Chevron Fold Zone are outlined by anastomosing high-strain zone array. Within lozenges the modal fold plunges are shown by the blue arrows, the modal lineation Lm attitudes by the black arrows and the modal So/Sm attitudes by the black strike/dip symbol. The constructed 3D fold geometric elements for each domain are shown in Figure 81. The stereonets show the fold axis attitudes for the Dove Schist (above the pink boundary, the quartzite sequence west and east (below the pink boundary). For the Dove Schist hinge calculations by GC and DRG from So/Sm field measurements are plotted as separate stereonets (see Figure 45 for Dove Schist-DRG. plot).

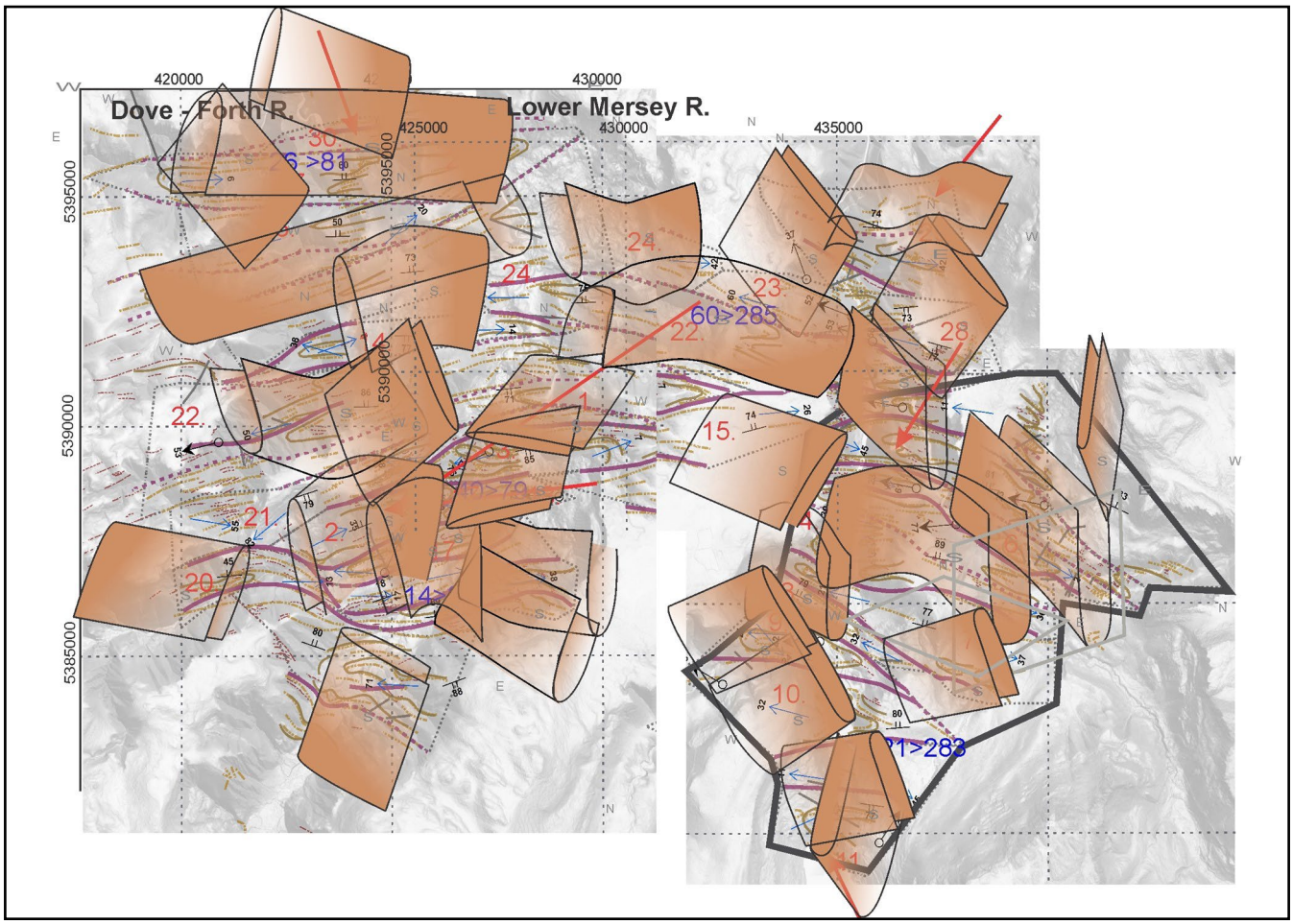

Figure 81. Individual fold-geometric elements and/or segments for the different domains highlighted in Figure 80. The elements have been constructed from the outcrop pattern and modal fold plunge within each lozenge (Cumming et al., 2025).

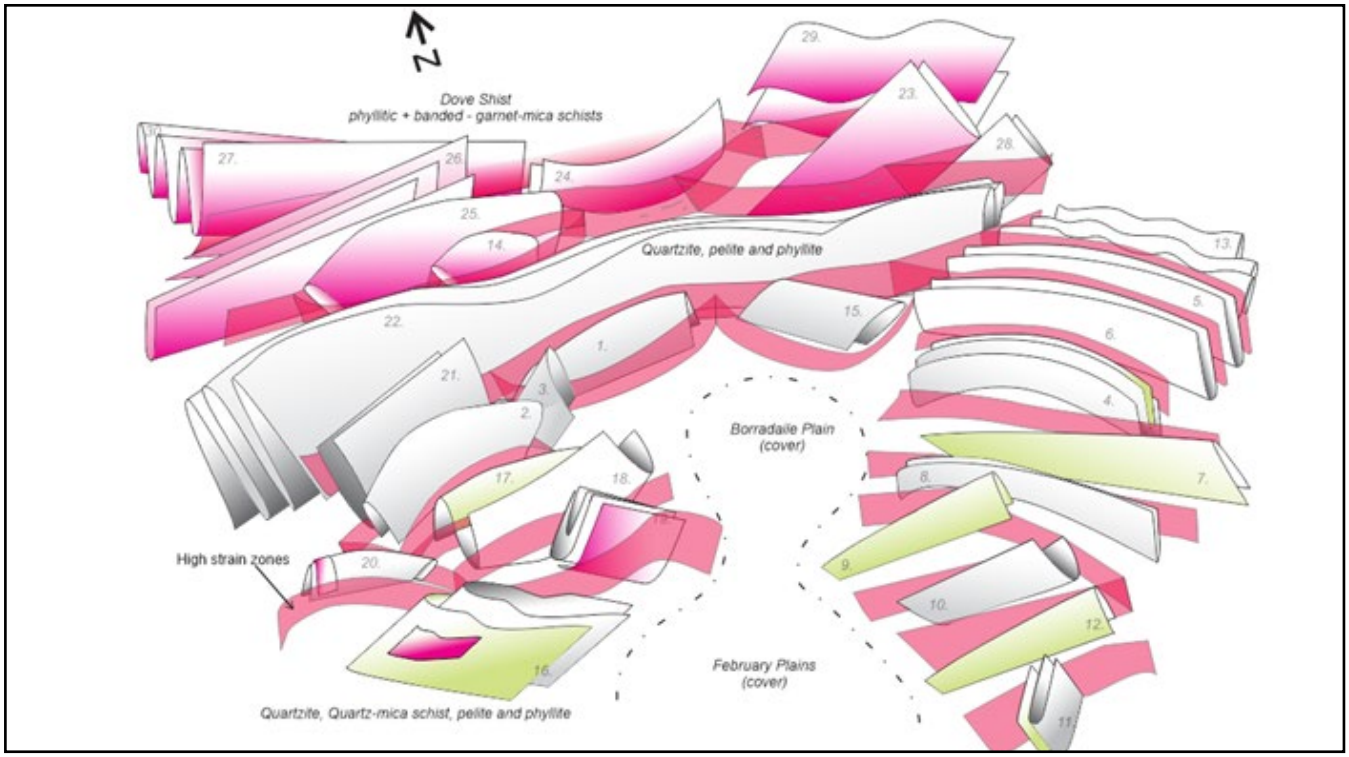

Figure 82. Schematic 3D geometric model of the complex folding across the Liena-Borradaile F3 Chevron Fold Zone. The diagram reflects the extremely irregular fold attitudes across the zone. The highlighted pink planes represent the high strain interfaces between the fold-hinge lozenges. Folds in the upper part of the figure highlighted by pink shading are within the high-grade Dove Schist. The fold elements with grey-green shading represent folds in the L-G quartzite, pelite and phyllite of the underlying rocks. (Figure from Cumming et al., 2025).

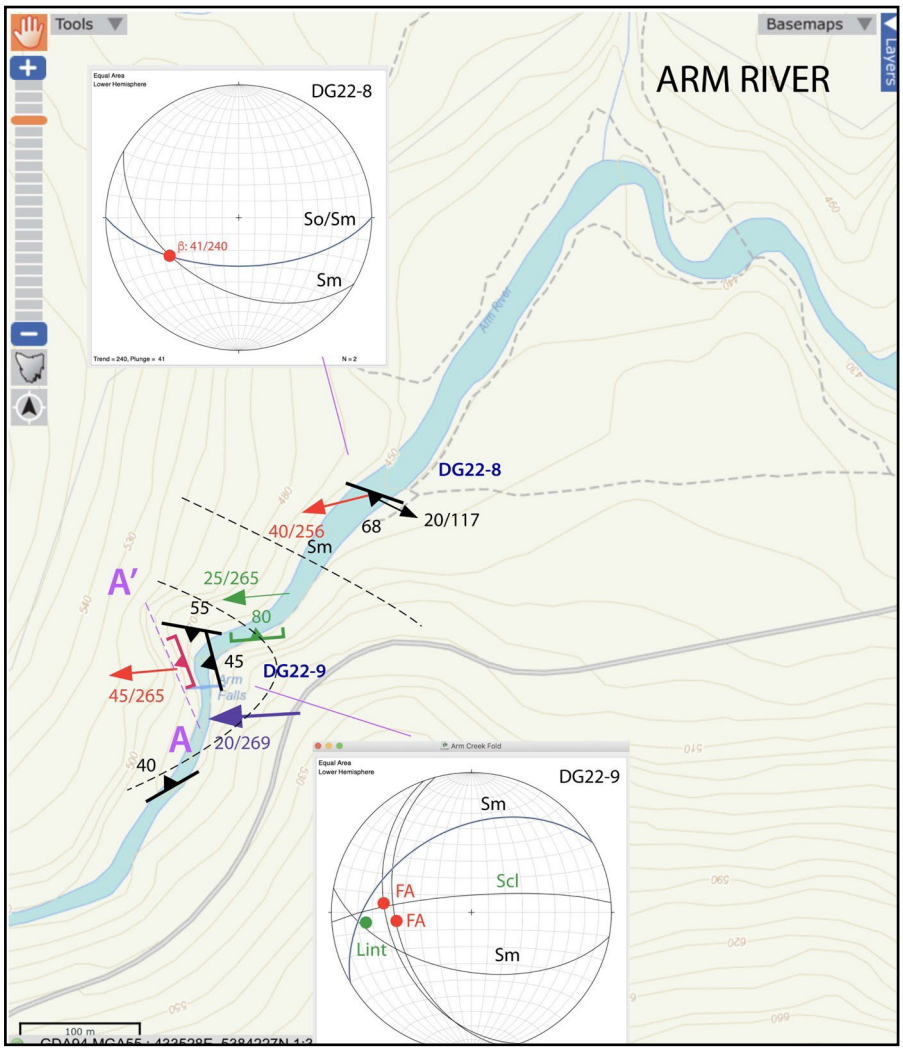

Figure 83 (Left). Structural map of a co-axially refolded early recumbent fold by a younger, west plunging F3 upright synformal fold highlighted by the Sm form lines (blue dashed lines). Both hinge zones can be seen in a cliff exposure on the Arm River (see Figure 84). The stereonets show the structural relationships at the two outcrop stations DG22-8 and DG22-9.

Map symbols: Red arrow and strike/dip symbol represent early isocline fold axis (FA) and axial surface attitude data. The green arrow and dip/strike symbol represent fold axis (Lint) and axial surface attitude data of the younger upright F3 fold.

Stereonet symbols: Red dots are measured fold axes (lower stereonet) and intersection lineation or equivalent fold axis (upper stereonet). The green dot (lower stereonet) is the intersection lineation for younger F3 fold axis. Scl is the younger fold axial surface cleavage (Scc3).

Figure 84 (Below). Cliff exposure on the Arm River. View is to the west. a) Upright, west plunging synformal closure in thick-bedded quartzite. The yellow dashed rectangle shows the F3 hinge area enlarged in (b). John Everard for scale. b) Detail of the early isoclinal folds within the hinge of the upright, west-plunging F3 synformal fold. c) F3 synformal closure at Arm River bend showing the line sketch of the folds and faults in (a). d) Stereonet of the Arm River bend folds showing the coaxial nature of the F2 and F3 folding.

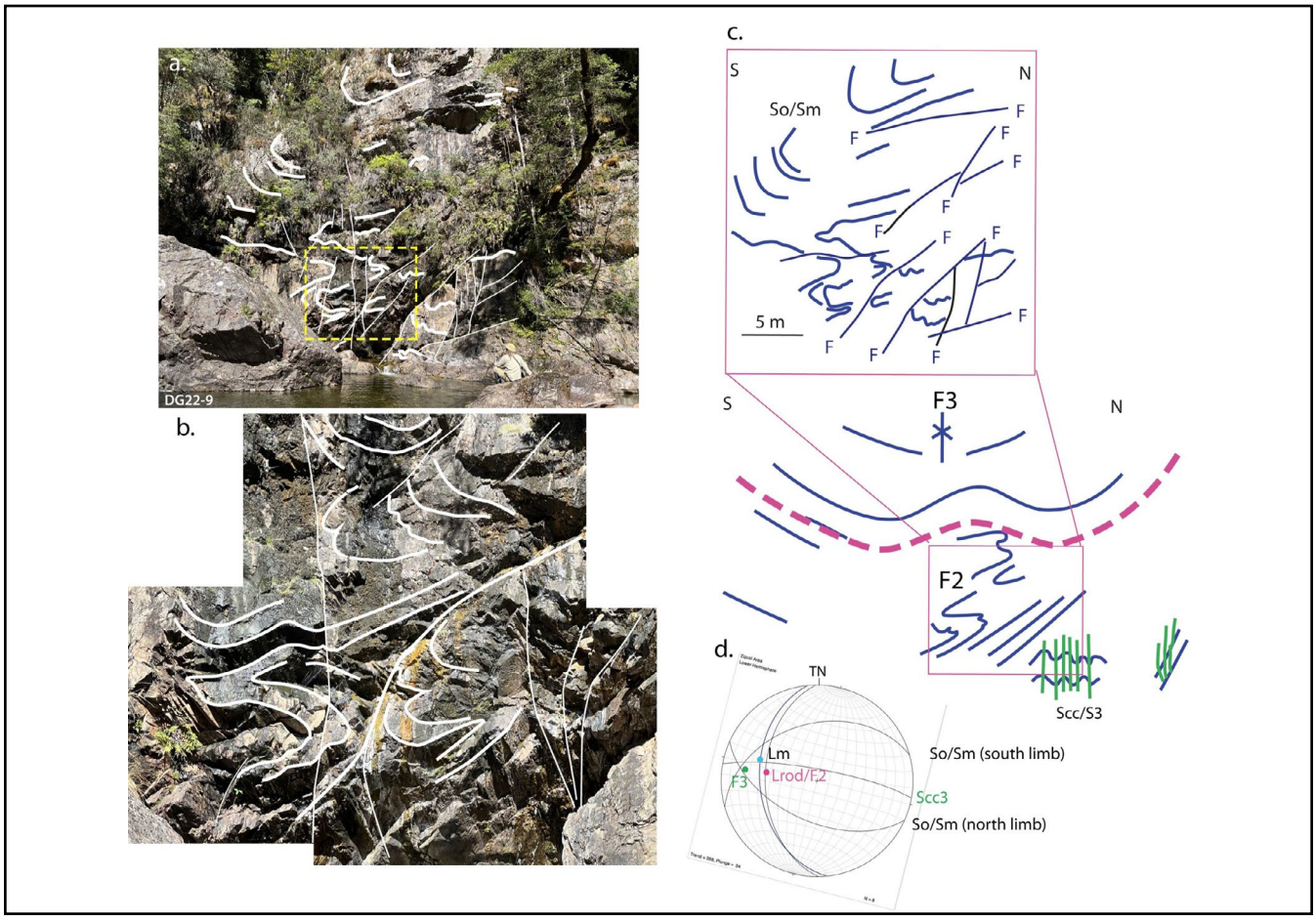

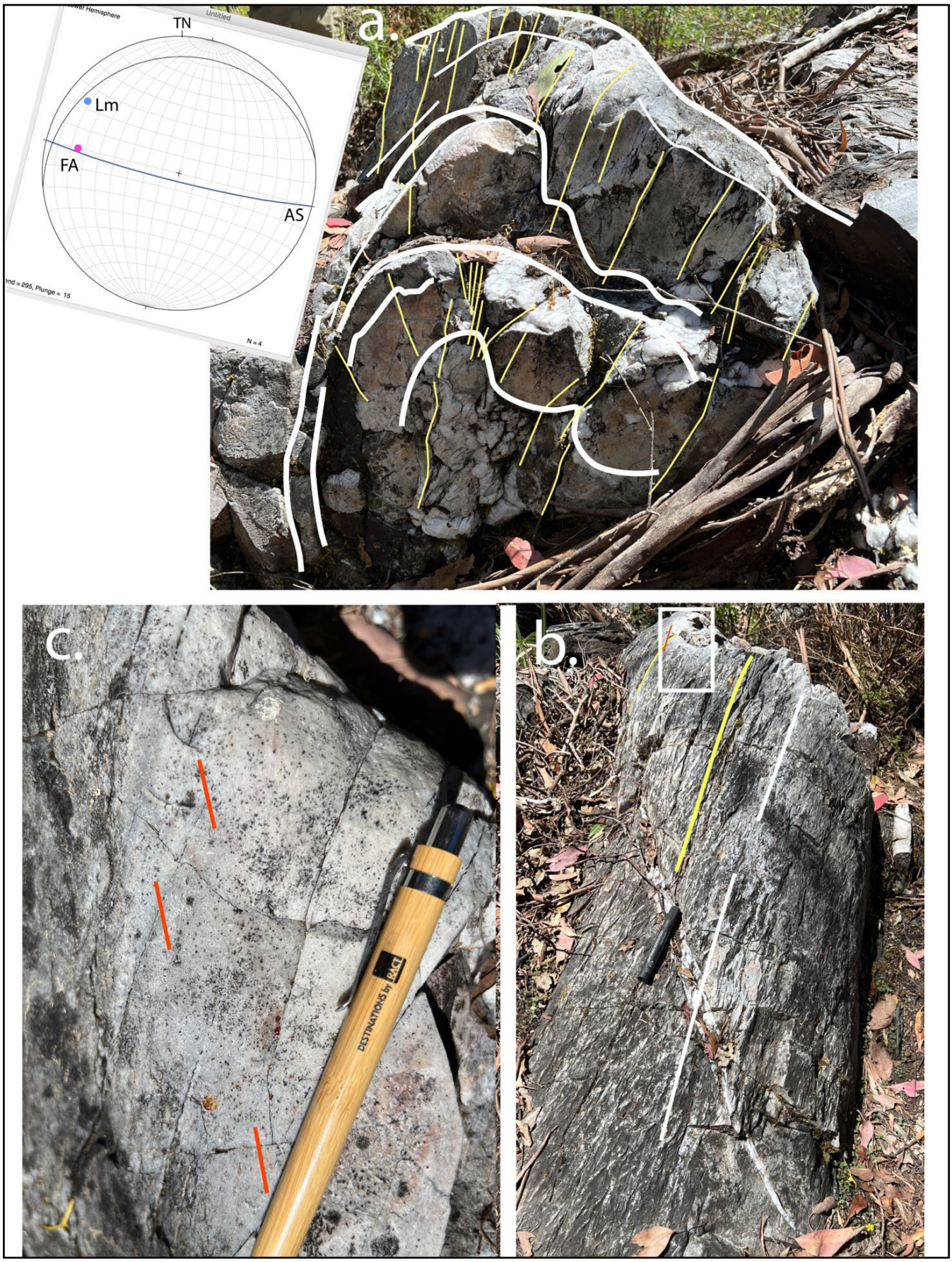

Figure 85. Small upright F3 fold along the Mersey River Road. a) Profile view of fold hinge showing a weakly fanned and refracted spaced cleavage across the fold hinge. The lobate nature of the base to the quartzite layers accentuates or focuses the spaced cleavage. The inset stereonet shows the attitudes (great circles) of the axial surface (AS) and the bedding surface containing the stretching lineation Lm. The measured fold axis is shown by the red dot and the measured lineation by the blue dot. b) View of the plunging fold hinge showing the intersection traces of the spaced cleavage (white line traces) on the bedding surfaces. The white rectangle shows the position of (c). The black marker pen highlights the position of a cross cutting thin quartz vein and remnants of mudcracks (see Figure 86). c) View of part of the plunging hinge line in the uppermost quartzite layer showing a quartz elongation lineation (parallel to red line traces). The yellow pen is aligned with the intersection traces of the spaced cleavage on the bedding surface of the quartzite. The stretching lineation is clearly folded across the F3 hinge. (Photo credits: David Gray).

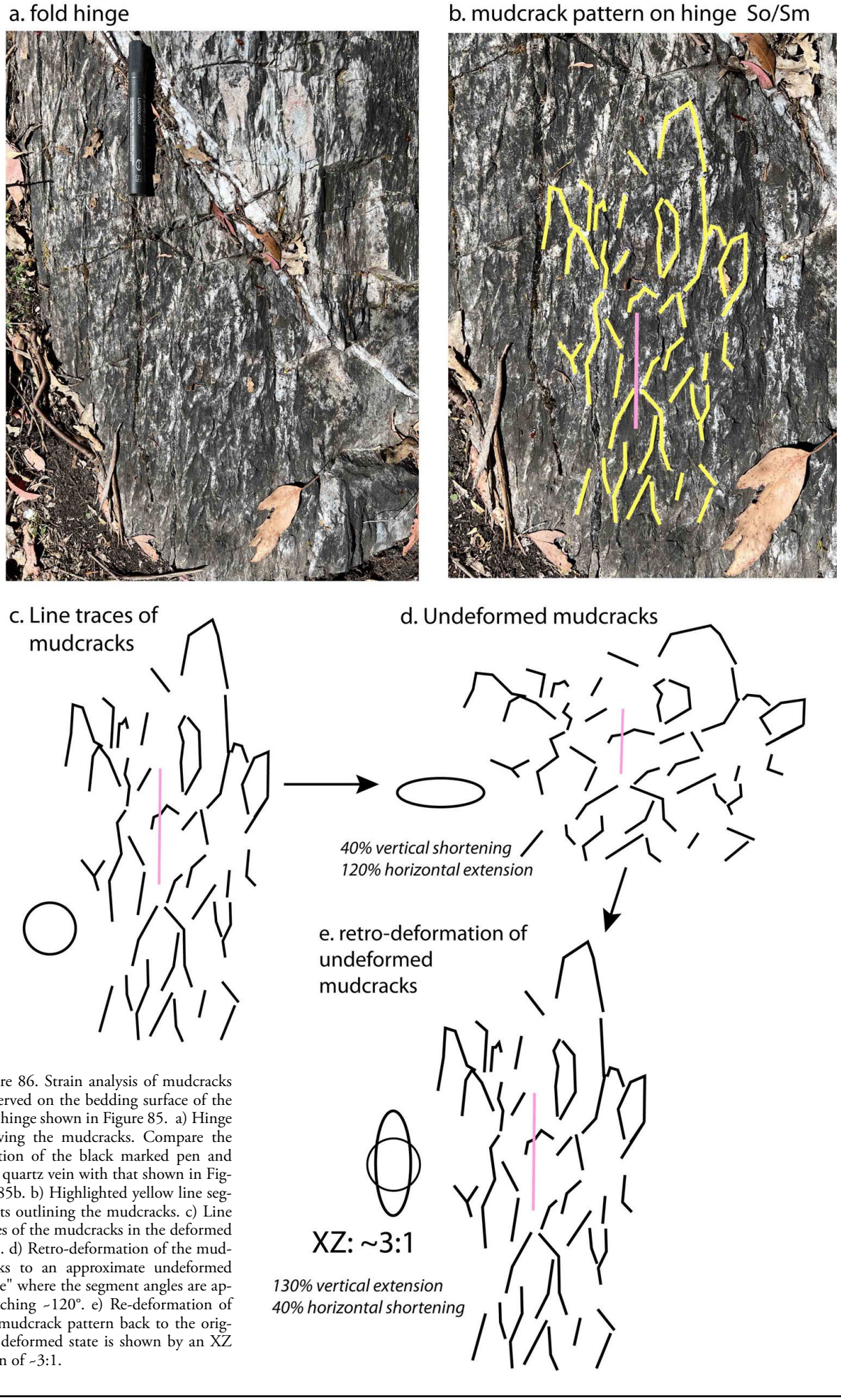

Figure 86. Strain analysis of mudcracks preserved on the bedding surface of the fold hinge shown in Figure 85. a) Hinge showing the mudcracks. Compare the position of the black marked pen and thin quartz vein with that shown in Figure 85b. b) Highlighted yellow line segments outlining the mudcracks. c) Line traces of the mudcracks in the deformed state. d) Retro-deformation of the mudcracks to an approximate undeformed "state" where the segment angles are approaching ~120°. e) Re-deformation of the mudcrack pattern back to the original deformed state is shown by an XZ strain of ~3:1.

5.3.3 Rowallan Fold Interference Zone (Area 3c, Figure 16)

The Lake Rowallan area has been treated separately within the Liena-Borradaile F3 chevron fold domain as it shows classic refolding of early isoclines by the east-west trending F3 folds in map view (Figures 87, 88 and 89). Outcrops now mostly submerged show early third order (metre-scale) and second order (tens of metre-scale) F1/F2 isoclines refolded by both open to tight upright, east-plunging upright F3 folds (Figures 87, 88 and 89). Structural mapping by Mattner (2015) when the lake level was lowered for dam wall remediation work has provided the data and photographs, and the basis of the interpretation and discussion (Figures 90 and 91).

Mattner (2015) subdivided the northern part of Lake Rowallan into three structural domains on the basis of foliation Sm pole plots (Figure 91). Each domain has a great circle fit to the pole pattern with a distinct π axis (equivalent fold axis) that Mattner considered were F3 generation. The variation in plunge and plunge direction was related to possible refolding or rotation associated with "hidden" shear zones between the domains.

A re-interpretation of the Mattner (2015) form line map shown in Figure 92 combined with π analysis of Sm defining individual fold hinges shows a complex fold interference pattern dominated by a large east-closing and east plunging F3 fold (Figure 92). North of this macro-fold are a series of inferred west-closing fold hinges with inferred intervening tight to isoclinal, cuspate east-closing hinges. Some of the folds approach reclined geometry with northwest plunges (red points on stereonets left side, Figure 92) suggesting these are early F1/F2 folds refolded by the east-trending F3 folds. The total fold axis stereonet (Figure 92b) shows two populations or unimodal clusters of determined fold axes, a dominant east plunging group and the small (n=2) northwest-plunging grouping. This pattern however may reflect a limited data sample dictated by the narrow, elongated form of the lake.

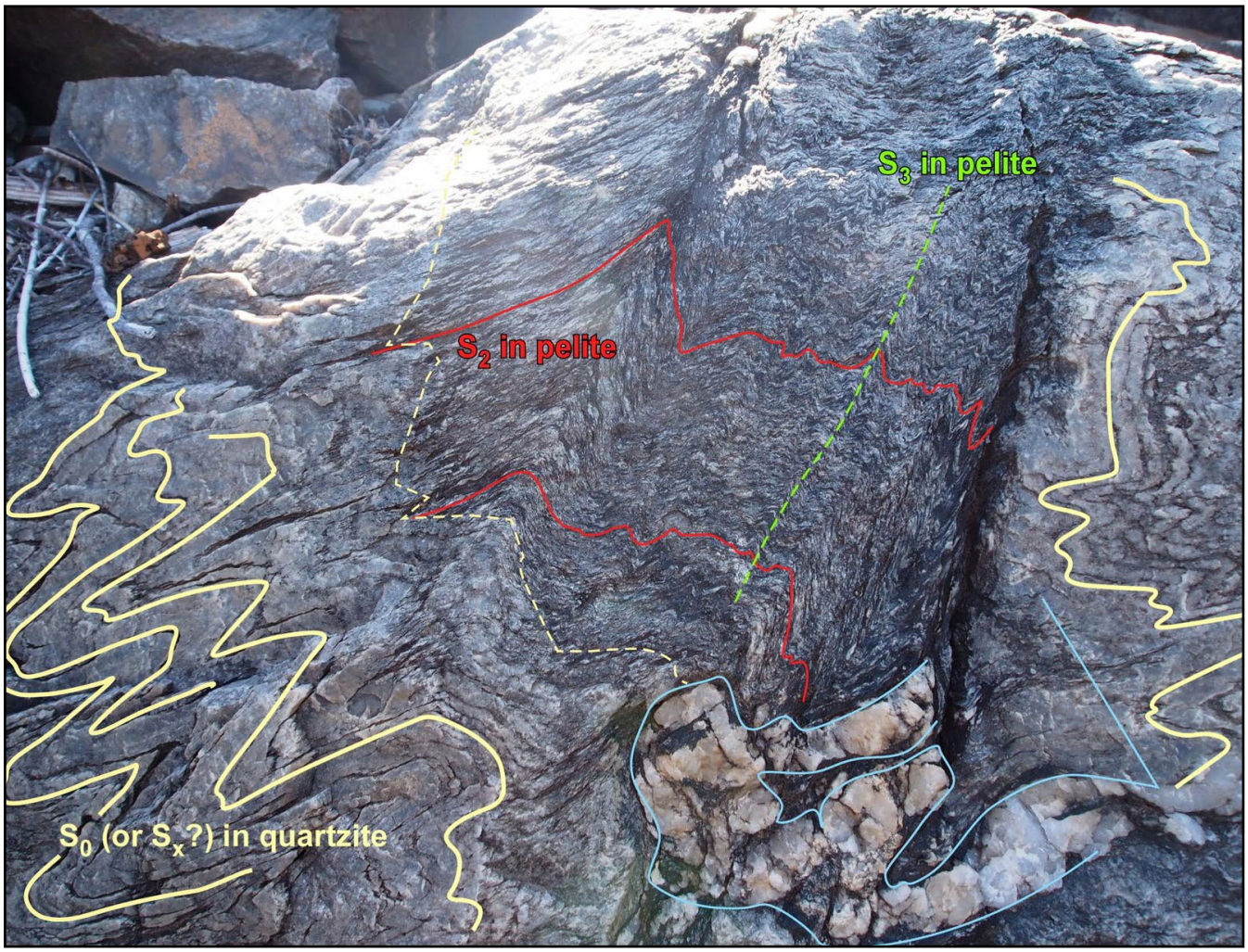

Figure 87. Refolding relationships at Lake Rowallan (Photo credit and annotation: Robert Scott). So/Sm: yellow line traces. S2 (Scc): red line traces. S3 (F3 axial surface traces): green dashed line traces. Isoclinal fold in quartz vein outline: light blue line trace (bottom right).

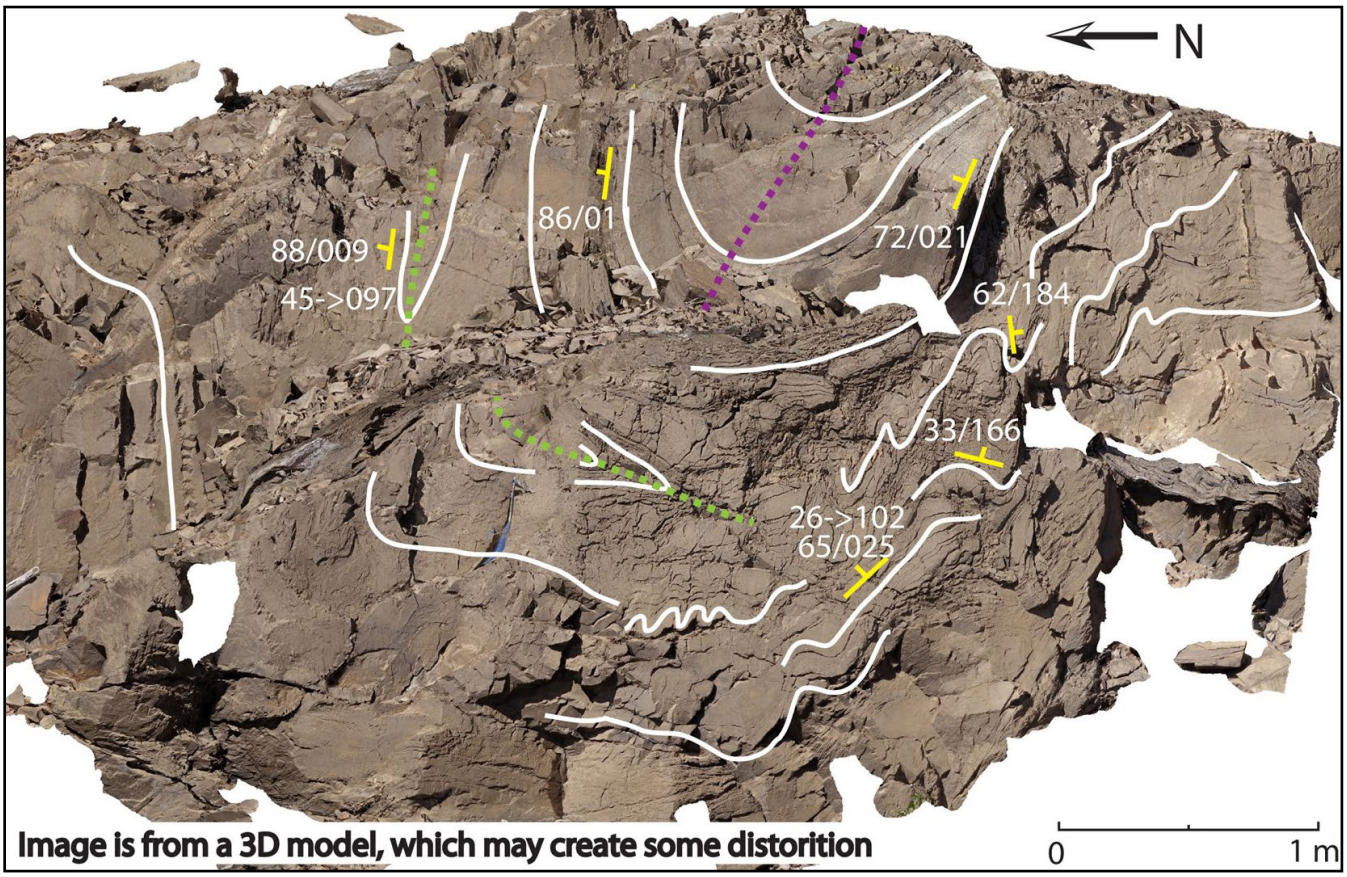

Figure 88 (Above). Image of a 3D outcrop model of a shoreline outcrop on Lake Rowallan (Mattner, 2015). For location see Figure 90. An upright east-west trending F3 fold refolds early isoclines within the So/Sm layering.

Figure 89 (Left). Photographs of early F1/F2 folds exposed along the shoreline of Lake Rowallan (Photo credits: Sally Mattner) a) Steeply and variably plunging symmetrical 'M'-folds within a large F2 fold hinge within a strongly deformed, intercalated quartzite and quartz-mica schist sequence. b) Tight to isoclinal approximately recumbent F2 chevron fold refolded by upright open F3 warps/folds. c) Enlargement of synformal closure at bottom left in photo (a).

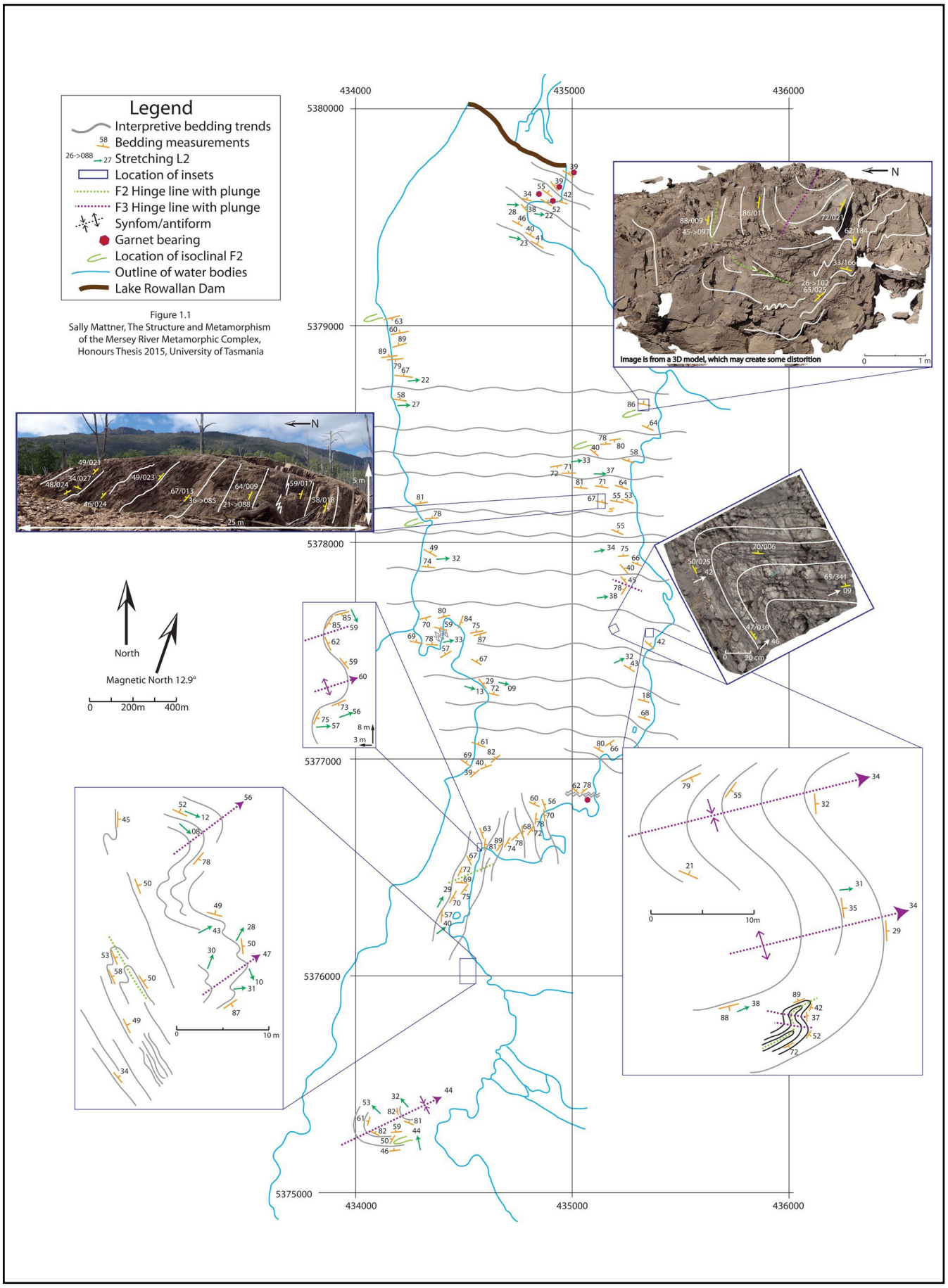

Figure 90. Mattner (2015) structural map of the northern part of Lake Rowallan. Form lines are shown by the thin black line traces. Purple arrows: F3 fold axes. Insets show areas of more detailed mapping and outcrop photographs. Orange symbols are foliation So/Sm strike/dip attitudes. Red dots are the garnet bearing schist localities.

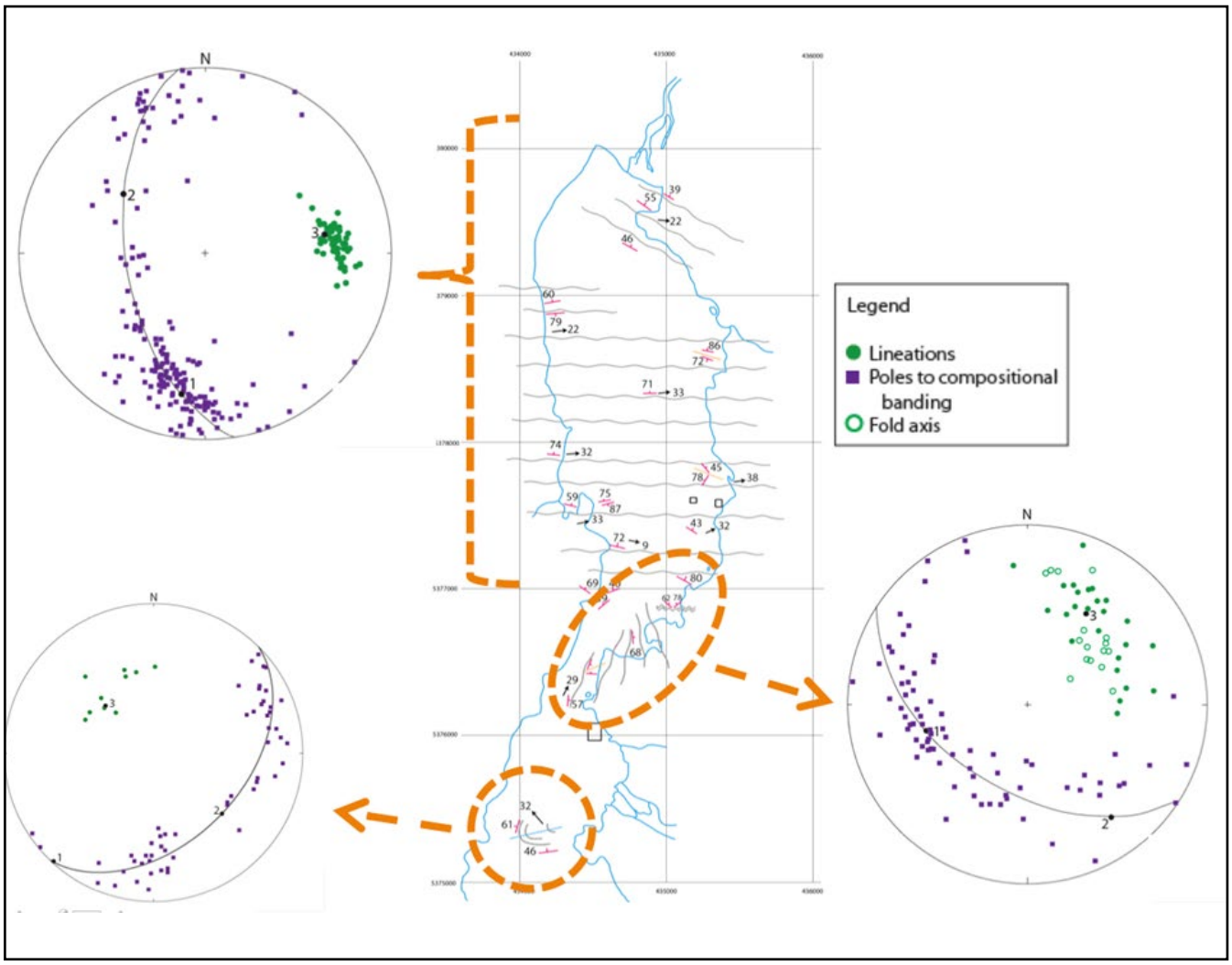

Figure 91. Mattner (2015) structural domain map with 3 domains categorised by stereonet plots of poles to compositional layering (purple dots), lineations Lm (green dots), fold axes (green circles) and best fit great circles.

At a more regional scale between Lakes Parangana and Rowallan (Figure 93) there are changes in the FA^Lm rotation direction suggesting the presence of regional scale sheath-like F2 folds with curved hinge lines. Variations in the rotation of FA^Lm are shown as clockwise at the Arm River and at the Lake Rowallan boat ramp and counter clockwise just north of Lake Rowallan. This suggests the presence of two early F1/F2 large-scale fold hinges in this area (Figure 93), a west-closing hinge at the north end of Lake Rowallan Dam and an F2 isoclinal fold pair further north up to Arm River. These folds are refolded by the east-west trending F3 folds (Mersey Synform) and overprinted by the S3 (Scc) cleavage (Figure 94).

The area of the boat ramp and quartzites along most of the Mersey valley show a pronounced intersection lineation (Lint) with colour (compositional) banding (So) traces on the foliation (Figure 95). Alignment of black lath-like minerals sub-parallel to Lint (see fig. 3.4, Mattner, 2015) indicates that Lint is parallel to the elongation direction (Lelong) within Sm.

A rodding lineation in the foliation Sm is also common in zones of intense transposition. Relicts of flattened and elongated, centimetre scale, isoclinal fold hinges are preserved on the Sm surface (Figure 96a) and in the transposition banding (Figure 96b). These are part of the higher strain zones.

The nature of the refolding is also shown at the Lake Rowallan boat ramp at the northeast end of the lake (Figures 97 and 98). Intercalated quartzite and garnet schist (the former Howell Group) is intensely folded, schistose and metamorphosed to lower amphibolite facies (Berry and Bull, 2004). South of the boat ramp the dominant foliation (Sm) trends northwest and has a northeast dip as part of an intensely foliated zone (high strain zone). It is a zone of intense transposition layering, showing asymmetric fold pairs (Figure 99) and a pronounced intersection lineation (Figure 100) and/or rodding lineation (Figure 101). The foliation flattens and changes to a north-northeast strike at the boat ramp (Figure 97b) associated with mesoscopic F3 folding, crenulations and crenulation lineation (Figures 104 and 105).

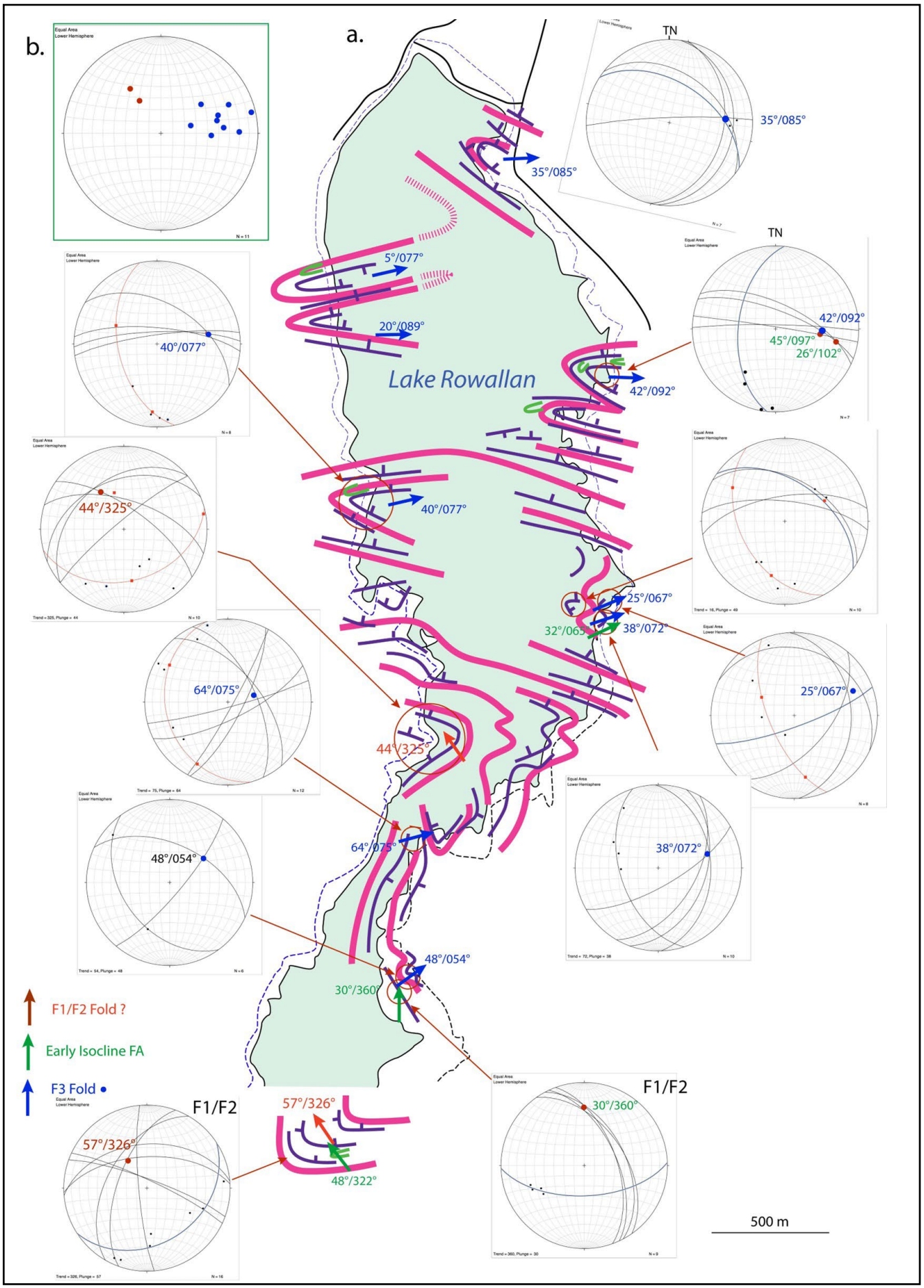

Figure 92. Lake Rowallan structural map and stereonets based on a folding model and the structural definition in the main part of the Liena-Borradaile zone. a) Structural form line map with the form line interpretation highlighted by the blue and heavy pink summary line traces. The initial interpretation (blue line traces) is based on Sm attitudes from the Mattner (2015) geology map base (Figure 90). Blue arrows arrows: F3 fold axes. Green arrows: early isocline F2 fold axes. Note the sub-parallelism of F2 and F3 hinge lines in the northern part of the map: coaxial refolding of F2 folds by F3 folds. b) Summary stereonet of fold axis determinations from the individual stereonets showing an apparent unimodal clustering of east plunging and northwest plunging fold sets.

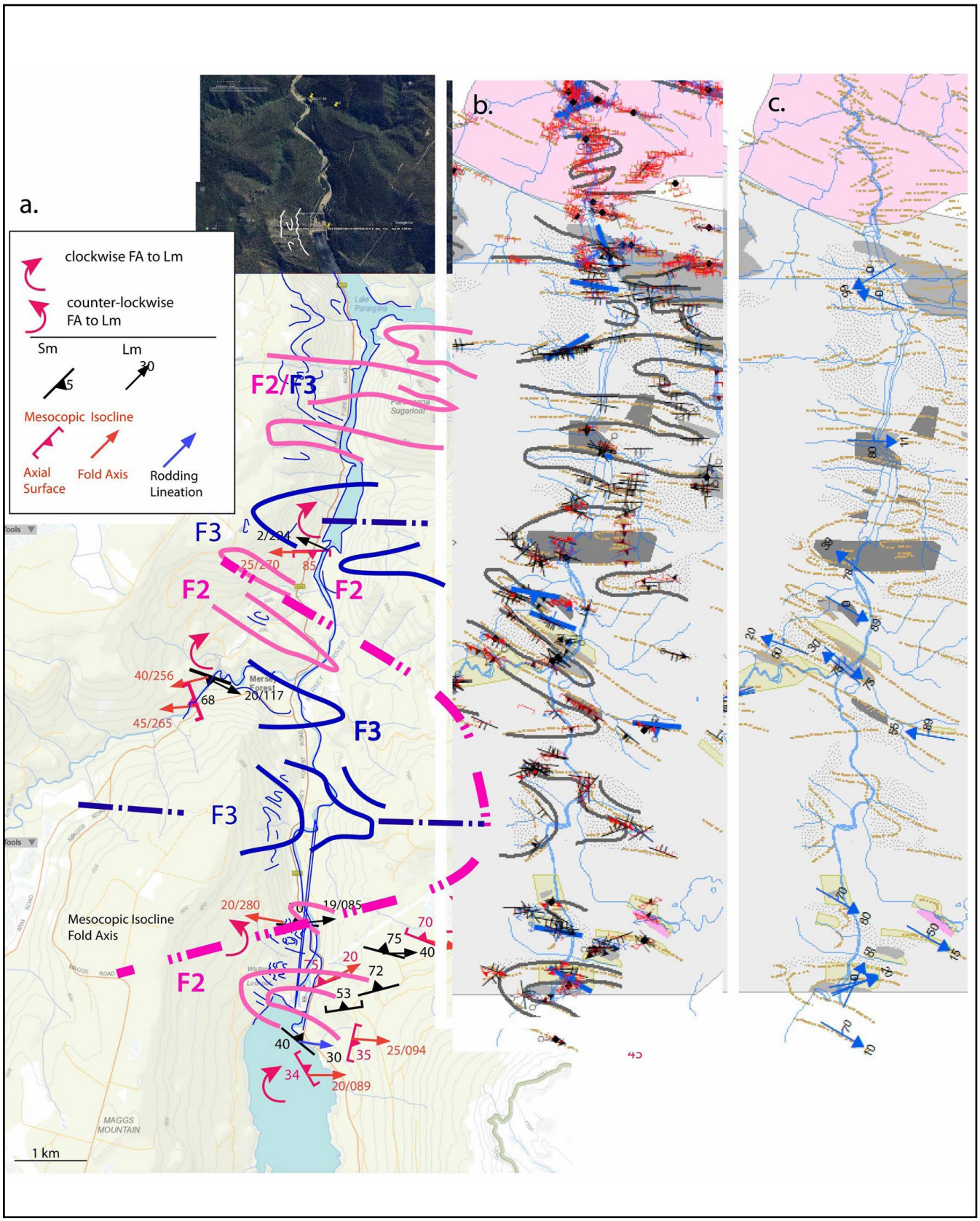

Figure 93. Structural strip maps of the Mersey Valley between Lake Parangana and the northern part of Lake Rowallan. a) Structural map based on structural data and observations collected by DRG with form lines in So/Sm by GC. Pink hinges within the form lines are interpreted as F2. They have almost isoclinal form and appear folded by the east-west F3 folds with hinge lines shown by the blue line traces. Variations in the rotation of FA^Lm are shown as clockwise rotation at the Arm River and at the Lake Rowallan boat ramp and counter clockwise just north of Lake Rowallan. These further suggest the presence of early F2 folds with curved hinge lines. The interpretation is based on sheath fold analysis after Alsop & Holdsworth (1999). ListMap topographic map as base. b) Form line strip map of the Mersey Valley based on MRT mapping by Cumming et al. (in prep, 2025). c) Form line strip map of the Mersey Valley showing early isocline fold axis plunges. Map segment and data collected by Cumming et al. (in prep, 2025).

Figure 94 (Left). Younger S3 cleavage/foliation (pink line traces) transecting and overprinting an asymmetric F2 isoclinal fold pair defined in So/Sm (purple line traces). Mersey Forest road outcrop 1 km south of Parangana Dam. View is to the west. (Photo credit: David Gray).

Figure 95 (Below). Views of the Sm foliation surface within quartzite from the outcrop shown in Figure 94 above. Road outcrop 1 km south of Parangana Dam. a) View normal to the Sm foliation in the quartzite showing a ~40°-50° plunging intersection lineation (Lint) with a corrugated ribbing appearance on some surfaces due to intersection of So/Sm. b) Close up of the foliation surface showing pronounced banding from quartz and quartz-mica layers in the quartzite. The Lmica lineation is an intersection of the strong S3 foliation that overprints the folded quartzite (see Figure 94). c) Enlarged view of the foliation showing the intersection (Lint) of a quartz-rich layer with Sm (white line traces), a quartz grain elongation lineation (Lelong) slightly oblique to Lint (yellow line traces) and the mica lineation related to the intersection of the strong S3 foliation (blue line trace) (Photo credit: David Gray).

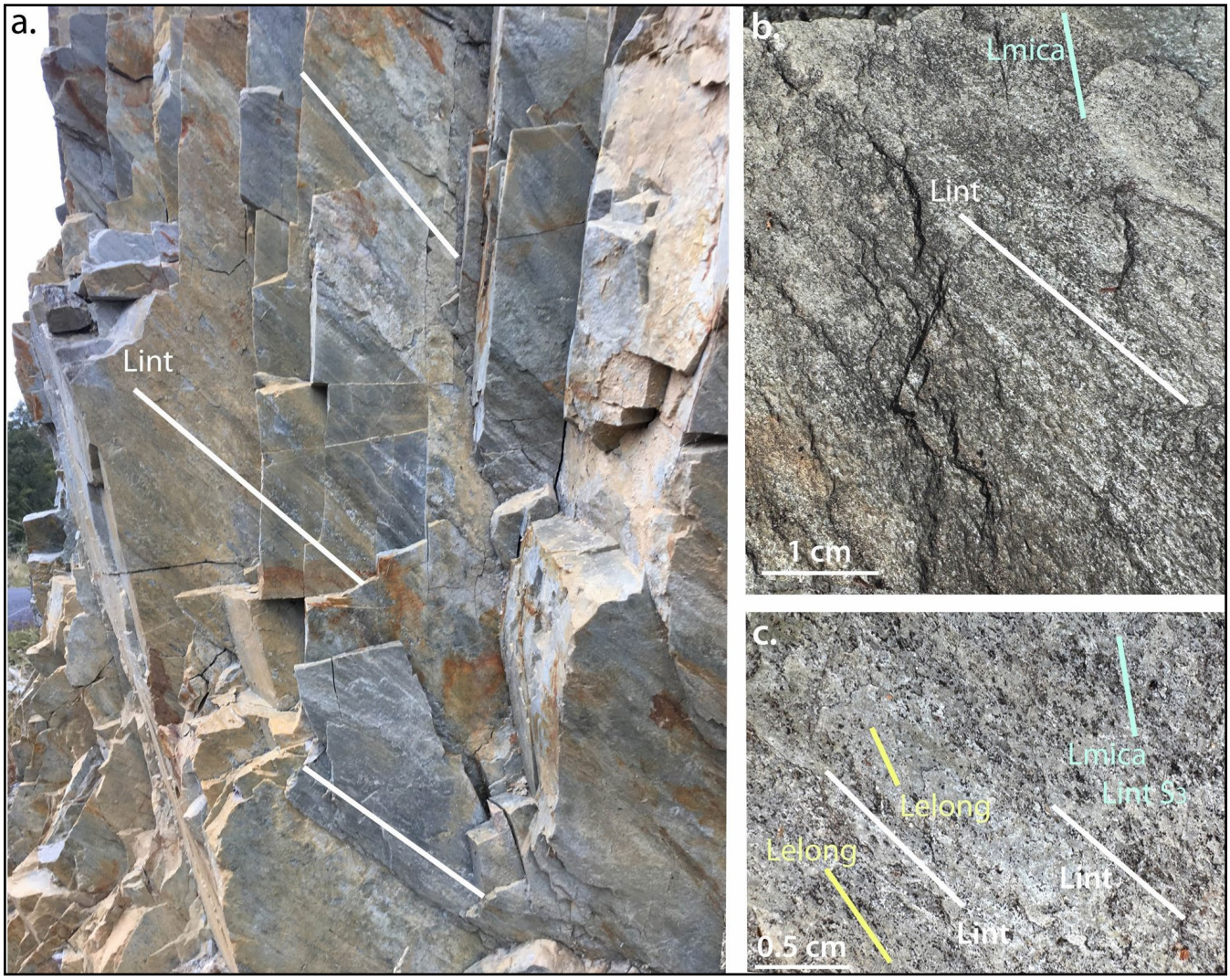

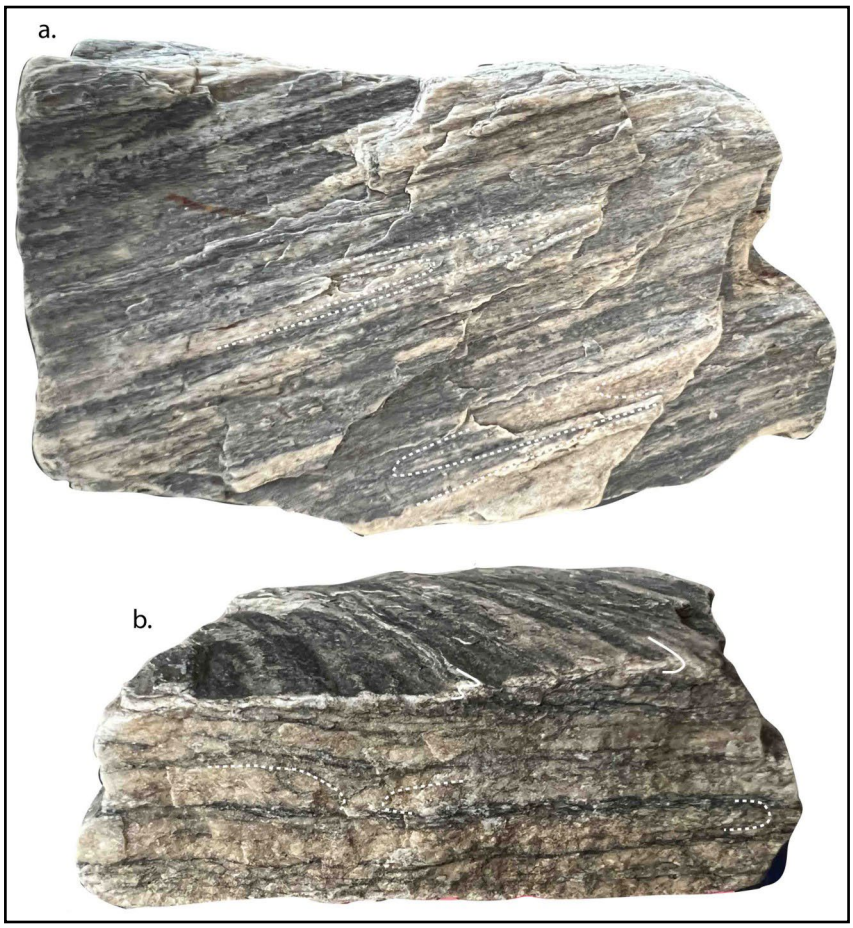

Figure 96 (Left). Rodding lineation and associated transposition layering typical of the quartzite-pelite sequence along the Mersey River valley (Photo credit: David Gray). a) View of foliation surface Sm showing an elongated and flattened isocline (fine white dashed lines) defined by So intersection with the Sm . b) Side view of sample showing the transposition layering consists of thin centimetre-scale quartzite bands separated by thin dark pelite selvedges. Relicts of isoclinal fold hinges are preserved in some of the quartzite "layers". Sample size is 10 cm.

Figure 97 (Below). Structure map of the Lake Rowallan Boat ramp area some ~250 m south of the dam wall. a) Simplified structural map showing foliation, lineation and fold axis attitudes. Outcrop locations for DG17-25, DG17-25 and DSG17-26 are shown. b) The stereonet (middle-right) plots foliation great circle traces from DG17-24, DG17-25 and DG17-26 giving a β point that is sub-parallel with the measured F2 fold axis. This indicates coaxial refolding by F3. The F3 fold is an upright, broad, open warp within Sm (see photo profile A-A', Figure 98b). It is associated with a sub-vertical, east-west trending crenulation cleavage Scc (S3).

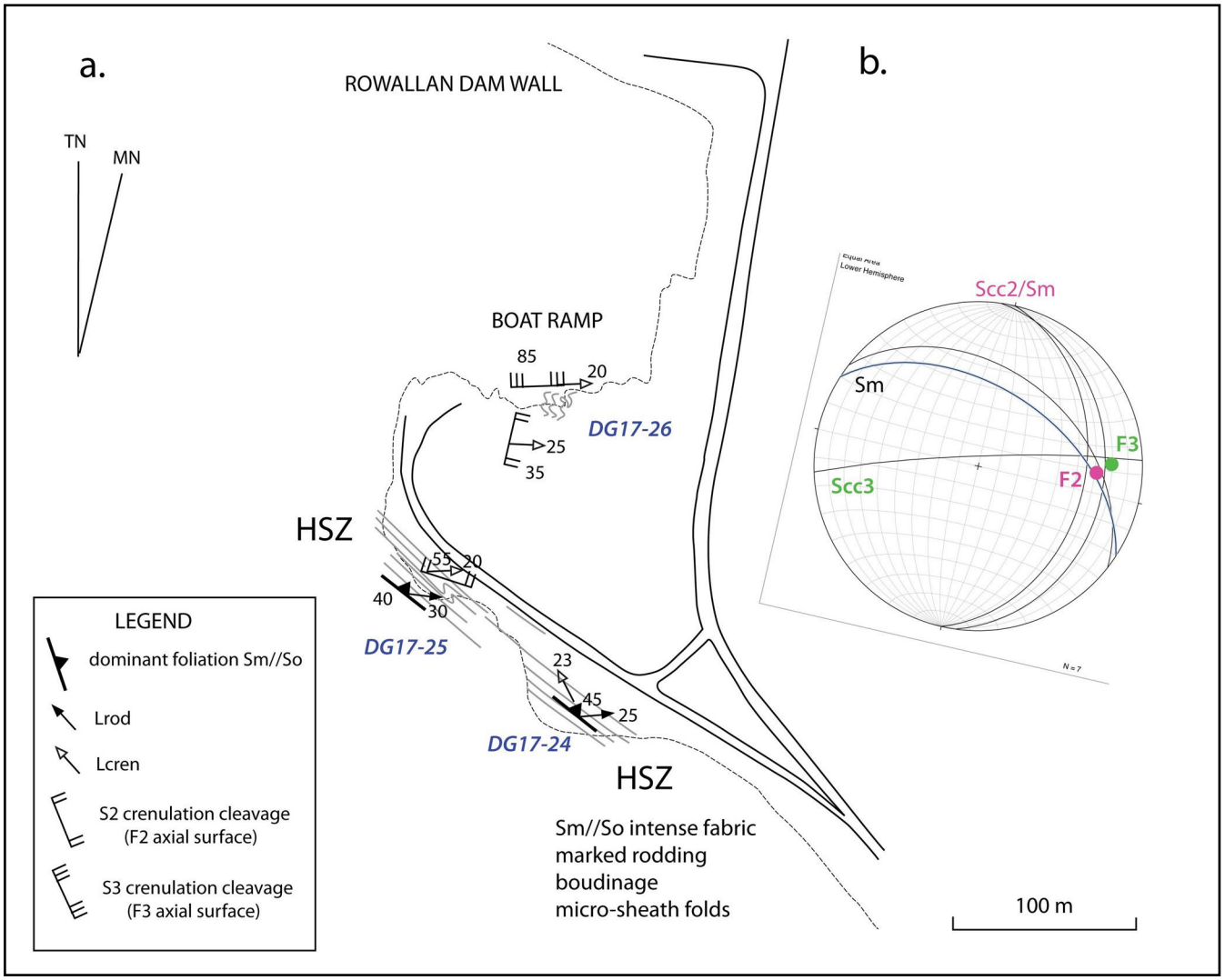

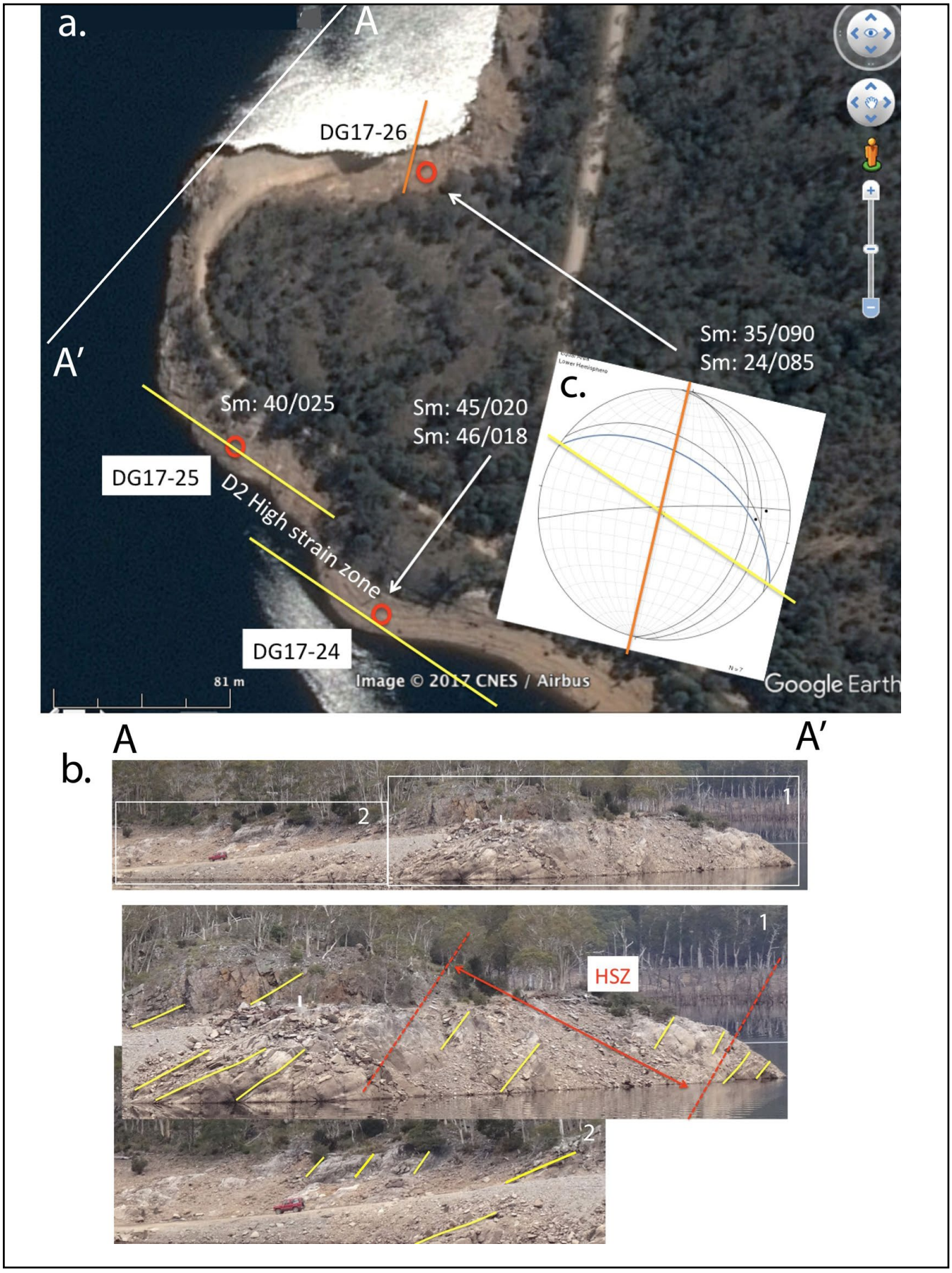

Figure 98. Lake Rowallan boat ramp simplified map and structural profile. a) Google satellite image of the shoreline at the Lake Rowallan boat ramp showing DG17 outcrop stations, the foliation trends at DG17-24 and DG17-25 (yellow line traces) and at DG17-26 (orange line trace). Foliation Sm measurements in white text are magnetic dip/dip azimuth. The position of photo profile A-A' is shown. b) Photo profile of the Lake Rowallan boat ramp showing the dominant foliation changing dip towards a broad open synformal F3 fold hinge (off photo left). c) Stereonet of the foliation Sm great circle traces at DG17-24, DG17-25 and DG17-26 with the yellow and orange strike traces superimposed. The β point coincides with measured F3 fold axes at DG17-26 with a steeply north-dipping axial surface Scc3 (see Figure 104c). (Photo credit: David Gray).

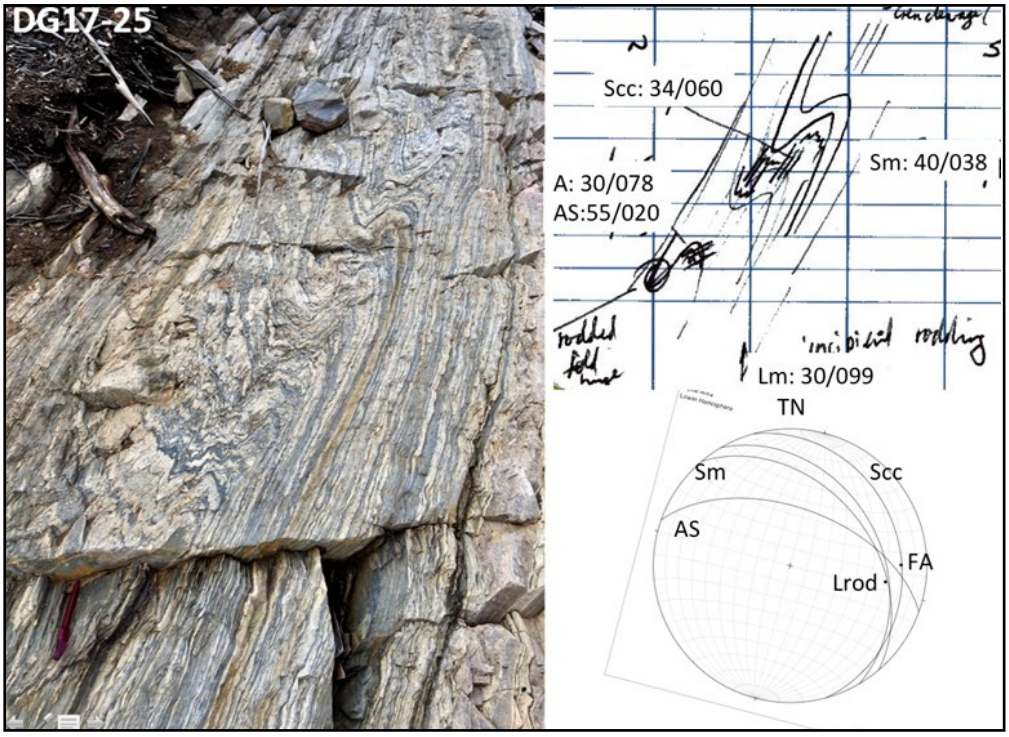

Figure 99. Asymmetric, S-symmetry F2 fold pair within strong to intense transposition layering So/Sm and with localised axial surface S2/Scc (see sketch top right). Location DG17-25. Note the limb Sm and the axial surface S2/Scc are sub-parallel and the rodding/intersection lineation is sub-parallel to the F2 fold axis (stereonet bottom left). Location DG17-25. (Photo credit: David Gray).

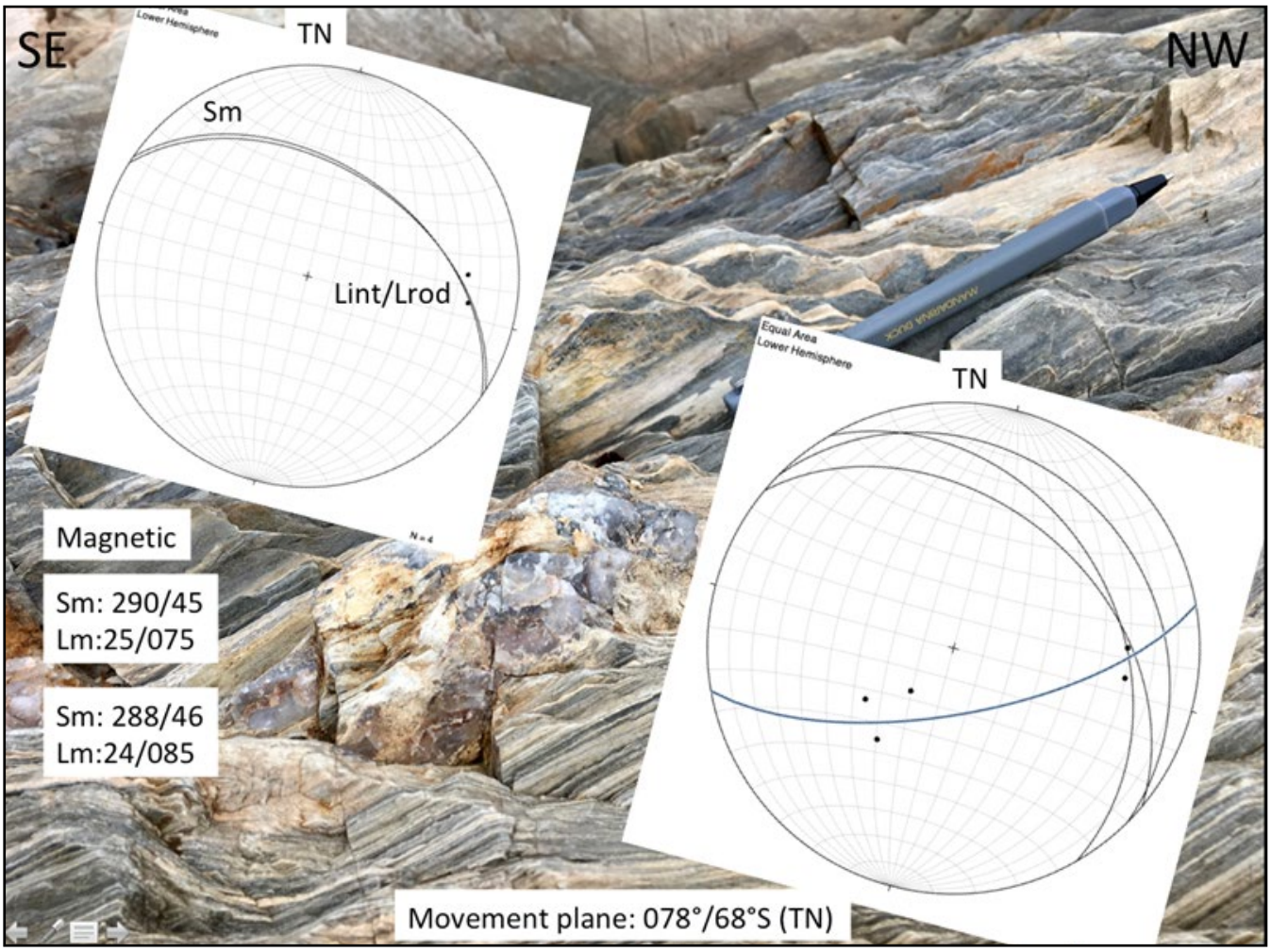

Figure 100. Pronounced east-plunging intersection lineation within intense transposition layering So/Sm at location DG17-24. Alignment of black lath-like minerals sub-parallel to Lint (see fig. 3.4, Mattner, 2015) indicate that Lrod/Lint is parallel to the elongation direction within Sm. The calculated movement plane (MP1) is east-west trending (blue great circle, lower right stereonet). MP1 is a great circle fit to the pole to Sm and the lineation Lint/rod (see Figure 25). (Photo credit: David Gray).

Figure 101. Incipient rodding intersection lineation parallel to the hinges of F2 asymmetric folds. Compare with Figure 100. Location DG17-25. (Photo credit: David Gray).

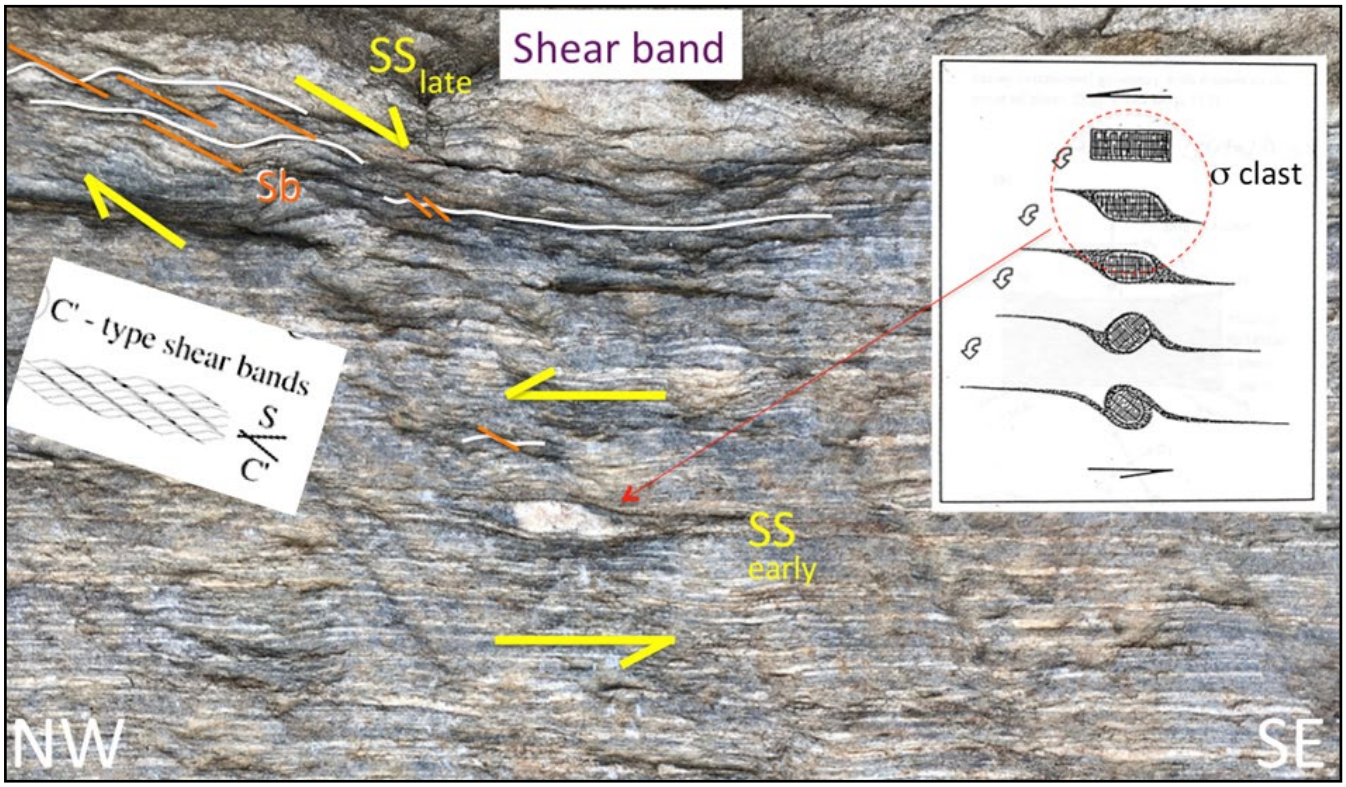

Figure 102. Transposition layering as thinly spaced banding (So/Sm) with a sigma "clast" (photo centre) and C' shear bands (top left). The sigma clast indicates top to the left (sinistral) shear sense whereas the shear bands give a top to the right (dextral) sense. Inset diagrams are from (Passchier & Trouw, 1996, fig.5.9 and Goscombe & Passchier, 2003, fig. 8) Location DG17-24. (Photo credit: David Gray).

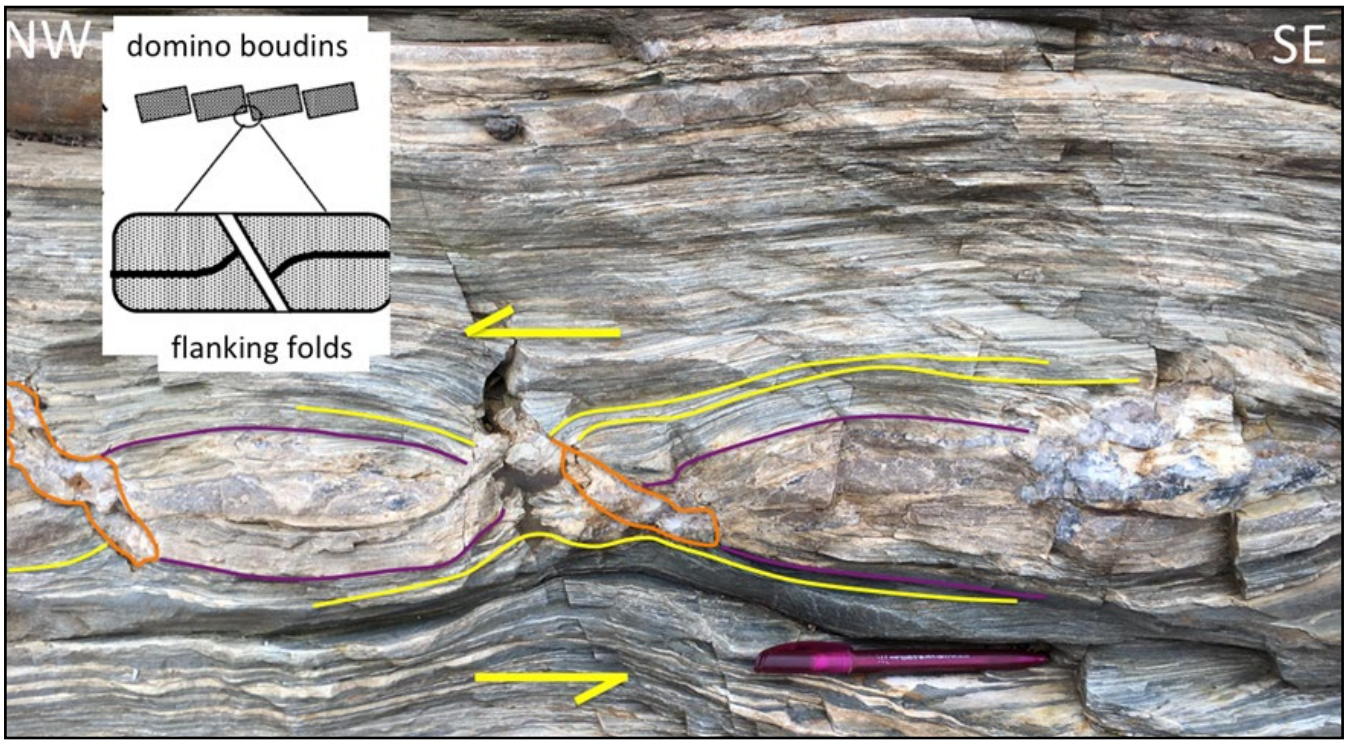

Figure 103 (Above). Boundinaged quartzite layer within quartz-mica schist showing quartz gash veins (orange outline) along the interboudin plane (Sib) and flanking folds at boudin necks (see inset top left). These are interpreted as domino boudins (inset fig. 8, Goscombe & Passchier, 2003) and indicate top to the left (sinistral) shear sense or southeast over northwest sense. Location Dg17-24. (Photo credit: David Gray).

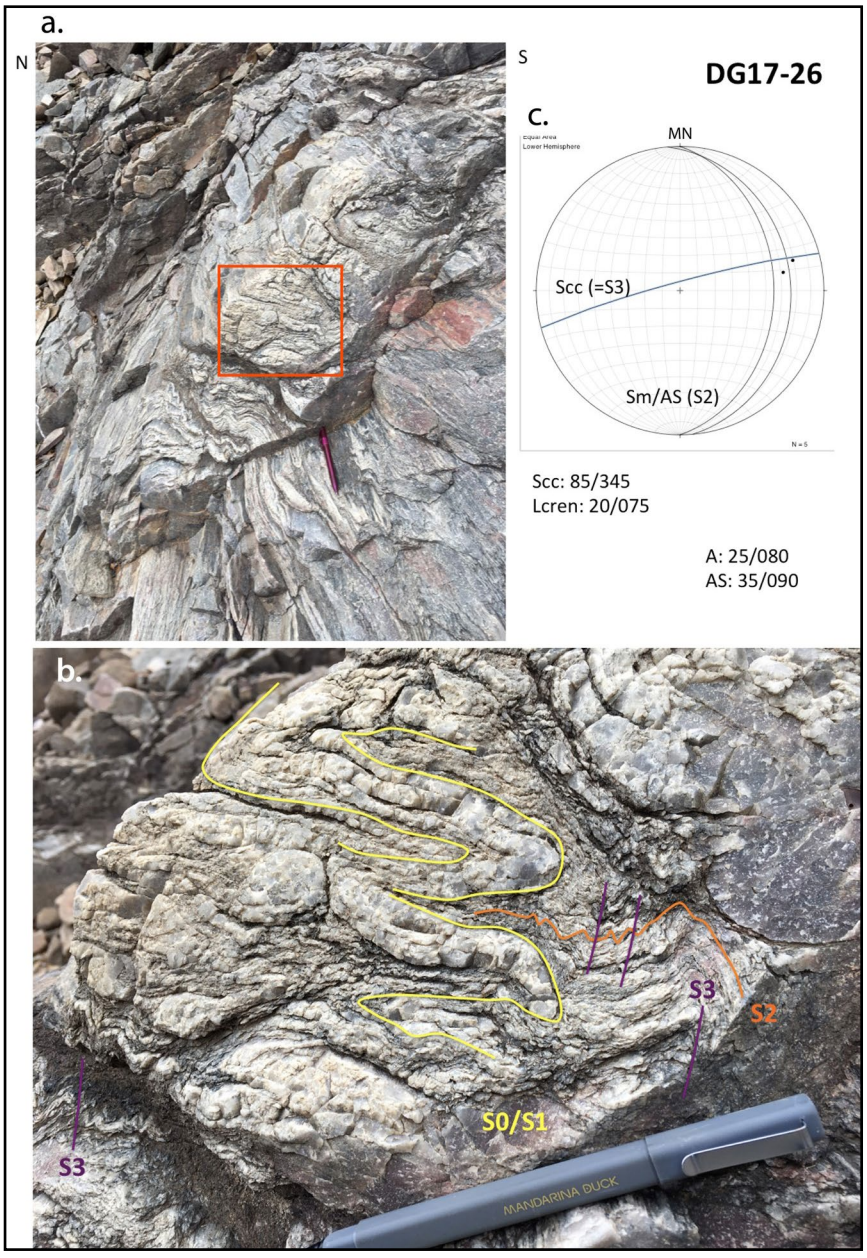

Figure 104 (Left). Structural relationships at outcrop DG17-26 above the boat ramp showing refolding of small recumbent isoclinal folds by upright F3 folds with a sub-vertical crenulation cleavage Scc3 (Photo credits: David Gray). a) Outcrop photo profile of both the F2 and F3 folds with view looking to the east. The enveloping surface containing the hinge points in So/Sm is steeply north-dipping. The red rectangle highlights the photo enlargement shown in (b). b) Enlarged part of the outcrop highlighted in (a) showing the coaxial refolding of early isoclinal folds by the upright F3 folds with an axial surface S3 crenulation cleavage (purple line traces). Yellow line traces: So/Sm compositional layering. Orange line traces: foliation S2 axial surface to F2 folds. c) Stereonet of the Sm/S2 foliation great circle traces. Structure measurements listed are magnetic.

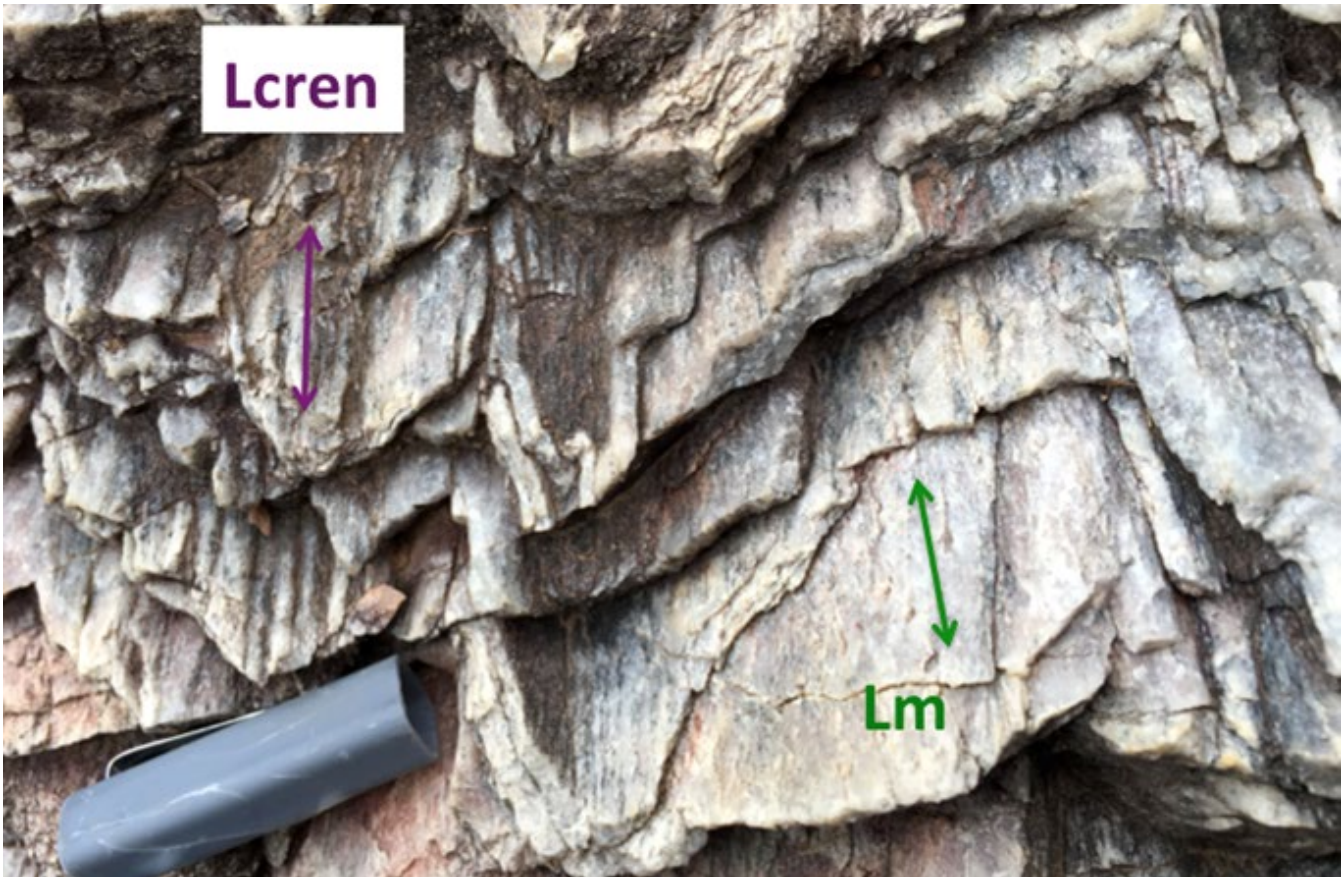

Figure 105. Small scale F3 folds with hinge lines and a crenulation lineation Lcren (purple arrow) sub-parallel to the mineral stretching lineation Lm (green arrow defined by elongated quartz grains within the dominant foliation So/Sm. Close up view of Outcrop DG17-26 (Figure 104) (Photo credit: David Gray).

The zone of strong transposition foliation south of the boat ramp, provide a number of shear sense examples ranging from asymmetric quartz fabrics in quartzite mylonite (Berry and Bull, 2004), shear bands (Figure 102), sigma clasts (Figure 102) and domino boudins (Figure 103). Berry and Bull (2004) argued for deformation involving a south-directed shear from quartz fabrics and southward verging F2 folds. The sigma clasts and domino boudins indicate left lateral shear sense or southeast-over-northwest sense in the early stages of transposition layering whereas the shear bands indicate dextral sense or northwest-over-southeast shear sense in a strain hardening or late phase.

5.4 Overland Track Zone (Area 4, Figure 16)

The Overland Track north of Lake Windemere to Old Pelion Hut (Figures 106 and 107) traverses strongly to intensely foliated quartzite with flattened mesoscopic, intrafolial isoclinal folds (Figure 107) and a strong rodding lineation (Figure 108). The foliated quartzite is broadly warped by open east-west trending F3 folds (Figure 107).

These folds commonly have curved hinge lines occurring as flattened tubes with sheath-like form (DG19-33 block diagrams, Figure 107). At many of these localities the rodding lineations show a herringbone pattern due to the superposition of multiple flattened tube-like isoclinal hinges (DG19-35 block diagram, Figure 107). Folded zones pass into intensely foliated, rodded quartzite with intrafolial isoclinal fold hinges (DG19-34, DG19-35, DG19-36 and DG19-39 block diagrams, Figure 107). The intensity of the foliation Sm and lineation Lm and Lrod incorporating rootless isoclinal folds and flattened tongue-like sheath-folds along this part of the Overland Track, are all suggestive of a significant high strain zone with a ~1.5 km thickness (based on the structural profile, Figure 107) at the probable base of the quartzite (cf. Frenchmans Cap profile in Gray and Vicary, 2021).

Shear bands at DG19-34 and DG19-36 (outcrop sketch profiles, Figure 107) show dextral, west-over-east shear sense as part of the basal zone.

5.4.1 North of Lake Windemere

The first outcrops of quartzite on the Overland Track after Cradle Mountain (Figure 108) are strongly foliated with homoclinal, south dipping compositional layering So/Sm containing coaxial folded asymmetric north-vergent F3 folds and F1/F2 isoclines within Sm (Figures 109, 110 and 111). Many of the isoclines have flattened, tongue-like sheath form within the foliation Sm (Figures 112 and 113). There is also a pronounced rodding lineation (Lrod) sub-parallel to Sm (Figures 109, 110 and 111). Stacked flattened isoclines with alternating limb intersections within Sm giving a "herringbone pattern" (Figure 111). This is typical of sheath fold evolution within small-scale (<1 m) folds flattened within the dominant foliation Sm.

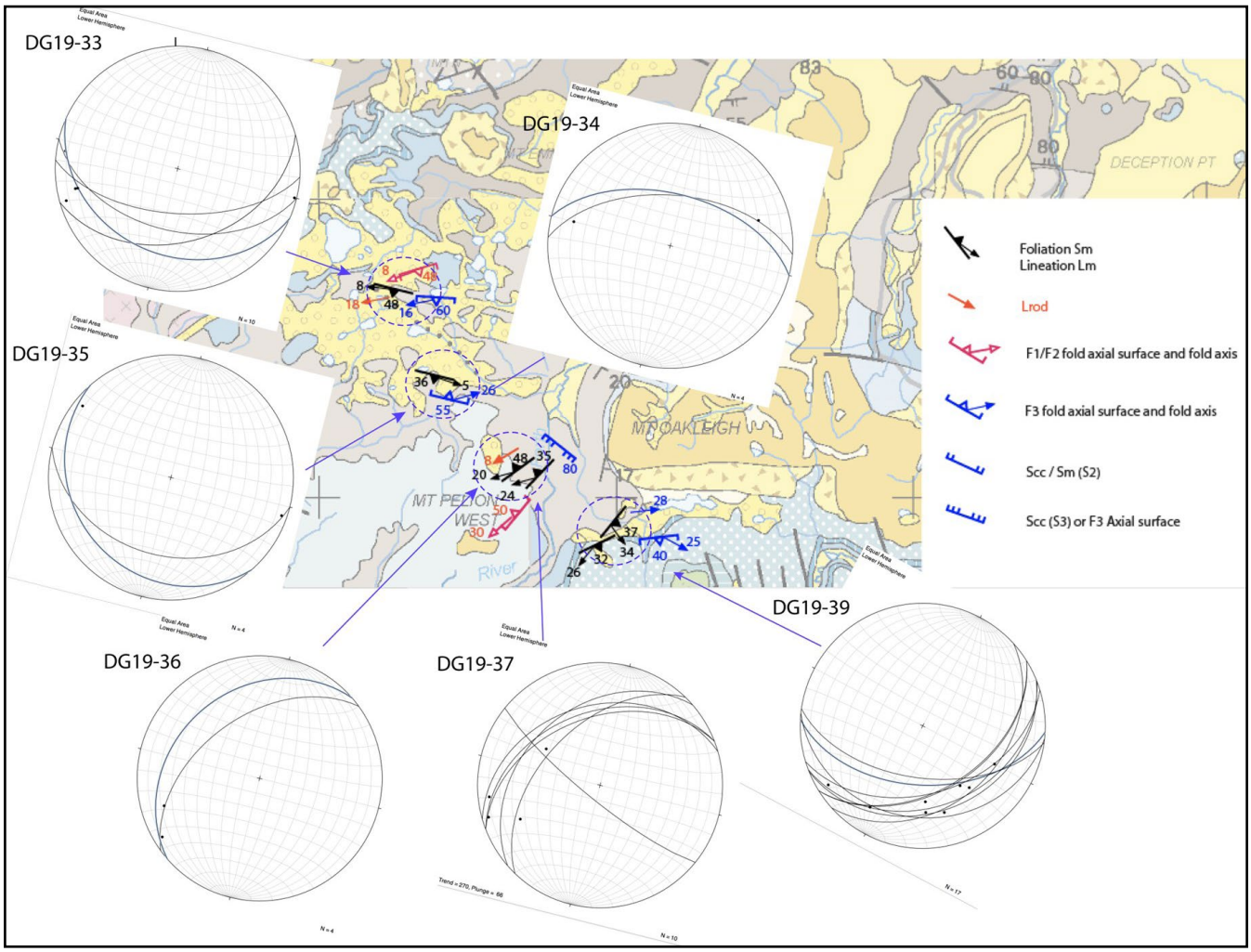

Figure 106. Structure map of the northern portion of the Overland Track from Lake Will to Old Pelion Hut. Map base is the MRT digital atlas 1:250,000 sheet. The inset stereonets show foliation Sm great circle traces and lineation Lm data (black dots). The stereonets are plotted magnetic readings with net rotated to TN.

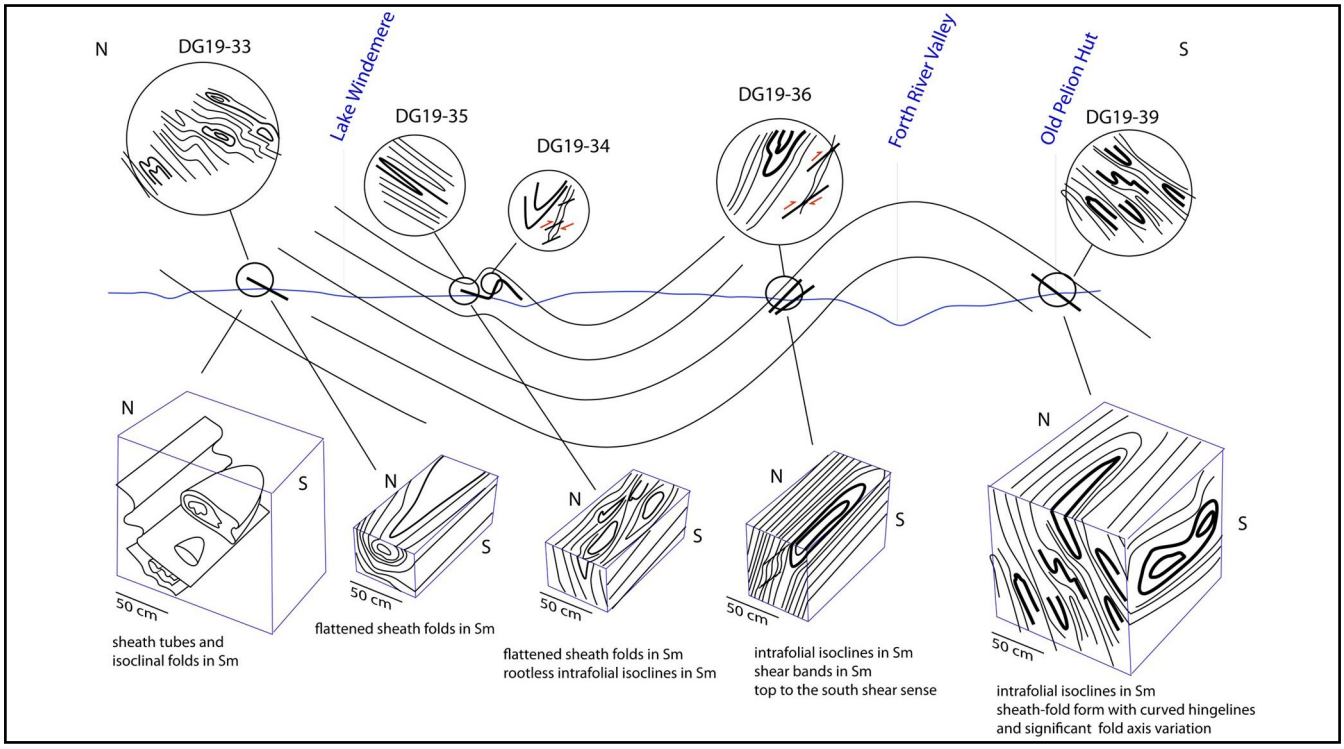

Figure 107. Structural profile of the northern portion of the Overland Track from Lake Will to Old Pelion Hut. Structural relationships at individual outcrops are shown by the sketch profiles and 3D block diagrams.

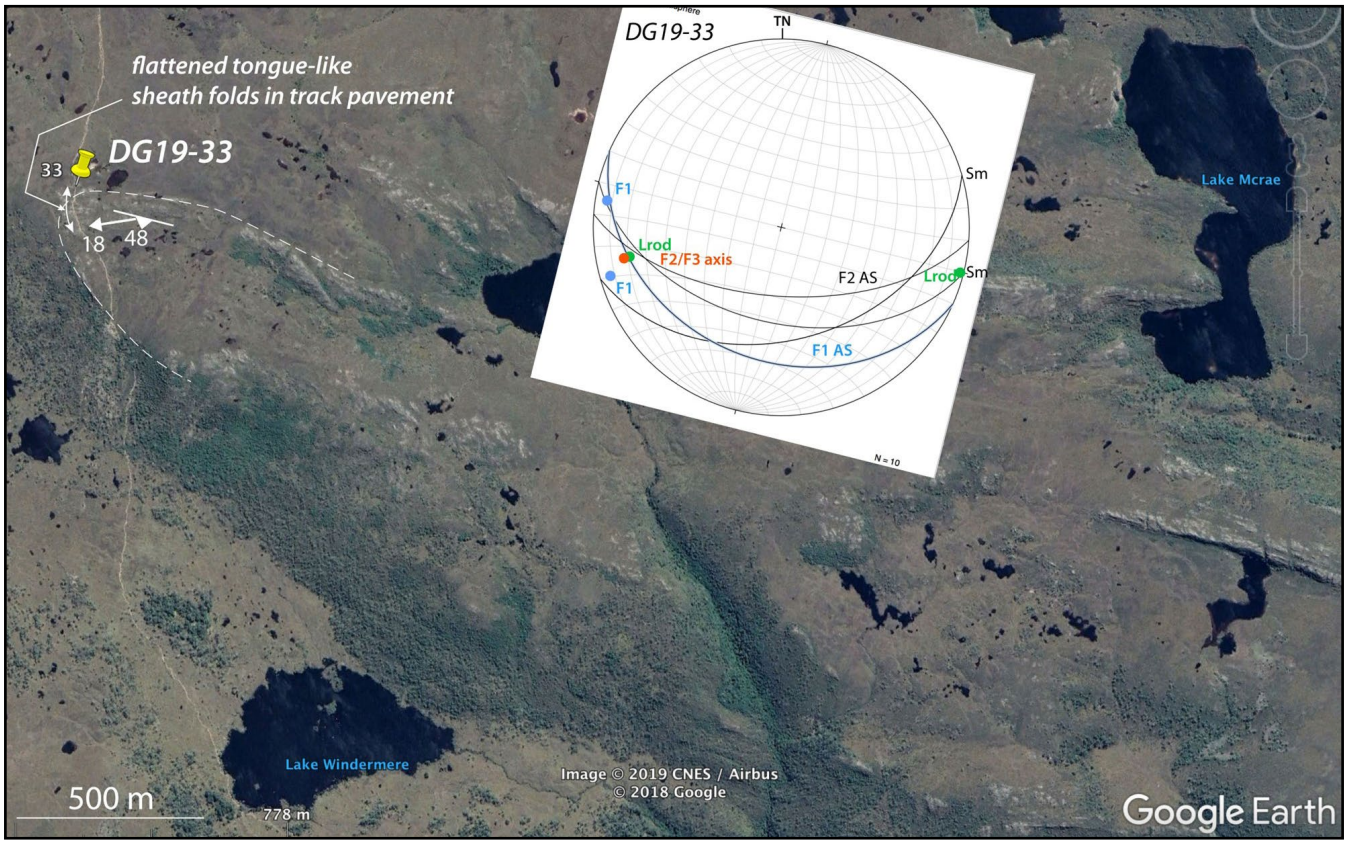

Figure 108 (Above). Google image of the Overland Track north of Lake Windemere (station DG17-33) showing west-northwest trending outcrop traces. The inset stereonet shows great circle traces of the south-dipping foliation Sm, F1 and F2 axial surfaces with blue dots representing F1 isocline axes, the red dot an F2/F3 fold axis and the green dots representing the rodding lineation (Lrod) attitudes.

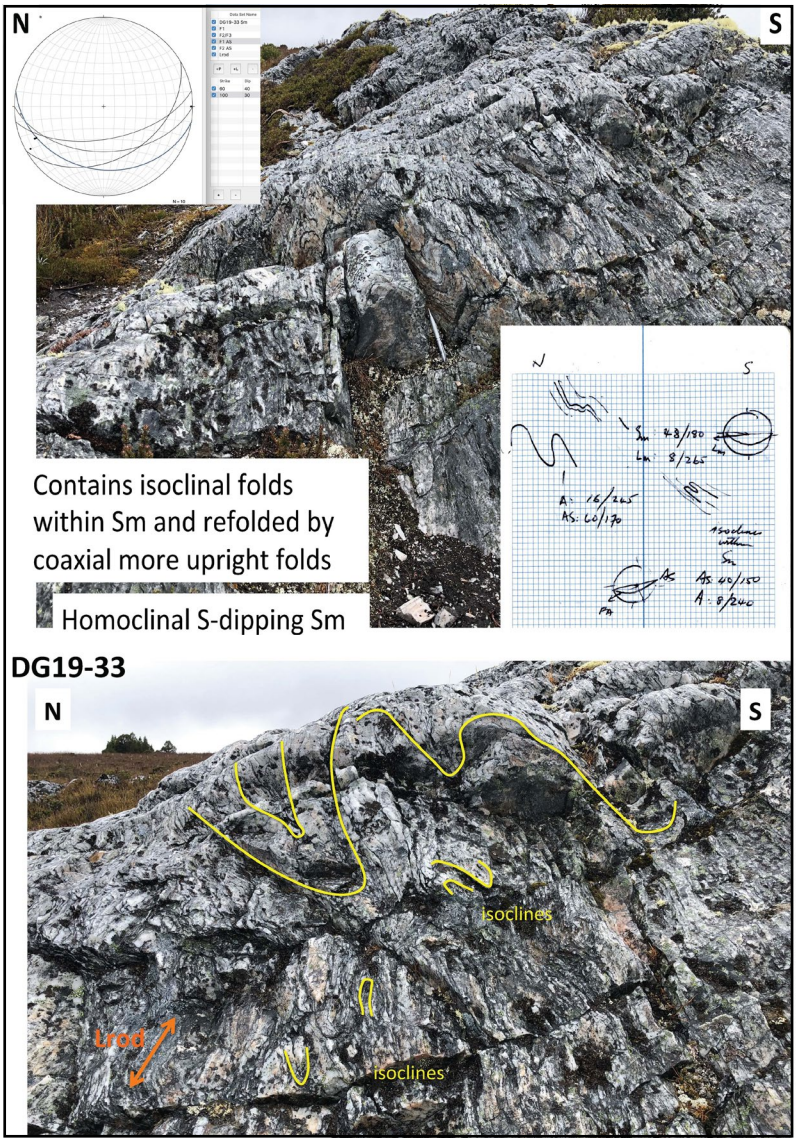

Figure 109 (Left). Profile view looking to the east of outcrop DG19-33 on the Overland Track north of Lake Windemere. Strongly to intensely foliated quartzite shows inclined, tight, north-vergent asymmetric folds that coaxially refold small-scale isoclines within Sm (compare with Figure 110) (Photo credits: David Gray).

Figure 110. Flattened, refolded isoclinal fold within lineated and rodded quartzite. Outcrop station DG19-33 north of Lake Windemere (Photo credit: David Gray).

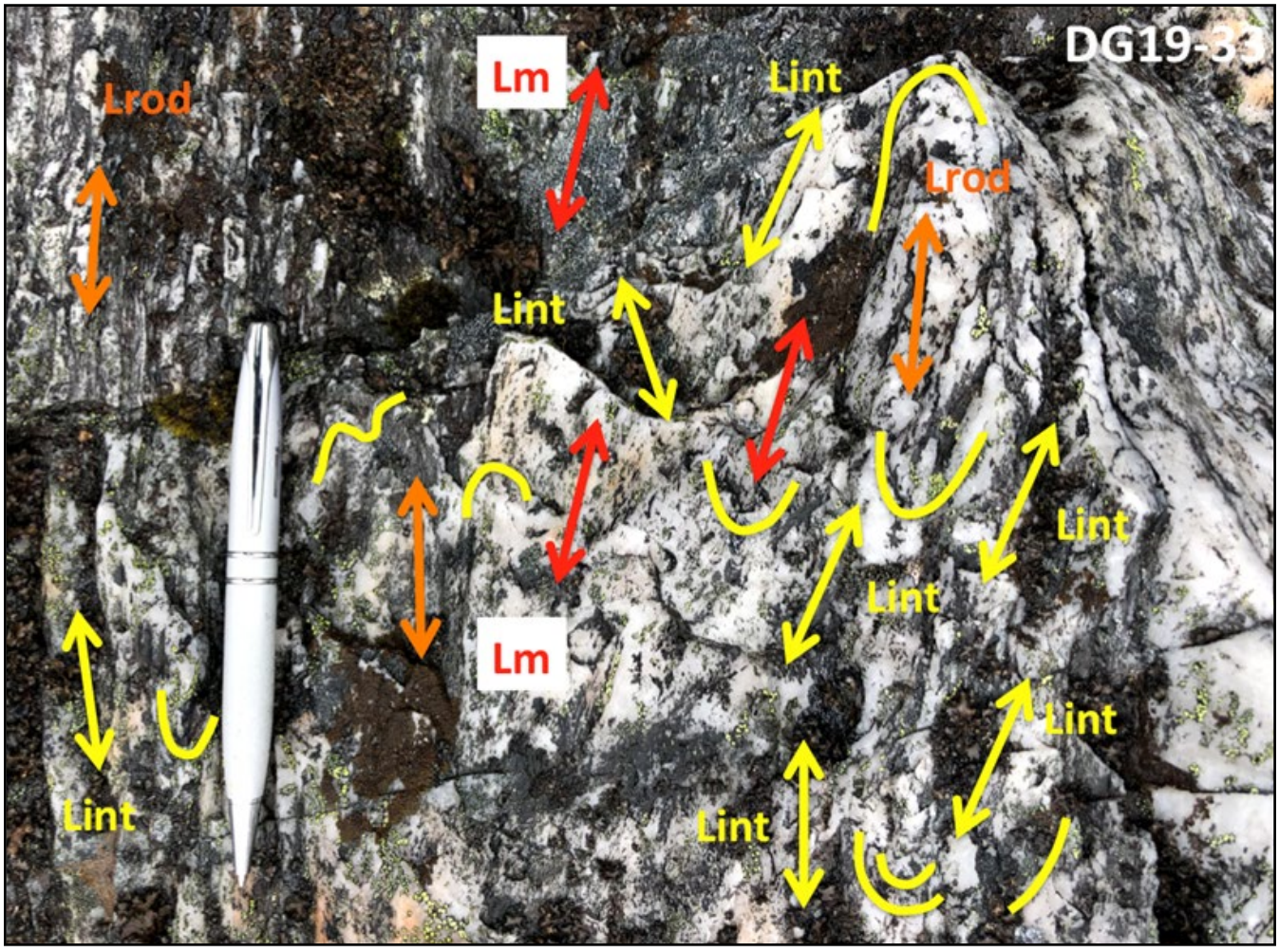

Figure 111. Sub-horizontal outcrop pavement view of quartzite foliation Sm. Outcrop station DG19-33. Remnants of flattened isoclinal sheath folds outlined by intersection of So/Sm with Sm (yellow line traces) produce a "herringbone" or crisscrossing pattern within Lint. This results in a rodding lineation Lrod (orange line traces) best seen in photo top left. Note Lrod is sub-parallel to the mineral stretching lineation Lm (red line trace) where the Lm is highlighted by a strong quartz grain elongation within Sm. (Photo credit: David Gray).

Figure 112 (Above). Flattened sheath-like isoclinal hinge within foliation Sm in strongly foliated quartzite with a pronounced mineral stretching lineation Lm (red arrow) (Photo credit: David Gray).

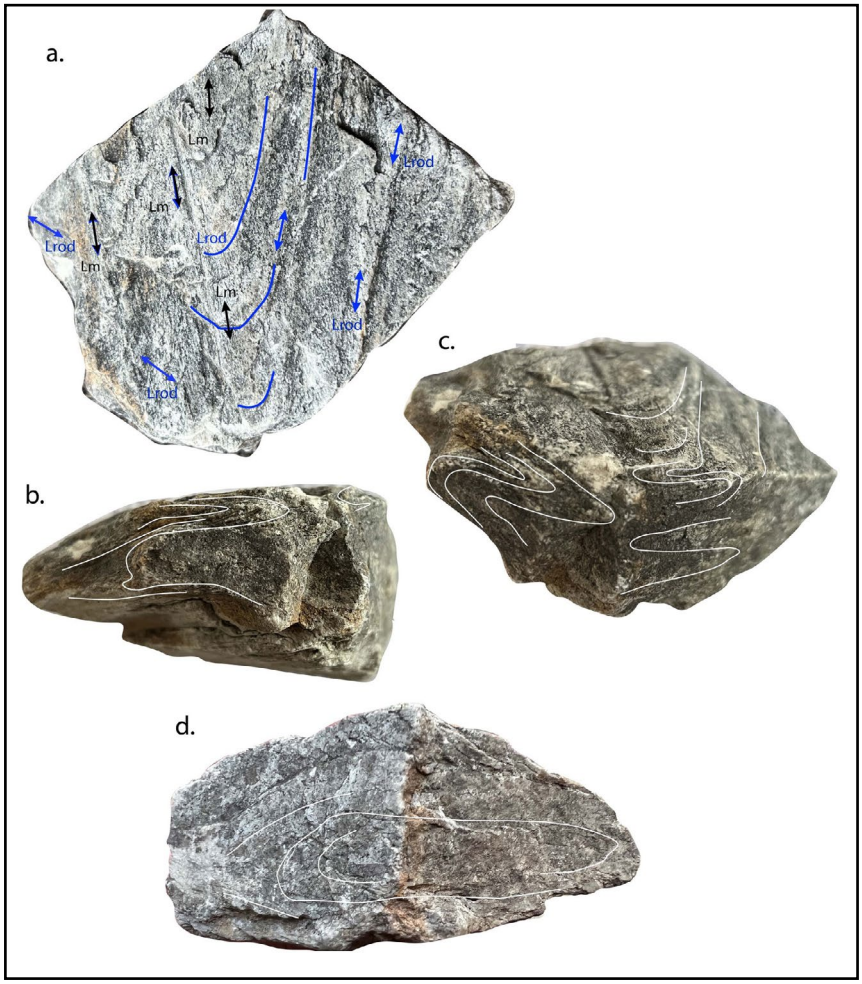

Figure 113 (Left). Small-scale sheath fold example from the Overland Track north of Lake Windemere (fig.11, Gray et al., 2024), Outcrop station DG19-33. Sample width is 10 cm. (a) View of upper surface showing flattened sheath form with curved intersection traces (Lint or Lrod) shown by the blue line traces within foliation (Sm), and the mineral lineation (Lm) by the black arrows. (b) Left side view showing the sheath fold lateral termination as an isoclinal fold. (c) Inclined frontal view showing the internal meso-fold interactions within the sheath. (d) Rear view of the sample showing the closed, ovoid form of the sheath fold core. Note that the sheath elongation is sub-parallel to the mineral lineation Lm and therefore the bulk stretch (Photo credits: David Gray).

5.4.2 Pine Forest Moor

Quartzite in the Pine Forest Moor area (Figure 114) has a northwest dipping foliation So/Sm containing a southwest plunging intense rodding lineation and mineral stretching lineation (Figures 114 and 115).

Flattened sheath-like isoclines form closed loop intersection traces on the foliation Sm (Figure 116). The north dipping foliation So/Sm occurs on the southern limb of a broad open, gently west-plunging synform (Figures 106 and 107).

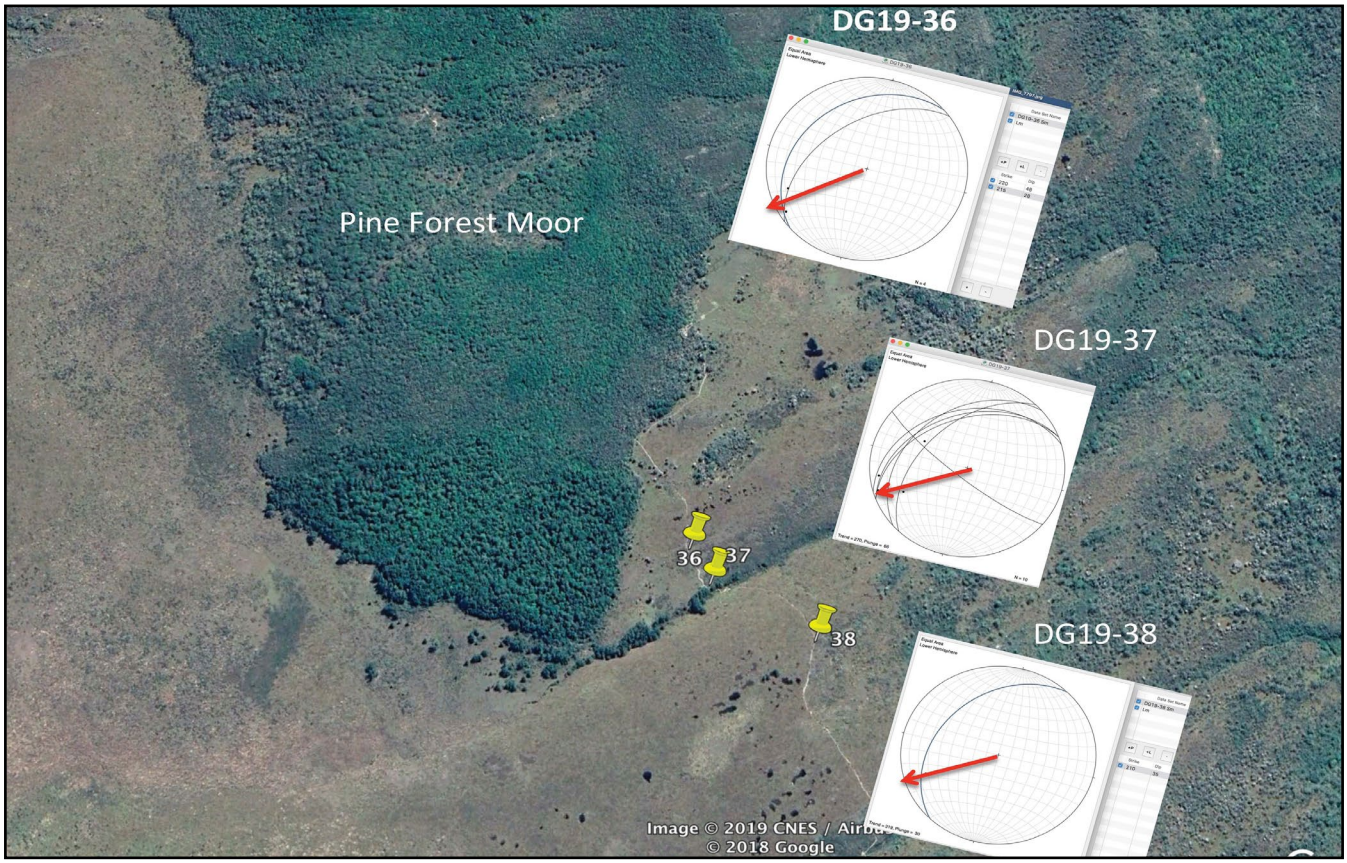

Figure 114. Pine Forest Moor Google satellite image showing stations DG19-36, 37 and 38 and stereonets displaying dominant lineation direction.

Figure 115. Pronounced stretching lineation in platy quartzite mylonite defined by a combined rodding/intersection lineation and quartz mineral elongation fabric (Photo credit: David Gray).

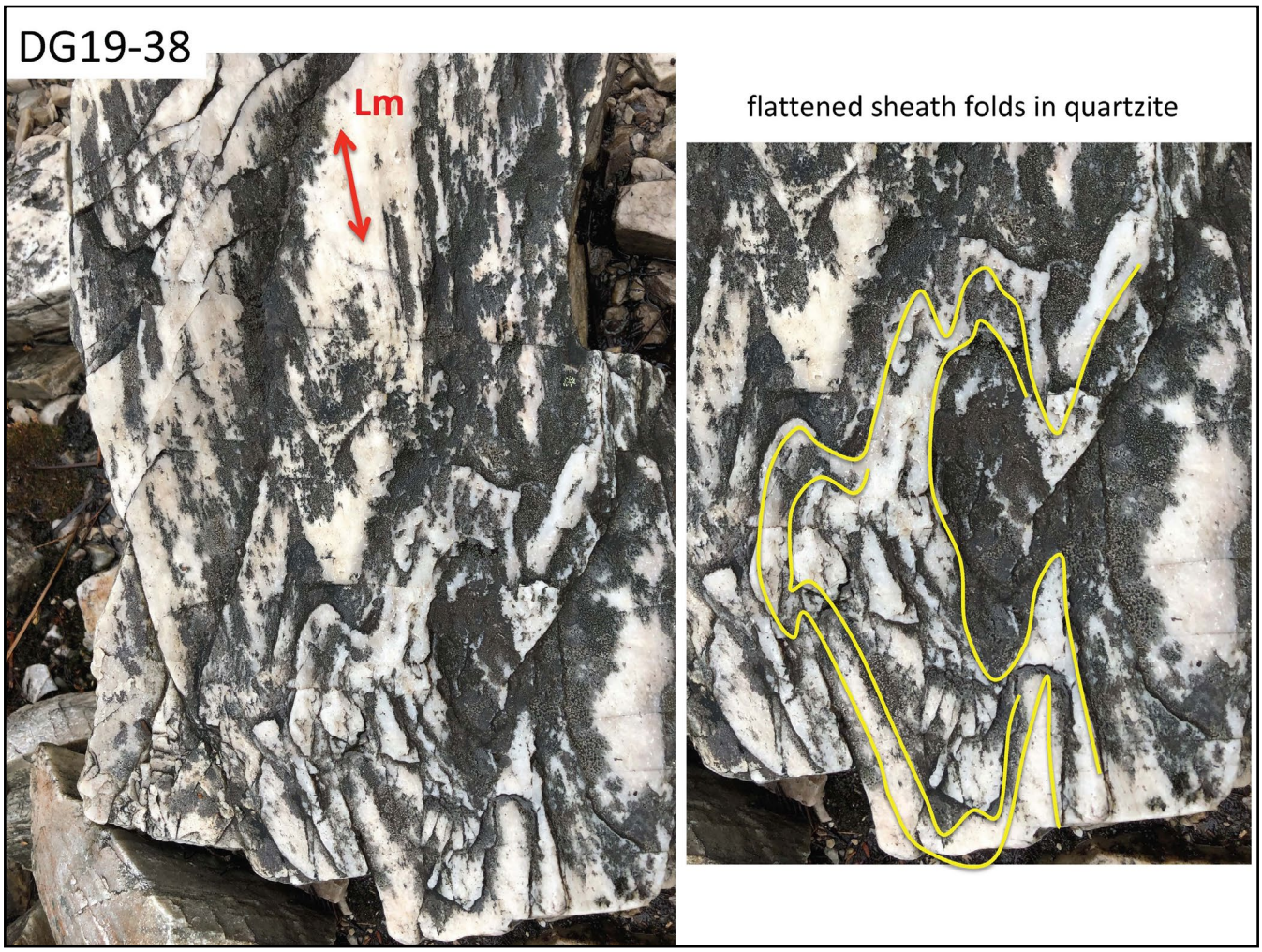

Figure 116. Stacked, flattened and elongated, "tongue-like" sheath folds in strongly foliated quartzite (photo left, lower right) with relationship to the mineral stretching lineation Lm shown by the red arrow. Enlargement (photo right) shows yellow line traces outlining the fold geometry as intersection traces of So/Sm with Sm. Outcrop DG19-38 (see Figure 114 for location). (Photo credit: David Gray).

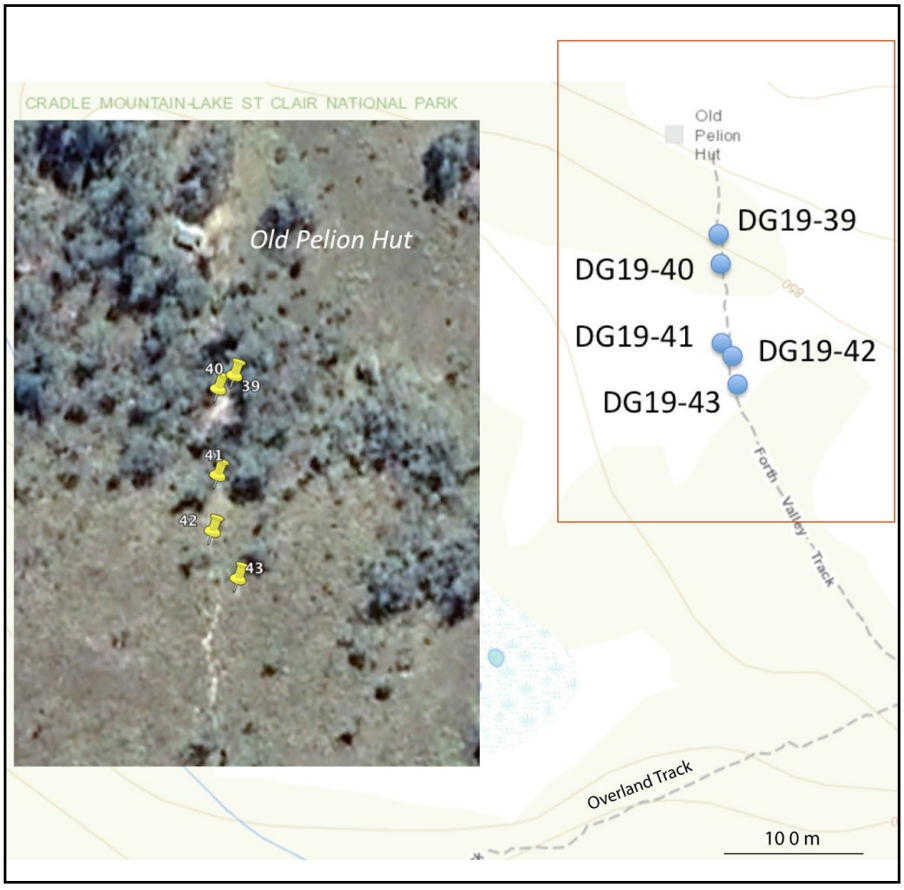

Figure 117. Old Pelion Hut map showing the positions of the outcrop stations DG19-39 to DG19-43. ListMap topographic map as base with Google satellite image as inset.

5.4.3 Old Pelion Hut Track

Quartzite along the Forth Valley Track into Old Pelion Hut (Figure 117) shows a consistent southeast dipping foliation Sm (Figures 118) containing isoclinal folds that have curved hinge lines and significant fold axis plunge and plunge direction variations (Figure 118). Isocline axes fan through 180° within the south-southeast dipping foliation Sm (Figure 118). These outcrops provide excellent examples of incipient sheath fold development (Figures 119, 120, 121 and 122), folding of the mineral lineation (Figure 123) and classic herringbone lint pattern (Figure 124), all part of the broadly folded basal high strain zone (HSZ) to the quartzite (Figure 107).

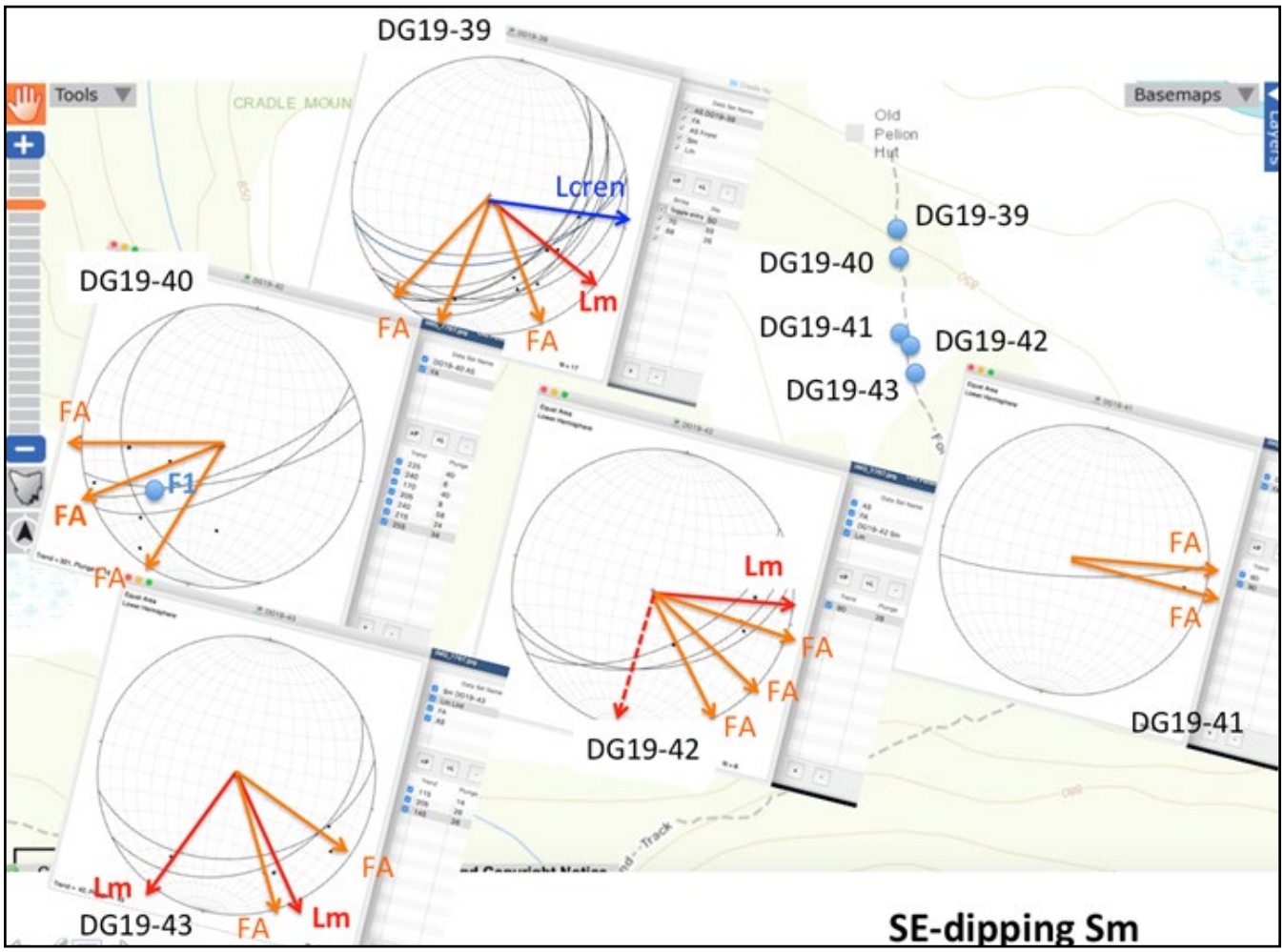

Figure 118 (Above). Old Pelion Hut structural data presented as individual stereonets for each DG19 station located by the blue dots on the underlying ListMap topographic base map. Isocline F1/F2 fold axis trends are shown by the orange arrows, mineral lineation Lm by the red arrows and crenulation lineation by the green arrow. The fold axes fan through 180° within the south-southeast dipping foliation. Lcren denotes the F3 fold axis trend.

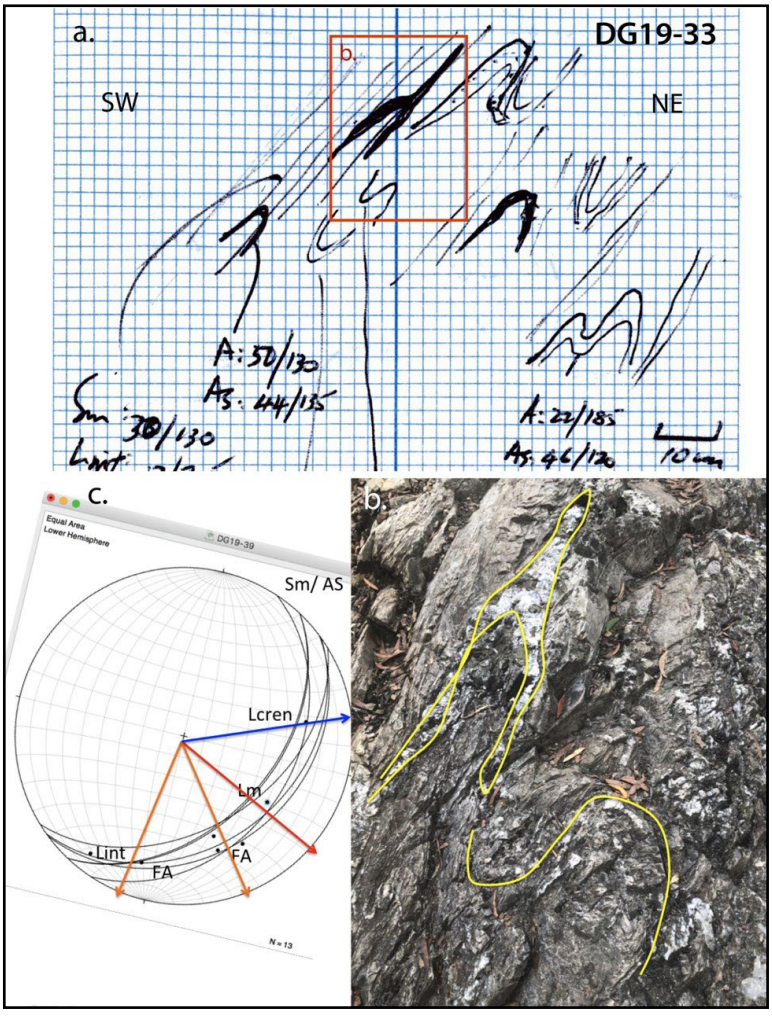

Figure 119 (Right). Profile view of fold stack within strongly to intensely foliated quartzite near Old Pelion Hut at DG19-39. a) Notebook sketch profile of dismembered to rootless asymmetric folds. The red rectangle shows the position of the outcrop photograph in (b). b) Flattened and elongated isocline nose in strongly foliated quartzite. c) Stereonet showing foliation Sm and isocline axial surfaces as great circles. Lineation and fold axis attitudes as black dots with trends highlighted by the coloured arrows. Orange: fold axis trend. Red: mineral lineation Lm trend. Blue: crenulation lineation trend (Photo credit: David Gray).

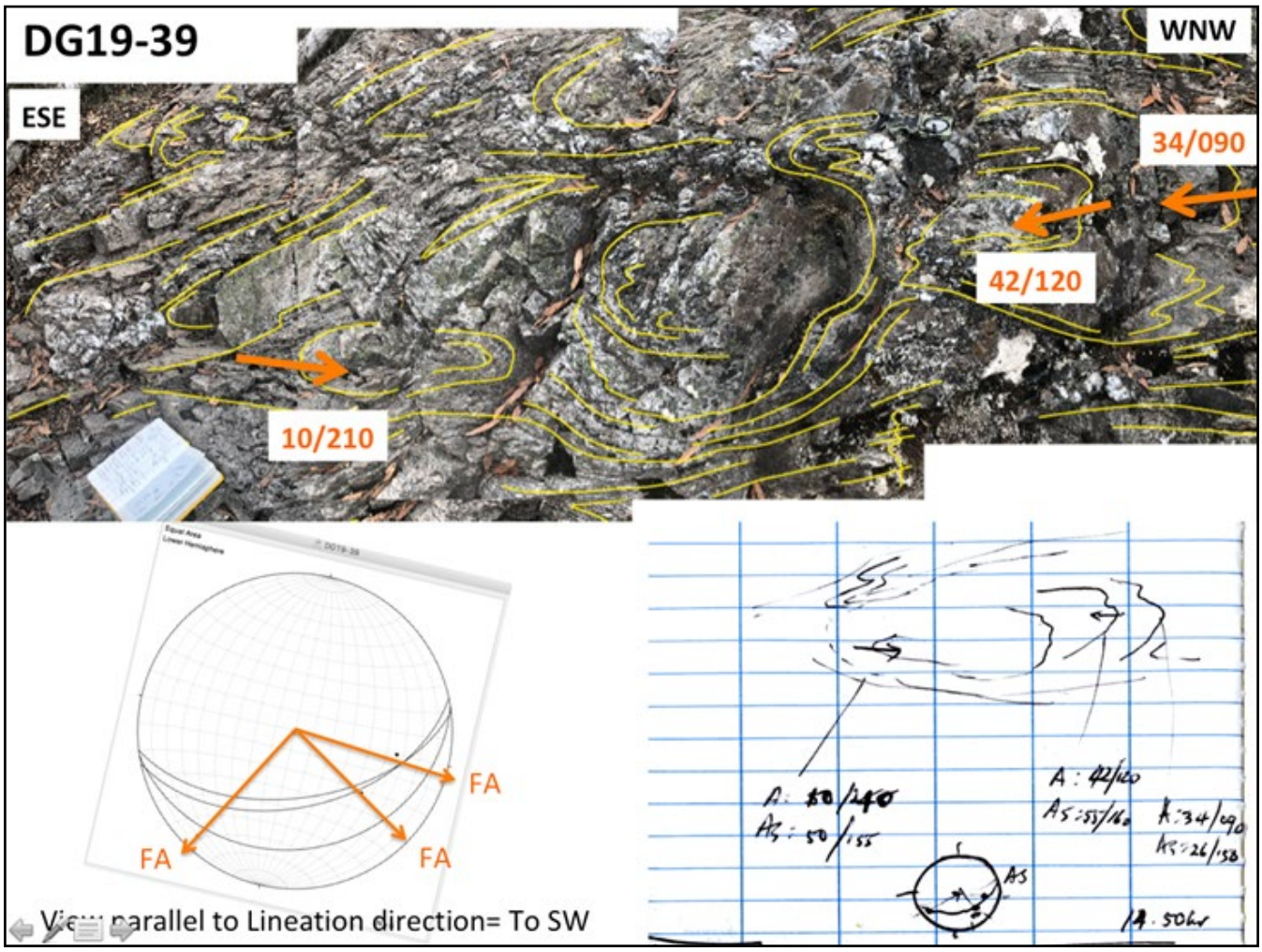

Figure 120 (Above). Strike-parallel view of the fold stack outcrop DG19-33 shown in Figure 119. This view (looking southwest) shows an ovoid shaped section through a sheath fold nose entrained within the south dipping foliation. The sheath closure displays opposite plunges at each end and displays varying fold plunges typical of a markedly curved hinge line (see stereonet inset) (Photo credit: David Gray).

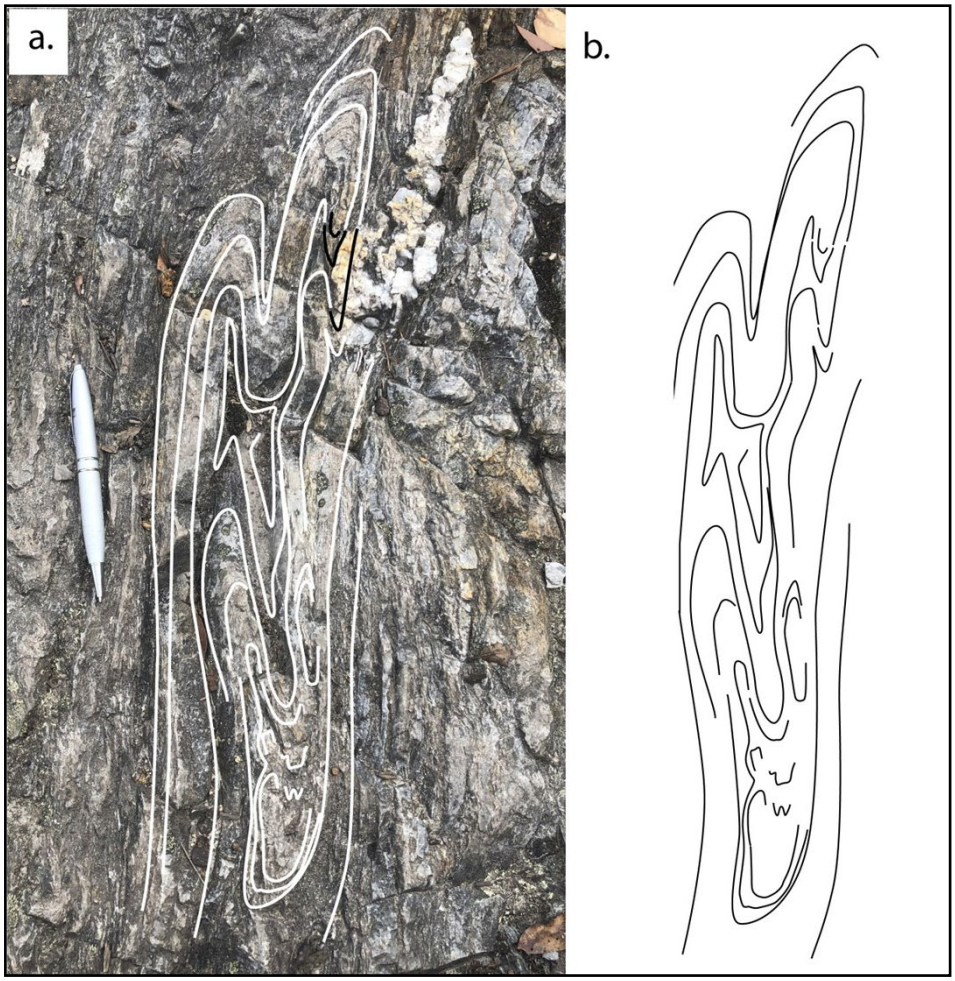

Figure 121 (Left). Plan view of variably plunging isoclinal fold hinges with overall closed loop outcrop traces in outcrop pavement at station DG19-40. This pattern is typical of early isoclinal folds with markedly curved hinge lines. (Photo credit: David Gray).

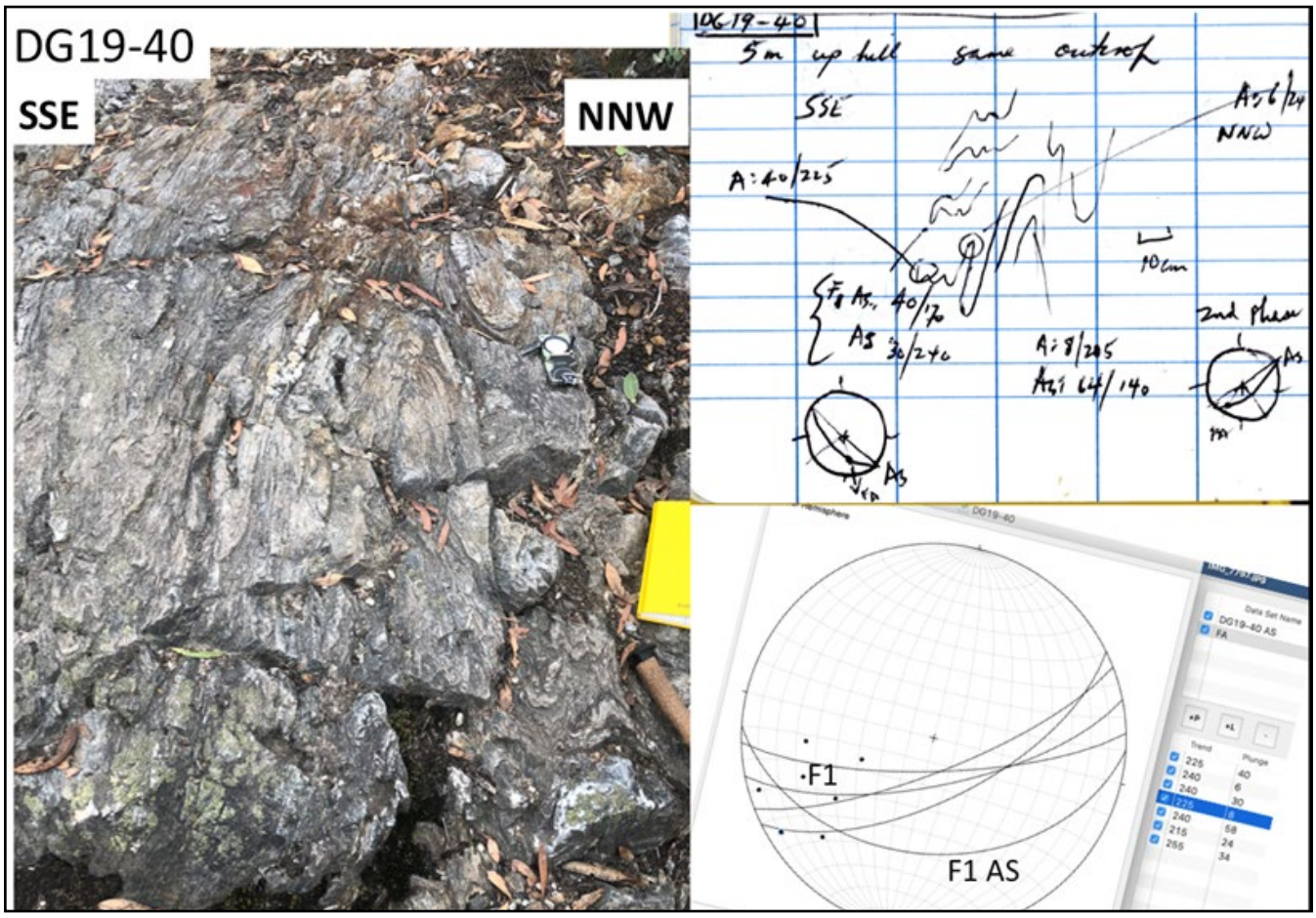

Figure 122. Profile view of outcrop DG19-40 with outcrop photograph (top left), Fieldbook outcrop sketch profile and measurements (top right) and structural data presented in stereonet form (bottom right) (Photo credit: David Gray).

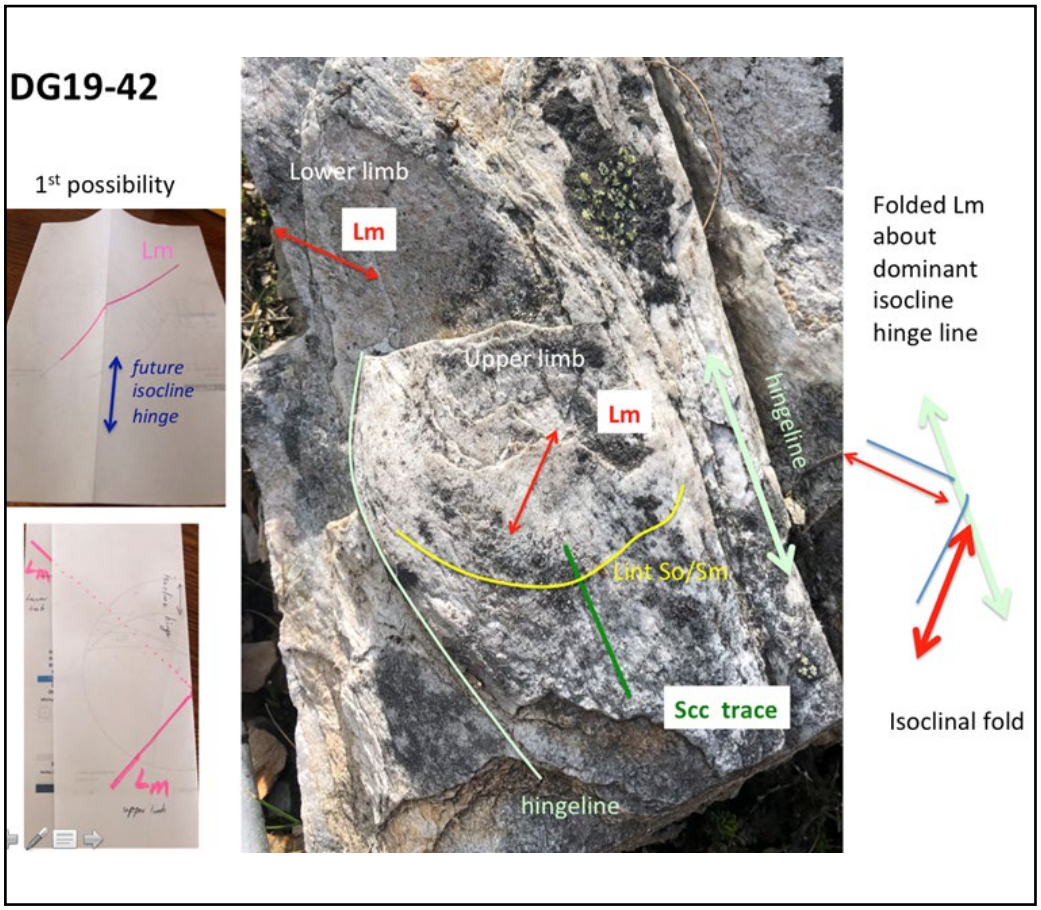

Figure 123 (Left). Folded lineation pattern across an isoclinal fold pair with weakly curved fold hinge lines.

Centre: Photo of the upper and lower isocline fold limbs with different Lm trends shown by the red arrows. Isocline hinge lines are shown by the light blue line traces. Left: Paper fold simulation of isoclinal folding a lineation (pink line) producing the pattern observed in the photo. Right: Geometrical relationships of the lineation pattern (dark blue line traces and red arrows) with respect to the fold hinge line (light blue trace). Compare with folded paper simulation on left (Photo credit: David Gray).

Figure 124. Typical herringbone rodding lineation pattern due to stacked, flattened isoclinal fold hinges flattened and extended within the transposition foliation Sm. The curvy nature of the So/Sm intersection traces on Sm (white line traces) is due to fold hinge lines having incipient sheath form. Lm: blue line traces. Loose block on the side of the Forth Valley track near Old Pelion Hut (Photo credit: David Gray).

6.0 IMPLICATIONS OF THE NORTHERN TYENNAN SUBDOMAIN STRUCTURE

The Northern Tyennan subdomain structure provides further examples and explanations of structural relationships developed in subducted and exhumed continental margin rocks during non-coaxial shear. These include the relationships within the rock fabrics, the Mt Kate macrofold, the relationships in bounding high strains and the Liena-Borradaile F3 chevron fold domain.

6.1 The Role of non-coaxial shear in Northern Tyennan Fabric Development

Strongly deformed quartzites in the Northern Tyennan subdomain show the evolution of a rodding lineation (Lrod) within Sm, herringbone rodding (Lrod) patterns, and flattened tongue-like sheath folds also in Sm as part of fabric evolution in non-coaxial general shear (Figures 125 and 126).

Folds initiate at high angle to the shear direction and with increasing shear strain develop curvilinear hinge lines (Figures 125a and 126a). At very high shear strains the folds become extremely elongated and flattened "tongue-like" tubes within the developing transposition foliation (Figures 125b and 126b, c). The flattened sheath folds occupy thin (1-2 cm thick) stacked sheets and commonly show overlapping hinges to produce a herringbone pattern of interfering rods on composite foliation surfaces (red lines in Figure 125c). At higher shear strains the rodding becomes more sub-parallel and approximates the stretching lineation Lm (compare the red and black line traces in Figure 125d).

6.2 The Role of non-coaxial shear in Northern Tyennan Fold Development

Curvilinear fold hinge lines (Figures 125a and 126a) are common at all scales in the Northern Tyennan subdomain. The fold hinge lines become markedly elongated and flattened with increasing shear strain $\gamma>5$ (Figures 125b and 126b, c).

As part of this general non-coaxial shear deformation a large part of the Northern Tyennan subdomain (Northern Tyennan F3 Chevron Fold Zone, Area 3, Figure 16) has undergone refolding (Figure 127b), fold tightening (Figure 127c) and subsequent rotation. This is analogous to interpreted poly-deformation within the core of the Eastern Tyennan (Gray and Vicary, 2024) and the internal parts of the Southern Tyennan mega-sheath folds (Gray and Vicary, 2023).

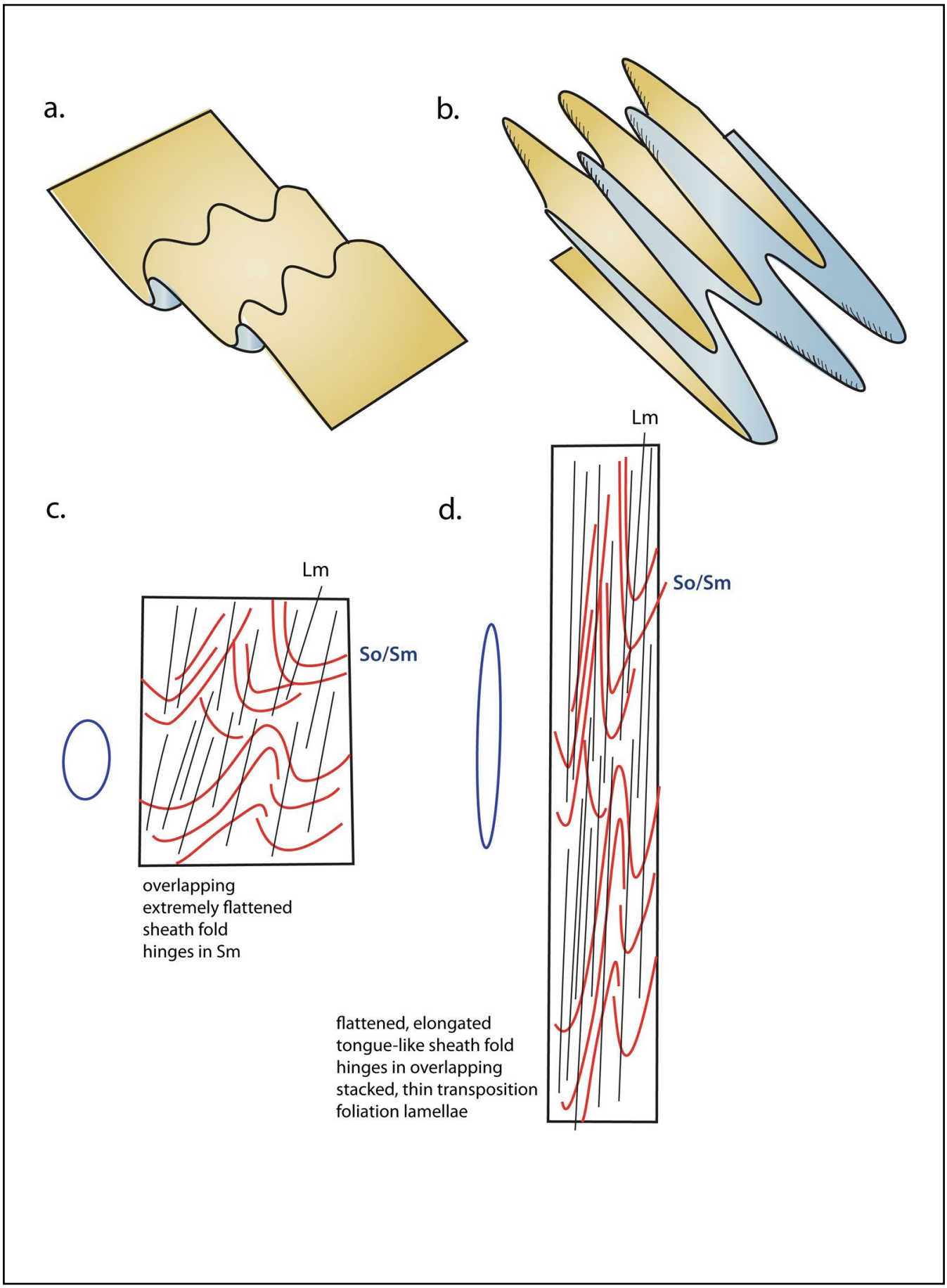

Figure 125. Schematic sheath fold evolution diagram (a. and b.) and rodding fabric in Sm diagram (c and d) developed in non-coaxial shear. a) Asymmetric fold couples developed in general non-coaxial shear (upper right-over lower left: sinistral shear). b) Resultant stacked sheath fold tubes developed from (a) at very high shear strains (γ >10). c) Incipient rodding/intersection lineation within Sm at low strain. d) Classic "herringbone" rodding lineation (Lrod) pattern developed from stacking overlapping, oppositely closing, sheath fold hinges at high strain. See ellipse shapes for strain comparison.

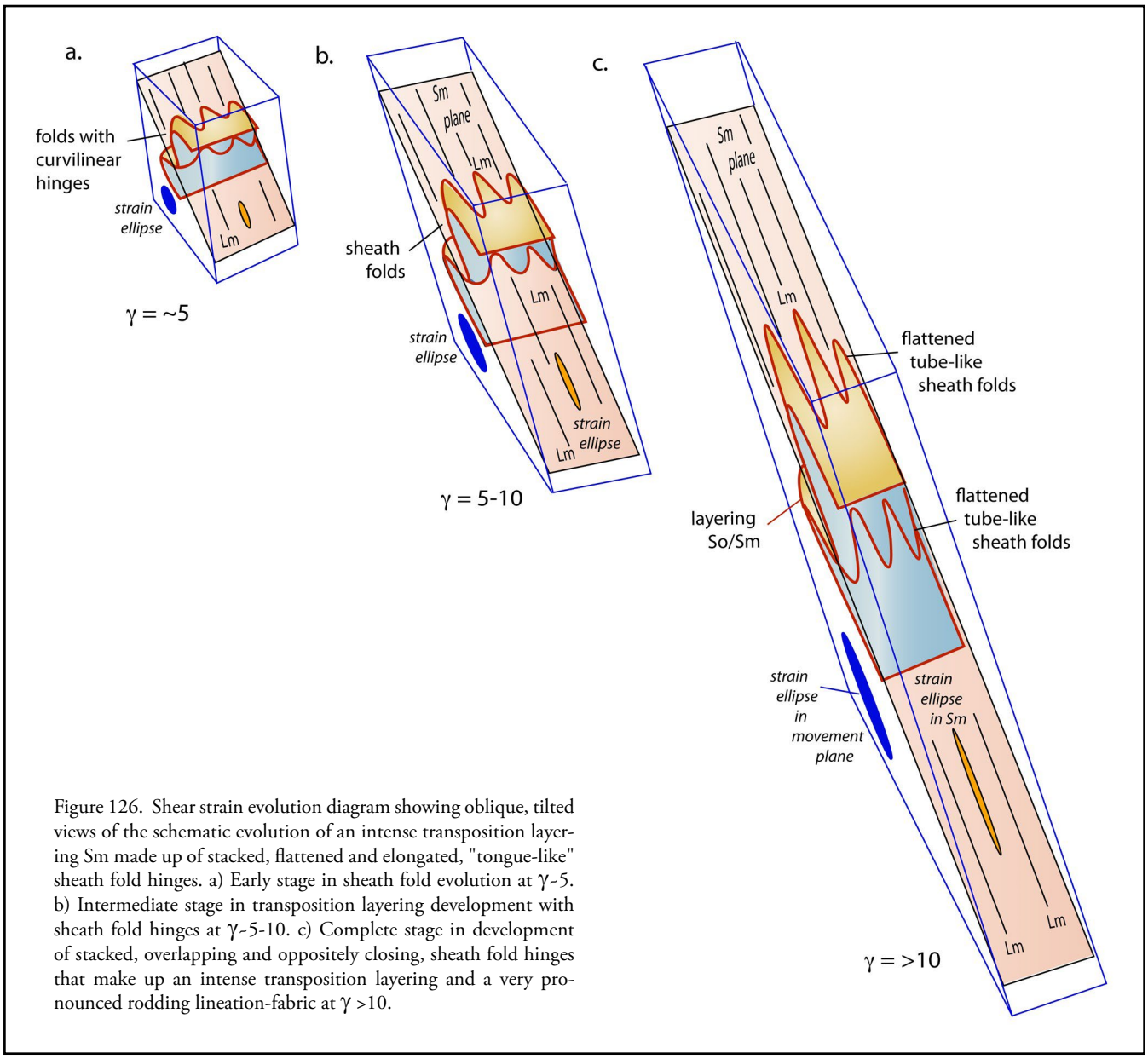

Figure 126. Shear strain evolution diagram showing oblique, tilted views of the schematic evolution of an intense transposition layering Sm made up of stacked, flattened and elongated, "tongue-like" sheath fold hinges. a) Early stage in sheath fold evolution at γ~5. b) Intermediate stage in transposition layering development with sheath fold hinges at γ~5-10. c) Complete stage in development of stacked, overlapping and oppositely closing, sheath fold hinges that make up an intense transposition layering and a very pronounced rodding lineation-fabric at γ >10.

The sub-vertical nature of the F3 folds (present state) in both the Eastern Tyennan and Northern Tyennan subdomains is however, somewhat problematical. Curved fold hinge lines coaxial refolding and overprinting relationships all suggest folding and refolding in progressive general or simple shear as shown in Figures 127 and 128. Given the F3 folds are now vertical the question is whether they formed in this attitude, or in another and were then subsequently rotated to the vertical during slab rebound and extension in the Late Cambrian. Shear-related folding and refolding combined with "rebound" to the sub-horizontal does not give the observed geometrical relationships (i.e. axial surfaces with a sub-vertical attitude and approximate orthogonal relationship to the So/Sm enveloping surface) (Figure 128). Folds produced in general shear as shown in Figure 128 for both dextral and sinistral cases have asymmetric form and dipping axial surfaces when the enveloping surface is rotated to the horizontal.

Another explanation for the F3 fold tightening and rotation may involve subduction channel "pinch-out" at the allochthon leading edge (Figure 129). This would result in a "wedge" between the floor (autochthon) and lid (obducting ophiolite sheet) of the channel effectively acting as a backstop or buttress to the ascending slab. This would cause buckle shortening (F3 folding) in the allochthon (Figure 129c) where earlier F3 folds formed in channel shear would also be further tightened and rotated into an orthogonal relationship with the subduction channel. On rebound the buttress F3 folds would also rotate into a sub-vertical attitude with an approximate orthogonal relationship with the So/Sm enveloping surface.

6.3 Shear Sense Explanation and Implications

Unlike other parts of the Tyennan Domain, the Northern Tyennan subdomain has an apparent complex movement history with east-over-west, south-over-north and north-over-south shear senses observed. The conflicting shear sense data are from different tectonic units and levels in the composite allochthon, but do not appear to fit simple subduction zone models (Figure 130). A discussion of MP1 and MP2 shear directions based on position in the litho-tectonic stack is included below.

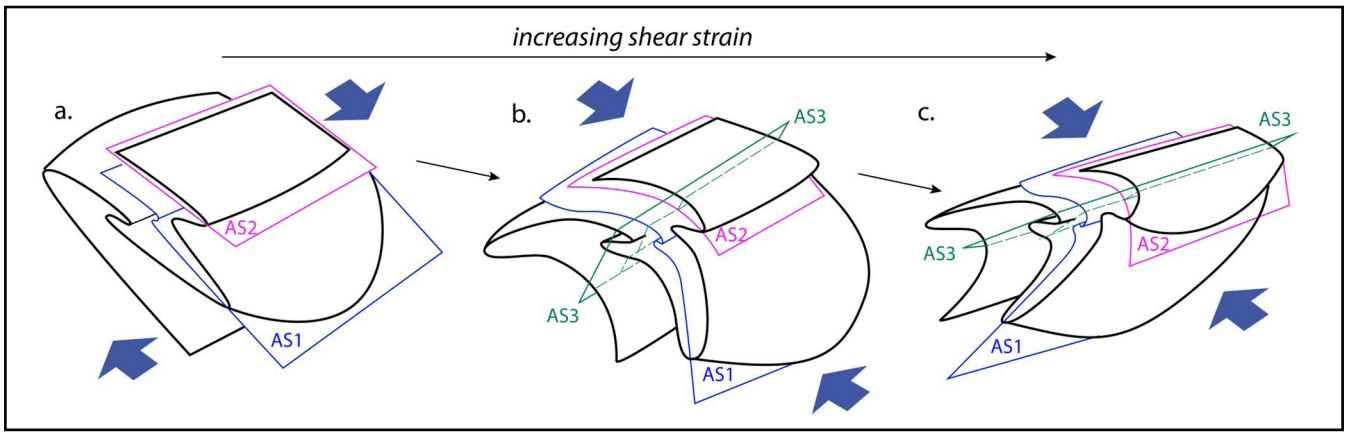

Figure 127 (Above). Refolding and poly-deformation in progressive, dextral non-coaxial shear (shear to the right of the diagram). a), b) and c) represent the initial, intermediate and final stages of the fold evolution in dextral shear with a third fold set (green AS3 axial surface) developing in (b) and tightening and rotating in (c). This process is envisaged to occur within a right-dipping subduction channel with later rebound such that AS3 becomes sub-vertical.

Figure 128 (Right). Schematic diagram of shear zones in profile illustrating angular relationships between asymmetric F3 folds and F3 axial surface attitude formed in i. general or simple shear in a west-dipping subduction channel with ii. "re-bound" rotation to the horizontal. a) dextral or west-over-east sense. b) sinistral or east-over-west sense. The schematic diagrams are looking north with west on the left and east on the right.

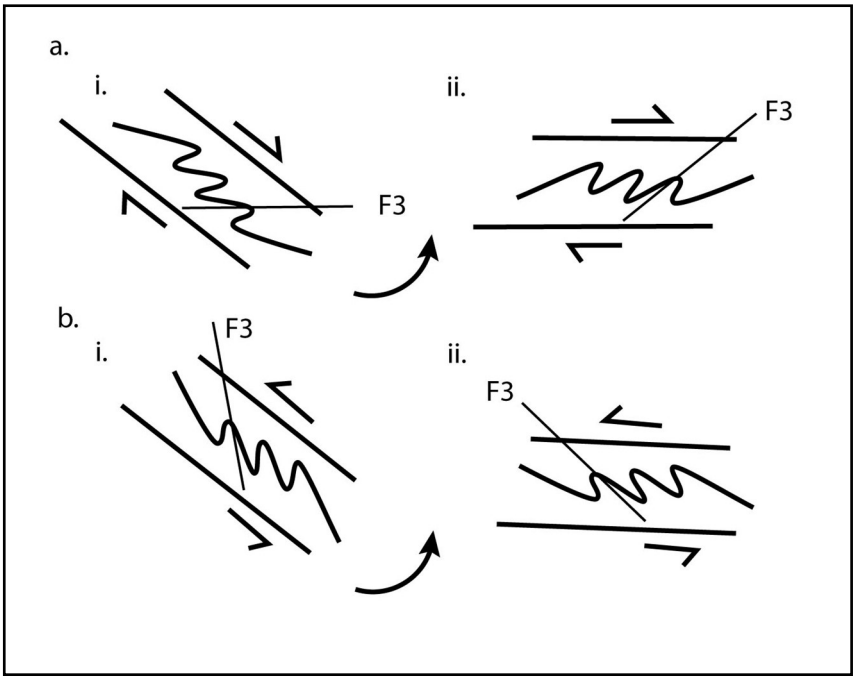

Figure 129 (Below). Simple, schematic crustal sections through an idealised subduction channel, where the channel is bounded by overriding ophiolite± asthenosphere and the underlying autochthon. A constrained wedge "backstop" can develop when the subduction channel narrows at the inflection point where the descending slab steepens at the subduction interface. Pinch-out of the ascending allochthon in the channel will occur at this inflection point constrained by the oceanic slab as a hanging wall "lid" to the channel. a) Steeper ascending wedge. b) Flatter wedge. c) Simple concept of channel pinch-out acting as a buttress or backstop to the ascending slab causing buckle shortening in the frontal part.

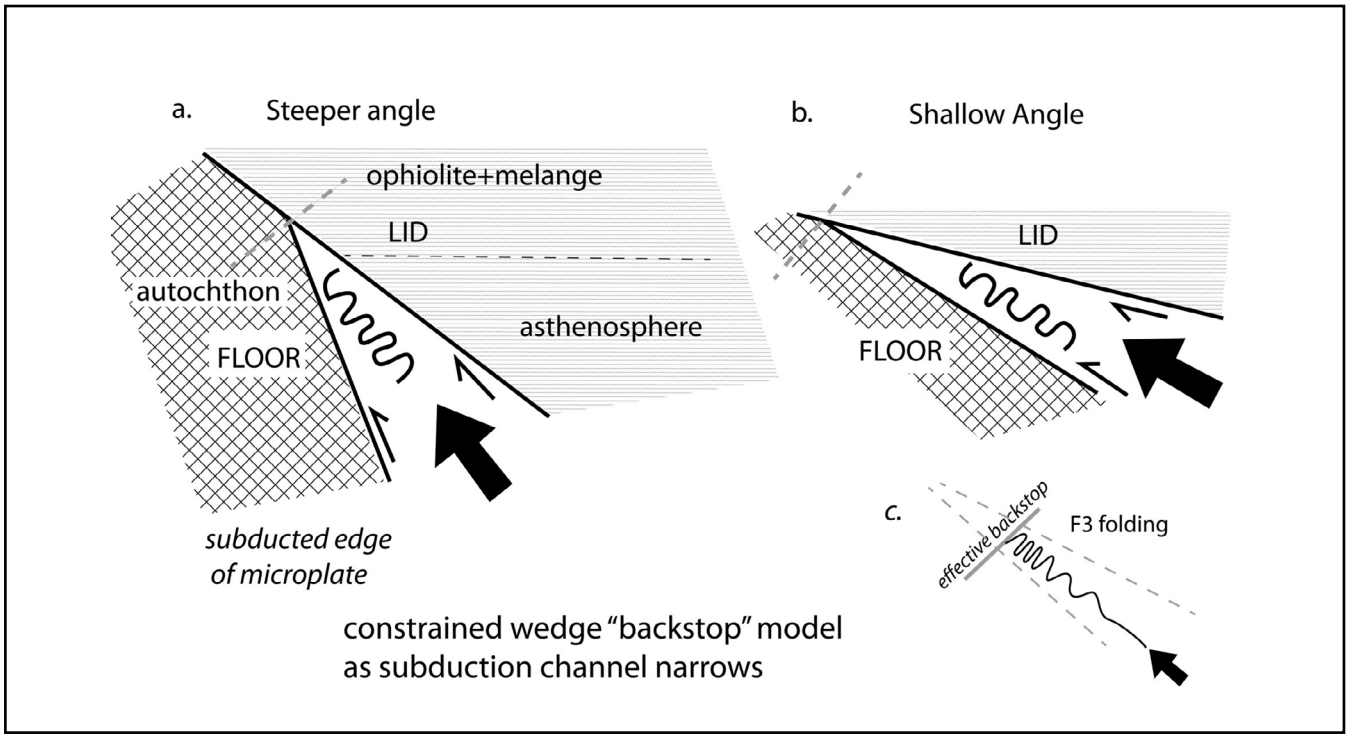

1) Base of the H-G layer (Dove Schist) (highest sheet)

MP1 and MP2 shear directions are approximately east-west trending but slightly discordant to the overall east-west strike of the eastern part of the Northern Tyennan subdomain. The shear sense indicated by shear bands in the high-strain margins of the high-grade schist (Figure 49) is sinistral, but with restoration of Sm to the horizontal give east-over-west shear sense. These margins are interpreted to represent the folded high strain base of the H-G schist "layer" and therefore require westward emplacement of the H-G "layer".

2) Within H-G layer (intercalated quartzite, quartz schist and garnet schist formerly the Howell Group) along the northeastern shoreline of Lake Rowallan. Shear sense within Sm is provided by:

- lineation MP1 movement plane (078°/68°S) (Figure 100): east-west movement plane
- sigma clasts (Figure 102): southeast-over-northwest
- domino-type boudins with flanking folds (Figure 103): southeast-over-northwest
- shear bands: northwest-over-southeast (Figure 102)

3) Base of the quartzite (lowest sheet) Along the Overland Track shear sense from shear bands was north-over-south (see DG19-35 and DG19-36 outcrop sketches, Figure 107) in the inferred basal part of the quartzite sitting above the (non-exposed) Scotchfire metamorphic sheet of the parautochthon.

Hypothetical shear sense variations are presented in two geometrical variants as profiles through the west-dipping subduction channel (Figure 130). The models assume strain partitioning through the allochthon constrained by shear strain along the upper and lower boundaries. During descent the leading edge of the Tasmanian microplate is "pulled" downwards by gravitational forces to depths of ~70-80 km with the potential shear bands shown. During buoyant ascent potential shear bands are also shown with opposite shear sense (Figure 130b)

But what are the current observations for the Tyennan Domain? All previous shear sense determinations in the Central and Eastern Tyennan subdomains have given west-over-east shear sense, particularly at the base of the H-G schist layer (Mt McCall and Collingwood Plain) and the basal part of the quartzite sequence (Frenchmans Cap) (see Gray and Vicary, 2021). This implies the same shear sense through the entire sheet even to the interface with the parautochthon (Scotchfire Sheet). Distinguishing between Stage 1 and Stage 2 shear bands is also problematical, although it is assumed that the shear bands develop mostly in Stage 2.

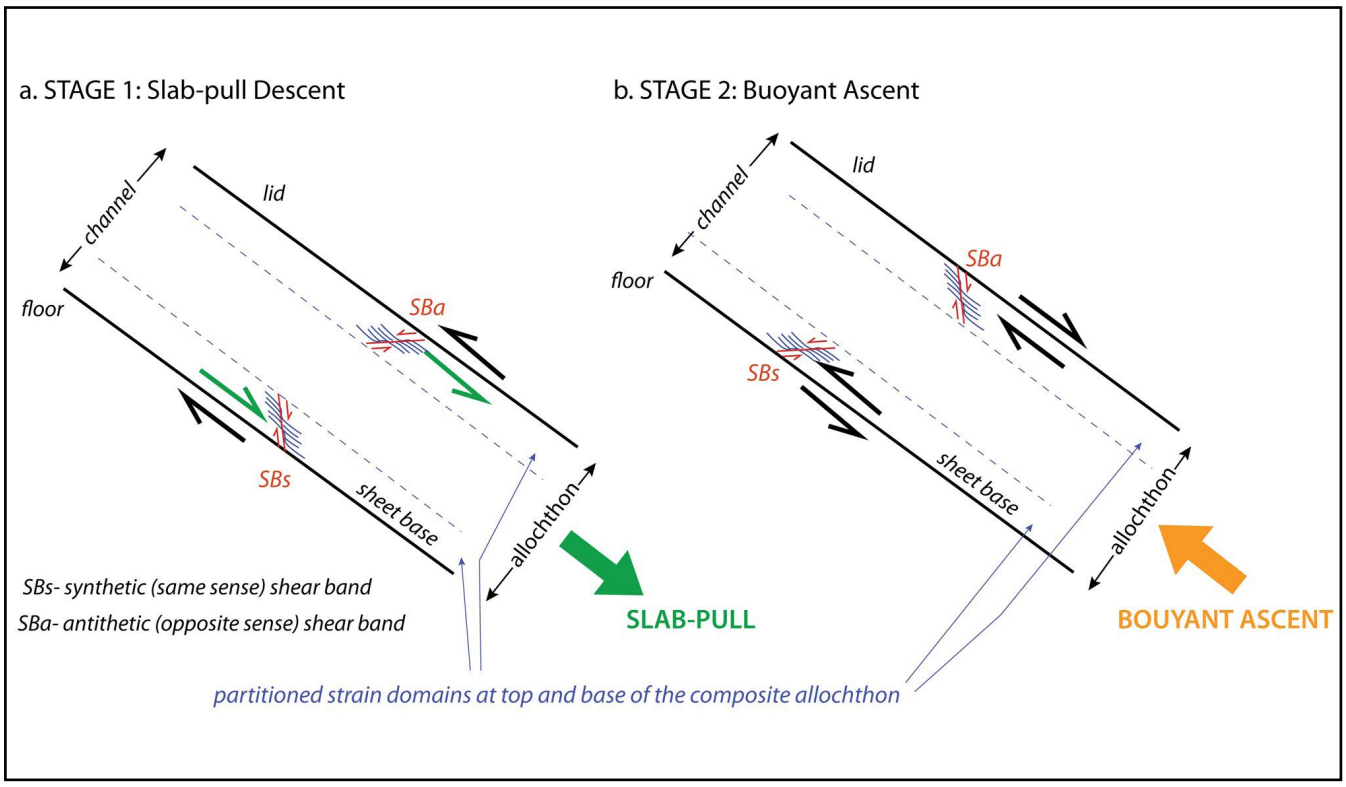

Figure 130. Simple, schematic subduction channel models in cross-section for distributed and/or partitioned strain during a) "Slab-Pull" descent and b) "Buoyant" ascent. Inferred movement is shown by the thick arrows for descent (green) and ascent (orange). The "allochthon" within the channel has upper and lower interfaces that show opposite sense shear. Hypothetical shear bands developed in the upper and lower partitioned strain zones also show different shear sense.

In summary, movement planes MP1 (derived from the lineation and foliation plane attitudes) and MP2 (derived from shear bands) represent the early stage shear direction and the late stage shear sense respectively. For the Northern Tyennan subdomain, these have a similar west-northwest trend, although there is evidence for a late stage? north-over-south shear sense in parts of the subdomain.

6.4 The Mt Kate Macro-fold Geometry

Understanding the Mt Kate recumbent macro-fold geometry is important for the Northern Tyennan subdomain structural evolution. Two variants are discussed:

1. The Gee et al. (1970) mapping suggests the Mt Kate macro-fold has a west-closing hinge with the hinge and lower limb truncated by a high strain zone (Waldheim HSZ). Quartzite layers that are structurally intercalated with the H-G garnet schist are truncated to the north by the inferred, but hidden, Late Cambrian Tyennan Margin Fault, and to the south by the Waldheim HSZ. The mineral lineation Lm is east-west trending approximately perpendicular to the curved hinges within the quartzite layers (Figures 36 and 37). The macro-fold is refolded by an, open, east-west trending antiform (Mt Kate antiform, Gee et al., 1970) to give a mushroom (Type 2 Ramsay, 1967) fold interference pattern.
2. Structural profiles across the Mt Kate macro-fold (Figures 31 and 38) combined with the FA^Lm rotation pattern (Figure 23) require the internal part of the macro-fold consists of an asymmetric west- and east-closing fold pair (see Section 3.6 and Figure 132). The rotation domain interface results from partial erosion of the upper limb of the east-closing sheath fold exposing the upper limb of the oppositely closing lower sheath fold as part of the asymmetric fold pair (Figure 24).

The relationships in (2) are critical to the Mt Kate macro-fold geometry. As part of this interpretation it is important that: i. The FA^Lm rotation pattern is preserved despite the tight to almost isoclinal chevron refolding of the internal macro-fold pair (Figure 133), and ii. The FA and Lm trend variations imply a marked curvature of the macro-fold pair hinge-lines. The overall geometric relationships cannot be explained by a west-closing sheath fold geometry as required by (1) (Figure 131).

In a simple schematic 3D geometry the Mt Kate macro-fold plunges west and has a now largely eroded, short, curved overturned limb with a long, originally planar lower limb, analogous to a "sled-runner" style geometry (Figure 134). The hinge to lower limb largely occupies the Northern Tyennan subdomain and subsequently gets refolded by the younger, upright (present state) F3 folds. An inner fold-nappe "core" exposed at Mt Kate consists of the oppositely east- and west-closing asymmetric fold pair (Figure 132b).

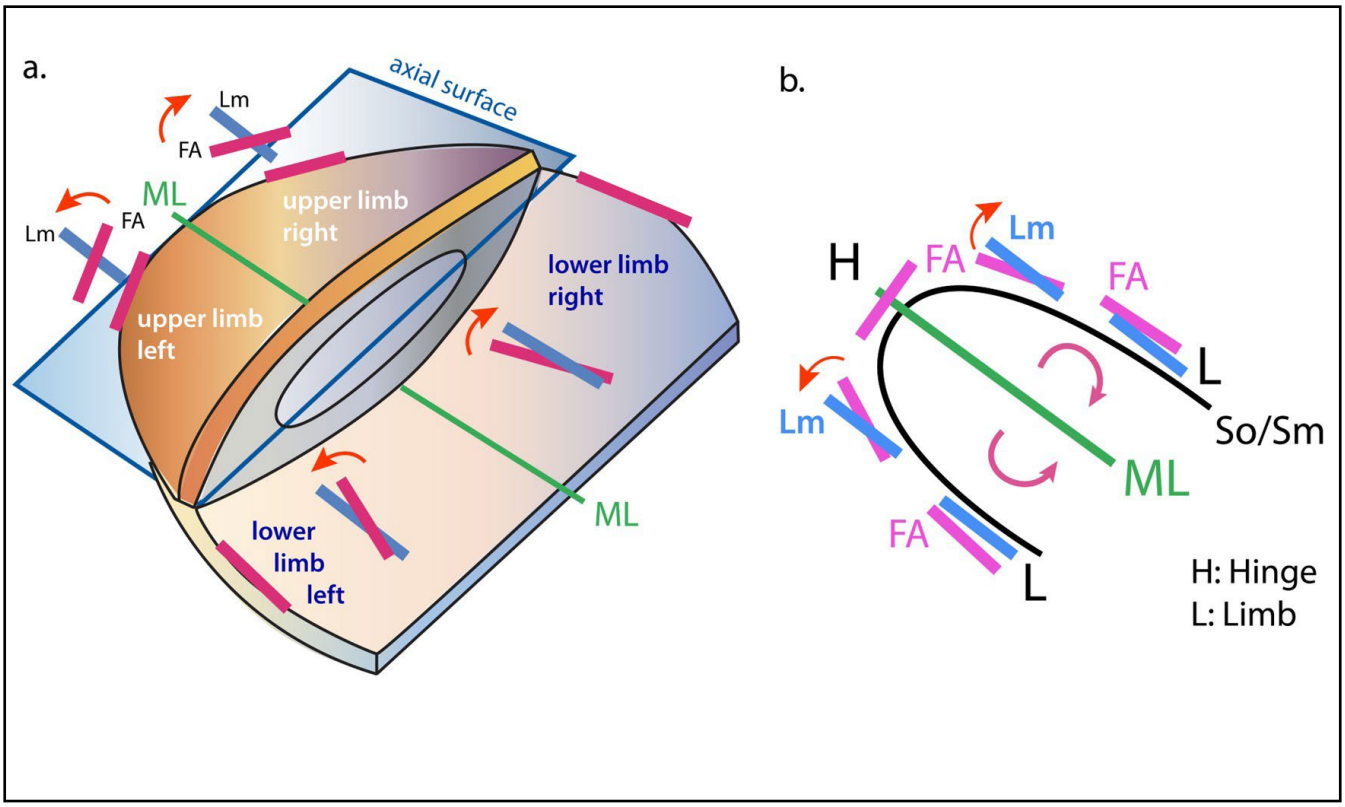

Figure 131. Schematic fold axis to Lm rotation (FA^Lm) diagrams (after Alsop & Holdsworth, 1999, 2004) for the assumed geometry of the Mt Kate west-closing, macro-sheath fold (i.e. west is to the top left in the direction of the green line ML). Upper and lower limb right and left rotation senses are shown. ML: sheath fold medial line. a) 3D form of the recumbent sheath fold. b) Plan view of the rotation relationships projected onto the axial surface showing clockwise and counter clockwise rotation domains relate to the hinge curvature of the macro-sheath fold.

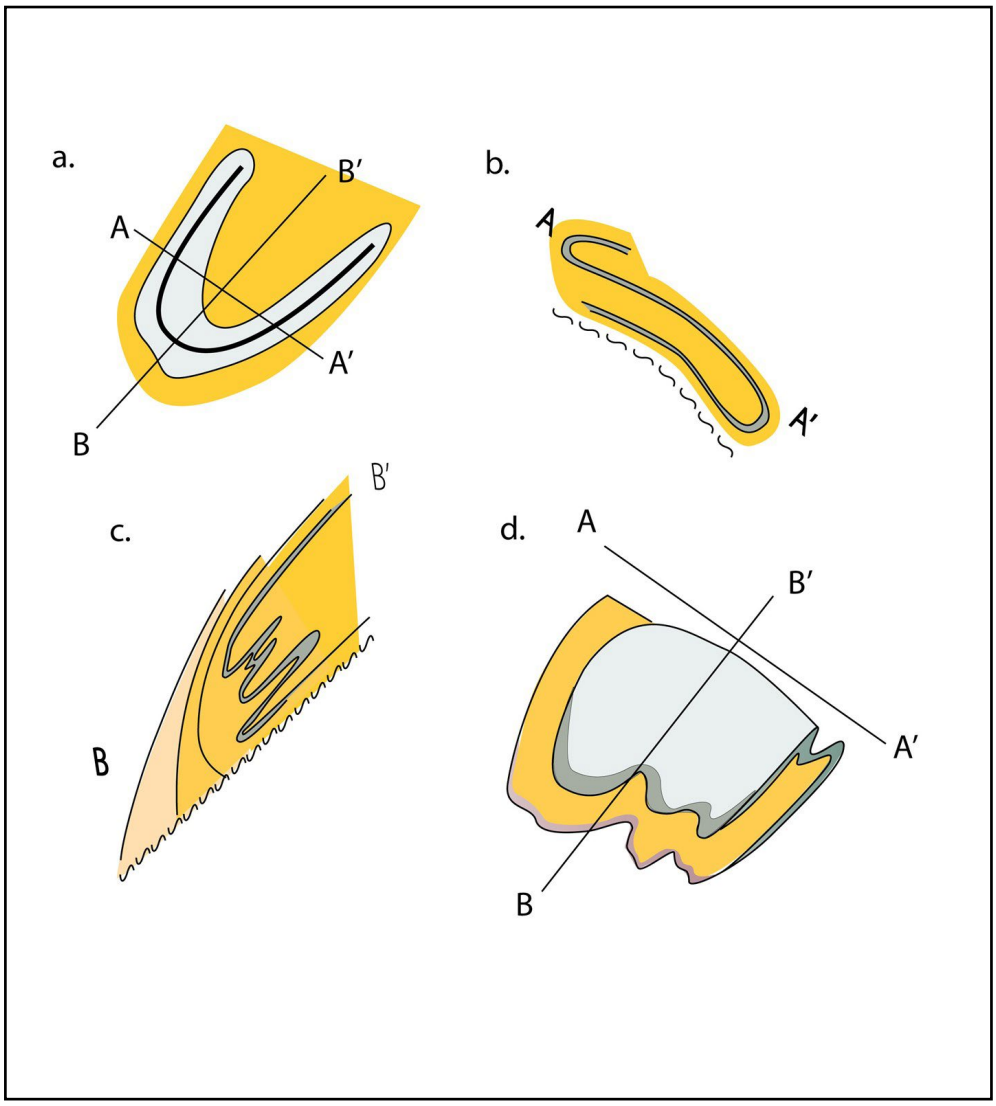

Figure 132. Geometry and form of the Mt Kate macro-fold shown in normal and longitudinal sections and a 3D diagram. a) Simplified map view with section lines A-A' and B-B' shown. b) Normal profile A-A' showing an interpreted asymmetric fold pair in the quartzite (see Figure 31). c) Longitudinal profile through the macro-fold showing truncation of the closure by the Waldheim High Strain Zone. d) 3D diagram showing the sheath-like macro-fold geometry within the asymmetric fold pair in the quartzite layer(s). The profile positions are shown.

Figure 133. Paper geometric model of refolded "sheath" fold pair (hinges or AST: blue-dash-dot line traces) by a chevron fold set (F3) approximately orthogonal to the initial or earlier F1/F2 folds (purple line traces). Note the original FA^Lm clockwise rotation on the sheath upper limb right (see Figure 131 above) remains consistent despite the later chevron fold overprint.

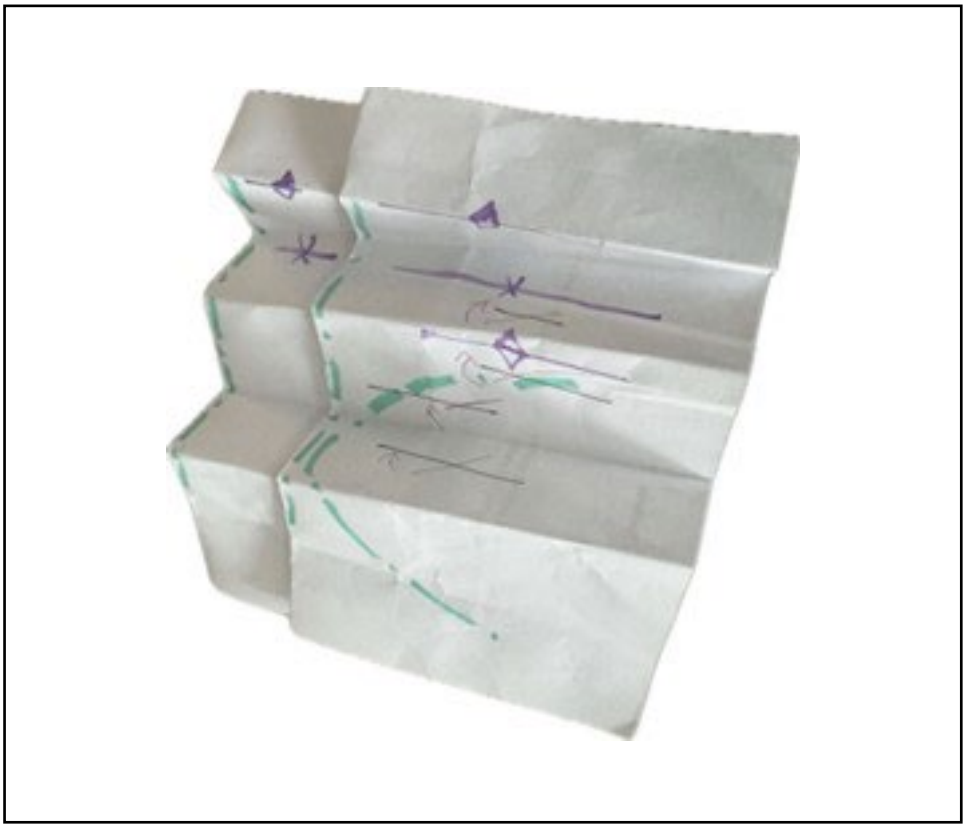

The macro-fold is considered to have undergone three "deformational" phases (Figure 134) including:

- **Phase 1a:** Development of the Mt Kate Macro-fold as part of the Tyennan leading-edge fold nappe.
- **Phase 1b:** Development of "trailing" asymmetric fold pairs during non-coaxial east-directed shear along the lower limb segment.
- **Phase 1c:** Continued non-coaxial shear with curvilinear, sheath-like hinge segments developing at high shear strains.
- **Phase 2a:** Continued non-coaxial shear with development of the chevron fold set (see Figure 135) that currently has an upright geometry and inferred sub-vertical stretch (present state). These folds refold the early F1/F2 Phase 1b recumbent, asymmetric folds (see inset sketch on lower right).
- **Phase 2b:** Continued non-coaxial shear with marked flattening and stretch to produce curvilinear, sheath-like hinge segments.
- **Phase 3:** bending of the leading edge fold-nappe with a strike change from north-south to east-west and development of sporadic north-west trending crenulation cleavage (Scc4).

Phase 2b folding is represented by upright extremely variably plunging F3 chevron folds in the eastern Liena-Borradaile domain (Area 3b, Figure 16). Geometrically these chevron folds tend to have broad, rounded antiformal hinges with intervening, narrow, tight cuspate synforms commonly bounded by zones of intense foliation Sm. In map view the hinge areas are shear zone-bounded, pod-like regions where So/Sm outcrop traces define ovoid to half-closed loops reflecting the curved and variably plunging nature (Figures 79 and 80). The resultant geometry is schematically shown in Figure 135.

In summary, the Mt Kate macro-fold has a compound geometry, with "sled-runner" style geometry as an "outer shell" and a sheath fold "core" internal to the outer nappe (Figure 134). Refolding by the F3 folds has produced a distinctive geometry (Figure 135), geometrically a product of non-coaxial general shear involving a sub-vertical stretch. The timing of F3 folding is discussed in Section 6.5 below.

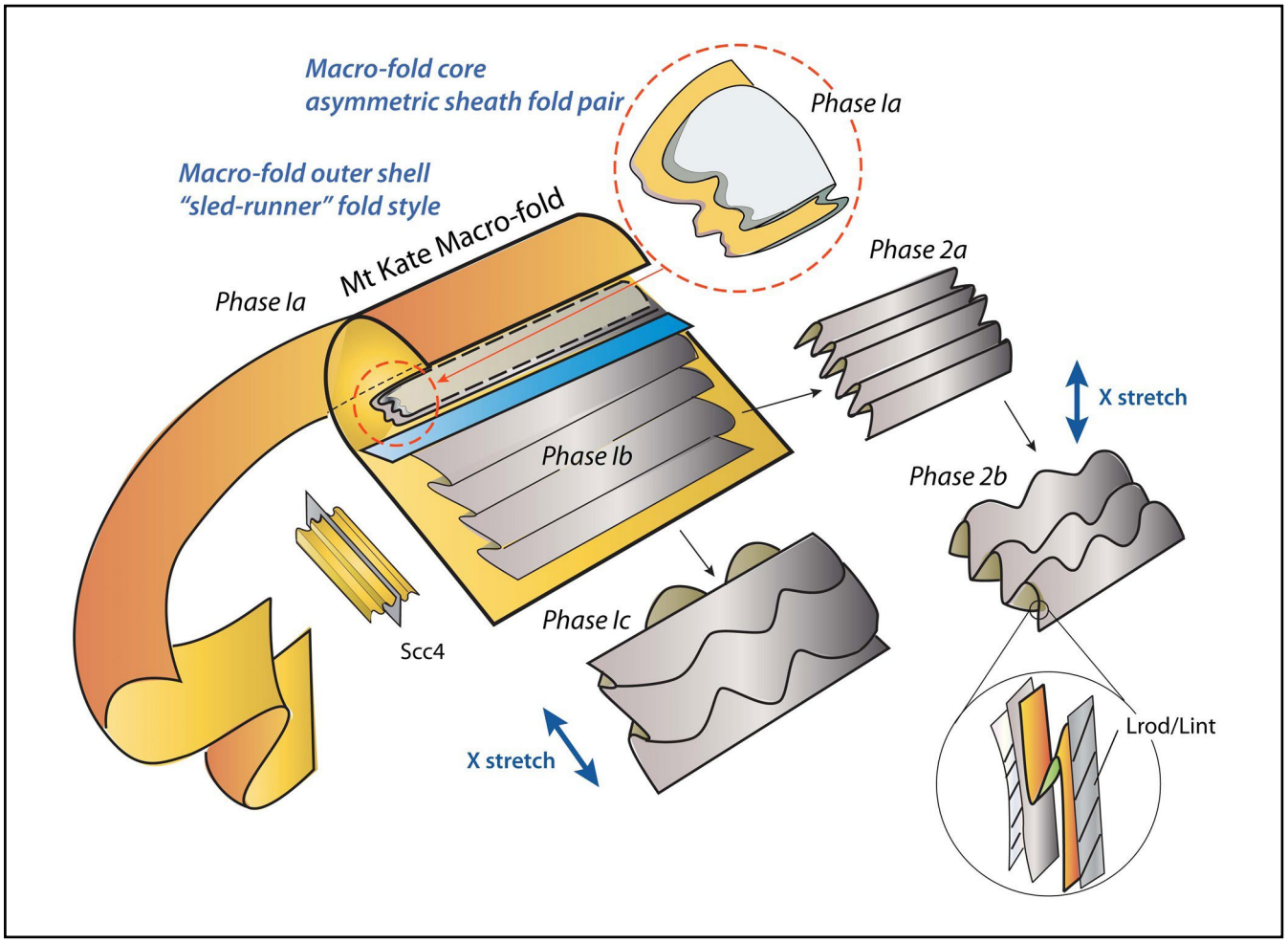

Figure 134: Schematic simplified geometry and interpreted evolution of the major structures within the Northern Tyennan subdomain. Three deformational phases are implied with Phase 1a being emplacement of the fold-nappe and 1b development of asymmetric folds along the nappe trailing limb, and 1c the development of curved sheath-like hinge lines of the trailing asymmetric folds during continued non-coaxial shear. Phase 2a involves refolding of the Mt Kate macro-fold by a set of open to tight chevron folds. Phase 2b involves development of curved hinge lines within the chevrons during continued non-coaxial shear.

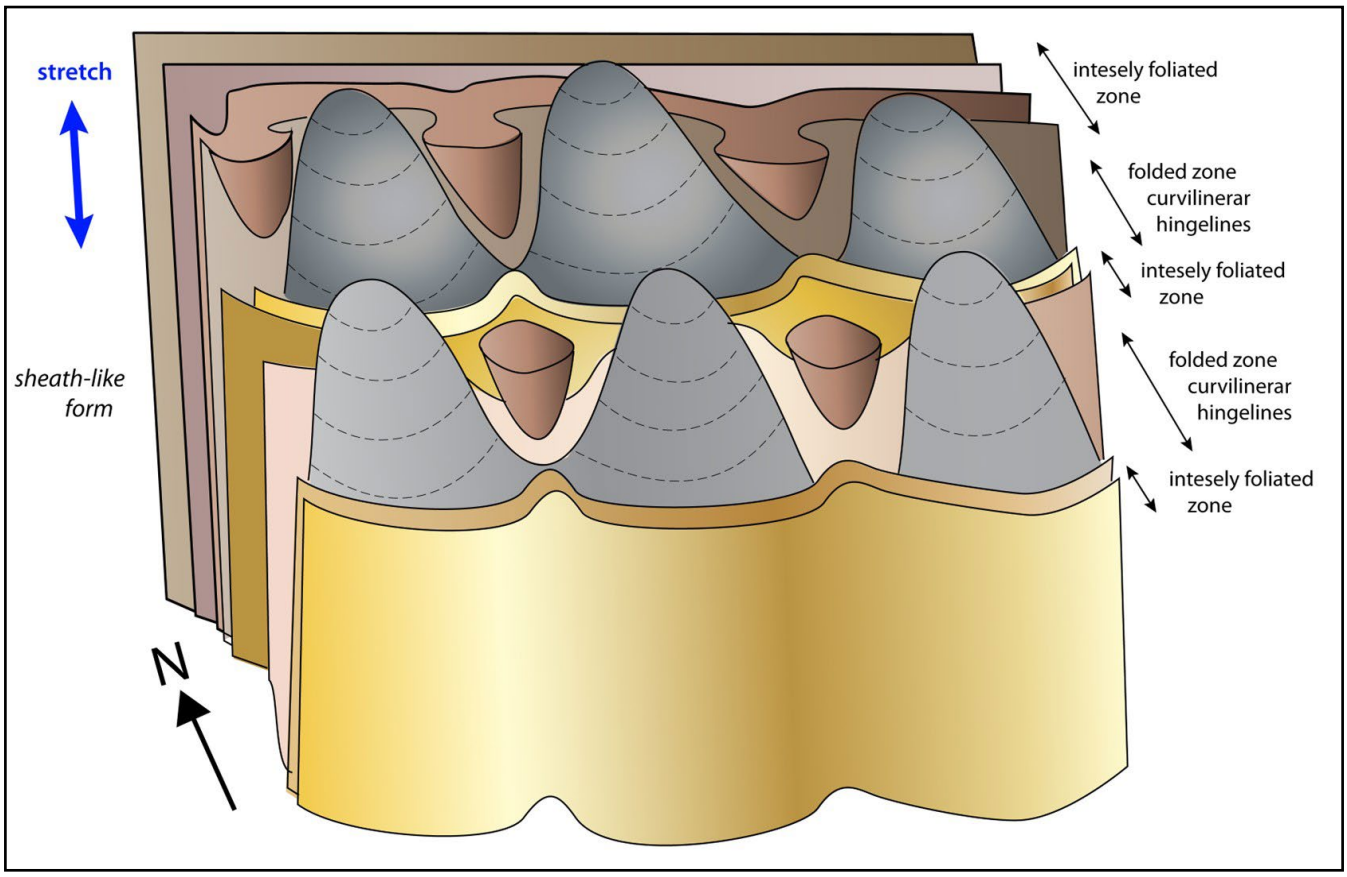

Figure 135. Schematic 3D sketch diagram of the interpreted Liena-Borradaile structural form incorporating steeply and variably plunging F3 fold hinge lines and hinge domains with closed to partially closed form lines in map view. These "fold hinge" domains are bounded by apparent high strain zones of strong to intense foliation.

Grey: low-grade quartzite.

Brown to burnt brown: pelite with strong to intense foliation (HSZ).

The cartoon is meant to exemplify the mapped relationships shown in Figures 79 and 80.

6.5 The Curvature of the Northern Tyennan Subdomain

Why is there a curvature change in the Northern Tyennan subdomain and what does it represent?

Curvature of the Northern Tyennan subdomain is an important element (Figure 19). In the Eastern and Southern Tyennan subdomains curvature changes show a radial pattern of the lineation Lm about local apparent rotation points (ARP) where the lineation remains approximately orthogonal to the So/Sm strike (see Gray and Vicary, 2021, 2024). In the Northern Tyennan however, the lineation Lm and the transport direction (TD) remain east-west trending despite the strike change.

The timing of this change in regional strike from north-south to east-west, relative to the development chronology of the major Northern Tyennan subdomain structures, is critical in the interpretation. Mapped major structural elements within the subdomain include the Mt Kate macro-fold as part of the leading edge fold-nappe, the mineral lineation (Lm), the transport direction (TD), and the F3 chevron folds. The timing and nature of the curvature is constrained by the geometrical relationships of these structural elements, particularly the timing relative to F3 folding.

Three scenarios to explain the curvature and relationships between the major structural elements of the Northern Tyennan subdomain are presented in schematic evolution diagrams (Figure 136). Each scenario involves deformation in an east-dipping, essentially planar north-south trending subduction channel, apart from scenario 3 that involves a curved subduction system at the northern end (Figure 136c). These include:

Scenario 1: F1/F2 and F3 folds form within an east-dipping subduction-obduction channel and are then subsequently rotated to an east-west orientation by simple clockwise rotation through ~90° about a pivot point (i.e. passive rotation of Sm, Lm, F1/F2 and F3 structural elements).

Scenario 2: F1/F2 folds form within an east-dipping subduction-obduction channel but the F3 folds develop syn-rotation with the east-west strike change. The rotation may be linked to a developing arcuate form or bend in the north-south trending subduction zone (i.e. passive rotation of Sm, Lm, F1/F2 but syn-rotation development of F3).

Scenario 3: F1/F2 and F3 folds form in an arcuate subduction zone with curved east- and south-dipping subduction-obduction channel, with the resultant pattern caused by the original subduction zone geometry (i.e. structures form "in situ" by "molding" of the allochthon and the contained structures to the shape of an inferred underlying curved subduction interface with F3 folding syn-emplacement).

The leading edge fold-nappe, common to all scenarios, formed in the first phase (Phase 1a) prior to the F3 folds (Phase 1b) as part of a non-coaxial general shear deformation in the subduction channel (see Gray et al., 2024). The differences in geometric evolution are:

Scenario1: All structures including the F3 chevron folds form pre-rotation and rotate passively to an east-west orientation (Figure 136a)

Scenario 2: All structures form pre-rotation, except the F3 chevron folds that form syn- to post rotation to an east-west orientation (Figure 136b)

Scenario 3: All structures form syn-emplacement of the Tyennan sheet along part of a curved subduction system (Figure 136c).

That Lm and TD remain approximately east-west trending despite the strike change means Scenarios 1 and 2 involving passive rotation cannot apply to the Northern Tyennan subdomain. This leaves the arcuate subduction zone of Scenario 3 where the current structural geometry "mirrors" the original subduction zone floor (Figures 137 and 138). The bend acts like a lateral ramp in a thrust-system with an upper sheet left (i.e. dextral) movement sense (Figure 137). This implies the overall curvature in So/Sm and the curvature in the Mt Kate axial surface trace are due to moulding of the sheet and contained fold-nappe to the bend in the subduction channel floor. The shear-related F3 chevron folds rotate late in the sequence due to blocking of the subduction channel by channel pinch-out (Figure 129). Narrowing or pinch-out of the subduction channel to a simple interface forms a wedge that effectively acts as a "backstop" constraining the movement of the ascending allochthonous "sheet", and therefore deformation at the leading edge. The trailing part of the leading edge fold-nappe undergoes buckle shortening by layer-parallel compression resulting in the localised zone of modified F3 folding.

The curved nature of the subduction zone may have developed during the Tyennan allochthon ascent within the subduction channel (Figure 139), where a varying allochthon thickness could lead to an effective "bend" in the subduction zone (diagram left, Figure 139). The final geometric anomaly could be a transform fault with a right step in the subduction zone. Preservation of this crustal-scale "transform" fault structure is potentially important for development of the Fossey part of the Dundas-Fossey graben system.

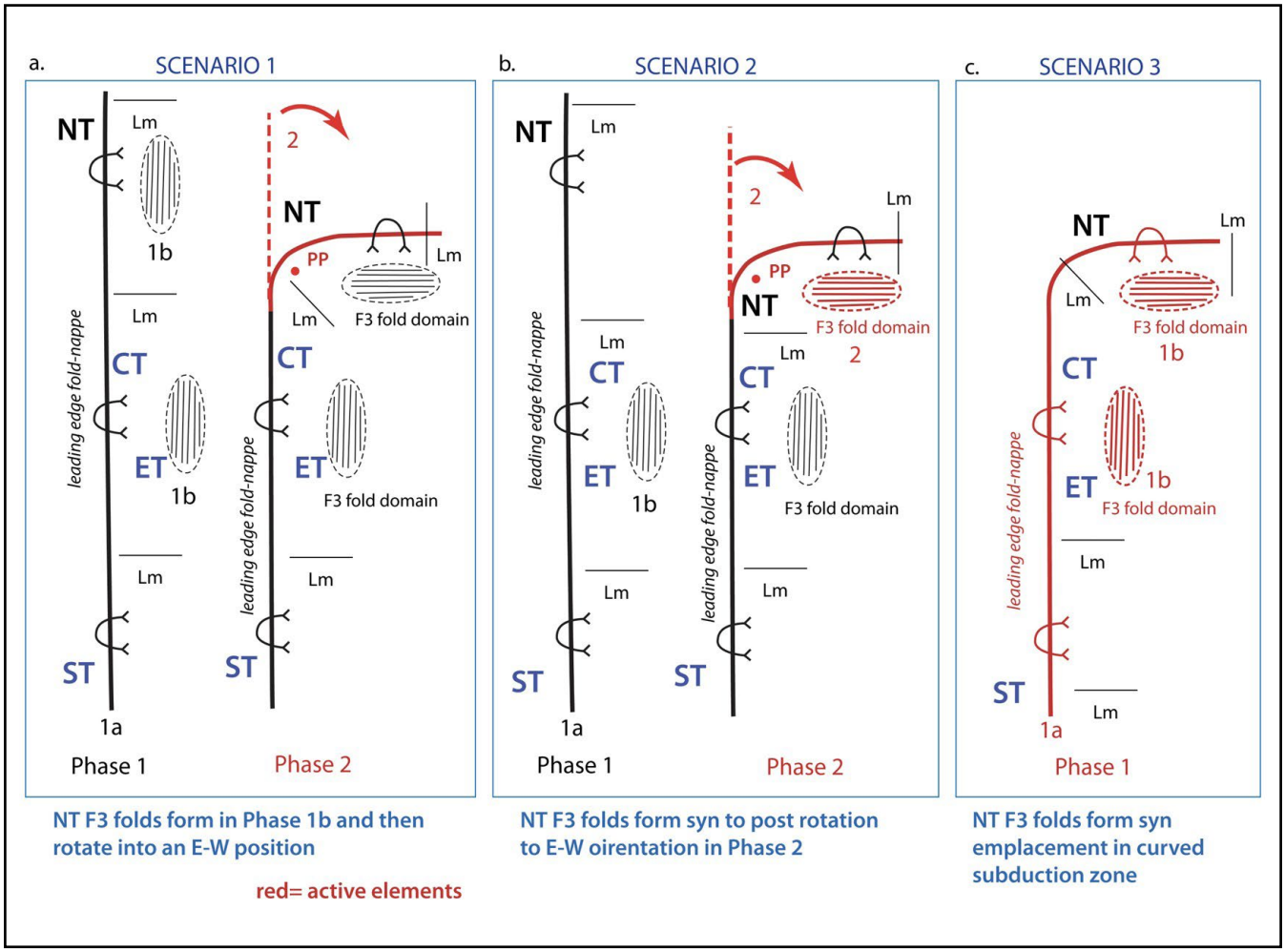

Figure 136. Schematic geometric evolution diagrams in plan view as three possible explanations of the curvature and strike change of the Northern Tyennan subdomain from a north-south to east-west trend. Black line work indicates structures formed pre-rotation highlighted by the red arrows. Red line work represents elements formed syn-rotation. Stage 1a represents leading edge fold-nappe development. Stage 1b represents F3 chevron fold development. PP: pivot point or apparent rotation point. Lm: mineral lineation. ST: Southern Tyennan subdomain. ET: Eastern Tyennan subdomain. CT: Central Tyennan subdomain. NT: Northern Tyennan subdomain.

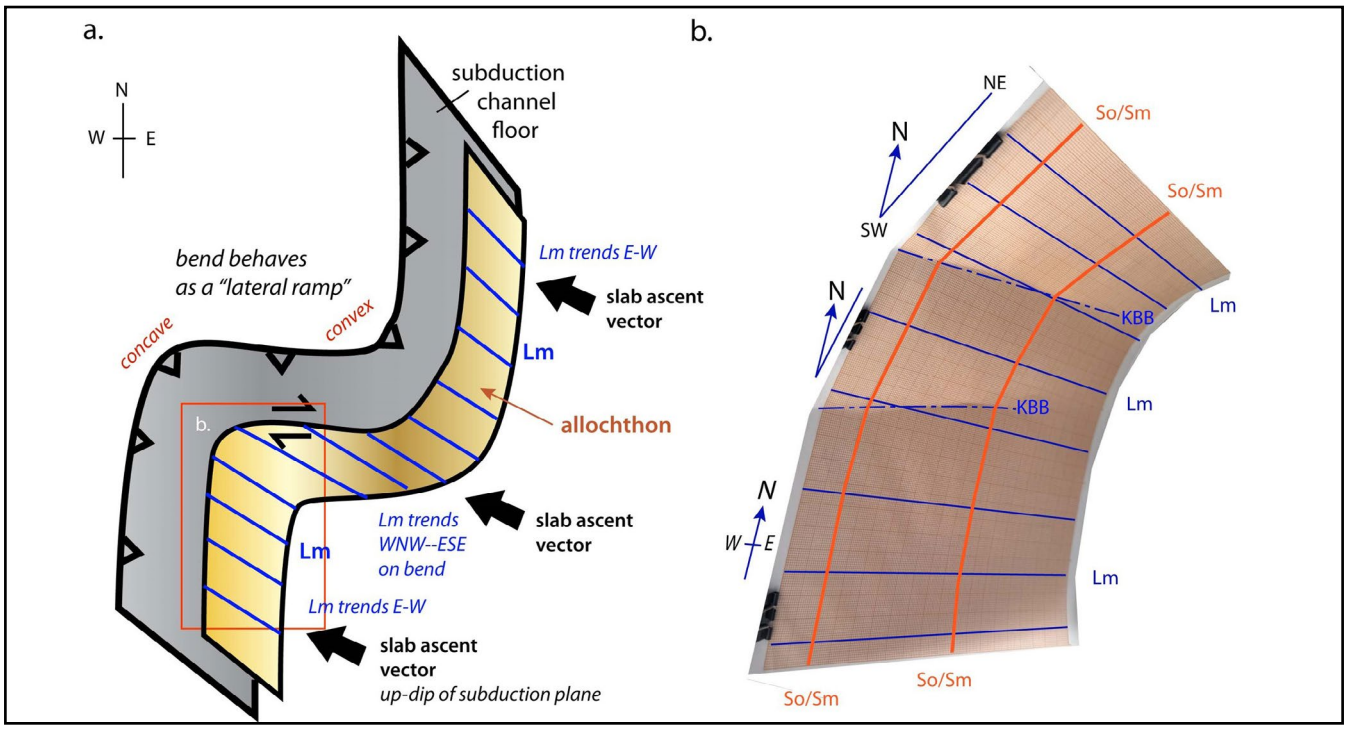

Figure 137: Schematic sketch "model" diagram of flexural bend in an east-dipping subduction zone. a) Oblique view of subduction zone with the allochthon (pale orange) "molded" to the subduction channel floor geometry (grey). Lm line markers (blue lines) show the orientation change of the pre-existing Lm around the flexural bend. Slab ascent is up the dip of the channel floor, with dextral sense oblique-slip motion on the bend as it acts like a lateral ramp in a thrust system. The red rectangle is the approximate position of the flexural model in (b). b) Simple geometric model of a flexural bend using graph paper attached to cardboard. Note the deviation in trend of the So/Sm strike (redline traces) and the Lm line markers (blue line traces) around the flexure in a modified kink flexure with kink band boundaries (KBB) shown by the blue dash-dot line traces. Compare with Figure 27.

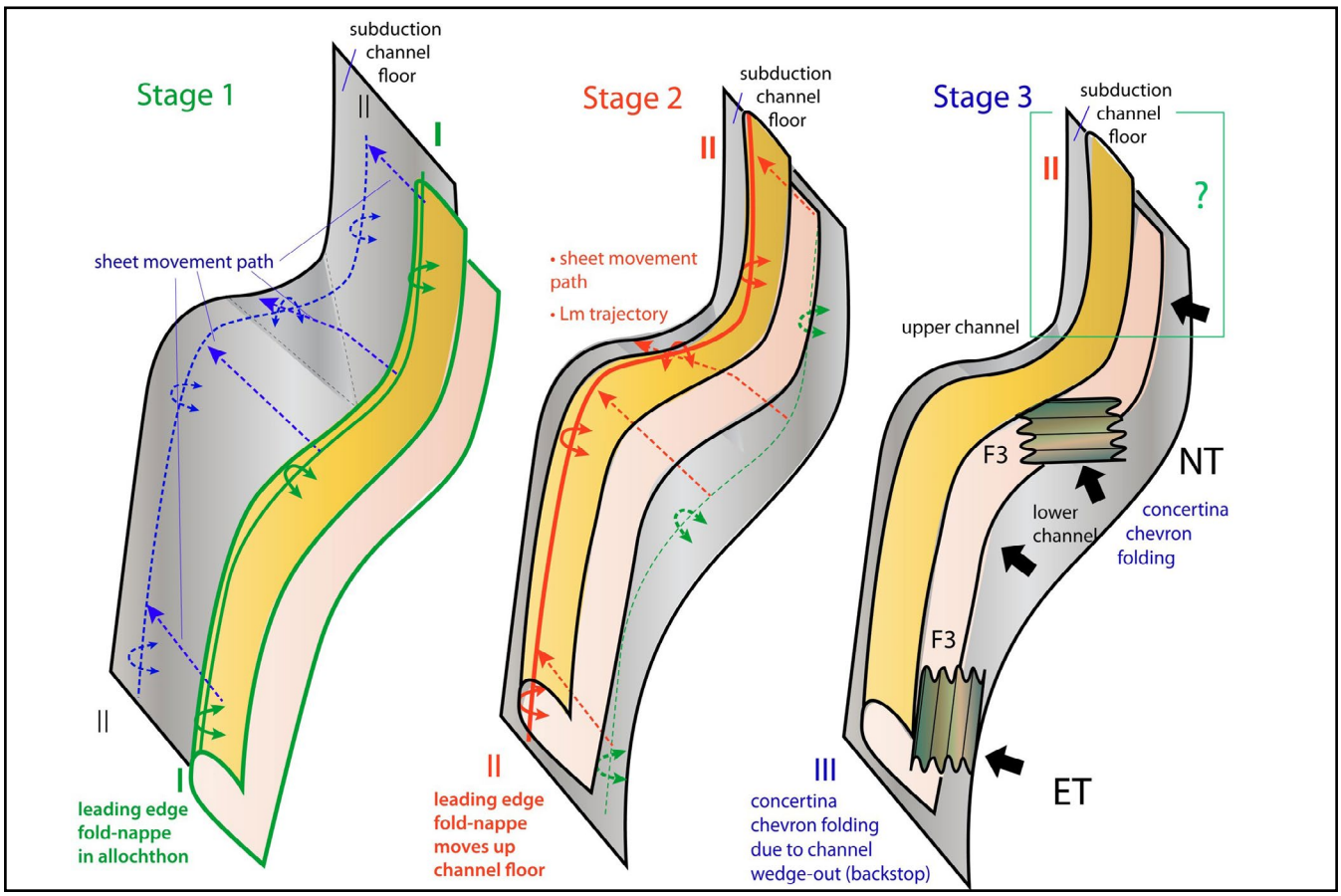

Figure 138: Northern Tyennan subdomain major structure evolution stages utilising a simple schematic diagram of a curved subduction channel in tilted, oblique view. Stage 1: Development of a leading edge fold-nappe at mid-channel depth (fold-nappe with green AST outline). Stage 2: Ascent of allochthon and leading edge fold-nappe to shallower depth (fold-nappe with red AST outline). The red dashed lines show the movement trajectory path of particles points on the axial surface trace (AST). Stage 3: Allochthon at final emplacement position due to close-out of the subduction channel. The model implies F1/F2 fold nappe curvature is due to molding of the allochthon sheet to the channel floor in the upper part with the F3 chevron folding forming late due to a buttressing effect by "blocking" of the subduction channel due to close-out (see Figure 129).

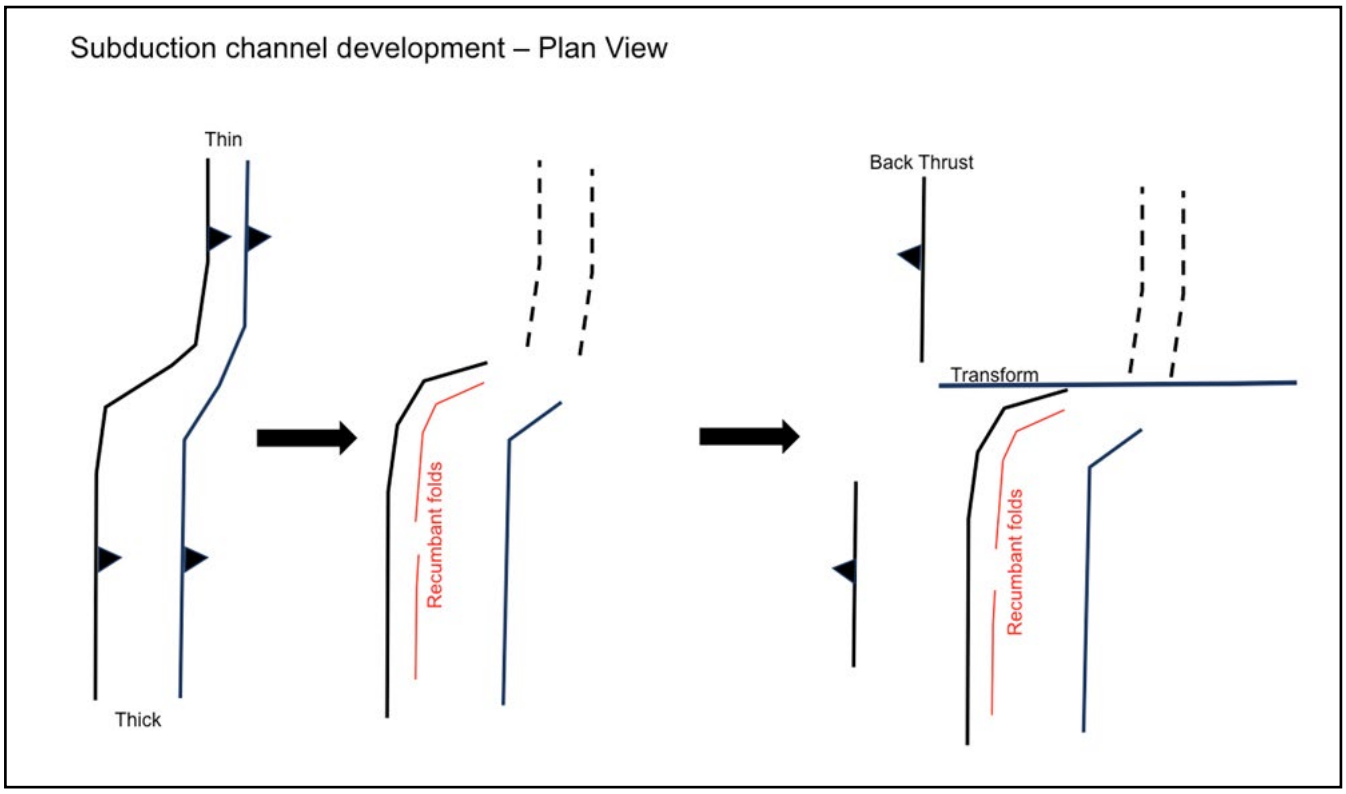

Figure 139. Plan view schematic diagram showing a three-stage evolution of a subduction zone anomaly (diagram left) into a subduction-transform zone (diagram right) during Tyennan allochthon ascent. The curved anomaly in the subduction zone is caused by a change in subduction zone channel width (thick versus thin channel). The channel and the contained allochthon sit between the two barbed interfaces (diagram left).

Although the curved subduction model explains the lineation relationships and the timing of F3 folding, issues remain with this interpretation. These are:

1. The subduction model has a concave bend coupled to a convex bend as part of the inferred right stepping of the subduction zone (Figure 137). This requires a synformal nature of the sheet at the bend in the Northern Tyennan subdomain. The bend north of Granite Tor plunges northwest and is therefore antiformal.

2. The basal shear zone of the high-grade unit (garnet schist) shows sinistral and not dextral sense as implied at the lateral ramp (Figure 137a)

3. The northern extension of the subduction system beyond the right step is not preserved in the rock record or has not been recognised at this stage.

4. Explanation of the emplacement involving a changing shear sense with an early east-over-west sense during emplacement (shown by the transposition foliation markers including sigma clast and domino boudins) and a late west-over-east sense and/or north-over-south sense (shown by shear bands).

The geometry of the rocks potentially continuous with the Tyennan Domain, including the North Coast Tyennan equivalent rocks (Forth massif) as well as the Great Bend belt of Proterozoic rocks, need documenting before The Northern Tyennan geometrical relationships can be resolved.

7.0 CONCLUSIONS

The Northern Tyennan subdomain has distinct geometry where Lm and TD are sub-parallel to the So/Sm strike, unlike other parts of the Tyennan Domain. The subdomain is structurally dominated by the Mt Kate recumbent macro-fold and a belt of upright F3 chevron folds. The chevron folds are bounded by anastomosing zones of strong to intense foliation and have curved hinge lines with marked changes in fold axis plunge and plunge direction. The upright chevron folds refold early recumbent isoclinal folds along the lower limb of the macro-fold.

The core of the macro-fold contains high-grade schist as the uppermost sheet in tectonic stack of garnet schist overlying low-grade pelite (phyllite) overlying quartzite. The basal part of the high-grade sheet is a high strain mylonitic zone that has sub-vertical attitude (present state) with sinistral shear sense. Restoration of the HSZ to the horizontal gives an east-over-west shear sense.

8.0 ACKNOWLEDGEMENTS

- Mineral Resources Tasmania (Andrew McNeill and Rebecca Sproule) for providing financial support for the Tyennan Structural Synthesis Project.
- Chris Large for editing and formatting this Tasmanian Geological Survey publication.
- Jason Bradbury NRE (Department of Natural Resources and Environment) for assistance with WHA and PWS permits for scientific research.
- Ron Berry and Rob Scott for supplying UTas student field mapping data along the Mersey River Road and at Lake Rowallan.

9.0 REFERENCES

Alsop, G.I. and Holdsworth, R.E., 1999. Vergence and facing patterns in large scale sheath folds. *Journal of Structural Geology*, 21, 1335-1349.

Alsop, G. and Holdsworth, R.E., 2004. The geometry and topology of natural sheath folds: a new tool for structural analysis. *Journal of Structural Geology*, 26, 1561-1589.

Barton, C. M.; Burns, K. L.; Gee, R. D.; Groves, D. I.; Gulline, A. B.; Jennings, D. J.; Longman, M. L.; Marshall, B.; Mathews, W. L.; Moore, W. R.; Naqvi, I. H.; Threader, V. M.; Urquhart, G. 1966. Geological Atlas 1 Mile Series. Zone 7 Sheet 44 (8014N). *Mackintosh*. Department of Mines, Tasmania.

Berry, R. F. 2014. Chapter 4.2 Cambrian Tectonics –The Tyennan Orogeny. In Corbett, K. D., Quilty, P.G & Calver, C. R. (Editors), Geological Evolution of Tasmania, pp 95-110. *Geological Society of Tasmania Special Publication*, 24, Geological Society of Australia (Tasmania Division), 270.

Berry, R.F. and Bull, S. 2004. *A Geological Excursion to Northwestern Tasmania*. Field Guide A2. 17th Australian Geological Convention, 8-13 February 2004, Hobart, Tasmania, Australia. Geological Society of Australia.

Berry, R. F. and Crawford, A. J. 1988. The tectonic significance of Cambrian allochthonous mafic-ultramafic complexes in Tasmania. *Australian Journal of Earth Sciences*, 35, 523-533.

Berry, R.F., Chmielowski, R.M., Steele, D.A. & Meffre, S. 2007. Chemical U-Th-Pb monazite dating of the Cambrian Tyennan Orogeny, Tasmania. *Australian Journal of Earth Sciences*, 54, 757-771. https://doi.org/10.1080/08120090701305269

Chmielowski, R. M. 2009. *The Cambrian metamorphic history of Tasmania*. PhD Thesis, University of Tasmania.

Chmielowski, R.M. & Berry, R.F. (2012). The Cambrian Metamorphic History of Tasmania: The Metapelites. *Australian Journal of Earth Sciences*, 59, 1007-1019. http://dx.doi.org/10.1080/08120099.2012.724449

Cumming, G.C., Everard, J.L. and Jackman, C. 2025. Mineral Resources Tasmania, *Geological Survey Paper*, 16, in prep.

Gee, R.D., Marshall, B and Burns, K.L. 1970. The metamorphic and structural sequence in the Precambrian of the Cradle Mountain area, Tasmania. *Geological Survey of Tasmania Report,* 11, 26.

Goscombe, B.D. and Passchier, C.W . 2003. Asymmetric boudins as shear sense indicators – an assessment from field data. J. *Structural Geology*, 25, 575-589.

Gray, D. R. and Vicary, M. J. 2021. Structural Geology of the Central Tyennan Region, Tasmania. *Mineral Resources Tasmania Geological Survey Paper*, 7, 69.

Gray, D. R. and Vicary, M. J. 2023. Structural Geology of the Southern Tyennan Domain, Tasmania—An Overview, Synthesis and Structural Implications.

Gray, D. R. and Vicary, M. J. 2024. Structural geology of the Eastern Tyennan subdomain, Tasmania - an overview and structural synthesis. *Mineral Resources Tasmania, Geological Survey Paper*, 14, 94.

Gray, D. R. and Vicary, M. J. 2025, Structural Geology of the central north region of Tasmania—Faults, Structural profiles, Fossey Basin Evolution and the central north 3D Model. *Mineral Resources Tasmania, Geological Survey Paper,* 18, in prep.

Gray, D. R., Vicary, M. J. and McNeill, A. W. 2024. The Tasmanian Tyennan Domain—a structural synthesis and review with tectonic and dynamic implications for continental margin subduction and exhumation. *Australian Journal of Earth Sciences*, 71(2), 153-210. https://doi.org/10.1080/08120099.2023.2280604.

Hopgood, D.N. 1980. A photo geological study of EL 2/78. Hunting Geology & Geophysics Australasia Unpublished Consulting Report for Alcoa of Australia Limited. Appendix A in Speijers, D.C. 1980. Tasmanian Company Report 80-1490.

Jennings, I. B.; Burns, K. L. 1958. Geological Atlas 1 Mile Series. Zone 7 Sheet 45. *Middlesex*. Department of Mines, Tasmania.

Jennings, I.B. 1963. *Geological Survey Explanatory Report*, one mile geological map series K55-6-45 Middlesex.

Mattner, S., 2015. *Structure and Metamorphism of the Mersey River Complex*. B.Sc. (Hons) Thesis, The University of Tasmania.

Meffre, S., Berry, R. F. & Hall, M. (2000). Cambrian metamorphic complexes in Tasmania: tectonic implications. *Australian Journal of Earth Sciences,* 47, 971 – 985. https://doi.org/10.1046/j.1440-0952.2000.00825.

Meffre, S., Berry, R.F., Hall, M. and McNeill, A., 2001. The Structural Style of Cambrian Metamorphic Complexes in Tasmania: SW Tasmanian examples. *Geological Society of Australia Abstracts*, 64, 118-120.

Passchier, C.W. and Trouw, R.A.J. 1996. *Micro-tectonics.* Springer Verlag. Berlin. 289.

Ramsay, J.G. 1967. *Folding and Fracturing of Rocks*. McGraw Hill, New York, 568p

Ramsay, J.G. and Huber, M,I., 1987. *The techniques of Modern Structural Geology, Vol. 2, Folds and Fractures*. Academic Press, London, 391.

Speijers, D.C. 1980. Report on Exploration of E.L.2/78 during 1980. Volume 1 and Appendices. Alcoa of Australia Limited: Exploration Division. *Tasmanian Company Report,* 80-1490, 82.

Spry, A.H., 1958. The Precambrian Rocks of Tasmania. Part III, Mersey-Forth Area. *Proceedings of the Royal Society of Tasmania*, 92, 117-138.

Spry, A.H., 1962. Notes on the Petrology and Structure of the Precambrian Metamorphic Rocks of the Upper Mersey-Forth Area. *Records of the Queen Victoria Museum Launceston*, New Series No 16, 1-11.

Spry, A.H. 1963. Precambrian rocks of Tasmania, Part V: Petrology and structure of the Frenchman's Cap area. *Papers and Proceedings of the Royal Society of Tasmania*, 97, 105-128.

Woodward, N.B., Gray, D.R. and Elliot, C.G. 1993. Repeated Palaeozoic thrusting and allochthoneity of Precambrian basement, northern Tasmania. *Australian Journal of Earth Sciences*, 40, 297-311.

APPENDIX 1

Enlarged maps of foliations, lineations and fold axes for the Northern Tyennan Subdomain

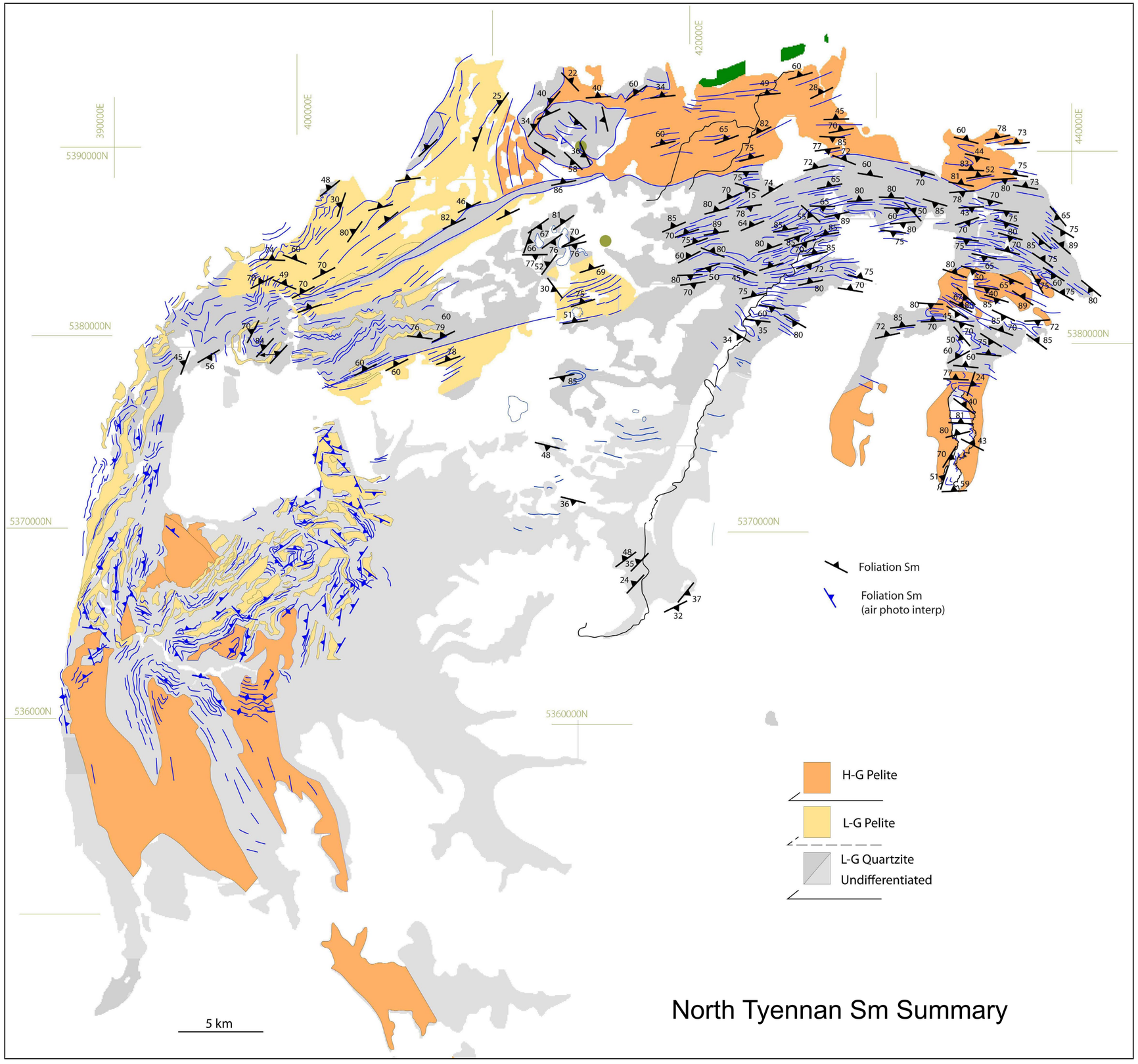
390000E
400000E
420000E
440000E
5390000N
5380000N
5370000N
536000N
5360000N
5 km
Foliation Sm
Foliation Sm
(air photo interp)
H-G Pelite
L-G Pelite
L-G Quartzite
Undifferentiated
North Tyennan Sm Summary

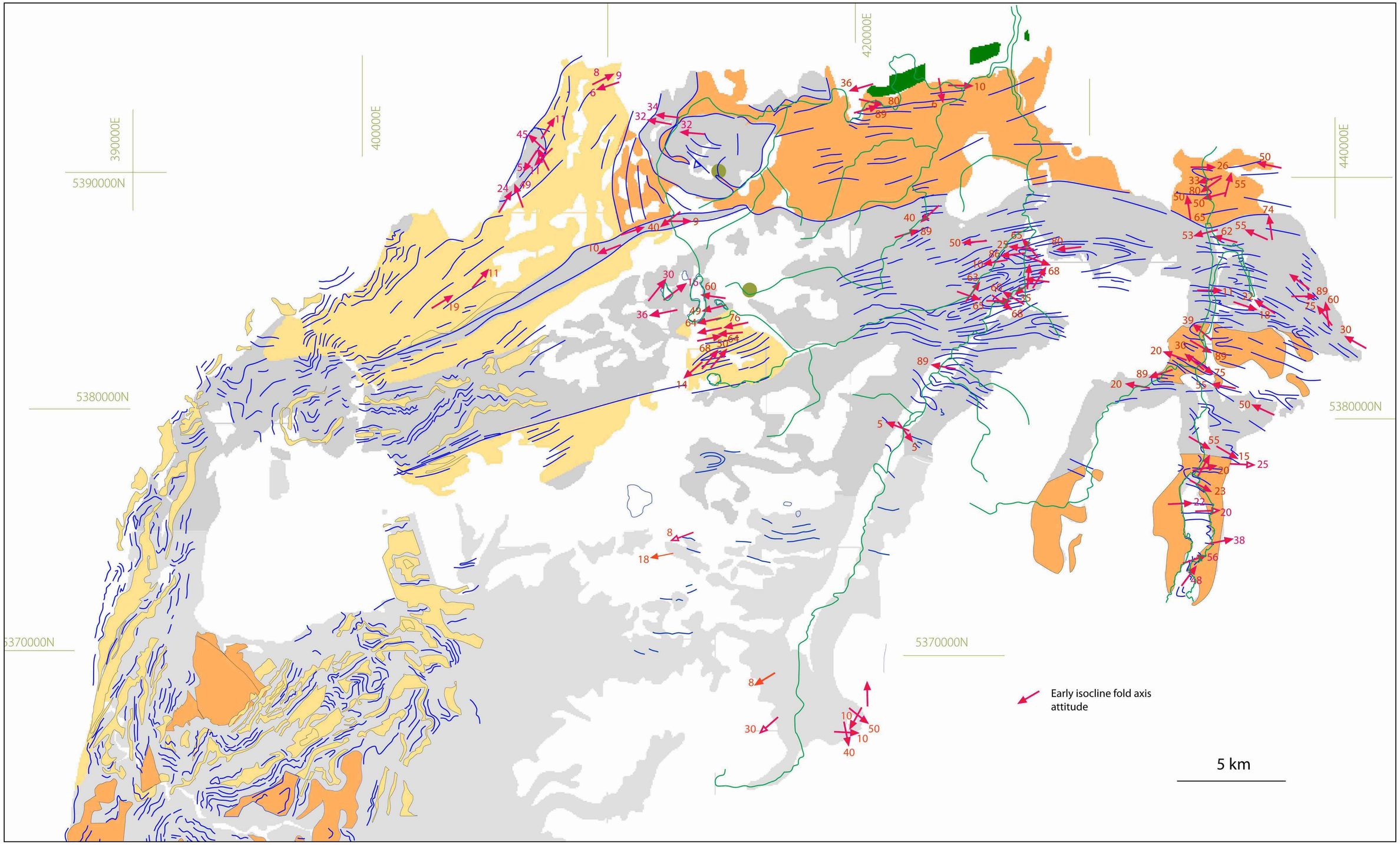

North Tyennan FA Summary

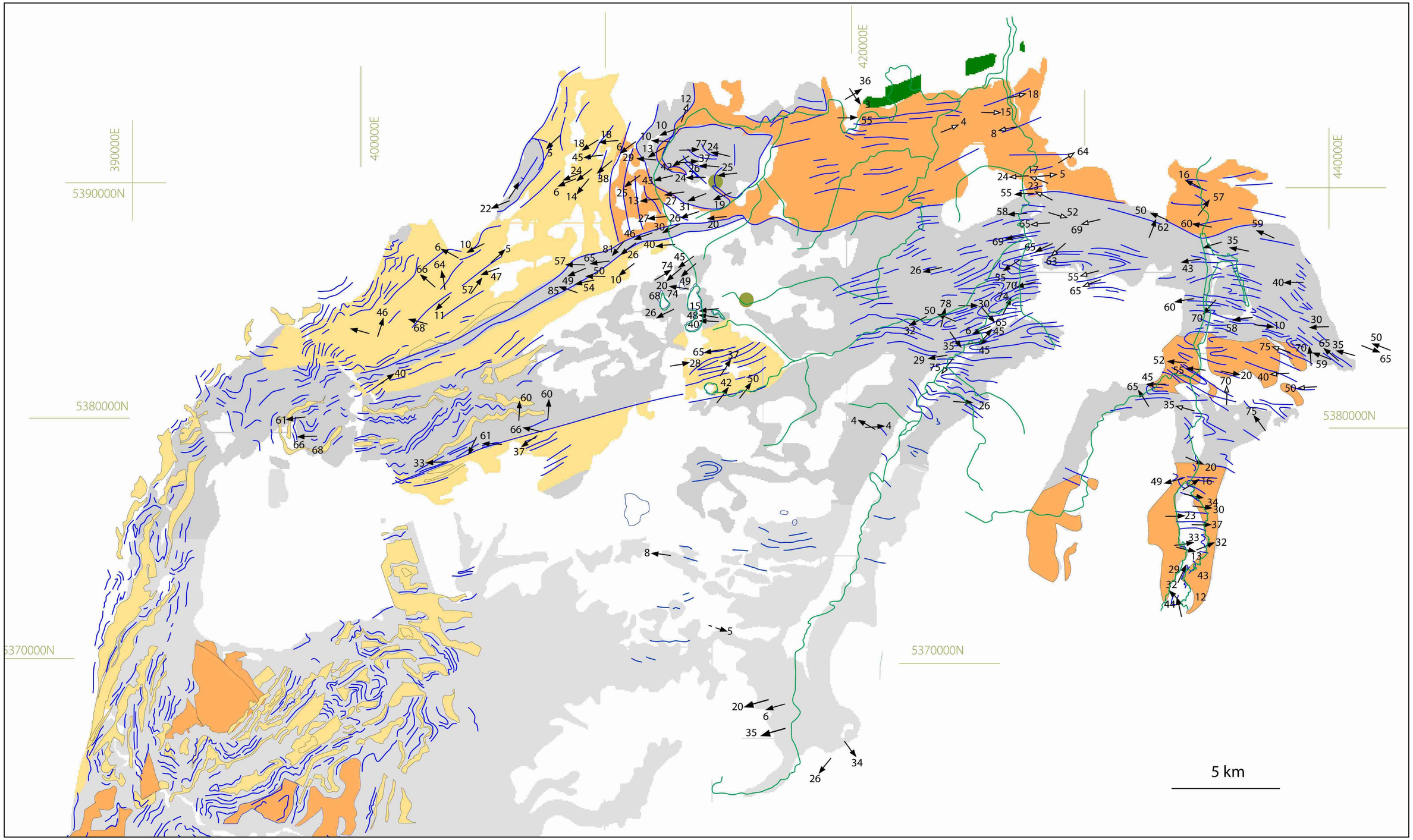

North Tyennan Lm Summary

APPENDIX 2

Structural Measurements (hard copy abbreviated)
Download file for comprehensive table

Structural Measurements download

Project	Structure	Structure Type Symbol	Dip *	Dip Direction *	Secondary Dip	Secondary Dip Direction	Reliability	Output Scale *	Comments	Lithology	Collection Date	Field #	Sample Description	Other References	Locality	X *	Y *	Positional Accuracy
Mersey	Metamorphic Foliation	Sag	78	358.6			1 - Most reliable	1:10,000	Sm		9/05/2017	DG17-23.1	weathered grey muscovite schist with psammite bands	DG17-23	Lake Rowallan area - Quarry, Lake MacKenzie Road	436584	5393301	10m
Mersey	Metamorphic Foliation	Sag	85	359.6			1 - Most reliable	1:10,000	Sm		9/05/2017	DG17-23.1	weathered grey muscovite schist with psammite bands	DG17-23	Lake Rowallan area - Quarry, Lake MacKenzie Road	436584	5393301	10m
Mersey	Vertical Metamorphic Foliation	Sah	90	13.6			1 - Most reliable	1:10,000	Sm		9/05/2017	DG17-23.2	Psamite dominate	DG17-23	Lake Rowallan area - Quarry, Lake MacKenzie Road	436584	5393301	10m
Mersey	Mineral Elongation Lineation	Lao	10	108.6			1 - Most reliable	1:10,000	Lm	psammite	9/05/2017	DG17-23.2	Psammite dominate	DG17-23	Lake Rowallan area - Quarry, Lake MacKenzie Road	436584	5393301	10m
Mersey	Fold with dip and dip direction of axial surface, Local age F2	Haq + Paq	40	281.6	76	198.6	1 - Most reliable	1:10,000	A	psammite	9/05/2017	DG17-23.2	Psammite dominate	DG17-23	Lake Rowallan area - Quarry, Lake MacKenzie Road	436584	5393301	10m
Mersey	Metamorphic Foliation	Sag	78	343.6			1 - Most reliable	1:10,000	Sm		9/05/2017	DG17-23.3	weathered grey muscovite schist with psammite bands	DG17-23	Lake Rowallan area - Quarry, Lake MacKenzie Road	436584	5393301	10m
Mersey	Mineral Elongation Lineation	Lao	4	68.6			1 - Most reliable	1:10,000	Lm		9/05/2017	DG17-23.3	weathered grey muscovite schist with psammite bands	DG17-23	Lake Rowallan area - Quarry, Lake MacKenzie Road	436584	5393301	10m
Mersey	Crenulation Lineation	Laj	58	283.6			1 - Most reliable	1:10,000	Lcren		9/05/2017	DG17-23.3	weathered grey muscovite schist with psammite bands	DG17-23	Lake Rowallan area - Quarry, Lake MacKenzie Road	436584	5393301	10m
Mersey	Fold, Local age F2	Haq	38	283.6			1 - Most reliable	1:10,000	A		9/05/2017	DG17-23.3	weathered grey muscovite schist with psammite bands	DG17-23	Lake Rowallan area - Quarry, Lake MacKenzie Road	436584	5393301	10m
Mersey	Metamorphic Foliation	Sag	80	143.6			1 - Most reliable	1:10,000	Sm	psammite	9/05/2017	DG17-23.4	weathered grey muscovite schist with psammite bands	5m NW of DG17-23	Lake Rowallan area - Quarry, Lake MacKenzie Road	436584	5393299	10m
Mersey	Metamorphic Foliation	Sag	80	328.6			1 - Most reliable	1:10,000	Sm	pelite	9/05/2017	DG17-23.4	weathered grey muscovite schist with psammite bands	5m NW of DG17-23	Lake Rowallan area - Quarry, Lake MacKenzie Road	436584	5393299	10m
Mersey	Metamorphic Foliation	Sag	45	33.6			1 - Most reliable	1:10,000	Sm		17/05/2017	DG17-24.1	transposed S0/Sm, interlayered quatzie and dark phyllite	DG17-24	Lake Rowallan area - 200m south boat ramp	434860	5379384	10m
Mersey	Mineral Elongation Lineation	Lao	25	88.6			1 - Most reliable	1:10,000	Lm		17/05/2017	DG17-24.1	transposed S0/Sm, interlayered quatzie and dark phyllite	DG17-24	Lake Rowallan area - 200m south boat ramp	434860	5379384	10m
Mersey	Metamorphic Foliation	Sag	46	31.6			1 - Most reliable	1:10,000	Sm		17/05/2017	DG17-24.2	transposed S0/Sm, interlayered quatzie and dark phyllite	DG17-24	Lake Rowallan area - 200m south boat ramp	434860	5379384	10m
Mersey	Mineral Elongation Lineation	Lao	24	98.6			1 - Most reliable	1:10,000	Lm		17/05/2017	DG17-24.2	transposed S0/Sm, interlayered quatzie and dark phyllite	DG17-24	Lake Rowallan area - 200m south boat ramp	434860	5379384	10m
Mersey	Ducitle Shear Band	Sau	64	63.6			1 - Most reliable	1:10,000	Fault		17/05/2017	DG17-24.3	transposed S0/Sm, interlayered quatztie and dark phyllite, flanking fault (margin of vein)	DG17-24	Lake Rowallan area - 200m south boat ramp	434860	5379384	10m
Mersey	Fold, Local age F1	Hal	21	93.6			1 - Most reliable	1:10,000	A		17/05/2017	DG17-24.4	Sheath folds	DG17-24	Lake Rowallan area - 200m south boat ramp	434860	5379384	10m
Mersey	Fold, Local age F1	Hal	12	288.6			1 - Most reliable	1:10,000	A		17/05/2017	DG17-24.4	Sheath folds	DG17-24	Lake Rowallan area - 200m south boat ramp	434860	5379384	10m
Mersey	Fold, Local age F1	Hal	42	78.6			1 - Most reliable	1:10,000	A		17/05/2017	DG17-24.4	Sheath folds	DG17-24	Lake Rowallan area - 200m south boat ramp	434860	5379384	10m
Mersey	Fold, Local age F1	Hal	26	93.6			1 - Most reliable	1:10,000	A		17/05/2017	DG17-24.4	Sheath folds	DG17-24	Lake Rowallan area - 200m south boat ramp	434860	5379384	10m
Mersey	Fold, Local age F1	Hal	10	98.6			1 - Most reliable	1:10,000	A		17/05/2017	DG17-24.4	Sheath folds	DG17-24	Lake Rowallan area - 200m south boat ramp	434860	5379384	10m
Mersey	Fold, Local age F1	Hal	32	88.6			1 - Most reliable	1:10,000	A		17/05/2017	DG17-24.4	transposed S0/Sm, interlayered quatztie and dark phyllite, flanking fault (margin of vein)	DG17-24	Lake Rowallan area - 200m south boat ramp	434860	5379384	10m
Mersey	Metamorphic Foliation	Sag	50	33.6			1 - Most reliable	1:10,000	Sm		17/05/2017	DG17-24.4	transposed S0/Sm, interlayered quatztie and dark phyllite, flanking fault (margin of vein)	DG17-24	Lake Rowallan area - 200m south boat ramp	434860	5379384	10m
Mersey	Mineral Elongation Lineation	Lao	30	93.6			1 - Most reliable	1:10,000	Lm		17/05/2017	DG17-24.4	transposed S0/Sm, interlayered quatztie and dark phyllite, flanking fault (margin of vein)	DG17-24	Lake Rowallan area - 200m south boat ramp	434860	5379384	10m
Mersey	Crenulation Lineation	Laj	23	333.6			1 - Most reliable	1:10,000	Lcren		17/05/2017	DG17-24.4	transposed S0/Sm, interlayered quatztie and dark phyllite, flanking fault (margin of vein)	DG17-24	Lake Rowallan area - 200m south boat ramp	434860	5379384	10m
Mersey	Crenulation Cleavage	Cai	34	58.6			1 - Most reliable	1:10,000	Scc		17/05/2017	DG17-25	transposed S0/Sm, interlayered quatztie and dark phyllite, flanking fault (margin of vein)	DG17-25	Lake Rowallan area - 50m south boat ramp	434786	5379455	10m
Mersey	Metamorphic Foliation	Sag	40	38.6			1 - Most reliable	1:10,000	Sm		17/05/2017	DG17-25	transposed S0/Sm, interlayered quatztie and dark phyllite, flanking fault (margin of vein)	DG17-25	Lake Rowallan area - 50m south boat ramp	434786	5379455	10m
Mersey	Fold with dip and dip direction of axial surface, Local age F1	Hal + Pap	20	88.6	55	18.6	1 - Most reliable	1:10,000	A		17/05/2017	DG17-25	transposed S0/Sm, interlayered quatztie and dark phyllite, flanking fault (margin of vein)	DG17-25	Lake Rowallan area - 50m south boat ramp	434786	5379455	10m
Mersey	Mineral Elongation Lineation	Lao	30	98.6			1 - Most reliable	1:10,000	Lm		17/05/2017	DG17-25	transposed S0/Sm, interlayered quatztie and dark phyllite, flanking fault (margin of vein)	DG17-25	Lake Rowallan area - 50m south boat ramp	434786	5379455	10m
Mersey	Crenulation Cleavage	Cai	20	73.6			1 - Most reliable	1:10,000	Scc (crosscutting)		17/05/2017	DG17-25	transposed S0/Sm, interlayered quatztie and dark phyllite, flanking fault (margin of vein)	DG17-25	Lake Rowallan area - 50m south boat ramp	434786	5379455	10m
Mersey	Crenulation Cleavage	Cai	34	58.6			1 - Most reliable	1:10,000	Scc (crosscutting)		17/05/2017	DG17-25	transposed S0/Sm, interlayered quatztie and dark phyllite, flanking fault (margin of vein)	DG17-25	Lake Rowallan area - 50m south boat ramp	434786	5379455	10m
Mersey	Fold with dip and dip direction of axial surface, Local age F1	Hal + Pap	25	93.6	35	103.6	1 - Most reliable	1:10,000	A		17/05/2017	DG17-26	thin bedded quartzite with minor schist layers	DG17-26	Lake Rowallan area - boat ramp	434896	5379577	10m
Mersey	Metamorphic Foliation	Sag	24	98.6			1 - Most reliable	1:10,000	Sm		17/05/2017	DG17-26	thin bedded quartzite with minor schist layers	DG17-26	Lake Rowallan area - boat ramp	434896	5379577	10m

Project	Structure	Structure Type Symbol	Dip *	Dip Direction *	Secondary Dip	Secondary Dip Direction	Reliability	Output Scale *	Comments	Lithology	Collection Date	Field #	Sample Description	Other References	Locality	X *	Y *	Positional Accuracy
Mersey	Crenulation Lineation	Laj	20	88.6			1 - Most reliable	1:10,000	Lcren		17/05/2017	DG17-26	thin bedded quartzite with minor schist layers	DG17-26	Lake Rowallan area - boat ramp	434896	5379577	10m
Mersey	Crenulation Cleavage	Cai	85	358.6			1 - Most reliable	1:10,000	Scc		17/05/2017	DG17-26	thin bedded quartzite with minor schist layers	DG17-26	Lake Rowallan area - boat ramp	434896	5379577	10m
Mersey	Metamorphic Foliation, parallel to bedding	Sak	77	3.6			1 - Most reliable	1:10,000	So/Sm		17/05/2017	DG17-27	thick bedded quartzite	DG17-27	Lake Rowallan area - quarry near junction	434981	5380885	10m
Mersey	Mineral Elongation Lineation	Lao	22	78.6			1 - Most reliable	1:10,000	Lm		17/05/2017	DG17-27	thick bedded quartzite	DG17-27	Lake Rowallan area - quarry near junction	434981	5380885	10m
Mersey	Metamorphic Foliation, parallel to bedding	Sak	82	178.6			1 - Most reliable	1:10,000	S0/Sm	quartzite	17/05/2017	DG17-28	quartzite	DG17-28	Lake Rowallan area - 1 km south of Parangana Dam	435419	5389744	10m
Mersey	Mineral Elongation Lineation	Lao	43	261.6			1 - Most reliable	1:10,000	Lm	quartzite	17/05/2017	DG17-28	quartzite	DG17-28	Lake Rowallan area - 1 km south of Parangana Dam	435419	5389744	10m
Mersey	Fold, Local age F1	Hal	48	263.6			1 - Most reliable	1:10,000	Lrod/FA	quartzite	17/05/2017	DG17-28	quartzite	DG17-28	Lake Rowallan area - 1 km south of Parangana Dam	435419	5389744	10m
Mersey							1 - Most reliable	1:10,000			17/05/2017	DG17-29	Contact between Fisher Quartzite and Dove Schists	DG17-29	Lake Rowallan area - Parangana Dam Wall	435358	5390668	10m
Mersey	Metamorphic Foliation	Sag	40	223.6			1 - Most reliable	1:10,000	Sm	pelite, graphitic-phyllitic	17/05/2017	DG17-30.1	black graphitic schist (Fisher Schist)	DG17-30	Lake Rowallan area - 3.2 km south of Lake MacKenzie Junction	435131	5392322	10m
Mersey	Mineral Elongation Lineation	Lao	39	233.6			1 - Most reliable	1:10,000	Lm	pelite, graphitic-phyllitic	17/05/2017	DG17-30.1	black graphitic schist (Fisher Schist)	DG17-30	Lake Rowallan area - 3.2 km south of Lake MacKenzie Junction	435131	5392322	10m
Mersey	Crenulation Cleavage	Cai	72	193.6			1 - Most reliable	1:10,000	Scc	pelite, graphitic-phyllitic	17/05/2017	DG17-30.2	black graphitic schist (Fisher Schist)	DG17-30	Lake Rowallan area - 3.2 km south of Lake MacKenzie Junction	435131	5392322	10m
Mersey	Metamorphic Foliation	Sag	44	243.6			1 - Most reliable	1:10,000	Sm	pelite, graphitic-phyllitic	17/05/2017	DG17-30.2	black graphitic schist (Fisher Schist)	DG17-30	Lake Rowallan area - 3.2 km south of Lake MacKenzie Junction	435131	5392322	10m
Mersey	Mineral Elongation Lineation	Lao	8	303.6			1 - Most reliable	1:10,000	Lm	pelite, graphitic-phyllitic	17/05/2017	DG17-30.2	black graphitic schist (Fisher Schist)	DG17-30	Lake Rowallan area - 3.2 km south of Lake MacKenzie Junction	435131	5392322	10m
Mersey	Mineral Elongation Lineation	Lao	16	298.6			1 - Most reliable	1:10,000	Lm	pelite, graphitic-phyllitic	17/05/2017	DG17-30.2	black graphitic schist (Fisher Schist)	DG17-30	Lake Rowallan area - 3.2 km south of Lake MacKenzie Junction	435131	5392322	10m
Cradle	Metamorphic Foliation	Sag	85	343.6			1 - Most reliable	1:10,000	Sm	quartzite	4/07/2017	DG17-69.1	steeply dipping thin bedded white quartzite	DG17-69	Dove Lake area - creek outlet near Lake Lilla	413023	5388577	10m
Cradle	Mineral Elongation Lineation	Lao	82	13.6			1 - Most reliable	1:10,000	Lm	quartzite	4/07/2017	DG17-69.1	steeply dipping thin bedded white quartzite, Lm 80 pitch NE (quartz elongation)	DG17-69	Dove Lake area - creek outlet near Lake Lilla	413023	5388577	10m
Cradle	Metamorphic Foliation, parallel to bedding	Sak	65	128.6			1 - Most reliable	1:10,000	So/Sm	quartzite	4/07/2017	DG17-69.2	steeply dipping thin bedded white quartzite	DG17-69	Dove Lake area - creek outlet near Lake Lilla	413023	5388577	10m
Cradle	Cleavage	Caa	55	63.6			3	1:10,000	S1	quartzite	4/07/2017	DG17-69.2	steeply dipping thin bedded white quartzite	DG17-69	Dove Lake area - creek outlet near Lake Lilla	413023	5388577	10m
Cradle	Metamorphic Foliation, parallel to bedding	Sak	88	343.6			1 - Most reliable	1:10,000	S0/Sm	quartzite	4/07/2017	DG17-69.2	steeply dipping thin bedded white quartzite	DG17-69	Dove Lake area - creek outlet near Lake Lilla	413023	5388577	10m
Cradle	M Fold with dip and dip direction of axial surface, Local age F2	Hak + Paq	56	68.6	85	158.6	1 - Most reliable	1:10,000	A	quartzite	4/07/2017	DG17-69.2	steeply dipping thin bedded white quartzite	DG17-69	Dove Lake area - creek outlet near Lake Lilla	413023	5388577	10m
Cradle	Bedding, no facing	Baf	80	343.6			1 - Most reliable	1:10,000	S0	quartzite	4/07/2017	DG17-69.2	steeply dipping thin bedded white quartzite	DG17-69	Dove Lake area - creek outlet near Lake Lilla	413023	5388577	10m
Cradle	Intersection Lineation	Laa	55	80.6			1 - Most reliable	1:10,000	Lint	quartzite	4/07/2017	DG17-69.2	steeply dipping thin bedded white quartzite	DG17-69	Dove Lake area - creek outlet near Lake Lilla	413023	5388577	10m
Cradle	Sinistral Wrench Fault	Las	70	143.6			1 - Most reliable	1:10,000	Fault (sinistral)	quartzite	4/07/2017	DG17-69.3	steeply dipping thin bedded white quartzite	DG17-69	Dove Lake area - creek outlet near Lake Lilla	413023	5388577	10m
Cradle	M Fold with dip and dip direction of axial surface, Local age F2	Hak + Paq	50	58.6	80	143.6	1 - Most reliable	1:10,000	A	quartzite	4/07/2017	DG17-69.3	steeply dipping thin bedded white quartzite	DG17-69	Dove Lake area - creek outlet near Lake Lilla	413023	5388577	10m
Cradle	Dextral Wrench Fault	Lar	80	63.6			1 - Most reliable	1:10,000	Fault (dextral)	quartzite	4/07/2017	DG17-69.4	steeply dipping thin bedded white quartzite	DG17-69	Dove Lake area - creek outlet near Lake Lilla	413023	5388577	10m
Cradle	M Fold, Local age F2	Hak	56	68.6			1 - Most reliable	1:10,000	A (F2)	quartzite	4/07/2017	DG17-69.4	steeply dipping thin bedded white quartzite	DG17-69	Dove Lake area - creek outlet near Lake Lilla	413023	5388577	10m
Cradle	Mineral Elongation Lineation	Lao	88	75.6	90	258.6	1 - Most reliable	1:10,000	Lrod	quartzite	4/07/2017	DG17-70	thin bedded quartzite with minor schist layers	DG17-70	Dove Lake area -Lake Lilla Tk, near Dove Lake Carpark	413449	5388364	10m
Cradle	Mineral Elongation Lineation	Lao	80	225.6			1 - Most reliable	1:10,000	Lrod	quartzite	4/07/2017	DG17-70	thin bedded quartzite with minor schist layers	DG17-70	Dove Lake area -Lake Lilla Tk, near Dove Lake Carpark	413449	5388364	10m
Cradle	Mineral Elongation Lineation	Lao	85	43.6			1 - Most reliable	1:10,000	Lrod	quartzite	4/07/2017	DG17-70	thin bedded quartzite with minor schist layers	DG17-70	Dove Lake area -Lake Lilla Tk, near Dove Lake Carpark	413449	5388364	10m
Cradle	Metamorphic Foliation, parallel to bedding	Sak	33	103.6			1 - Most reliable	1:10,000	S0/Sm env	quartzite	4/07/2017	DG17-70	thin bedded quartzite with minor schist layers	DG17-70	Dove Lake area -Lake Lilla Tk, near Dove Lake Carpark	413449	5388364	10m
Cradle	Metamorphic Foliation, parallel to bedding	Sak	85	145.6			1 - Most reliable	1:10,000	S0/Sm	quartzite	4/07/2017	DG17-70	thin bedded quartzite with minor schist layers	DG17-70	Dove Lake area -Lake Lilla Tk, near Dove Lake Carpark	413449	5388364	10m
Cradle	Metamorphic Foliation, parallel to bedding	Sak	75	305.6			1 - Most reliable	1:10,000	S0/Sm	quartzite	4/07/2017	DG17-70	thin bedded quartzite with minor schist layers	DG17-70	Dove Lake area -Lake Lilla Tk, near Dove Lake Carpark	413449	5388364	10m
Cradle	Metamorphic Foliation, parallel to bedding	Sak	84	165.6			1 - Most reliable	1:10,000	S0/Sm	quartzite	5/07/2017	DG17-71	quartzite	DG17-71	Dove Lake area -Hansens Peak Track, 20m below ridge with Mt Campbell	414021	5387512	10m
Cradle	Cleavage	Caa	75	8.6			1 - Most reliable	1:10,000	S1	quartzite	5/07/2017	DG17-71	quartzite	DG17-71	Dove Lake area -Hansens Peak Track, 20m below ridge with Mt Campbell	414021	5387512	10m

Project	Structure	Structure Type Symbol	Dip *	Dip Direction *	Secondary Dip	Secondary Dip Direction	Reliability	Output Scale *	Comments	Lithology	Collection Date	Field #	Sample Description	Other References	Locality	X *	Y *	Positional Accuracy
Cradle	Fold with dip and dip direction of axial surface, Local age F3	Has + Par	60	153.6	78	63.6	1 - Most reliable	1:10,000	A	quartzite	5/07/2017	DG17-71	quartzite	DG17-71	Dove Lake area -Hansens Peak Track, 20m below ridge with Mt Campbell	414021	5387512	10m
Cradle	Cleavage	Caa	80	3.6			1 - Most reliable	1:10,000	S1	quartzite	5/07/2017	DG17-72	quartzite	DG17-72	Dove Lake area -Steps up to Hansens Peak Track	414164	5386998	10m
Cradle	Metamorphic Foliation, parallel to bedding	Sak	80	177.6			1 - Most reliable	1:10,000	S0/Sm	quartzite	5/07/2017	DG17-72	quartzite	DG17-72	Dove Lake area -Steps up to Hansens Peak Track	414164	5386998	10m
Cradle	Mineral Elongation Lineation	Lao	15	71.6			1 - Most reliable	1:10,000	Lrod	quartzite	5/07/2017	DG17-72	quartzite	DG17-72	Dove Lake area -Steps up to Hansens Peak Track	414164	5386998	10m
Cradle	Metamorphic Foliation	Sag	85	145.6			1 - Most reliable	1:10,000	Sm	phyllite	5/07/2017	DG17-73.1	intensely foliated black phyllite and grey silstone, intrafolial folds	DG17-73 (WPT594)	Dove Lake area -Lake Lilla Track	412582	5389244	10m
Cradle	Intersection Lineation	Laa	65	247.6			1 - Most reliable	1:10,000	Lint	phyllite	5/07/2017	DG17-73.1	intensely foliated black phyllite and grey silstone, intrafolial folds	DG17-73 (WPT594)	Dove Lake area -Lake Lilla Track	412582	5389244	10m
Cradle	Metamorphic Foliation	Sag	84	305.6			1 - Most reliable	1:10,000	Sm	quartzite	5/07/2017	DG17-73.1	intensely foliated black phyllite and grey silstone, quartzite layer	DG17-73 (WPT594)	Dove Lake area -Lake Lilla Track	412582	5389244	10m
Cradle	Fold with dip and dip direction of axial surface, Local age F1	Hal + Pap	62	63.6	85	157.6	1 - Most reliable	1:10,000	A		5/07/2017	DG17-73.2	intensely foliated black phyllite and grey silstone	DG17-73 (WPT594)	Dove Lake area -Lake Lilla Track	412582	5389244	10m
Cradle	Metamorphic Foliation	Sag	84	305.6			1 - Most reliable	1:10,000	Sas (bounding HSZ)	quartzite	5/07/2017	DG17-74.1	White quartzite/mica schist	DG17-74 ((WPT595)	Dove Lake area -first ridge outcrop	412826	5389070	10m
Cradle	Metamorphic Foliation	Sag	83	338.6			1 - Most reliable	1:10,000	Sm (modal)	quartzite	5/07/2017	DG17-74.1	White quartzite/mica schist	DG17-74 ((WPT595)	Dove Lake area -first ridge outcrop	412826	5389070	10m
Cradle	Mineral Elongation Lineation	Lao	68	253.6			1 - Most reliable	1:10,000	Lm	quartzite	5/07/2017	DG17-74.1	White quartzite/mica schist, fold axis variable about mineral lineation (quartzite)	DG17-74 ((WPT595)	Dove Lake area -first ridge outcrop	412826	5389070	10m
Cradle	Metamorphic Foliation	Sag	84	305.6			1 - Most reliable	1:10,000	Sm	quartzite	5/07/2017	DG17-74.2	White quartzite/mica schist	DG17-74 ((WPT595)	Dove Lake area -first ridge outcrop	412826	5389070	10m
Cradle	Metamorphic Foliation	Sag	84	325.6			1 - Most reliable	1:10,000	Sm	quartzite	5/07/2017	DG17-74.2	White quartzite/mica schist, pavement	DG17-74 ((WPT595)	Dove Lake area -first ridge outcrop	412826	5389070	10m
Cradle	Metamorphic Foliation	Sag	83	338.6			1 - Most reliable	1:10,000	Sm	quartzite	5/07/2017	DG17-74.3	White quartzite/mica schist, pavement	DG17-74 ((WPT595)	Dove Lake area -first ridge outcrop	412826	5389070	10m
Cradle	Metamorphic Foliation	Sag	84	329.6			1 - Most reliable	1:10,000	Sm	quartzite	5/07/2017	DG17-74.3	White quartzite/mica schist, pavement	DG17-74 ((WPT595)	Dove Lake area -first ridge outcrop	412826	5389070	10m
Cradle	Fold with dip and dip direction of axial surface, Local age F1	Hal + Pap	59	279.6	76	335.6	1 - Most reliable	1:10,000	A	quartzite	5/07/2017	DG17-74.4	White quartzite/mica schist, pavement	DG17-74 ((WPT595)	Dove Lake area -first ridge outcrop	412826	5389070	10m
Cradle	Metamorphic Foliation	Sag	84	339.6			1 - Most reliable	1:10,000	Sm	quartzite	5/07/2017	DG17-74.5	White quartzite/mica schist, pavement	DG17-74 ((WPT595)	Dove Lake area -first ridge outcrop	412826	5389070	10m
Cradle	Mineral Elongation Lineation	Lao	68	253.6			1 - Most reliable	1:10,000	Lm	quartzite	5/07/2017	DG17-74.5	White quartzite/mica schist, pavement	DG17-74 ((WPT595)	Dove Lake area -first ridge outcrop	412826	5389070	10m
Cradle	Mineral Elongation Lineation	Lao	60	255.6			1 - Most reliable	1:10,000	Lm	quartzite	5/07/2017	DG17-74.6	White quartzite/mica schist, pavement	DG17-74 ((WPT595)	Dove Lake area -first ridge outcrop	412826	5389070	10m
Cradle	Mineral Elongation Lineation	Lao	80	269.6			1 - Most reliable	1:10,000	Lm	quartzite	5/07/2017	DG17-74.6	White quartzite/mica schist, pavement	DG17-74 ((WPT595)	Dove Lake area -first ridge outcrop	412826	5389070	10m
Cradle	Mineral Elongation Lineation	Lao	56	275.6			1 - Most reliable	1:10,000	Lm	quartzite	5/07/2017	DG17-74.6	White quartzite/mica schist, pavement	DG17-74 ((WPT595)	Dove Lake area -first ridge outcrop	412826	5389070	10m
Cradle	Metamorphic Foliation	Sag	80	335.6			1 - Most reliable	1:10,000	Sm	quartzite	5/07/2017	DG17-74.6	White quartzite/mica schist, pavement	DG17-74 ((WPT595)	Dove Lake area -first ridge outcrop	412826	5389070	10m
Cradle	Mineral Elongation Lineation	Lao	76	263.6			1 - Most reliable	1:10,000	Lrod	quartzite	5/07/2017	DG17-74.7	White quartzite/mica schist, pavement	DG17-74 ((WPT595)	Dove Lake area -first ridge outcrop	412826	5389070	10m
Cradle	Fold with dip and dip direction of axial surface, Local age F1	Hal + Pap	80	231.6	86	155.6	1 - Most reliable	1:10,000	A	quartzite	5/07/2017	DG17-74.8	White quartzite/mica schist, pavement	DG17-74 ((WPT595)	Dove Lake area -first ridge outcrop	412826	5389070	10m
Cradle	Fold with dip and dip direction of axial surface, Local age F1	Hal + Pap	40	65.6	88	339.6	1 - Most reliable	1:10,000	A	quartzite	5/07/2017	DG17-74.9	White quartzite/mica schist, pavement	DG17-74 ((WPT595)	Dove Lake area -first ridge outcrop	412826	5389070	10m
Cradle	Fold, Local age F1	Hal	85	71.6			1 - Most reliable	1:10,000	A	quartzite	5/07/2017	DG17-74.10	White quartzite/mica schist, pavement	DG17-74 ((WPT595)	Dove Lake area -first ridge outcrop	412826	5389070	10m
Cradle	Fold, Local age F1	Hal	68	256.6			1 - Most reliable	1:10,000	A	quartzite	5/07/2017	DG17-74.11	White quartzite/mica schist, pavement	DG17-74 ((WPT595)	Dove Lake area -first ridge outcrop	412826	5389070	10m
Cradle	Vertical Metamorphic Foliation	Sah	90	245.6			1 - Most reliable	1:10,000	Sm	quartzite	5/07/2017	DG17-74.12	White quartzite/mica schist, pavement	DG17-74 ((WPT595)	Dove Lake area -first ridge outcrop	412826	5389070	10m
Cradle	Fold with dip and dip direction of axial surface, Local age F1	Hal + Pap	46	247.6	80	3.6	1 - Most reliable	1:10,000	A	quartzite	5/07/2017	DG17-74.13	White quartzite/mica schist, pavement	DG17-74 ((WPT595)	Dove Lake area -first ridge outcrop	412826	5389070	10m
Cradle	Fold with dip and dip direction of axial surface, Local age F1	Hal + Pap	36	251.6	82	345.6	1 - Most reliable	1:10,000	A	quartzite	5/07/2017	DG17-74.14	White quartzite/mica schist, pavement	DG17-74 ((WPT595)	Dove Lake area -first ridge outcrop	412826	5389070	10m
Cradle	Mineral Elongation Lineation	Lao	28	254.6			1 - Most reliable	1:10,000	Lrod	quartzite	5/07/2017	DG17-75	thin bedded quartzite and platy quartzite mylonite	DG17-75 (WPT596)	Dove Lake area	412892	5389019	10m
Cradle	Metamorphic Foliation	Sag	88	343.6			1 - Most reliable	1:10,000	Sm	quartzite	5/07/2017	DG17-75	thin bedded quartzite and platy quartzite mylonite	DG17-75 (WPT596)	Dove Lake area	412892	5389019	10m
Cradle	Fold with dip and dip direction of axial surface, Local age F1	Hal + Pap	35	253.6	70	175.6	1 - Most reliable	1:10,000	A	quartzite	5/07/2017	DG17-75	thin bedded quartzite and platy quartzite mylonite	DG17-75 (WPT596)	Dove Lake area	412892	5389019	10m

Project	Structure	Structure Type Symbol	Dip *	Dip Direction *	Secondary Dip	Secondary Dip Direction	Reliability	Output Scale *	Comments	Lithology	Collection Date	Field #	Sample Description	Other References	Locality	X *	Y *	Positional Accuracy
Cradle	Fold with dip and dip direction of axial surface, Local age F3	Has + Par	30	39.6	15	58.6	1 - Most reliable	1:10,000	A	quartzite	5/07/2017	DG17-77	thin bedded quartzite and platy quartzite mylonite	DG17-77	Dove Lake area - Crater Lake cirque wall	411975	5387771	25m
Cradle	Fold, Local age F1	Hal	22	273.6			1 - Most reliable	1:10,000	A	schist, quartz-mica	5/07/2017	DG17-78	Mica quartz schist, high stain zone, isoclinal folds in qtz veins	DG17-78 (WPT597)	Dove Lake area - Ronny Creek Carpark	412434	5390558	10m
Cradle	Metamorphic Foliation	Sag	86	359.6			1 - Most reliable	1:10,000	Sm	schist, quartz-mica	5/07/2017	DG17-78	Mica quartz schist, high stain zone	DG17-78 (WPT597)	Dove Lake area - Ronny Creek Carpark	412434	5390558	10m
Cradle	Crenulation Lineation	Laj	22	270.6			1 - Most reliable	1:10,000	Lcren	schist, quartz-mica	5/07/2017	DG17-78	Mica quartz schist, high stain zone	DG17-78 (WPT597)	Dove Lake area - Ronny Creek Carpark	412434	5390558	10m
Cradle	Mineral Elongation Lineation	Lao	40	265.6			1 - Most reliable	1:10,000	Lrod	schist, quartz-mica	5/07/2017	DG17-78	Mica quartz schist, high stain zone, rodding lineation in qtz vein	DG17-78 (WPT597)	Dove Lake area - Ronny Creek Carpark	412434	5390558	10m
Cradle	Metamorphic Foliation	Sag	80	189.6			1 - Most reliable	1:10,000	Sm	schist, quartz-mica	5/07/2017	DG17-79	White mylonitic quartzite	DG17-79	Dove Lake area boardwalk track from Ronny Carpatk	412446	5390544	10m
Cradle	Mineral Elongation Lineation	Lao	60	277.6			1 - Most reliable	1:10,000	Lrod	schist, quartz-mica	5/07/2017	DG17-79	White mylonitic quartzite	DG17-79	Dove Lake area boardwalk track from Ronny Carpatk	412446	5390544	10m
Cradle	Fold with dip and dip direction of axial surface, Local age F3	Has + Par	15	253.6	80	168.6	1 - Most reliable	1:10,000	A		5/07/2017	DG17-80.1	bedded quartzite	DG17-80 (WPT598)	Dove Lake area, outcrop near bridge	412350	5390672	10m
Cradle	Fold with dip and dip direction of axial surface, Local age F3	Has + Par	15	269.6	80	165.6	1 - Most reliable	1:10,000	A		5/07/2017	DG17-80.2	bedded quartzite	DG17-80 (WPT598)	Dove Lake area, outcrop near bridge	412350	5390672	10m
Cradle	Bedding, no facing	Baf	40	319.6			1 - Most reliable	1:10,000	S0	quartzite	7/07/2017	DG17-81	intensely foliated pelitic quartzite, transposed So, sheathlike folds	DG17-81 (WPT599)	Dove River Gorge Track	411860	5394787	10m
Cradle	Metamorphic Foliation	Sag	50	295.6			1 - Most reliable	1:10,000	Sm	quartzite	7/07/2017	DG17-81	intensely foliated pelitic quartzite, transposed So, sheathlike folds	DG17-81 (WPT599)	Dove River Gorge Track	411860	5394787	10m
Cradle	Mineral Elongation Lineation	Lao	40	283.6			1 - Most reliable	1:10,000	Lm	quartzite	7/07/2017	DG17-81	intensely foliated pelitic quartzite, transposed So, sheathlike folds	DG17-81 (WPT599)	Dove River Gorge Track	411860	5394787	10m
Cradle	Fold, Local age F1	Hal	28	283.6			1 - Most reliable	1:10,000	A	quartzite	7/07/2017	DG17-81	intensely foliated pelitic quartzite, transposed So, sheathlike folds,intrafolial isoclines	DG17-81 (WPT599)	Dove River Gorge Track	411860	5394787	10m
Cradle	Fold, Local age F1	Hal	32	281.6			1 - Most reliable	1:10,000	A	quartzite	7/07/2017	DG17-81	intensely foliated pelitic quartzite, transposed So, sheathlike folds, isoclines in quartz veins	DG17-81 (WPT599)	Dove River Gorge Track	411860	5394787	10m
Cradle	Metamorphic Foliation, parallel to bedding	Sak	40	309.6			1 - Most reliable	1:10,000	S0/Sm	quartzite	7/07/2017	DG17-82	bedded quartzite, mullion structure, intense Lm parallel to Fold axis	DG17-82 (WPT600)	Dove River Gorge Track, bridge	412161	5394923	10m
Cradle	Mineral Elongation Lineation	Lao	34	277.6			1 - Most reliable	1:10,000	Lm	quartzite	7/07/2017	DG17-82	bedded quartzite, mullion structure, intense Lm parallel to Fold axis, mineral lineation	DG17-82 (WPT600)	Dove River Gorge Track, bridge	412161	5394923	10m
Cradle	Intersection Lineation	Laa	12	23.6			1 - Most reliable	1:10,000	Lint	quartzite	7/07/2017	DG17-82	bedded quartzite, mullion structure, intense Lm parallel to Fold axis	DG17-82 (WPT600)	Dove River Gorge Track, bridge	412161	5394923	10m
Cradle	Fold, Local age F1	Hal	32	275.6			1 - Most reliable	1:10,000	A	quartzite	7/07/2017	DG17-82	bedded quartzite, mullion structure, intense Lm parallel to Fold axis	DG17-82 (WPT600)	Dove River Gorge Track, bridge	412161	5394923	10m
Cradle	Metamorphic Foliation	Sag	34	336.6			1 - Most reliable	1:10,000	Sm	schist, quartz-mica	7/07/2017	DG17-83	foliated qtz-mica schist, boudinaged isoclinally folded thin quartz veins, rodded veins	DG17-83 (WPT601)	Dove River Gorge Track	412570	5394757	10m
Cradle	Mineral Elongation Lineation	Lao	8	275.6			1 - Most reliable	1:10,000	Lm	schist, quartz-mica	7/07/2017	DG17-83	foliated qtz-mica schist, boudinaged isoclinally folded thin quartz veins, rodded veins, mineral lineation	DG17-83 (WPT601)	Dove River Gorge Track	412570	5394757	10m
Cradle	Mineral Elongation Lineation	Lao	12	279.6			1 - Most reliable	1:10,000	Lrod	schist, quartz-mica	7/07/2017	DG17-83	foliated qtz-mica schist, boudinaged isoclinally folded thin quartz veins, rodded veins. Lrod = quartz veins	DG17-83 (WPT601)	Dove River Gorge Track	412570	5394757	10m
Cradle	Metamorphic Foliation, parallel to bedding	Sak	34	305.6			1 - Most reliable	1:10,000	S0/Sm	quartzite	7/07/2017	DG17-84	thick bedded quartzite	DG17-84 (WPT602)	Dove River Gorge Track - head of gorge	412285	5394316	10m
Cradle	Mineral Elongation Lineation	Lao	29	275.6			1 - Most reliable	1:10,000	Lm	quartzite	7/07/2017	DG17-84	thick bedded quartzite, mineral lineation	DG17-84 (WPT602)	Dove River Gorge Track - head of gorge	412285	5394316	10m
Cradle	Mineral Elongation Lineation	Lao	14	245.6			1 - Most reliable	1:10,000	Lrod	quartzite	7/07/2017	DG17-84	thick bedded quartzite, quatz veins	DG17-84 (WPT602)	Dove River Gorge Track - head of gorge	412285	5394316	10m
Cradle	Metamorphic Foliation, parallel to bedding	Sak	63	323.6			1 - Most reliable	1:10,000	S0/Sm	quartzite	8/03/2019	DG19-30.1	Bedded quartzite	DG19-30 (WPT623)	Crater Lake	412653	5387637	10m
Cradle	Intersection Lineation	Laa	6	48.6			1 - Most reliable	1:10,000	Lint	quartzite	8/03/2019	DG19-30.1	Bedded quartzite	DG19-30 (WPT623)	Crater Lake	412653	5387637	10m
Cradle	Mineral Elongation Lineation	Lao	26	243.6			1 - Most reliable	1:10,000	Lm	quartzite	8/03/2019	DG19-30.1	Bedded quartzite	DG19-30 (WPT623)	Crater Lake	412653	5387637	10m
Cradle	Metamorphic Foliation, parallel to bedding	Sak	54	138.6			1 - Most reliable	1:10,000	S0/Sm	quartzite	8/03/2019	DG19-30.2	Bedded quartzite	DG19-30 (WPT623)	Crater Lake	412653	5387637	10m
Cradle	Fold with dip and dip direction of axial surface	Haa + Pac	16	58.6	80	143.6	1 - Most reliable	1:10,000	A	quartzite	8/03/2019	DG19-30.3	Bedded quartzite	DG19-30 (WPT623) ~ 20m south	Crater Lake	412653	5387617	10m

Project	Structure	Structure Type Symbol	Dip *	Dip Direction *	Secondary Dip	Secondary Dip Direction	Reliability	Output Scale *	Comments	Lithology	Collection Date	Field #	Sample Description	Other References	Locality	X *	Y *	Positional Accuracy
Cradle	Strike and dip of metamorphic foliation other than cleavage, local age S1	Say	32	278.6			1 - Most reliable	1:10,000	S1/Sm	quartzite	8/03/2019	DG19-31.1	Platy Quartzite	DG19-31 (WPT624)	Marions Lookout	412681	5387135	10m
Cradle	Metamorphic Foliation	Sag	80	178.6			1 - Most reliable	1:10,000	Sm	quartzite	8/03/2019	DG19-31.1	Platy Quartzite	DG19-31 (WPT624)	Marions Lookout	412681	5387135	10m
Cradle	Mineral Elongation Lineation	Lao	36	258.6			1 - Most reliable	1:10,000	Lrod	quartzite	8/03/2019	DG19-31.1	Platy Quartzite	DG19-31 (WPT624)	Marions Lookout	412681	5387135	10m
Cradle	Mylonitic Foliation	Sas	75	173.6			1 - Most reliable	1:10,000	Sm (mylonitic)	quartzite	8/03/2019	DG19-31.2	Platy Quartzite	DG19-31 (WPT624)	Marions Lookout	412681	5387135	10m
Cradle	Mineral Elongation Lineation	Lao	32	283.6			1 - Most reliable	1:10,000	Lm	quartzite	8/03/2019	DG19-31.2	Platy Quartzite	DG19-31 (WPT624)	Marions Lookout	412681	5387135	10m
Cradle	Kink Fold with dip and dip direction of axial surface	Hau + Pao	62	148.6	75	63.6	1 - Most reliable	1:10,000	Kink A	quartzite	8/03/2019	DG19-31.3	Platy Quartzite, Kink Bands (Chevrons)	DG19-31 (WPT624)	Marions Lookout	412681	5387135	10m
Cradle	Metamorphic Foliation	Sag	72	193.6			1 - Most reliable	1:10,000	Sm	quartzite	8/03/2019	DG19-32.1	Platy quartzite mylonite; boudinaged folded quartz veins	DG19-32	track above s end Dove Lake	412641	5387083	10m
Cradle	Fold	Haa	70	133.6			1 - Most reliable	1:10,000	FA	quartzite	8/03/2019	DG19-32.1	Platy quartzite mylonite; boudinaged folded quartz veins	DG19-32	track above s end Dove Lake	412641	5387083	10m
Cradle	Mineral Elongation Lineation	Lao	68	143.6			1 - Most reliable	1:10,000	Lfibre	quartzite	8/03/2019	DG19-32.1	Platy quartzite mylonite; boudinaged folded quartz veins	DG19-32	track above s end Dove Lake	412641	5387083	10m
Cradle	Cleavage	Caa	62	158.6			1 - Most reliable	1:10,000	S1	quartzite	8/03/2019	DG19-32A	quartzite	DG19-32A	Near Kitchen Hut	412287	5385687	10m
Cradle	Metamorphic Foliation	Sag	48	193.6			1 - Most reliable	1:10,000	Sm	quartzite	9/03/2019	DG19-33.1	Platy quartzite mylonite, homoclinally dipping	DG19-33 (WPT625)	N of Pine Forest Moor	412441	5377250	10m
Cradle	Mineral Elongation Lineation	Lao	8	278.6			1 - Most reliable	1:10,000	Lm	quartzite	9/03/2019	DG19-33.1	Platy quartzite mylonite, homoclinally dipping	DG19-33 (WPT625)	N of Pine Forest Moor	412441	5377250	10m
Cradle	Fold with dip and dip direction of axial surface	Haa + Pac	16	258.6	60	183.6	1 - Most reliable	1:10,000	A	quartzite	9/03/2019	DG19-33.2	Platy quartzite mylonite, homoclinally dipping	DG19-33 (WPT625)	N of Pine Forest Moor	412441	5377250	10m
Cradle	Fold with dip and dip direction of axial surface, Local age F1	Hal + Pap	8	253.6	40	163.6	1 - Most reliable	1:10,000	A early	quartzite	9/03/2019	DG19-33.3	Platy quartzite mylonite, homoclinally dipping; isoclines within Sm	DG19-33 (WPT625)	N of Pine Forest Moor	412441	5377250	10m
Cradle	Mineral Elongation Lineation	Lao	2	103.6			1 - Most reliable	1:10,000	Lrod	quartzite	9/03/2019	DG19-33.4	Platy quartzite mylonite, homoclinally dipping; rodding lineations define a herring-bone pattern	DG19-33 (WPT625)	N of Pine Forest Moor	412441	5377250	10m
Cradle	Mineral Elongation Lineation	Lao	18	258.6			1 - Most reliable	1:10,000	Lrod	quartzite	9/03/2019	DG19-33.4	Platy quartzite mylonite, homoclinally dipping;	DG19-33 (WPT625)	N of Pine Forest Moor	412441	5377250	10m
Cradle	Fold with dip and dip direction of axial surface	Haa + Pac	6	253.6	30	203.6	1 - Most reliable	1:10,000	A	quartzite	9/03/2019	DG19-33.5	Platy quartzite mylonite, homoclinally dipping	DG19-33 (WPT625)	N of Pine Forest Moor	412441	5377250	10m
Cradle	Metamorphic Foliation, parallel to bedding	Sak	56	3.6			1 - Most reliable	1:10,000	S0/Sm	quartzite	9/03/2019	DG19-34.1	strongly lineated quartzite	DG19-34 (WPT626)	N of Pine Forest Moor	413808	5374133	10m
Cradle	Mineral Elongation Lineation	Lao	20	283.6			1 - Most reliable	1:10,000	Lm	quartzite	9/03/2019	DG19-34.1	strongly lineated quartzite	DG19-34 (WPT626)	N of Pine Forest Moor	413808	5374133	10m
Cradle	Fold with dip and dip direction of axial surface	Haa + Pac	26	73.6	55	13.6	1 - Most reliable	1:10,000	A	quartzite	9/03/2019	DG19-34.2	strongly lineated quartzite	DG19-34 (WPT626)	N of Pine Forest Moor	413808	5374133	10m
Cradle	Metamorphic Foliation	Sag	36	193.6			1 - Most reliable	1:10,000	Sm	quartzite	9/03/2019	DG19-35.1	Lineated quartzite, folded Sm	DG19-35 (WPT627)	N of Pine Forest Moor	413808	5374133	10m
Cradle	Mineral Elongation Lineation	Lao	5	108.6			1 - Most reliable	1:10,000	Lm	quartzite	9/03/2019	DG19-35.1	Lineated quartzite	DG19-35 (WPT627)	N of Pine Forest Moor	413808	5374133	10m
Cradle	Metamorphic Foliation	Sag	8	23.6			1 - Most reliable	1:10,000	Sm	quartzite	9/03/2019	DG19-35.2	Lineated quartzite	DG19-35 (WPT627)	N of Pine Forest Moor	413808	5374133	10m
Cradle	Metamorphic Foliation	Sag	12	228.6			1 - Most reliable	1:10,000	Sm	quartzite	9/03/2019	DG19-35.2	Lineated quartzite	DG19-35 (WPT627)	N of Pine Forest Moor	413808	5374133	10m
Cradle	Mineral Elongation Lineation	Lao	8	308.6			1 - Most reliable	1:10,000	Lm	quartzite	9/03/2019	DG19-35.2	Lineated quartzite	DG19-35 (WPT627)	N of Pine Forest Moor	413808	5374133	10m
Cradle	Metamorphic Foliation	Sag	48	323.6			1 - Most reliable	1:10,000	Sm	quartzite	10/03/2019	DG19-36.1	Lineated quartzite	DG19-36 (WPT628)	S of Pine Forest Moor	416113	5371008	10m
Cradle	Mineral Elongation Lineation	Lao	20	253.6			1 - Most reliable	1:10,000	Lm	quartzite	10/03/2019	DG19-36.1	Lineated quartzite	DG19-36 (WPT628)	S of Pine Forest Moor	416113	5371008	10m
Cradle	Metamorphic Foliation, parallel to bedding	Sak	28	318.6			1 - Most reliable	1:10,000	So/Sm	quartzite	10/03/2019	DG19-36.2	Lineated quartzite	DG19-36 (WPT628)	S of Pine Forest Moor	416113	5371008	10m
Cradle	Mineral Elongation Lineation	Lao	8	238.6			1 - Most reliable	1:10,000	Lm	quartzite	10/03/2019	DG19-36.2	Lineated quartzite	DG19-36 (WPT628)	S of Pine Forest Moor	416113	5371008	10m
Cradle	Metamorphic Foliation	Sag	44	338.6			1 - Most reliable	1:10,000	Sm	quartzite	10/03/2019	DG19-37.1	Layered schist/quartzite, quartzite bands	DG19-37 (WPT629)	S of Pine Forest Moor	416140	5370959	10m
Cradle	Intersection Lineation	Laa	10	263.6			1 - Most reliable	1:10,000	Lm/Lint	quartzite	10/03/2019	DG19-37.1	Layered schist/quartzite, quartzite bands	DG19-37 (WPT629)	S of Pine Forest Moor	416140	5370959	10m
Cradle	Metamorphic Foliation	Sag	35	343.6			1 - Most reliable	1:10,000	Sm	schist	10/03/2019	DG19-37.2	Layered schist/quartzite, schist	DG19-37 (WPT629)	S of Pine Forest Moor	416140	5370959	10m
Cradle	Mineral Elongation Lineation	Lao	6	243.6			1 - Most reliable	1:10,000	Lm	schist	10/03/2019	DG19-37.2	Layered schist/quartzite, schist	DG19-37 (WPT629)	S of Pine Forest Moor	416140	5370959	10m
Cradle	Crenulation Lineation	Laj	46	303.6	80	218.6	1 - Most reliable	1:10,000	A cren	schist	10/03/2019	DG19-37.3	Layered schist/quartzite, crenulations	DG19-37 (WPT629)	S of Pine Forest Moor	416140	5370959	10m
Cradle	Metamorphic Foliation	Sag	36	318.6			1 - Most reliable	1:10,000	Sm	schist	10/03/2019	DG19-37.4	Layered schist/quartzite	DG19-37 (WPT629)	S of Pine Forest Moor	416140	5370959	10m
Cradle	Crenulation Cleavage	Cai	80	218.6			1 - Most reliable	1:10,000	Scc	schist	10/03/2019	DG19-37.4	Layered schist/quartzite	DG19-37 (WPT629)	S of Pine Forest Moor	416140	5370959	10m

Project	Structure	Structure Type Symbol	Dip *	Dip Direction *	Secondary Dip	Secondary Dip Direction	Reliability	Output Scale *	Comments	Lithology	Collection Date	Field #	Sample Description	Other References	Locality	X *	Y *	Positional Accuracy
Cradle	Fold with dip and dip direction of axial surface, Local age F1	Hal + Pap	30	228.6	40	338.6	1 - Most reliable	1:10,000	A F1	schist	10/03/2019	DG19-37.5	Layered schist/quartzite	DG19-37 (WPT629)	S of Pine Forest Moor	416140	5370959	10m
Cradle	Fold with dip and dip direction of axial surface, Local age F1	Hal + Pap	45	328.6	50	333.6	1 - Most reliable	1:10,000	AS F1	schist	10/03/2019	DG19-37.5	Layered schist/quartzite	DG19-37 (WPT629)	S of Pine Forest Moor	416140	5370959	10m
Cradle	Metamorphic Foliation	Sag	24	313.6			1 - Most reliable	1:10,000	Sm	quartzite	10/03/2019	DG19-38.1	Lineated quartzite/sheath folds	DG19-38 (WPT630)	S of Pine Forest Moor	416274	5370882	10m
Cradle	Mineral Elongation Lineation	Lao	35	253.6			1 - Most reliable	1:10,000	Lm	quartzite	10/03/2019	DG19-38.1	Lineated quartzite/sheath folds	DG19-38 (WPT630)	S of Pine Forest Moor	416274	5370882	10m
Cradle							1 - Most reliable	1:10,000		quartzite	10/03/2019	WPT631	last outcrop of quatzite	(WPT631)	S of Pine Forest Moor	416431	5370482	10m
Cradle	Fold with dip and dip direction of axial surface, Local age F1	Hal + Pap	50	143.6	44	148.6	1 - Most reliable	1:10,000	A	quartzite	10/03/2019	DG19-39.1	thin bedded quartzite with minor schist layers	DG19-39 (WPT632)	Old Pelion Hut	419953	5369026	10m
Cradle	Fold with dip and dip direction of axial surface, Local age F1	Hal + Pap	28	151.6	34	123.6	1 - Most reliable	1:10,000	A	quartzite	10/03/2019	DG19-39.2	thin bedded quartzite with minor schist layers	DG19-39 (WPT632)	Old Pelion Hut	419953	5369026	10m
Cradle	Fold with dip and dip direction of axial surface, Local age F1	Hal + Pap	22	198.6	46	133.6	1 - Most reliable	1:10,000	A	quartzite	10/03/2019	DG19-39.3	thin bedded quartzite with minor schist layers	DG19-39 (WPT632)	Old Pelion Hut	419953	5369026	10m
Cradle	Metamorphic Foliation	Sag	30	143.6			1 - Most reliable	1:10,000	Sm	quartzite	10/03/2019	DG19-39.4	thin bedded quartzite with minor schist layers	DG19-39 (WPT632)	Old Pelion Hut	419953	5369026	10m
Cradle	Intersection Lineation	Laa	12	218.6			1 - Most reliable	1:10,000	Lint	quartzite	10/03/2019	DG19-39.4	thin bedded quartzite with minor schist layers	DG19-39 (WPT632)	Old Pelion Hut	419953	5369026	10m
Cradle	Crenulation Lineation	Laj	28	83.6			1 - Most reliable	1:10,000	Lcren	quartzite	10/03/2019	DG19-39.4	thin bedded quartzite with minor schist layers	DG19-39 (WPT632)	Old Pelion Hut	419953	5369026	10m
Cradle	Fold with dip and dip direction of axial surface, Local age F1	Hal + Pap	38	163.6	45	133.6	1 - Most reliable	1:10,000	A	quartzite	10/03/2019	DG19-39.5	thin bedded quartzite with minor schist layers	DG19-39 (WPT632)	Old Pelion Hut	419953	5369026	10m
Cradle	Mineral Elongation Lineation	Lao	34	143.6			1 - Most reliable	1:10,000	Lm	quartzite	10/03/2019	DG19-39.6	thin bedded quartzite with minor schist layers	DG19-39 (WPT632)	Old Pelion Hut	419953	5369026	10m
Cradle	Metamorphic Foliation	Sag	37	128.6			1 - Most reliable	1:10,000	Sm	quartzite	10/03/2019	DG19-39.6	thin bedded quartzite with minor schist layers	DG19-39 (WPT632)	Old Pelion Hut	419953	5369026	10m
Cradle	Fold with dip and dip direction of axial surface, Local age F1	Hal + Pap	10	223.6	50	168.6	1 - Most reliable	1:10,000	A	quartzite	10/03/2019	DG19-39.7	thin bedded quartzite with minor schist layers	DG19-39 (WPT632)	Old Pelion Hut	419953	5369026	10m
Cradle	Fold with dip and dip direction of axial surface, Local age F1	Hal + Pap	42	133.6	55	173.6	1 - Most reliable	1:10,000	A	quartzite	10/03/2019	DG19-39.8	thin bedded quartzite with minor schist layers	DG19-39 (WPT632)	Old Pelion Hut	419953	5369026	10m
Cradle	Fold with dip and dip direction of axial surface, Local age F1	Hal + Pap	34	103.6	26	163.6	1 - Most reliable	1:10,000	A	quartzite	10/03/2019	DG19-39.9	thin bedded quartzite with minor schist layers	DG19-39 (WPT632)	Old Pelion Hut	419953	5369026	10m
Cradle	Fold with dip and dip direction of axial surface, Local age F1	Hal + Pap	40	183.6	40	183.6	1 - Most reliable	1:10,000	A	quartzite	10/03/2019	DG19-40.1	thin bedded quartzite with minor schist layers	DG19-40	Old Pelion Hut	419949	5369022	25m
Cradle	Fold with dip and dip direction of axial surface, Local age F2	Haq + Paq	40	238.6	30	253.6	1 - Most reliable	1:10,000	A	quartzite	10/03/2019	DG19-40.1	thin bedded quartzite with minor schist layers	DG19-40	Old Pelion Hut	419949	5369022	25m
Cradle	Fold, Local age F2	Haq	6	37.6			1 - Most reliable	1:10,000	A	quartzite	10/03/2019	DG19-40.2	thin bedded quartzite with minor schist layers	DG19-40	Old Pelion Hut	419949	5369022	25m
Cradle	Fold with dip and dip direction of axial surface, Local age F2	Haq + Paq	8	218.6	64	153.6	1 - Most reliable	1:10,000	A	quartzite	10/03/2019	DG19-40.3	thin bedded quartzite with minor schist layers	DG19-40	Old Pelion Hut	419949	5369022	25m
Cradle	Fold with dip and dip direction of axial surface, Local age F2	Haq + Paq	58	268.6	70	178.6	1 - Most reliable	1:10,000	A	quartzite	10/03/2019	DG19-40.4	thin bedded quartzite with minor schist layers	DG19-40	Old Pelion Hut	419949	5369022	25m
Cradle	Fold with dip and dip direction of axial surface, Local age F2	Haq + Paq	34	268.6	76	178.6	1 - Most reliable	1:10,000	A	quartzite	10/03/2019	DG19-40.5	thin bedded quartzite with minor schist layers	DG19-40	Old Pelion Hut	419949	5369022	25m
Cradle	Fold, Local age F2	Haq	6	253.6			1 - Most reliable	1:10,000	A	quartzite	10/03/2019	DG19-40.6	thin bedded quartzite with minor schist layers	DG19-40	Old Pelion Hut	419949	5369022	25m
Cradle	Fold, Local age F1	Hal	24	228.6			1 - Most reliable	1:10,000	A	quartzite	10/03/2019	DG19-40.7	thin bedded quartzite with minor schist layers	DG19-40	Old Pelion Hut	419949	5369022	25m
Cradle	Fold with dip and dip direction of axial surface, Local age F2	Haq + Paq	10	93.6	80	181.6	1 - Most reliable	1:10,000	A	quartzite	10/03/2019	DG19-41.1	thin bedded quartzite with minor schist layers	DG19-41	Old Pelion Hut	419951	5368999	25m
Cradle	Fold, Local age F2	Haq	12	103.6			1 - Most reliable	1:10,000	A	quartzite	10/03/2019	DG19-41.2	thin bedded quartzite with minor schist layers	DG19-41	Old Pelion Hut	419951	5368999	25m
Cradle	Fold, Local age F1	Hal	32	133.6			1 - Most reliable	1:10,000	A	quartzite	10/03/2019	DG19-42.1	thin bedded quartzite with minor schist layers	DG19-42	Old Pelion Hut	419951	5368984	25m
Cradle	Fold with dip and dip direction of axial surface, Local age F1	Hal + Pap	30	113.6	46	163.6	1 - Most reliable	1:10,000	A1	quartzite	10/03/2019	DG19-42.2	thin bedded quartzite with minor schist layers	DG19-42	Old Pelion Hut	419951	5368984	25m
Cradle	Metamorphic Foliation	Sag	44	173.6			1 - Most reliable	1:10,000	Sm	quartzite	10/03/2019	DG19-42.3	thin bedded quartzite with minor schist layers	DG19-42	Old Pelion Hut	419951	5368984	25m
Cradle	Mineral Elongation Lineation	Lao	28	93.6			1 - Most reliable	1:10,000	Lm	quartzite	10/03/2019	DG19-42.3	thin bedded quartzite with minor schist layers	DG19-42	Old Pelion Hut	419951	5368984	25m

Project	Structure	Structure Type Symbol	Dip *	Dip Direction *	Secondary Dip	Secondary Dip Direction	Reliability	Output Scale *	Comments	Lithology	Collection Date	Field #	Sample Description	Other References	Locality	X *	Y *	Positional Accuracy
Cradle	Fold with dip and dip direction of axial surface, Local age F1	Hal + Pap	56	158.6	57	153.6	1 - Most reliable	1:10,000	A	quartzite	10/03/2019	DG19-42.4	thin bedded quartzite with minor schist layers	DG19-42	Old Pelion Hut	419951	5368984	25m
Cradle	Fold, Local age F1	Hal	34	108.6			1 - Most reliable	1:10,000	A2	quartzite	10/03/2019	DG19-42.5	thin bedded quartzite with minor schist layers	DG19-42	Old Pelion Hut	419951	5368984	25m
Cradle	Metamorphic Foliation	Sag	32	153.6			1 - Most reliable	1:10,000	Sm	quartzite	10/03/2019	DG19-43.1	thin bedded quartzite with minor schist layers	DG19-43 (WPT633)	Old Pelion Hut	419959	5368972	10m
Cradle	Intersection Lineation	Laa	14	128.6			1 - Most reliable	1:10,000	Lint	quartzite	10/03/2019	DG19-43.1	thin bedded quartzite with minor schist layers	DG19-43 (WPT633)	Old Pelion Hut	419959	5368972	10m
Cradle	Mineral Elongation Lineation	Lao	26	218.6			1 - Most reliable	1:10,000	Lm	quartzite	10/03/2019	DG19-43.1	thin bedded quartzite with minor schist layers	DG19-43 (WPT633)	Old Pelion Hut	419959	5368972	10m
Cradle	Mineral Elongation Lineation	Lao	26	158.6			1 - Most reliable	1:10,000	Lm	quartzite	10/03/2019	DG19-43.2	thin bedded quartzite with minor schist layers	DG19-43 (WPT633)	Old Pelion Hut	419959	5368972	10m
Cradle	Fold, Local age F1	Hal	28	163.6			1 - Most reliable	1:10,000	A	quartzite	10/03/2019	DG19-43.3	thin bedded quartzite with minor schist layers	DG19-43 (WPT633)	Old Pelion Hut	419959	5368972	10m
Cradle	Local age F2	Hal + Pap	25	118.6	40	173.6	1 - Most reliable	1:10,000	A	quartzite	10/03/2019	DG19-43.4	thin bedded quartzite with minor schist layers	DG19-43 (WPT633)	Old Pelion Hut	419959	5368972	10m
Cradle	Metamorphic Foliation	Sag	85	193.6			1 - Most reliable	1:10,000	Sm	quartzite	19/10/2020	DG20.30.1	qtzite steeply dipping	DG20.30	Cradle	414207	5387173	10m
Cradle	Metamorphic Foliation	Sag	50	88.6			1 - Most reliable	1:10,000	Sm	quartzite	19/10/2020	DG20.30.1	qtzite steeply dipping	DG20.30	Cradle	414207	5387173	10m
Cradle	Mineral Elongation Lineation	Lao	15	163.6			1 - Most reliable	1:10,000	Lm	quartzite	19/10/2020	DG20.30.1	qtzite steeply dipping	DG20.30	Cradle	414207	5387173	10m
Cradle	Metamorphic Foliation	Sag	65	143.6			1 - Most reliable	1:10,000	Sm	quartzite	19/10/2020	DG20.30.2	qtzite steeply dipping	DG20.30	Cradle	414207	5387173	10m
Cradle	Metamorphic Foliation	Sag	80	173.6			1 - Most reliable	1:10,000	S???	quartzite	19/10/2020	DG20.30.2	qtzite steeply dipping	DG20.30	Cradle	414207	5387173	10m
Cradle	Fold	Haa	65	242.6			1 - Most reliable	1:10,000	Beta calc	quartzite	19/10/2020	DG20.30.2	qtzite steeply dipping	DG20.30	Cradle	414207	5387173	10m
Cradle	Metamorphic Foliation	Sag	55	208.6			1 - Most reliable	1:10,000	Sm	quartzite	19/10/2020	DG20.30 5mN.1	early fold	DG20.30 5mN	Cradle	414207	5387178	10m
Cradle	Metamorphic Foliation	Sag	40	353.6			1 - Most reliable	1:10,000	Sm	quartzite	19/10/2020	DG20.30 5mN.2	early fold	DG20.30 5mN	Cradle	414207	5387178	10m
Cradle	Fold	Haa	17	285.6			1 - Most reliable	1:10,000	Beta calc	quartzite	19/10/2020	DG20.30 5mN.3	early fold	DG20.30 5mN	Cradle	414207	5387178	10m
Cradle	Dip direction and dip of axial surface of minor fold	Pac			80	13.6	1 - Most reliable	1:10,000	As	quartzite	19/10/2020	DG20.30 5mN.4	early fold	DG20.30 5mN	Cradle	414207	5387178	10m
Cradle	Fold with dip and dip direction of axial surface	Haa + Pac	50	273.6	65	283.6	1 - Most reliable	1:10,000	FA	quartzite	19/10/2020	DG20.31.1	reclined folds	DG20.31	Cradle	414180	5387207	10m
Cradle	Axial surface of minor fold	Pac	40	238.6			1 - Most reliable	1:10,000	FA	quartzite	20/10/2020	DG20.32.1	fractured white quartzite	DG20.32	Cradle	412184	5385238	10m
Cradle	Metamorphic Foliation	Sag	40	193.6			1 - Most reliable	1:10,000	Sm	quartzite	20/10/2020	DG20.32.2	fractured white quartzite	DG20.32	Cradle	412184	5385238	10m
Cradle	Metamorphic Foliation	Sag	85	148.6			1 - Most reliable	1:10,000	Sm	quartzite	20/10/2020	DG20.32.3	fractured white quartzite	DG20.32	Cradle	412184	5385238	10m
Cradle	Metamorphic Foliation	Sag	55	68.6			1 - Most reliable	1:10,000	Sm		21/10/2020	DG20.33.1	prominent rodding in Sm	DG20.33	Cradle	414181	5386873	10m
Cradle	Mineral Elongation Lineation	Lao	48	61.6			1 - Most reliable	1:10,000	Lelong		21/10/2020	DG20.33.2	prominent rodding in Sm	DG20.33	Cradle	414181	5386873	10m
Cradle	Fold with dip and dip direction of axial surface	Haa + Pac	35	48.6	60	283.6	1 - Most reliable	1:10,000	FA/AS		21/10/2020	DG20.33.3	prominent rodding in Sm	DG20.33	Cradle	414181	5386873	10m
Cradle	Metamorphic Foliation	Sag	55	68.6			1 - Most reliable	1:10,000	Sm		21/10/2020	DG20.33.4	prominent rodding in Sm	DG20.33	Cradle	414181	5386873	10m
Cradle	Mineral Elongation Lineation	Lao	48	61.6			1 - Most reliable	1:10,000	Lm		21/10/2020	DG20.33.4	prominent rodding in Sm	DG20.33	Cradle	414181	5386873	10m
Cradle	Metamorphic Foliation	Sag	55	68.6			1 - Most reliable	1:10,000	Sm		21/10/2020	DG20.33.5	prominent rodding in Sm	DG20.33	Cradle	414181	5386873	10m
Cradle	Mineral Elongation Lineation	Lao	48	61.6			1 - Most reliable	1:10,000	Lm		21/10/2020	DG20.33.5	prominent rodding in Sm	DG20.33	Cradle	414181	5386873	10m
Cradle	Metamorphic Foliation	Sag	56	69.6			1 - Most reliable	1:10,000	Sm		21/10/2020	DG20.33.6	prominent rodding in Sm	DG20.33	Cradle	414181	5386873	10m
Cradle	Mineral Elongation Lineation	Lao	50	63.6			1 - Most reliable	1:10,000	Lm		21/10/2020	DG20.33.6	prominent rodding in Sm	DG20.33	Cradle	414181	5386873	10m
Cradle	Metamorphic Foliation	Sag	48	61.6			1 - Most reliable	1:10,000	Sm		21/10/2020	DG20.34.1		DG20.34	Cradle	414195	5386297	10m
Cradle	Mineral Elongation Lineation	Lao	42	55.6			1 - Most reliable	1:10,000	Lm		21/10/2020	DG20.34.2		DG20.34	Cradle	414195	5386297	10m
Cradle	Fold	Haa	15	28.6			1 - Most reliable	1:10,000	FA		21/10/2020	DG20.35.1		DG20.35	Cradle	414187	5386826	10m
Cradle	Fold with dip and dip direction of axial surface	Haa + Pac	10	23.6	85	98.6	1 - Most reliable	1:10,000	FA/AS		21/10/2020	DG20.35.2		DG20.35	Cradle	414187	5386826	10m
Cradle	Metamorphic Foliation	Sag	56	69.6			1 - Most reliable	1:10,000	Sm		21/10/2020	DG20.35.3		DG20.35	Cradle	414187	5386826	10m
Cradle	Mineral Elongation Lineation	Lao	55	68.6			1 - Most reliable	1:10,000	Lrod		21/10/2020	DG20.35.3		DG20.35	Cradle	414187	5386826	10m
Cradle	Metamorphic Foliation	Sag	65	78.6			1 - Most reliable	1:10,000	Sm		21/10/2020	DG20.35.4		DG20.35	Cradle	414187	5386826	10m
Cradle	Mineral Elongation Lineation	Lao	58	71.6			1 - Most reliable	1:10,000	Lm		21/10/2020	DG20.35.4		DG20.35	Cradle	414187	5386826	10m

Project	Structure	Structure Type Symbol	Dip *	Dip Direction *	Secondary Dip	Secondary Dip Direction	Reliability	Output Scale *	Comments	Lithology	Collection Date	Field #	Sample Description	Other References	Locality	X *	Y *	Positional Accuracy
Cradle	Metamorphic Foliation, parallel to bedding	Sak	85	98.6			1 - Most reliable	1:10,000	So	pelite	21/10/2020	DG20.36.1	thinly laminated grey pelite	DG20.36	Cradle	414187	5386810	10m
Cradle	Metamorphic Foliation	Sag	78	91.6			1 - Most reliable	1:10,000	S1/Sm	pelite	21/10/2020	DG20.36.2	thinly laminated grey pelite	DG20.36	Cradle	414187	5386810	10m
Cradle							1 - Most reliable	1:10,000		pelite	21/10/2020	DG20.36.3	pelite	DG20.36	Cradle	414195	5386985	10m
Cradle	Fold with dip and dip direction of axial surface	Haa + Pac	30	43.6	85	98.6	1 - Most reliable	1:10,000	FA/AS	pelite	21/10/2020	DG20.37.1	pelite	DG20.37	Cradle	414199	5386766	10m
Cradle	Metamorphic Foliation, parallel to bedding	Sak	40	53.6			1 - Most reliable	1:10,000	So	pelite	21/10/2020	DG20.37.2	pelite	DG20.37	Cradle	414199	5386766	10m
Cradle	Cleavage	Cae	90	103.6			1 - Most reliable	1:10,000	S1	pelite	21/10/2020	DG20.37.3	pelite	DG20.37	Cradle	414199	5386766	10m
Cradle	Metamorphic Foliation, parallel to bedding	Sak	86	99.6			1 - Most reliable	1:10,000	So	quartzite	21/10/2020	DG20.38.1	qtzite core of folded isocline	DG20.38	Cradle	414199	5386766	10m
Cradle	Metamorphic Foliation	Sag	90	103.6			1 - Most reliable	1:10,000	S1/Sm	quartzite	21/10/2020	DG20.38.2	qtzite core of folded isocline	DG20.38	Cradle	414199	5386766	10m
Cradle	Metamorphic Foliation	Sag	80	93.6			1 - Most reliable	1:10,000	Sm	quartzite	21/10/2020	DG20.39.1		DG20.39	Cradle	414196	5386705	10m
Cradle	Mineral Elongation Lineation	Lao	45	58.6			1 - Most reliable	1:10,000	Lm	quartzite	21/10/2020	DG20.39.2		DG20.39	Cradle	414196	5386705	10m
Cradle	Fold	Haa	40	53.6			1 - Most reliable	1:10,000	FA	quartzite	21/10/2020	DG20.40.1	qtzite	DG20.40	Cradle	414072	5386437	10m
Cradle	Mineral Elongation Lineation	Lao	12	25.6			1 - Most reliable	1:10,000	Lelong	quartzite	21/10/2020	DG20.40.2	qtzite	DG20.40	Cradle	414072	5386437	10m
Cradle	Metamorphic Foliation	Sag	40	53.6			1 - Most reliable	1:10,000	Sm	quartzite	21/10/2020	DG20.40.3	qtzite	DG20.40	Cradle	414072	5386437	10m
Cradle	Metamorphic Foliation	Sag	70	83.6			1 - Most reliable	1:10,000	Sm	quartzite	21/10/2020	DG20.40.4	qtzite	DG20.40	Cradle	414072	5386437	10m
Cradle	Mineral Elongation Lineation	Lao	40	53.6			1 - Most reliable	1:10,000	Lelong	quartzite	21/10/2020	DG20.40.5	qtzite	DG20.40	Cradle	414072	5386437	10m
Cradle	Fold	Haa	34	47.6			1 - Most reliable	1:10,000	Beta calc	quartzite	21/10/2020	DG20.40.6	qtzite	DG20.40	Cradle	414072	5386437	10m
Cradle	Metamorphic Foliation, parallel to bedding	Sak	75	88.6			1 - Most reliable	1:10,000	So/Sm		21/10/2020	DG20.41.1	qtzite	DG20.41	Cradle	414047	5386393	10m
Cradle	Unspecified Lineation	Lae	62	75.6			1 - Most reliable	1:10,000	Lmullion		21/10/2020	DG20.41.1	qtzite	DG20.41	Cradle	414047	5386393	10m
Cradle	Cleavage	Cae	76	89.6			1 - Most reliable	1:10,000	S1		21/10/2020	DG20.41.2	qtzite	DG20.41	Cradle	414047	5386393	10m
Cradle	Metamorphic Foliation	Sag	35	48.6			1 - Most reliable	1:10,000	Sm		21/10/2020	DG20.42.1	south side of whaleback ridge in qtzite	DG20.42	Cradle	414012	5386318	10m
Cradle	Intersection Lineation	Laa	33	46.6			1 - Most reliable	1:10,000	Lint		21/10/2020	DG20.42.2	south side of whaleback ridge in qtzite	DG20.42	Cradle	414012	5386318	10m
Cradle	Metamorphic Foliation	Sag	75	88.6			1 - Most reliable	1:10,000	Sm		21/10/2020	DG20.42.3	south side of whaleback ridge in qtzite	DG20.42	Cradle	414012	5386318	10m
Cradle	Intersection Lineation	Laa	30	43.6			1 - Most reliable	1:10,000	Lint		21/10/2020	DG20.42.4	south side of whaleback ridge in qtzite	DG20.42	Cradle	414012	5386318	10m
Cradle	Fold with dip and dip direction of axial surface	Haa + Pac	35	48.6	90	103.6	1 - Most reliable	1:10,000	FA/AS		21/10/2020	DG20.43.1		DG20.43	Cradle	414396	5386355	10m
Cradle	Mineral Elongation Lineation	Lao	35	48.6			1 - Most reliable	1:10,000	Lm		21/10/2020	DG20.43.2		DG20.43	Cradle	414396	5386355	10m
Cradle	Metamorphic Foliation	Sag	37	50.6			1 - Most reliable	1:10,000	Sm		21/10/2020	DG20.43.3		DG20.43	Cradle	414396	5386355	10m
Cradle	Unspecified Lineation	Lae	36	49.6			1 - Most reliable	1:10,000	Lmullion		21/10/2020	DG20.43.4		DG20.43	Cradle	414396	5386355	10m
Cradle	Metamorphic Foliation	Sag	42	55.6			1 - Most reliable	1:10,000	Sm	quartzite	21/10/2020	DG20.44.1	qtzite	DG20.44	Cradle	414634	5386630	10m
Cradle	Intersection Lineation	Laa	30	43.6			1 - Most reliable	1:10,000	Lint	quartzite	21/10/2020	DG20.44.2	qtzite	DG20.44	Cradle	414634	5386630	10m
Cradle	Metamorphic Foliation	Sag	45	58.6			1 - Most reliable	1:10,000	Sm	pelite	21/10/2020	DG20.45.1	laminated grey pelite	DG20.45	Cradle	414706	5386814	10m
Cradle	Intersection Lineation	Laa	50	63.6			1 - Most reliable	1:10,000	Lint	pelite	21/10/2020	DG20.45.2	laminated grey pelite	DG20.45	Cradle	414706	5386814	10m
Borradaile	Metamorphic Foliation, parallel to bedding	Sak	70	83.6			1 - Most reliable	1:10,000	So/Sm		19/01/2022	DG22.1.1	quarry near Lake Rowallan, dip slip movement on bedding plane, Lm pitch = 21E	DG22.1	Borradaile	434965	5380887	25m
Borradaile	Fold	Haa	20	33.6			1 - Most reliable	1:10,000	FA		19/01/2022	DG22.1.3	quarry near Lake Rowallan, dip slip movement on bedding plane	DG22.1	Borradaile	434965	5380887	25m
Borradaile	Fold with dip and dip direction of axial surface	Haa + Pac	65	78.6	78	-268.4	1 - Most reliable	1:10,000	FA/AS		19/01/2022	DG22.2.1		DG22.2	Borradaile	435079	5380139	25m
Borradaile	Fold with dip and dip direction of axial surface	Haa + Pac	50	63.6	75	-271.4	1 - Most reliable	1:10,000	FA/AS		19/01/2022	DG22.2.2		DG22.2	Borradaile	435079	5380139	25m
Borradaile	Fold with dip and dip direction of axial surface	Haa + Pac	55	68.6	74	87.6	1 - Most reliable	1:10,000	FA/AS		19/01/2022	DG22.2.3		DG22.2	Borradaile	435079	5380139	25m
Borradaile	Fold with dip and dip direction of axial surface	Haa + Pac	20	33.6	75	88.6	1 - Most reliable	1:10,000	FA/AS		19/01/2022	DG22.2.4		DG22.2	Borradaile	435079	5380139	25m
Borradaile	Fold	Haa	17	30.6			1 - Most reliable	1:10,000	FA		19/01/2022	DG22.2.4		DG22.2	Borradaile	435079	5380139	25m
Borradaile	Fold	Haa	40	53.6			1 - Most reliable	1:10,000	FA		19/01/2022	DG22.2.5		DG22.2	Borradaile	435079	5380139	25m

Project	Structure	Structure Type Symbol	Dip *	Dip Direction *	Secondary Dip	Secondary Dip Direction	Reliability	Output Scale *	Comments	Lithology	Collection Date	Field #	Sample Description	Other References	Locality	X *	Y *	Positional Accuracy
Borradaile	Fold	Haa	50	63.6			1 - Most reliable	1:10,000	FA		19/01/2022	DG22.2.6		DG22.2	Borradaile	435079	5380139	25m
Borradaile	Fold	Haa	65	78.6			1 - Most reliable	1:10,000	FA		19/01/2022	DG22.2.6		DG22.2	Borradaile	435079	5380139	25m
Borradaile	Fold	Haa	55	68.6			1 - Most reliable	1:10,000	FA		19/01/2022	DG22.2.6		DG22.2	Borradaile	435079	5380139	25m
Borradaile	Fold with dip and dip direction of axial surface	Haa + Pac	20	33.6	75	88.6	1 - Most reliable	1:10,000	FA/AS		19/01/2022	DG22.2.7		DG22.2	Borradaile	435079	5380139	25m
Borradaile	Metamorphic Foliation, parallel to bedding	Sak	72	-274.4			1 - Most reliable	1:10,000	So/Sm		19/01/2022	DG22.2.8		DG22.2	Borradaile	435079	5380139	25m
Borradaile	Metamorphic Foliation	Sag	63	-283.4			1 - Most reliable	1:10,000	Sm		19/01/2022	DG22.2.8		DG22.2	Borradaile	435079	5380139	25m
Borradaile	Metamorphic Foliation, parallel to bedding	Sak	90	103.6			1 - Most reliable	1:10,000	So/Sm		19/01/2022	DG22.2.9		DG22.2	Borradaile	435079	5380139	25m
Borradaile	Metamorphic Foliation	Sag	53	66.6			1 - Most reliable	1:10,000	Sm		19/01/2022	DG22.2.9		DG22.2	Borradaile	435079	5380139	25m
Borradaile	Metamorphic Foliation	Sag	75	88.6			1 - Most reliable	1:10,000	Sm	Schist	19/01/2022	DG22.3.1	albite schist with qtzite bands	DG22.3	Borradaile	436101	5380731	25m
Borradaile	Mineral Elongation Lineation	Lao	40	53.6			1 - Most reliable	1:10,000	Lm	Schist	19/01/2022	DG22.3.2	albite schist with qtzite bands, Pitch 35E	DG22.3	Borradaile	436101	5380731	25m
Borradaile	Fold with dip and dip direction of axial surface	Haa + Pac	10	23.6	70	83.6	1 - Most reliable	1:10,000	FA/AS	Schist	19/01/2022	DG22.3.3	albite schist with qtzite bands	DG22.3	Borradaile	436101	5380731	25m
Borradaile	Mineral Elongation Lineation	Lao	40	53.6			1 - Most reliable	1:10,000	Lm1	Schist	19/01/2022	DG22.3.4	albite schist with qtzite bands	DG22.3	Borradaile	436101	5380731	25m
Borradaile	Mineral Elongation Lineation	Lao	55	68.6			1 - Most reliable	1:10,000	Lm2	Schist	19/01/2022	DG22.3.5	albite schist with qtzite bands	DG22.3	Borradaile	436101	5380731	25m
Borradaile	Intersection Lineation	Laa	10	23.6			1 - Most reliable	1:10,000	Lint	Schist	19/01/2022	DG22.3.6	albite schist with qtzite bands	DG22.3	Borradaile	436101	5380731	25m
Borradaile	Fold with dip and dip direction of axial surface	Haa + Pac	24	37.6	55	68.6	1 - Most reliable	1:10,000	FA/AS		19/01/2022	DG22.4.1		DG22.4	Borradaile	434964	5386165	25m
Borradaile	Fold	Haa	75	88.6			1 - Most reliable	1:10,000	FA		19/01/2022	DG22.4.1		DG22.4	Borradaile	434964	5386165	25m
Borradaile	Mineral Elongation Lineation	Lao	2	15.6			1 - Most reliable	1:10,000	Lm		19/01/2022	DG22.4.2		DG22.4	Borradaile	434964	5386165	25m
Borradaile	Metamorphic Foliation	Sag	16	29.6			1 - Most reliable	1:10,000	Sm		19/01/2022	DG22.4.3		DG22.4	Borradaile	434964	5386165	25m
Borradaile	Ducitle Shear Band	Sau	35	48.6			1 - Most reliable	1:10,000	Sb		19/01/2022	DG22.5.1	Shear bands with SW over NW movement	DG22.5	Borradaile	435129	5392376	25m
Borradaile	Metamorphic Foliation	Sag	60	73.6			1 - Most reliable	1:10,000	Sm		19/01/2022	DG22.5.2	Shear bands with SW over NW movement	DG22.5	Borradaile	435129	5392376	25m
Borradaile	Fault	Faa	70	83.6			1 - Most reliable	1:10,000	F		19/01/2022	DG22.6.1	Fisher River Power Station	DG22.6	Borradaile	439256	5385958	25m
Borradaile	Unspecified Lineation	Lae	40	53.6			1 - Most reliable	1:10,000	Kink band?		19/01/2022	DG22.6.2	Fisher River Power Station	DG22.6	Borradaile	439256	5385958	25m
Borradaile	Metamorphic Foliation	Sag	84	97.6			1 - Most reliable	1:10,000	Sm		19/01/2022	DG22.6.3	Fisher River Power Station	DG22.6	Borradaile	439256	5385958	25m
Borradaile	Metamorphic Foliation	Sag	70	83.6			1 - Most reliable	1:10,000	Sm		19/01/2022	DG22.7.1	Fisher River Power Station, prominent Lint and Lcren, pitch = 50W	DG22.7	Borradaile	439315	5385938	25m
Borradaile	Metamorphic Foliation, parallel to bedding	Sak	68	81.6			1 - Most reliable	1:10,000	So/Sm		20/01/2022	DG22.8.1	Arm River Falls	DG22.8	Borradaile	433425	5384220	25m
Borradaile	Metamorphic Foliation, parallel to bedding	Sak	20	33.6			1 - Most reliable	1:10,000	So/Sm		20/01/2022	DG22.8.2	Arm River Falls, Lm with pitch = 20SE	DG22.8	Borradaile	433425	5384220	25m
Borradaile	Fold	Haa	40	53.6			1 - Most reliable	1:10,000	FA		20/01/2022	DG22.8.4	Arm River Falls	DG22.8	Borradaile	433425	5384220	25m
Borradaile	Metamorphic Foliation, parallel to bedding	Sak	45	58.6			1 - Most reliable	1:10,000	So/Sm		20/01/2022	DG22.8.5	Arm River Falls	DG22.8	Borradaile	433425	5384220	25m
Borradaile	Metamorphic Foliation, parallel to bedding	Sak	60	73.6			1 - Most reliable	1:10,000	So/Sm		20/01/2022	DG22.8.6	Arm River Falls	DG22.8	Borradaile	433425	5384220	25m
Borradaile	Metamorphic Foliation, parallel to bedding	Sak	45	58.6			1 - Most reliable	1:10,000	So/Sm		20/01/2022	DG22.9.1	Bend on Arm River	DG22.9	Borradaile	433291	5384093	25m
Borradaile	Mineral Elongation Lineation	Lao	37	50.6			1 - Most reliable	1:10,000	Lrod		20/01/2022	DG22.9.2	Bend on Arm River	DG22.9	Borradaile	433291	5384093	25m
Borradaile	Unspecified Lineation	Lae			40	53.6	1 - Most reliable	1:10,000	Lmullion		20/01/2022	DG22.9.3	Bend on Arm River, Lineation pitch = 70N	DG22.9	Borradaile	433291	5384093	25m
Borradaile	Fold with dip and dip direction of axial surface	Haa + Pac	25	38.6	70	-276.4	1 - Most reliable	1:10,000	FA/AS		20/01/2022	DG22.9.4	Bend on Arm River	DG22.9	Borradaile	433291	5384093	25m
Borradaile	Fold with dip and dip direction of axial surface	Haa + Pac	25	38.6	80	-266.4	1 - Most reliable	1:10,000	FA/AS		20/01/2022	DG22.9.5	Bend on Arm River	DG22.9	Borradaile	433291	5384093	25m
Borradaile	Mineral Elongation Lineation	Lao					1 - Most reliable	1:10,000	Lm		20/01/2022	DG22.9.5	Bend on Arm River	DG22.9	Borradaile	433291	5384093	25m
Borradaile	Fold	Haa	40	53.6			1 - Most reliable	1:10,000	FA		20/01/2022	DG22.9.6	Bend on Arm River	DG22.9	Borradaile	433291	5384093	25m
Borradaile	Fold	Haa	30	43.6			1 - Most reliable	1:10,000	FA		20/01/2022	DG22.9.7	Bend on Arm River	DG22.9	Borradaile	433291	5384093	25m
Borradaile	Fold	Haa	30	43.6			1 - Most reliable	1:10,000	FA		20/01/2022	DG22.9.8	Bend on Arm River	DG22.9	Borradaile	433291	5384093	25m
Borradaile	Fold with dip and dip direction of axial surface	Haa + Pac	45	58.6	40	53.6	1 - Most reliable	1:10,000	FA/AS (av)		20/01/2022	DG22.9.9	Bend on Arm River, estimate of fold DG22.9.6 - DG22.9.8	DG22.9	Borradaile	433291	5384093	25m

Project	Structure	Structure Type Symbol	Dip *	Dip Direction *	Secondary Dip	Secondary Dip Direction	Reliability	Output Scale *	Comments	Lithology	Collection Date	Field #	Sample Description	Other References	Locality	X *	Y *	Positional Accuracy
Borradaile	Metamorphic Foliation, parallel to bedding	Sak	45	58.6			1 - Most reliable	1:10,000	So/Sm		20/01/2022	DG22.9.10	Bend on Arm River	DG22.9	Borradaile	433291	5384093	25m
Borradaile	Cleavage	Cae	80	93.6			1 - Most reliable	1:10,000	Scl		20/01/2022	DG22.9.11	Bend on Arm River	DG22.9	Borradaile	433291	5384093	25m
Borradaile	Metamorphic Foliation	Sag	55	68.6			1 - Most reliable	1:10,000	Sm		20/01/2022	DG22.9.12	Bend on Arm River	DG22.9	Borradaile	433291	5384093	25m
Borradaile	Intersection Lineation	Laa	22	35.6			1 - Most reliable	1:10,000	Lint		20/01/2022	DG22.9.13	Bend on Arm River	DG22.9	Borradaile	433291	5384093	25m
Borradaile	Mineral Elongation Lineation	Lao	24	37.6			1 - Most reliable	1:10,000	Lm		20/01/2022	DG22.9.14	Bend on Arm River	DG22.9	Borradaile	433291	5384093	25m
Borradaile	Metamorphic Foliation, parallel to bedding	Sak	40	53.6			1 - Most reliable	1:10,000	So/Sm		20/01/2022	DG22.9.15	Bend on Arm River	DG22.9	Borradaile	433291	5384093	25m

Tasmanian Government

Mineral Resources Tasmania
PO Box 56 Rosny Park
Tasmania Australia 7018
Ph: +61 3 6165 4800

info@mrt.tas.gov.au www.mrt.tas.gov.au